Study of the physicochemical properties of an extinguishing powder for sodium fires : aging, fabrication, and mechanism of extinction

Nur Andriani Pramudita Kusumanindyah

Université Fédérale
Toulouse Midi-Pyrénées

THÈSE

En vue de l'obtention du

DOCTORAT DE L'UNIVERSITÉ DE TOULOUSE

Délivré par :

École Nationale Supérieure des Mines d'Albi-Carmaux

Présentée et soutenue par :
Nur Andriani Pramudita KUSUMANINDYAH

le Mardi, 13 Décembre 2016

Titre :

Study of the physicochemical properties of
an extinguishing powder for sodium fires:
aging, fabrication, and mechanism of extinction

École doctorale et discipline ou spécialité :
ED MEGEP : Génie des procédés et de l'Environnement

Unité de recherche :
RAPSODEE CNRS-UMR 5302 Mines Albi

Directeur/trice(s) de Thèse :

Henri BERTHIAUX (Directeur de Thèse Mines Albi)
Laurent BRISSONNEAU (Co-Directeur de Thèse/Correspondant CEA)

Jury :

Khashayar SALEH (Université de Technologie Compiègne, Rapporteur)
Jean-Louis CONSALVI (Université Aix-Marseille, Rapporteur)
André LAURENT (Université de Lorraine ENSIC - Lorraine INP, Examinateur)
Loïc FAVERGEON (École Nationale Supérieure des Mines de Saint Étienne, Président)
Cendrine GATUMEL (Co-encadrant Mines Albi, Examinateur)
Thierry GILARDI (Co-encadrant CEA, Membre Invité)
Philippe BICHON (Ingénieur R&D Société Ai-GROUP, Membre Invité)

"There is no growth in a comfort zone and there is no comfort in a growth zone. I must leave my comfort zone to grow"

(Muhammad Assad – Notes from Qatar)

A la mémoire de mon cher Papa et de Nicole

REMERCIEMENTS

Ces trois dernières années sont une expérience inoubliable et très enrichissante, non seulement sur le plan professionnel mais aussi sur le plan personnel. Je suis arrivée en France il y a 4 ans afin de poursuivre mes études supérieures, après 4 années de formation continue en Licence et Master1 en Indonésie. Partir aussi loin de mon pays natal n'était pas si facile. Je quittais ma zone de confort, ma famille, et mes ami(e)s. Je dédie tous mes travaux de Doctorat à mon cher Papa et à Nicole que j'avais rencontrée lors de mon stage de Master 2 car tous deux croyaient en moi et m'ont guidée sur cette voix. Malheureusement, la vie ne leur a pas permis d'être là aujourd'hui pour voir l'aboutissement de mon travail.

Mon cher Papa, je te remercie d'avoir toujours été disponible pour me donner tes précieux conseils à n'importe quelle heure du jour ou de la nuit ; le décalage horaire compliquait parfois les choses ! Je me souviens quand tu m'as demandée, la veille de mon départ pour la France, si j'étais prête pour entreprendre cette grande aventure. Tu m'avais dit qu'une fois partie, il ne faudrait pas revenir en arrière et que je devais réussir ma vie. Tu as toujours été mon premier et mon plus grand soutien. Tu m'as guidée pour faire ces choix et tu m'as montré la route à suivre pour avancer dans la vie. Je tiendrai la promesse que je t'ai faite à tout mettre en œuvre pour réussir et honorer ton souvenir. Je t'aime Papa.

Nicole, je ne t'ai connue que 5 mois seulement lors de mon stage de Master 2 et qui avait marqué le début de mon travail à Cadarache. Notre rencontre a été la plus belle qui me soit arrivée. Malgré mes faibles compétences en Français au début, tu as été la première personne à me témoigner ta confiance en me donnant l'opportunité de faire mon doctorat au CEA et en me proposant ce sujet de thèse riche en partie expérimentale. Je me souviens comme si c'était hier quand tu m'as convaincue que je devrais revenir après mon stage pour préparer ma thèse. Tu me rassurais sur la barrière de la langue et tu m'expliquais que je ne devrais ma réussite qu'à mes seuls efforts. J'ignorais à ce moment-là que ce serait tes derniers messages qui m'ont toujours motivée pour donner le meilleur de moi-même. Encore merci de m'avoir sélectionnée en tant que ta thésarde.

Ensuite, je tiens à remercier tous mes encadrants de thèse. Laurent tout d'abord : Tu as été mon encadrant après le départ de Nicole, j'ai beaucoup appris avec toi de par ton exigence notamment. Je détestais presque cela parfois je l'avoue dans le quotidien de mon travail et en même temps j'admirais cette qualité d'encadrant. Je détestais car il m'arrivait d'avoir le sentiment de ne pas fournir un travail suffisant ; j'appréciais car je comprenais que tu avais raison. Je viens de loin pour apprendre et je te remercie de m'avoir appris beaucoup des choses. C'est grâce à ton exigence que j'ai appris à être plus exigeante encore avec moi-même pour fournir un travail de qualité. Ta dédicace pour la recherche, toujours donner le meilleur de soi-même en sachant prendre le temps pour atteindre au mieux la perfection sont les choses que j'ai le plus appréciées en toi. Je te remercie pour tout le temps de discussions qu'on a passées ensemble.

Puis Thierry : Les derniers mois au cours desquels nous avons travaillé pour construire des modèles sous COMSOL sont des expériences mémorables. J'ai beaucoup apprécié ta patience pour essayer de comprendre une problématique et y répondre : c'est une formidable qualité de chercheur. Sur le plan personnel, il était très agréable de travailler avec toi. Ta vision toujours

positive des choses m'a beaucoup aidé pour finaliser la rédaction de ma thèse et préparer ma soutenance, surtout dans les dernières semaines juste après le départ de Papa. Tu essayais toujours de me remonter le moral ; sur le plan humain, c'est une qualité exceptionnelle. Je t'en suis très reconnaissante.

Quant à vous, Henri et Cendrine, je vous remercie de votre grande disponibilité pour répondre à mes questions. J'ai beaucoup appris des moyens expérimentaux des poudres lors de mon séjour à l'Ecole des Mines d'Albi Carmaux. Je vous remercie de votre soutien moral pendant la conférence AIChE à San Francisco. Cette période restera toujours un bon souvenir.

Je tiens à également remercier toute les membres de jury M. Saleh, M. Consalvi, M. Favergeon, et M. Laurent, d'avoir accepté de lire attentivement le manuscrit et donner leur avis qui est très constructif pour améliorer le travail.

Ensuite, mes chers Bibi et Serge, « mes parents du labo », je ne sais pas comment j'aurais pu réussir à finir ma thèse sans vous ! On oublie trop souvent que l'expérimental n'est pas toujours identique à la théorie. Vous m'avez aidé à régler les soucis que je rencontrais dans mes travaux au cours des expériences. Je vous remercie également d'avoir été à mon écoute, de m'avoir apporté votre soutien jusqu'au bout, de me crier sans cesse « Nur, tu vas y arriver ! » à chaque fois que je croyais que je ne pourrai pas finir mes manips dans les délais impartis. Il y a toujours une solution ! Vous m'avez appris cela et je n'oublierai jamais dans la suite de ma carrière.

A toute l'équipe du LIPC : les ingénieurs Pierre, Anna, Karine, Michele, Aurélien, Vincent ; les techniciens Aurore, mon « beau » Vincent, Cyril ; les thésard(e)s, stagiaires et apprenti(e)s Alice Plantamp, Jérémy, Marie Lacroix, Marie Gabard, Yanis, Daniele, encore un autre Vincent (Anjard), « petit » Pierre, Florian, J.C, Emilie, Camille, Alice Goffan, Alice Huynh, Morgan, Finlay, Joachim, Karine, et Emeline. Sans oublier mes chères secrétaires Petra et Florence ! Merci d'avoir toujours su entretenir une ambiance chaleureuse et dynamique au labo et de m'avoir transmis la culture française pour que je me sente comme chez moi. Je garderai toujours le souvenir de cette belle ambiance.

Un grand merci à toutes les personnes que m'ont aidée durant ces 3 années de travail : Christophe Perrais et J.P. Ferraud qui m'a reçue dans le labo LIPC ; Dominique Pecheur et Christophe Tiffreau qui m'a accueillie au sein du SMTA ; Christian Latgé, Olivier Gastaldi qui m'a donné ses précieux conseils autour de projet TECNA ; Thierry Bonhomme, Nawelle, Hélène, Jean Peybernes du LTRS qui m'ont apporté leur soutien lors de campagne d'essai Chris(X)ti-Na ; Philippe Bichon de Ai-Group qui m'a beaucoup aidée pour réaliser très rapidement la manip Chri(X)ti-Na ; Claude Berton et Michel Soucille qui m'a aidée sur l'analyse de risque Chris(X)ti-Na, son conseil et encouragement ; Thierry Abran de FLS ; l'équipe de l'Ecole des Mines : Laurent, Séverine, Sylvie, Nathalie, Christine, Chrystelle, les thésard(e)s Léonard, Tina, Lucia, Haithem, Andres, Margot, Hugo grâce à qui j'ai beaucoup apprécié mes séjours à Albi ; mon professeur de français Evelyn ; mes ami(e)s Diogo, Marie Trijau, Benoit, Claire, Céline, Nicholas, Tangi, Eva ; et mes amies de voyages Shinta, Yuko, Ari toujours de bonne humeur !

A mes meilleures amies que je considère comme de vraies sœurs : Anais, ma voisine de bureau, « mon SOS câlin » ; ma coloc Faoulat ; Nayiri ; Sarah ; Anike je vous remercie de votre présence à mes côtés dans les moments les plus difficiles de ma vie. C'était une véritable chance de vous avoir rencontrées. Merci de m'avoir toujours répété que je n'étais pas seule et que je pouvais compter sur vous !

Enfin, je remercie toute ma famille, surtout ma Maman, ma sœur, et Budhe Titiek qui m'a soutenue jusqu'au bout et qui m'a rappelée que même si la distance nous sépare, le plus important est l'amour qui nous unie. Et un dernier remerciement à ma « maman française », Dominique, que j'ai rencontrée en arrivant en France à l'Université : elle m'a toujours soutenue, encouragée, accompagnée, écoutée et conseillée pendant toutes ces années comme elle l'aurait fait avec sa propre fille.

RÉSUMÉ ÉTENDU

Cette étude est réalisée dans le cadre du développement de la filière des Réacteurs nucléaires à Neutrons Rapides refroidis au sodium (RNR-Na). Il est largement connu que le sodium a des propriétés bénéfiques du fait qu'il ne ralentit pas les neutrons, qu'il est faiblement activé, compatible avec les aciers inoxydables, et qu'il présente de bonnes propriétés thermiques (conductivité, évacuation de la chaleur) ainsi qu'une viscosité et une densité faibles. Cependant son opacité et sa réactivité chimique importante avec l'eau et l'air sont ses inconvénients majeurs. La réaction sodium-air peut provoquer un feu de sodium. Par conséquent, il est impératif, pour assurer la sécurité en fonctionnement d'un circuit sodium, de proposer une méthode capable de lutter contre l'incendie en cas de fuite de sodium. Le Commissariat à l'Energie Atomique et aux énergies alternatives (CEA) a breveté une poudre extinctrice, baptisée Marcalina, à base d'un mélange de carbonate de lithium et de carbonate de sodium faiblement hydraté (3,5 – 5,4% d'eau) dans une proportion proche de l'eutectique, dont la température de fusion est d'environ 500°C, associé à du graphite. Il est considéré que cette poudre possède de meilleures performances que les poudres extinctrices commerciales disponibles jusque-là. Elle a été fabriquée depuis les années 1980 jusqu'à la fin des années 1990 par la société CACI, qui a cessé son activité. D'une part, la production industrielle de cette poudre est projetée dans un proche avenir du fait de la relance des programmes sur les réacteurs rapides (liés au projet ASTRID); d'autre part, le CEA a aujourd'hui à sa disposition un stock important de lots de poudres inutilisés. Ainsi, la réutilisation de ces lots pose la question de leur efficacité pour éteindre un feu de sodium, notamment en raison de leur entreposage à long terme qui pourrait modifier leur composition. Pour cette raison, des analyses physico-chimiques de ces poudres sont menées afin de connaître l'évolution de leur composition et leurs caractéristiques pour les différents lots. Pour le CEA, l'intérêt de cette étude est de saisir tout particulièrement s'il est possible de réutiliser directement ces poudres ou, si tel n'est pas le cas, d'étudier la possibilité de les régénérer ou sinon de les fabriquer de nouveau. Les objectifs de cette thèse sont de caractériser le vieillissement de la poudre, de connaître sa méthode de fabrication ainsi que de comprendre le mécanisme d'extinction du feu de sodium lié à ses propriétés physicochimiques.

La première partie de cette étude comporte diverses analyses physico-chimiques qui ont été réalisées pour caractériser ces poudres. Trois poudres appelées poudres A, B et C ont été choisies comme poudres Marcalina de référence pour la suite de cette étude. Les analyses chimiques réalisées sont :

1. *L'analyse thermo gravimétrique (ATG) couplée à la micro chromatographie gazeuse (µ-GC)*
   Cette analyse permet de rapporter la perte de mas. d'échantillon observée par l'ATG aux gaz dégagés lors du chauffage mesurés par µ-GC. Les résultats ont montré une perte de mas. importante de 11,8% pour les poudres B et C, ce qui correspond aux dégagements d'eau et de CO_2 pendant le chauffage jusqu'à 200°C. Tandis que la poudre A a la plus faible perte de mas. avec 4,8%

2. *La diffraction des rayons X (DRX)*
   L'analyse XRD permet d'identifier les composants de la poudre. Les analyses qualitatives ont été réalisées en identifiant les phases d'un échantillon par rapport à celles référencées. Une analyse semi quantitative (SQ) a également été effectuée afin d'estimer les proportions des différentes phases en utilisant les méthodes RIR (Ratio Intensité de Référence). Cinq composants ont été détectés: le carbonate de sodium monohydrate ($Na_2CO_3.H_2O$), le carbonate de lithium (Li_2CO_3), le graphite, le lithium sodium carbonate ($LiNaCO_3$) et le trona ($Na_2CO_3.NaHCO_3.2H_2O$). Ces deux derniers composés ne sont pas mentionnés dans les brevets, devenant ainsi les composants à étudier plus en détail. Les pics les plus forts de $LiNaCO_3$ ont été observés dans la poudre A avec 42%mass. Ils sont beaucoup plus faibles

pour la poudre C, alors qu'ils sont presque non détectés dans la poudre B. D'autre part, le trona n'a pas été observé dans la poudre A, contrairement aux pics forts identifiés dans les deux poudres B et C avec 31%mass et 39%mass respectivement. La nature lamellaire des cristaux de graphite provoque une imprécision des résultats en raison de son orientation préférentielle. Néanmoins, l'analyse SQ permet d'estimer l'ordre de grandeur des compositions.

3. *La filtration de graphite et la spectroscopie d'absorption atomique (SAA)*
   La filtration de graphite et la SAA ont été effectuées pour mesurer la composition élémentaire des poudres. Les poudres doivent être déshydratées auparavant pour doser la teneur en eau et en CO_2. L'acide sulfurique 1M a utilisé pour ensuite dissoudre l'échantillon. La filtration est suivie d'un lavage du résidu avec de l'eau déminéralisée et d'un séchage dans un four pendant 2 heures à 100°C afin d'obtenir la quantité de graphite. L'analyse AAS permet alors de doser les concentrations de sodium et de lithium dans le filtrat récupéré de la filtration.

4. *L'analyse thermique différentielle (ATD)*
   Cette analyse a été utilisée pour détecter les transformations de phases lors du chauffage de la poudre de 25 à 600°C (fusion) puis en la refroidissant jusqu'à ce qu'elle atteigne la température ambiante (cristallisation). Les poudres ayant des quantités plus élevées de trona se décomposent à une température légèrement supérieure (environ 90°C) pour les poudres B et C que la poudre A (à 80°C) et absorbent environ deux fois plus d'énergie. Pendant le refroidissement, un pic exothermique a été observé à environ 488°C pour ces trois poudres.

La combinaison des analyses TGA-µGC, filtration au graphite et AAS permet de calculer la composition en poudre. Trona est relativement abondant et stable jusqu'à 57°C dans des conditions sèches. Une décomposition en une étape se produit dans une plage de température de 77-214°C sous atmosphère de N_2 en Na_2CO_3, H_2O et CO_2, ce qui explique le dégagement de CO_2 détecté par µGC. Sur la base de la réaction de décomposition de trona, sa formation pourrait être produite à partir de Na_2CO_3 et/ou $Na_2CO_3.H_2O$, selon les teneurs en humidité et CO_2 pendant le stockage. Par conséquent, on a supposé que trona est un produit du vieillissement, une hypothèse qui sera validée par les expériences de vieillissement qui seront développées et discutées ultérieurement. Le cristal $LiNaCO_3$ a été découvert à partir de l'étude du diagramme de phases du carbonate de lithium et du carbonate de sodium. En effet, le résultat de l'expérience réalisée en ATD avec un mélange de 50:50% en moles de Li_2CO_3 et Na_2CO_3 montre le pic endothermique à 499 $\pm$ 0,5°C résultant de sa formation, ce qui est cohérent avec le diagramme de Cairns et coll. Ainsi, son existence dans le mélange pourrait être liée au procédé de fabrication de la poudre (qu'elle soit produite par fusion à haute température ou par d'autres procédés?), qui n'est malheureusement pas connu du fait de l'arrêt d'activité du fabriquant. Par conséquent, une étude de l'effet de broyage du mélange de Na_2CO_3-Li_2CO_3 et/ou $Na_2CO_3.H_2O$-Li_2CO_3 a ensuite été réalisée pour vérifier si cette étape du procédé pouvait être à l'origine de sa formation. Au contraire, le vieillissement en stockage peut provoquer sa décomposition, comme on le verra de façon plus détaillée dans les essais de vieillissement.

La transformation de la composition chimique peut potentiellement modifier les propriétés physiques de ces poudres. Pour cela, les caractérisations physiques suivantes sont également effectuées :

5. *Le microscope électronique à balayage (MEB)*
   Les analyses par MEB ont été utilisées pour caractériser la microstructure des poudres. La poudre A est constituée de particules en forme de bâtonnets de forme régulière (longueur 5µm), qui coexistent avec des particules plus grosses de 20µm de longueur. D'autre part, la poudre B est constituée de particules beaucoup plus grosses et arrondies de formes

irrégulières de 100µm (avec des particules agglomérées en forme d'aiguille). La poudre C ressemble plus à la poudre A, bien que la plupart de ses particules en forme d'aiguilles semblent être brisées par rapport à la poudre A.

6. *L'analyse de la granulométrie*
   La distribution granulométrique de la poudre a été déterminée en utilisant un équipement de diffraction laser. Un léger agrandissement des particules a été observé dans la poudre C avec 7,43µm (distribution monomodale) par rapport à la poudre A, alors que les particules B étaient six fois plus grandes que la poudre A avec une taille moyenne de 30,3µm et une distribution multimodale.

7. *Les essais d'écoulement par FT4 poudre rhéomètre*
   Un rhéomètre en poudre FT4 de Freeman Technology (Gloucestershire, RU) est conçu pour caractériser la rhéologie ou les propriétés d'écoulement des poudres. Il mesure la résistance de la poudre à l'écoulement en mouvement. Plusieurs essais de cisaillement ont été effectués à différents niveaux de contraintes normales pour mesurer le comportement de la poudre pendant la transition de l'absence à la présence de l'écoulement. Les données produites représentent la relation entre la contrainte de cisaillement et la contrainte normale, qui peut être tracée pour définir le lieu cinématique de rupture de la poudre. Pour chaque échantillon, le lieu cinématique de rupture a été obtenu pour 2, 4, 8 et 16 kPa. Il montre que la poudre A présente une caractéristique cohésive dans 2 kPa. Plus la contrainte de consolidation appliquée est élevée, moins elle devient cohésive. Néanmoins, la poudre serait encore classée comme une poudre cohésive à une valeur de contrainte élevée. Il s'est avéré qu'à des contraintes plus élevées, la poudre C a la même tendance que la poudre A à être cohésive, tandis que la poudre B est capable de s'écouler facilement. Ainsi, les résultats sont en bon accord avec les mesures granulométriques. Ayant la taille des particules plus grandes, la poudre B est plus facile à s'écouler contrairement à poudre A et C dont les tailles sont plus petites, elles sont plus difficile à s'écouler (cohésive).

8. *Le voluménomètre*
   Les masses volumiques tassées ont été mesurées par un voluménomètre d'Erweka. Les poudres A et C ont des masses volumiques semblables, alors que la valeurs est doublée pour la poudre B. Selon l'indice de Carr, ces trois poudres sont comprises dans la catégorie de flux modéré, tandis que l'indice de Hausner les considère comme légèrement compressibles et cohésives. Ces résultats sont en contradiction avec ceux obtenus à partir de mesure FT4. Cela peut s'expliquer par un phénomène d'agglomération qui se produirait plus facilement pour les poudres A et C pendant le tassement permettant aux particules d'occuper un plus grand volume et d'être moins denses que dans la poudre B.

9. *Le pycnomètre en hélium*
   Cet appareil a été utilisé pour mesurer la vraie densité de particules qui représente le rapport du poids sur le volume des grains. Les résultats pour les trois poudres sont de même valeur avec 2,2 $g.mL^{-1}$. La poudre A et C sont constituées de 86% de porosité, à comparer avec la poudre moins poreuse B avec 75% de porosité.

10. *Le dynamique vapeur sorption (DVS)*
    Le DVS est une technique gravimétrique dans laquelle un échantillon de poudre est soumis à des conditions variables d'humidité de l'air et de température. La température d'analyse est réglée à 25°C. L'humidité est variée entre 0 et 90% par incréments de 10% pour le cycle d'adsorption poursuivi par le cycle de désorption commencé de 90 à 0% d'humidité avec les mêmes incréments. Cette analyse permet d'obtenir une première estimation des gains de mas. à différentes conditions d'humidité qui peuvent être représentatives de conditions de stockage différentes. Ces trois poudres commencent à prendre de la mas. sous 78,5% HR pendant le cycle d'adsorption. La poudre A présente le plus grand changement de mas. avec

44,6%, tandis que les deux poudres B et C gagnent moins de la moitié de celle-ci avec respectivement 20,4% et 14,6%. Le cycle de désorption des produits démontre la recristallisation de poudre A qui se transforme en deux produits séparés avec une différence de couleur distincte. Le même comportement est également observé pour les poudres B et C. L'hystérésis représente la stabilité de l'échantillon en fonction de la fluctuation de l'humidité. Cette hystérésis pourrait correspondre au passage du carbonate de sodium monohydrate au décahydrate qui commence à 70% HR à température ambiante. Ainsi, elle concerne la stabilité de l'échantillon.

La deuxième partie de l'étude concerne sur le vieillissement de la poudre qui a été menée afin de comprendre son mécanisme. Considérant que la poudre est initialement composée de $Na_2CO_3.H_2O$ et de Li_2CO_3 dans le brevet, $Na_2CO_3.H_2O$ est alors pris comme échantillon pur d'intérêt. Cependant, le $LiNaCO_3$ est censé faire partie de la composition initiale de la poudre car l'étude de la littérature indique qu'elle ne peut être formée que lors de la fusion des carbonates de sodium et de lithium à haute température. De plus, la poudre dont la teneur en eau est supérieure à celle de la spécification a une quantité moindre de $LiNaCO_3$. Par conséquent, il est également devenu objet d'observation. En outre, comme la poudre A est le seul échantillon dont la teneur en eau est encore dans la plage de spécification, il est choisi comme échantillon Marcalina de référence. Du $Na_2CO_3.H_2O$ commercial de pureté de 99,5% a été utilisé. Comme le $LiNaCO_3$ n'est pas disponible dans le commerce, il a été produit par chauffage du Na_2CO_3 et du Li_2CO_3 dans des proportions molaires de 50:50 à 600°C pour obtenir la fusion des sels puis la recristallisation en carbonate mixte pendant le refroidissement.

Pour les essais, les échantillons ont été placés dans des dessiccateurs contenant des solutions salines saturées pour contrôler l'humidité relative à des valeurs faibles (8%, KOH), modérées (33%, $MgCl_2$) et élevées (75%, NaCl). Outre l'humidité, le rôle du dioxyde de carbone de l'air ambiant a également été étudié. Par conséquent, deux méthodes de conditionnement (avec et sans passage d'air) ont été appliquées. L'évolution des compositions de poudre a été suivie par analyse DRX, avec des prélèvements effectués tous les 2 mois. Les expériences ont été réalisées pendant 8 mois. L'analyse des essais a montré que les grains des poudres de LiNaCO3 et de $Na_2CO_3.H_2O$ utilisées étaient trop gros pour fournir des cinétiques suffisamment rapides pour être observées. Par conséquent, seuls les résultats de la poudre A, constituée de petits grains, seront examinés plus en détail.

Les résultats des analyses semi-quantitatives de DRX pour l'évolution de la composition de la poudre A pendant 8 mois dans 75% HR avec passage d'air ont montré que la quantité de trona augmente et la quantité de $LiNaCO_3$ diminue avec le temps. $LiNaCO_3$ se décompose presque complètement en $Na_2CO_3.H_2O$, Li_2CO_3 et peu de trôna après deux mois. $LiNaCO_3$ n'est plus observable après 8 mois de vieillissement dans cette condition. Entre le deuxième et le quatrième mois, le $Na_2CO_3.H_2O$ se transforme complètement en trôna. Cependant en l'absence de CO_2, $LiNaCO_3$ est complètement décomposé après deux mois en $Na_2CO_3.H_2O$, Li_2CO_3 et un peu de $Na_2CO_3.7H_2O$. Aucune trona n'est observée à ce moment. À des temps plus longs, les teneurs en trona et $Na_2CO_3.7H_2O$ augmentent, aux dépens de $Na_2CO_3.H_2O$. Au bout de huit mois , ce dernier semble augmenter aux dépens de $Na_2CO_3.7H_2O$, bien qu'il soit discutable (compte tenu de la présence de trona), si les conditions d'étanchéité à l'air ont été conservés dans les derniers mois.

Dans des conditions d'air moins humides, la cinétique de décomposition de $LiNaCO_3$ et de formation de trona est beaucoup plus lente. Il est donc intéressant de remettre en question les conditions limites, relatives aux niveaux d'humidité et de présence de CO_2, dans lesquelles les deux réactions sont thermodynamiquement possibles. La légère baisse de 10%mas. de $LiNaCO_3$ et l'augmentation de 9%mas. de $Na_2CO_3.H_2O$ due à la décomposition de $LiNaCO_3$ ont été observées dans une condition étanche à 8% HR après huit mois. Cela démontre que $LiNaCO_3$ s'est décomposé plus rapidement sans la présence de CO_2 sur la base des résultats comparatifs de l'échantillon conservé dans des conditions étanche et ouverte à faible humidité (HR 8%).

La comparaison de la variation de composition de la poudre A au bout de 8 mois pour les trois conditions d'humidité avec ou sans air a montré que dans des conditions ouvertes, la moindre présence de trona (2% en mas.) est obtenue pour 8%HR. Sa quantité est de 9 fois et 24 fois plus élevée dans les conditions de 32%HR + air et 75%HR + air, respectivement. Ici, l'augmentation du trona est en corrélation avec la diminution de $LiNaCO_3$ et $Na_2CO_3.H_2O$. Dans le cas de faible humidité 8%HR + air, sa quantité est relativement constante avec seulement 1%mas. d'augmentation au bout de 8 mois. Au contraire, trona est beaucoup plus difficile à former sans la présence de CO_2 même à humidité élevée (75% RH). Cependant le $LiNaCO_3$ s'est avéré être complètement décomposé et 23% de trona a été formé pendant en condition étanche à 75%HR. Encore une fois, la présence de trona remet en question l'étanchéité à l'air des conditions d'HR à 75%. Il est également possible que l'essai à 8%HR ne soit pas étanche mais que la transformation en trôna soit beaucoup plus lente dans cette condition.

Les résultats expérimentaux du vieillissement ont donc démontré deux réactions différentes qui pourraient se produire simultanément, dont la cinétique de réaction dépend de la condition de stockage:

- La condition de HR élevée en atmosphère ouverte (présence de CO_2) favorise la formation de trona,

$$3\ Na_2CO_3.H_2O + 2\ H_2O + CO_2 \rightarrow 2\ [Na_2CO_3.NaHCO_3.2H_2O]$$

- La condition de HR élevée en atmosphère fermée (présence limitée de CO_2) est favorable à la décomposition de $LiNaCO_3$,

$$2\ LiNaCO_3 + H_2O \rightarrow Li_2CO_3 + Na_2CO_3.H_2O$$

La poudre B résulte des deux réactions, tandis que la décomposition réactionnelle de $LiNaCO_3$ dans la poudre C est plus contrôlée (cinétique de réaction limitée par la présence de CO_2 ?). Cela peut être dû à la différence des conditions de stockage appliquées aux deux poudres. Il est suggéré de contrôler la condition d'humidité inférieure à 50% pour éviter la réaction de vieillissement. Ces deux mécanismes nous permettent d'estimer la composition de la poudre après le vieillissement si les deux réactions se produisaient totalement. Le résultat a montré que 58w% de trona pourrait être formé, ce qui correspond approximativement à 11.6w% d'eau d'hydratation. En outre, il semble que la taille des particules puisse influencer la cinétique des deux réactions. En présence de particules plus grosses, les résultats des échantillons purs de $Na_2CO_3.H_2O$ et $LiNaCO_3$ après 8 mois de vieillissement ont montré une formation plus lente de trona et une décomposition de $LiNaCO_3$ par rapport à la poudre A.

Le $LiNaCO_3$ est soupçonné d'être un composant de départ, du fait qu'il se détériore au cours du temps pendant le stockage. De plus, l'étude bibliographique du mélange eutectique de Li_2CO_3 et de Na_2CO_3 montre qu'il se forme par fusion à haute température (500°C). Une étude approfondie sur la formation de ce composant permet d'éclairer le moyen de fabrication de cette poudre. Pour cela, des essais de broyage des mélanges des carbonates lithium et sodium ont été réalisées.

Les matériaux originaux mentionnés dans les brevets relatifs à Marcalina, qui comprennent le Li_2CO_3, le $Na_2CO_3.H_2O$, le graphite, ainsi que le Na_2CO_3, sont les échantillons choisis pour les tests. Deux types d'appareils de broyage ont été utilisés: broyeur en mortier et broyeur planétaires. Ces broyeurs sont choisis afin de comparer la composition du produit après broyage avec différents type de broyeur (technique/mécanisme différents). Cette information sera utile pour considérer le choix du broyeur dans la perspective de l'application industrielle.

En effet, les résultats expérimentaux ont montré que $LiNaCO_3$ peut être produit par réaction mécanochimique pendant le processus de broyage. Pour les mélanges de carbonates anhydres, la réaction se produit comme suit:

$$Li_2CO_3 + Na_2CO_3 \rightarrow 2\ LiNaCO_3$$

La réaction mécanochimique entre deux constituants se produit en raison des contraintes mécaniques appliquées dans les particules. La rupture de ces particules se produit ainsi, créant des surfaces propres car le broyage et les poudres se mélangeant de cette manière permettent un contact très intime entre les constituants. Ceci peut expliquer pourquoi le $LiNaCO_3$ qui doit être produit de façon classique à environ 500°C pourrait être formé par une réaction mécanochimique. Cependant, comme lors des essais avec $Na_2CO_3.H_2O$ seul, broyage n'est pas capable de diminuer la quantité d'eau (comme observé par ATG à 80°C), ceci prouve que des hausses de température élevées ne sont pas produites dans le broyeur. Dans ce cas, seule la réduction de la taille des cristallites probablement se produit. Cependant, le broyeur à mortier et le broyeur planétaires ont montré des résultats contradictoires. Le $LiNaCO_3$ ne peut pas être formé avec le broyeur de mortier à partir de carbonate de sodium anhydre, contrairement au broyeur planétaire, pour lequel $LiNaCO_3$ est apparu plus facile avec du carbonate de sodium hydrate. Cela pourrait être dû au fait que le traitement mécanochimique commence par un raffinement de particules et de cristallites. Les poudres résultant du broyeur de mortier peuvent avoir une taille de cristallites plus grande que celle produite par le broyeur planétaire en raison de sa moindre performance. Il est donc très possible que dans ce cas, $LiNaCO_3$ ne soit pas encore formé. Le produit final dépend avant tout des conditions de broyage, par conséquent, différents types de broyeurs ou l'altération des paramètres de broyage peuvent donner lieu à divers chemins de réaction pour la réaction mécanochimique. Il apparaît que les solides comprenant de l'oxygène et de l'hydrogène, y compris les acides et bases solides, les sels acides et basiques, les hydrates cristallins ou les substances réagissant les uns avec les autres, libèrent de l'eau, possèdent une réactivité plus élevée que les substances anhydres. La dureté de ces composés est 3-4 fois inférieure à celle des oxydes anhydres qui permet de diminuer le niveau de charge mécanique et de passer à des conditions d'activation plus souples. L'influence de l'eau ou des groupes hydroxyle sur les réactions mécanochimiques a été étudiée de manière approfondie par plusieurs auteurs. Dans l'ensemble, les réactions mécanochimiques dans un certain nombre de cas se produisent plus rapidement dans les mélanges d'oxydes hydratés que dans les oxydes anhydres. C'est la raison pour laquelle, il est possible que dans le broyeur de mortier, $LiNaCO_3$ puisse être produit en utilisant $Na_2CO_3.H_2O$ comme réactif mais pas pour Na_2CO_3 anhydre. Cela pourrait être dû au fait que la présence d'hydrate rend la formation de $LiNaCO_3$ moins énergique que l'utilisation de composé anhydre comme réactif.

Les résultats expérimentaux ont confirmé que $LiNaCO_3$ peut également être produit à partir de la réaction mécanochimique du carbonate de lithium et du carbonate de sodium monohydrate selon:

$$Li_2CO_3 + Na_2CO_3.H_2O \rightarrow 2\ LiNaCO_3 + H_2O$$

Ces résultats d'expériences expliquent également la diminution de la teneur en eau dans la plage de spécification qui peut être obtenue si la composition du produit de départ contient de 7% massique d'eau d'hydratation (comme ce qui est mentionné sur le brevet). Si le fabricant a réduit la taille de grains de ses poudres par co broyage de Li_2CO_3 et Na_2CO_3, H_2O, il a involontairement formé du $LiNaCO_3$, diminuant en cela la teneur en eau de sa poudre. Cependant, il est également possible que le producteur n'ait pas soupçonné que le dégagement de la teneur en eau ait pu également provoquer la formation de $LiNaCO_3$. De plus, seule l'analyse de DRX est capable de détecter la présence de ce composé, ce qui n'est pas le cas de la méthode analytique utilisée pendant les années de production pour contrôler la qualité du produit.

La suite partie de l'étude est centrée sur la compréhension du comportement des poudres avec différentes compositions sur l'extinction des feux de sodium, notamment liée à l'effet du vieillissement sur la capacité d'extinction due à la présence de trôna et à l'influence de $LiNaCO_3$. Pour cela, un dispositif expérimental dédié pour cette étude, baptisé Chris(X)ti-Na (eXtinction Na), a été développé. Il se compose d'un dispositif d'épandage de poudre placé au-dessus d'un petit creuset de sodium chauffé avec une plaque chauffante et de dispositifs de mesure (contrôle de la température à des positions différentes et enregistrement vidéo). Cette installation permet d'étudier les phénomènes d'extinction des poudres en fonction de leur composition chimique, notamment dans la proportion maximum du trôna et $LiNaCO_3$, dans le but d'étudier le rôle de l'eau sous forme hydrate et la fusion de composant eutectique des carbonates. Les poudres synthétisées avec des compositions variables ont été préparées et testées sur le dispositif.

Dix grammes de sodium sont utilisés dans chaque expérience remplissant 19,6 cm^2 de surface. Deux méthodes d'épandage ont été étudiées à l'aide de deux dispositifs d'épandage de poudre: (a) le tamis vibrant et (b) le fond escamotable, pour deux modes d'épandage différents: continu et direct. Les tamis vibrants permettent d'étaler la poudre en continu, ce qui permet d'observer l'influence des propriétés chimiques de manière plus lente et plus proche à la réalité. Par contre le fond escamotable permet à la poudre de se répandre une fois de façon directe dans laquelle on maintiendra la même quantité de poudre (5 g) à chaque essai, ce qui permet de comparer l'efficacité des poudres indépendamment de l'influence de granulométrie des poudres. Les analyses DRX du résidu d'extinction ont été réalisées. La séquence des expériences a été enregistrée par une caméra vidéo. Les personnels d'essai étaient protégés par des combinaisons Nomex ©, des gants résistants au feu et des masques de protection complets.

Quatre groupes d'études de composition de poudre sont choisis:

- *Le rôle de l'eau d'hydratation*
  Il est étudié en fonction des différentes proportions contenues dans les composants purs. Le carbonate de sodium anhydre, le sodium carbonate monohydrate et le trôna ont été choisis avec 0%mas., 13,2%mas. et 18,1%mas. de teneur en eau d'hydratation respectivement. L'effet de la décomposition (déshydratation) du carbonate de sodium monohydrate et trôna à une température relativement basse suivie par la fusion à température élevée du carbonate de sodium anhydre pendant l'extinction est étudiée.

- *Le rôle du mélange eutectique avec et sans eau d'hydratation dans le carbonate de sodium*.
  La composition de la Marcalina telle que présentée dans le brevet est adoptée. Par conséquent, cela représente respectivement 7%mas. et 0%mas. de teneur en eau d'hydratation. L'effet de la décomposition (déshydratation) de la poudre et sa fusion à une température relativement basse à l'extinction est observée.

- *L'impact de la teneur en eau d'hydratation supérieure, inferieur et dans la plage de spécification recommandée par CACI*.
  La présence de trona avec et sans $LiNaCO_3$ dans le mélange est comparée en considérant qu'elle influencera la teneur en eau d'hydratation, à 5,6%mas. et 8,9%mas. respectivement.

- *L'influence de $LiNaCO_3$ pour l'extinction*
  Cet examen est mené afin de comprendre la nécessité de son existence dans le mélange. Son intérêt est douteux, car $LiNaCO_3$ est un composé qui fond à 500,6° C, tandis que les carbonates de sodium et de lithium forment un eutectique à 498 ° C, dont la fusion peut être obtenue s'ils sont suffisamment mélangés. Pour cette raison, le $LiNaCO_3$ pur a été mélangé avec 9% de graphite. En outre, sa présence dans le mélange de Marcalina est étudiée avec 2,9w% d'eau d'hydratation. Cette étude est essentielle pour expliquer si elle pourrait améliorer sensiblement la qualité d'extinction ou si elle ne contribuera qu'à la réduction de

la teneur en eau d'hydratation (dans le cas d'une production involontaire, ou non, pendant le broyage).

La comparaison des profils de température pour différentes teneurs en eau en épandage continu a montré qu'avecdes poudres ayant une teneur en eau d'hydratation plus élevée, une élévation de température était observée avant une extinction relativement rapide. Il semble que cette tendance soit observée dans la plage de 5,6 à 18,1% d'eau d'hydratation. Cette diminution rapide de la température montre le rôle précieux de l'eau d'hydratation en termes de capacité d'extinction rapide contrairement à celle avec une teneur en eau d'hydratation inférieure ou même nulle. En fait, 0,5 à 0,9 g d'eau est nécessaire pour éteindre un feu de sodium en nappe de 19,6 cm^2, soit en moyenne 0,036 g d'eau/cm^2. Cela implique que 1 à 2 g de NaOH (équivalant à 0,3-0,6 mm de hauteur de NaOH pour 19,6 cm^2) est réellement nécessaire pour couvrir complètement la surface de sodium. Cette valeur correspond approximativement à la valeur présentée dans la thèse de M. Reuillon, à l'origine de la fabrication de la poudre Marcalina.

Bien qu'il y ait évidemment une légère élévation de température due à la réaction exothermique de Na-H_2O en surface, la diminution de température due à la formation de NaOH liquide est plus importante pour assurer la séparation de Na et O_2, qui est le rôle clé dans les performances d'extinction. Une teneur en eau d'hydratation insuffisante semble être seulement capable de fournir un effet d'étouffement lent du feu avec la formation d'une couche poreuse qui favorise les ré-inflammations. Ces poudres sont encore en mesure d'éteindre un feu, mais cela peut prendre un temps beaucoup plus long et quantité plus élevée de sorte que leur efficacité est considérée comme moindre.

La teneur en eau minimale, qui correspond à une poudre encore efficace dans l'extinction d'un feu, est de 5,6%, c'est-à-dire la limite supérieure des teneurs en eau recommandée par le producteur il y a plusieurs années. Cependant, les poudres qui sont près de 13w% de l'eau d'hydratation semblent plus susceptibles de produire une forte flamme vigoureuse avant l'extinction. Cette flamme est attribuée à l'hydrogène produit lors de la réaction de l'eau avec le sodium.

Il a été montré que la présence de trôna n'altérait pas la capacité d'extinction de la poudre. Il contribue à augmenter la teneur en eau d'hydratation, ce qui augmente la production de NaOH (et H_2) pendant l'extinction. Cependant, il convient de noter que la même quantité de NaOH peut être produite par une mas. similaire de trona et $Na_2CO_3.H_2O$. Sachant que la trona libère presque deux fois plus d'hydrogène, ceci rend sa présence moins intéressante que celle du carbonate de sodium monohydrate.

Dans le cas d'une température superficielle élevée du sodium (>550°C), $LiNaCO_3$ pourrait avoir plus de contribution en facilitant la fusion des carbonates (assurance de fusion par rapport à des poudres de carbonates de lithium et sodium plus ou moins bien mélangées). Néanmoins, sa fusion prend plus de temps que celle du NaOH. Il a une viscosité plus élevée que le NaOH, ce qui rend difficile pour lui de produire une couche liquide suffisamment homogène pour assurer une séparation totale du sodium et de l'oxygène. Et surtout, la couche de carbonates pendant le refroidissement est sensible à la fissuration à une température relativement élevée, exposant de nouveau la surface de sodium chaud à l'air, provoquant ainsi des ré-inflammations.

La taille des particules n'a apparemment pas d'influence majeure sur les performances d'extinction. Les tailles de particules plus grandes montrent réellement un temps d'extinction plus rapide. En fait, elle affecte notamment la performance d'épandage. Les particules plus petites semblent plus difficilement couvrir la surface de sodium de façon homogène.
Deux étapes de mécanismes d'extinction sont proposées qui incluent (1) la formation d'hydroxyde de sodium liquide et (2) la fusion de carbonates eutectiques. L'étape 1 peut se produire directement :

- par la réaction directe de trona et/ou $Na_2CO_3.H_2O$ avec $Na_{(g)}$ et/ou $Na_2O_{(s)}$
  $Na_2CO_3.NaHCO_3.2H_2O_{(s)} + 3\,Na_{(g)} \rightarrow 2\,Na_2CO_3 + 2\,NaOH_{(l)} + \frac{3}{2}H_{2(g)}$
  $Na_2CO_3.NaHCO_3.2H_2O_{(s)} + 3\,Na_2O_{(s)} \rightarrow 2\,Na_2CO_3 + 5\,NaOH_{(l)}$
  ou
  $Na_2CO_3.H_2O_{(s)} + Na_{(g)} \rightarrow Na_2CO_3 + NaOH_{(l)} + \frac{1}{2}H_{2(g)}$
  $Na_2CO_3.H_2O_{(s)} + Na_2O_{(s)} \rightarrow Na_2CO_3 + 2\,NaOH_{(l)}$

- indirectement par la réaction de décomposition de trona et $Na_2CO_3.H_2O$ avant la réaction de H_2O(g) libéré avec Na et Na_2O)
  $Na_2CO_3.NaHCO_3.2H_2O_{(s)} \rightarrow \frac{3}{2}Na_2CO_3 + \frac{5}{2}H_2O_{(l,g)} + \frac{1}{2}CO_{2(g)}$
  $\frac{5}{2}Na_{(g)} + \frac{5}{2}H_2O_{(g)} \rightarrow \frac{5}{2}NaOH_{(l)} + \frac{5}{4}H_{2(g)}$
  $\frac{5}{2}Na_2O_{(s)} + \frac{5}{2}H_2O_{(g)} \rightarrow 5NaOH_{(l)}$
  ou
  $Na_2CO_3.H_2O_{(s)} \rightarrow Na_2CO_3 + H_2O_{(g)}$
  $Na_{(g)} + H_2O_{(g)} \rightarrow NaOH_{(l)} + \frac{1}{2}H_{2(g)}$
  $Na_2O_{(s)} + H_2O_{(g)} \rightarrow 2NaOH_{(l)}$

Cependant, comme les deux réactions se produisent très rapidement pendant l'extinction, elles sont difficiles à distinguer dans nos expériences.

Les résultats de cette étude démontrent l'effet bénéfique de l'eau d'hydratation qui joue un rôle majeur sur l'extinction, bien plus que le mélange de carbonate eutectique. Cependant, il est possible que les réactions exothermiques et la formation d'hydrogène induites par la réaction de l'eau avec l'oxyde de sodium ou de sodium puissent être un problème, en particulier si la flamme d'hydrogène peut nuire à la personne pendant l'intervention. Par conséquent, il est d'abord nécessaire de confirmer la présence d'une telle flamme en utilisant une mesure technique appropriée. Les technologies de détection comprennent des détecteurs de flammes qui détectent le spectre non visible des rayonnements électromagnétiques, tels que les rayonnements ultraviolets (UV) et infrarouges (IR). En outre, l'effet de cette flamme devrait être étudié à une échelle beaucoup plus grande. Ceci est important pour savoir si les phénomènes observés dans les expériences à petite échelle menées dans l'installation expérimentale de Chris(X)ti-Na sont reproductibles à d'autres échelles. Une plus grande quantité de sodium devrait être utilisée et ainsi, des quantités plus importantes de poudre seraient employées. Les résultats de ces tests seront précieux pour évaluer la spécification de la poudre liée à la teneur en eau d'hydratation et quelle sera la limite de tolérance de trona pour un emploi efficace. Cette information sera utilisée pour déterminer si les poudres actuellement en stock peuvent être réutilisées ou si une nouvelle poudre avec un seuil différent en eau d'hydratation doit être développé. Par ailleurs, il serait intéressant d'étudier l'emploi de ces poudres sur les feux en nappe de sodium à des températures basses (environ 300°C) et à des températures beaucoup plus élevées (au-dessus de 500°C), car cela confirmerait le rôle bénéfique ou non de $LiNaCO_3$ pour l'extinction à des températures plus élevées.

Le rôle des propriétés physiques semble être significatif lors de l'épandage de la poudre. Une quantité différente de teneur en eau d'hydratation peut affecter la taille des particules. De plus, le phénomène observé au cours de l'essai lié à l'agglomération et à l'homogénéisation pourrait affecter la performance d'épandage. Ainsi, les effets des compositions chimiques sur la performance d'étalement doivent être étudiés. Des poudres ayant différentes compositions chimiques peuvent être testées dans différents dispositifs d'épandage. Les effets liés à

l'évolution de la composition due à différentes manipulations de poudres telles que le transport et la fluidisation sont nécessaires pour garantir la qualité de la poudre utilisée ou si un nouveau procédé ou méthode de diffusion doit être développé dans le futur.

La fabrication de nouvelles poudres pourrait être envisagée. Le processus de broyage joue un rôle important dans la production de poudres avec une bonne homogénéisation. Selon les résultats des études d'extinction à plus grande échelle et d'épandage avec différents dispositifs, une nouvelle gamme de tailles de particules pourrait être proposée. Les résultats des tests d'extinction sur les feux à grande échelle peuvent donner l'information de la nécessité d'avoir $LiNaCO_3$ dans la poudre. D'après les résultats de cette thèse, on a trouvé que ce composé était bénéfique dans certains tests lorsque la teneur en eau d'hydratation était faible (5,6%mas.). S'il est prouvé qu'il apporte un effet substantiel sur l'efficacité d'extinction à grande échelle, sa formation doit être étudiée en utilisant différents types de broyeurs et de procédures (liées à la durée du broyage, de l'atmosphère) pour contrôler sa formation. Le test d'épandage peut donner l'indication sur la gamme de tailles de particules qui pourraient être utilisées pour améliorer sa performance. Cette valeur contribue également à déterminer une méthode de broyage adéquate pendant le procédé de fabrication. Il faut garder à l'esprit que la production de $LiNaCO_3$ par une réaction mécanochimique peut réduire la teneur en eau de la poudre, de sorte que la composition peut être ajustée pour fournir la teneur finale en eau cible dans la poudre.

En ce qui concerne les conditions de stockage, il serait intéressant de conserver les poudres dans des récipients étanches et de contrôler régulièrement les conditions d'humidité <50% HR. Concernant l'emballage, il est recommandé de choisir un emballage (ex: plastique) imperméable au CO_2. Ces conditions pourraient limiter non seulement la transformation chimique en trona, mais aussi la décomposition de $LiNaCO_3$ (s'il s'avère être un composé intéressant pour l'extinction à grande échelle).

Afin d'anticiper l'absorption d'eau qui pourrait se produire pendant la manipulation de la poudre et le stockage, il est suggéré d'avoir les compositions de poudre initiales avec une teneur en eau d'hydratation comprise entre 5,6 et 7%mas. du mélange de carbonate sodium monohydrate, carbonate de lithium et graphite. 5,6%mas. est la limite minimale, car la poudre avec moins d'eau est considérée comme ayant une mauvaise performance pendant l'extinction, tandis que 7%mas. est la composition originale de Marcalina comme recommandé dans le brevet. Cependant, la détermination de cette fourchette est basée sur les résultats obtenus à partir de cette thèse qui doivent être confrontés en termes d'effet sur les feux à grande échelle et les phénomènes de manipulation du transport (agglomération, ...) lors de la manipulation des poudres.

Enfin, une approche de modélisation pourrait être élaborée sur la base des données préliminaires recueillies et discutées dans cette étude. Le transfert de masse et de chaleur pendant l'extinction est considéré comme intéressant à analyser afin d'avoir plus de compréhension en ce qui concerne le mécanisme d'extinction proposé. Plusieurs possibilités de réactions pouvant survenir pendant l'extinction peuvent être analysées afin d'estimer la quantité d'hydroxyde de sodium et d'hydrogène qui pourrait être produite pendant l'extinction.

INTRODUCTION

As the population growth is expected to keep expanding throughout the following years, the energy demand will continuously increase. With 437 power reactors currently operating in 31 countries, having a combined capacity of over 380 GWe and producing 16% of the world's electricity, nuclear is one of the major energy sources available nowadays. In order to enhance the future role of nuclear, the innovative nuclear energy system known as Generation IV is proposed. Unlike its predecessors, this generation comprises the nuclear reactor and its energy conversion systems, as well as the necessary facilities for the entire fuel cycle from ore extraction to final waste disposal. It is supposed to be a highly economical reactor with enhanced safety, minimal waste, and resistant to proliferation. Ten countries, including France, have joined together to form the Generation IV International Forum (GIF). The goal is to have different Gen IV systems available for international deployment in 2030 [1].

Sodium cooled Fast Reactors (SFR) is one of the six systems selected by the GIF where France has brought a major contribution to development, relying on its large experience [2]. It features a fast-neutron spectrum and a closed fuel cycle for efficient conversion of fertile uranium and management of actinides. It can consume more than 80% of uranium resources and burn the minor actinides while producing electricity. Thus, it participates to the reduction of the ultimate radioactive waste quantity and lifetime [3]. Figure 1 shows the operating principle of an integrated type SFR where sodium is used as a coolant in the primary and secondary circuit. The unpressurized core primary system (sodium core outlet temperatures are 530-550°C) is integrated into the main vessel containing the intermediate heat exchangers and the primary pumps, whereas the secondary sodium acts as a barrier between the primary sodium and the energy conversion system.

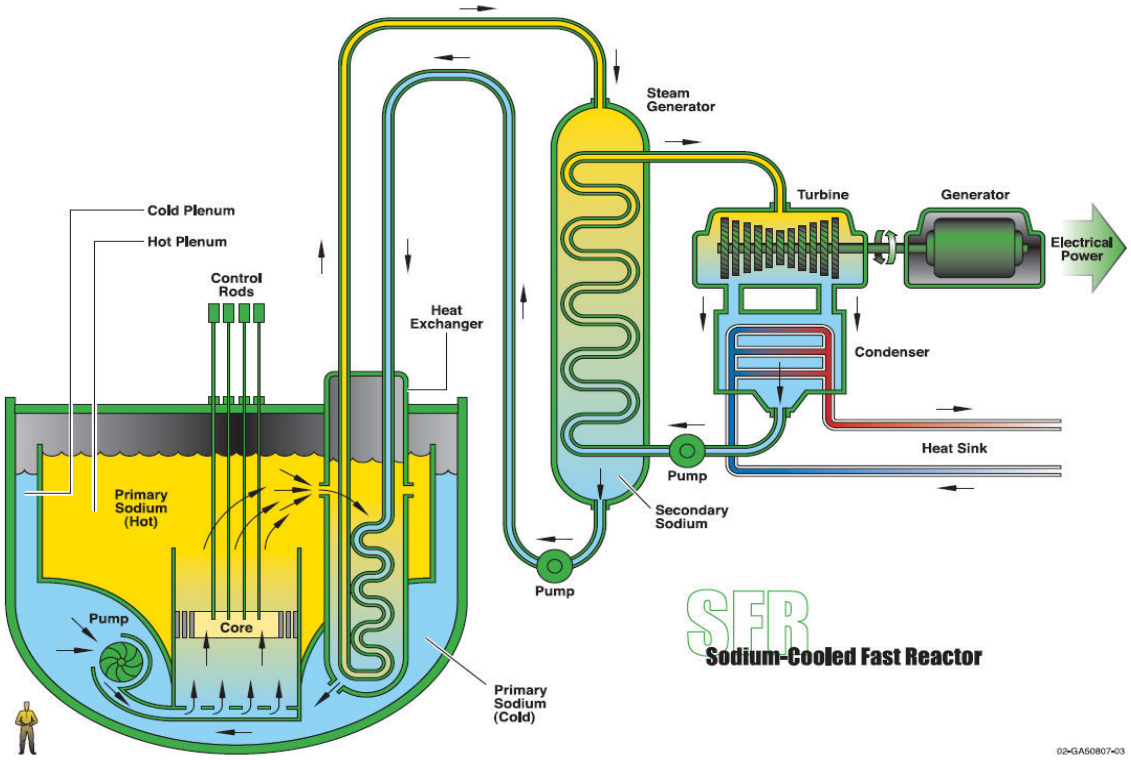

Figure 1. The schematic diagram of SFR operating system [1]

This thesis is carried out within the framework of nuclear 4th generation future reactor prototype, named ASTRID (Advanced Sodium Technological Reactor for Industrial Demonstration), currently under research and development phase at the CEA (Commissariat à l'Energie Atomique et aux énergies alternatives). It is pursued as a part of safety study of the SFR, particularly related to the extinction of sodium fire in case of sodium release. Indeed, the sodium has attractive physical characteristics that make it suitable to be used as a coolant. This includes a large temperature range in the liquid state, allowing its utilization at normal atmospheric pressure, an excellent thermal conductivity (100 times higher than water) and a low activation under neutron flux. It is compatible with stainless steels. At 400°C, its viscosity and density equivalent of the ones of water at 20°C make it possible to perform the hydraulic simulations using water as a model. The low vapor pressure in the normal operating conditions produced very limited amounts of aerosols. It also conveys very well the sound waves, ultrasound, and electricity as well as having paramagnetic properties, which can be used in sensors. Furthermore, sodium is the most common alkali metals. It ranks sixth as the most abundant element on the earth's crust at its natural state, which exists only in the form of sodium ion (Na^+) notably in the form of ocean salts (sodium chloride, sodium bromide, sodium iodide). For the nuclear industry, the "refined sodium" or "nuclear quality sodium" is used with a calcium concentration of <2 ppm in order to avoid the activation of impurities [4].

However it should be underlined that sodium is a very strong reductant. Its opacity and its significant chemical reactivity with water and air are its major drawbacks [3]. The exothermic reaction, producing soda and hydrogen, is the results of its strong chemical reactivity when in contact with water. Consequently, an intermediary sodium circuit is generally located between the primary sodium and the water vapor generator. In addition, it spontaneously ignites upon contact with air or oxygen above 130°C. Thus, all the circuits need to be operated under inert atmosphere. A leak detection system is also necessary to be able to prevent and to limit the consequences of a sodium fire after sodium release [4]. Four major accidents due to the sodium-air reaction in the world includes [5]:

- The Ilona test facility encountered a sodium leak (110°C < T Na < 140°C) that resulted in sodium fire of 4500 kg of sodium and significant sodium-concrete interactions (Germany, 1992);
- A design defect during startup produced a slow sodium leak (0.04 $kg.s^{-1}$) and caused a sodium pool fire in the Monju prototype fast breeder reactor (Japan, 1994). The design was then improved and a new monitoring system was then adopted to enhance the prevention;
- Numerous sodium fires occurred in the early years of reactor BN-600 operation (Russia, 1993) due to pipe and weld cracking ;
- Almeria solar plant facility experienced a large sodium spray fire (Spain, 1986) during a routine maintenance event. Powder Graphex CK23 was not capable of extinguishing the fire. At this plant, sodium was used as a mean to store and transport heat to power conversion components of the plant. Prior to the accident, the plant had been shut down to repair a leaking sodium valve.

As for France, several sodium leaks, which might lead to sodium-air reactions, were encountered in all three SFRs [6]: small sodium leaks were detected at the end of 1978 causing the reduction of RAPSODIE's operational capacity to about 22 MWh followed by another small leak in the nitrogen system, which ended up on the shutdown decision on October 1982 ; the first real sodium fire occurred in the PHENIX plant on October 1976, nevertheless the fire could be successfully extinguished manually ; during the operational period of SUPERPHENIX, a small sodium leak from the main fuel storage tank was detected on April 1987 and led to a 10 month shutdown. Hence, each of these incidents demonstrates the urgency of implementing a sodium leak detection system to prevent the sodium fire for the next generation of SFR. More importantly, a system capable of achieving a rapid extinction in case of sodium fire is ultimately required.

Many researches have proposed various methods of extinction, either by passive devices such as leak collection trays [5,6,7] or by active means like extinguishing powders. In 1978, CEA developed an extinguishing powder, known as Marcalina, which was proven to be very effective in suppressing a sodium fire due to its efficiency (low amount of deposited powder) of achieving fire suppression both at low and high sodium temperatures. It is composed mainly of lithium carbonate and low-hydrated sodium carbonate in a near eutectic proportion, of which melting temperature is around 500°C, associated with graphite [10]. It has been produced between the early 1980s to the late 1990s by CACI, a company that ceased its production nowadays. Sodium fire became no longer a risk following the terminated exploitation of sodium in several facilities. CEA has then, at its disposal, an abundant stock of unused powder batches, some of which are being conserved in an unadapted manner ever since the dismantling of the facilities. Hence, the reutilization of these powders initiates the questions about their efficiency to extinguish a sodium fire after long term storage.

The objective of this thesis is to study, on one hand, the effect of physicochemical phenomenon that might influence the storage and production methods. On the other hand, it aims to examine the physicochemical reaction impact towards the extinction capacity. As a matter of perspective, these informations will be helpful in:

- The understanding of powder behavior during storage (powder aging).
  It is important to recognize the evolution of physical and chemical properties of the powder over time so that the ideal storage condition (to prevent the evolution) could be determined. This result also contributes to the powder handling (e.g. transportation).
- The insight of the production method.
  Due to the cease of powder production, nowadays there is no longer commercial extinguishing powder for sodium fire with the same quality and efficiency than Marcalina®. Thus, it would be a great interest to be able to re-manufacture it.
- The comprehension of the role of extinguishing properties.
  This is the key information to understand the role of each component on the extinction. It is a valuable knowledge to determine their specification in order to maintain and/or even optimize their performance.

This thesis aims at addressing the points raised above and is divided into five parts: *First*, the theoretical background related to the liquid metal fire, particularly sodium, which includes the ignition, combustion, until extinction. *Second*, the experimental materials and methods used for the physicochemical characterization of the powder as well as the experimental device that has been specifically developed to understand the role of the extinguishing properties. *Third*, the effect of aging towards the physicochemical properties of the powder and also the influence of grinding process included in the fabrication on their physicochemical characteristics. *Fourth*, the impact of the evolution of physicochemical properties during the storage and fabrication on the extinction performance. *Finally*, the conclusion and perspectives of study.

BIBLIOGRAPHY OF INTRODUCTION

[1] U.S. DOE Nuclear Energy Research Advisory Committee and the Generation IV International Forum, *A technology roadmap for generation IV nuclear energy systems*. 2002.

[2] CEA, "4th-Generation sodium cooled fast reactors: The ASTRID technological demonstrator." Dec-2012.

[3] Gauché F, "ASTRID, Generation IV advanced sodium technological reactor for industrial demonstration," *Clefs CEA: Low carbon energies*, no. 61, pp. 26–28, Sep-2013.

[4] G. Rodriguez, "Le caloporteur sodium." Techniques de l'Ingénieur, 01-Oct-2004.

[5] Olivier T.J. , Radel R.F, Nowlen S.P, Blanchat T.K, & Hewson J.C, "Metal Fire Implications for Advanced Reactors, Part 1: Literature Review," Sandia National Laboratories., SAND2007-6332, Oct. 2007.

[6] M. Schneider, "Fast breeder reactors in France," *Sci. Glob. Secur.*, vol. 17, pp. 36–53, 2009.

[7] F. Huber, P. Menzenhauer, and W. Peppler, "Investigation of sodium area conflagrations and testing of a protective system," *Nucl. Eng. Des.*, vol. 35, no. 1, pp. 155–162, 1975.

[8] S. V. Diwakar, T. Sundararajan, S. K. Das, P. M. Rao, and N. Kasinathan, "Development of mathematical model for optimization of sodium leak collection tray," *Nucl. Eng. Des.*, vol. 238, no. 10, pp. 2684–2692, Oct. 2008.

[9] S. V. Diwakar, P. Mangarjuna Rao, N. Kasinathan, S. K. Das, and T. Sundararajan, "Numerical prediction of fire extinguishment characteristics of sodium leak collection tray in a fast breeder reactor," *Nucl. Eng. Des.*, vol. 241, no. 12, pp. 5189–5202, Dec. 2011.

[10] Reuillon M. , Mellottee H. , Devillers B. , Alfille L.,Duco J. , Fruchard Y. , Malet J.C. , et Chappellier A., "Procédé et poudre pour l'extinction des feux de métaux liquides," 75 36225, 03-Mar-1978.

Table of Contents

List of Figures

List of Tables

CHAPTER I
State of the art: Literature review on the sodium fire and the extinguishing powders

As briefly described in the introduction, several sodium leaks might lead to sodium-air reactions, thus provoking a sodium fire. Indeed, a sodium fire cannot be excluded in the accident scenario of SFR. Therefore a review of the nature of sodium fires and advanced study concerning their extinction is likely inevitable. This chapter is dedicated particularly to the comprehension of the nature of sodium fire from the ignition, combustion, until extinction. 3 types of sodium fires will be briefly introduced and then the discussion around sodium pool fire will be more emphasized. The overview of the extinction mechanisms will be developed, although the active method of extinction by an extinguishing powder would be the ultimate information. The comparison of several commercial extinguishing powders will be presented especially for the benefit of the powder developed by the CEA. The literature information about the physicochemical characteristics of this powder will be the base of study for the next chapters. Finally, the grinding and mixing process are introduced to give the brief insights for general fabrication method of powder.

1.1 Literature review of sodium fire

As classified as class D fires, designated for combustible metals, sodium fires have particular characteristics. There are three types of sodium fires [1]:

- **Spray/pulverized fire** happens when the sodium is finely divided in air (spontaneous combustion) when it is ejected under pressure and burns in the form of droplets or when the sodium jet impacts an obstacle (e.g. grid, wall…), or when the reaction sodium – concrete reaction happened. In this case, the kinetics of combustion is much faster. The energy released brutally causes more severe consequences on the buildings. The only way to prevent this type of fire is based on the conception of the plant.
- **Pool fire** happens when the sodium mass is not finely divided (low heat, short flames) and it occurs when the metal is spread over a floor area. This thesis will concentrate on this type of fire. It happens in case of a low-pressure sodium leak. A sodium pool ignites at a temperature around 125^0C. For combustion to occur, the premises moisture must be between 30-70% and the oxygen concentration higher than 3% [1]. It should be noted that this is a self-extinguishing fire from lack of oxygen. The prevention of this type of fire is based on the employment of leak collection trays (passive device) and extinguishing powders (active device).
- **Mixed fire** when both pool and spray fires occurs at the same time. They correspond to a sodium flows that smashed an obstacle. The kinetics and thermal effects will relate to the two previous configurations.

Sodium inflames at low temperatures, a value depending on the geometry, and for oxygen concentrations higher than 3%. A drop of sodium starts to burn at 125°C and a heated pool kindles at around 200°C. The flame temperature is noted to be at 1350°C where monoxide and peroxide of sodium are the combustion products. The room humidity reacts with sodium peroxide producing the toxic sodium hydroxide. The 40% weight of burnt sodium is present in the form of smoky white aerosol, which causes a really low visibility in the room [1]. Another feature of sodium fire is that it forms an oxide blanket on the surface at relatively low temperature, i.e. below 400-450°C, which somewhat protects the metal in contact with air and

consequently delays the ignition. However at higher temperatures, this oxide layer flows and dissolves within the liquid metal, thus liberating the surface thereof. Therefore it will be neglected in future discussion. Furthermore, due to its high thermal conductivity, the whole mass of sodium reaches high temperatures during the fires. This is not the case for other fuels, like hydrocarbons, for which only the sole blazing surface of which have a relatively high temperature. Moreover, this temperature is considerably superior to the auto-ignition temperature. Hence, the metallic surface needs to be isolated from the ambient atmosphere in order to stop the combustion [2].

This part will discuss the theoretical background of sodium fire that consists of three main aspects: *firstly*, the study of flammability limits allowing the sodium users to know the conditions from which the sodium ignites; *secondly*, the study of combustion in order to define the thermodynamic effects of such fire; and *finally*, the study of the suitable separation method of fuel (sodium) and oxidant (oxygen) capable of achieving the extinction.

1.1.1 The ignition of sodium

A. Theories related to the ignition

As most metal fires, sodium ignition is preceded by a reaction occurring at the surface of the metal. It corresponds to the formation of a superficial oxide layer, the protective or porous nature of which will determine the beginning of ignition. The oxidation happens slowly at the beginning (pre-ignition phase). As the heat source brings enough energy to the system, the reaction rate increases rapidly. Like many chemical reactions, the oxidation rate (r) of metals obeys an Arrhenius law [3]:

$$r = A \exp\left(-\frac{E_a}{RT}\right) \quad (1\text{-}1)$$

where A is the pre-exponential factor of the reaction rate ; E_a is the activation energy ; R is the universal gas constant; T is temperature.

The evolution of the oxidation rate according to the temperature, determined experimentally, corresponds to the general expression [4]:

$$\frac{da}{dt} = \frac{k_n}{a^{n-1}} \quad (1\text{-}2)$$

with a = mass of oxygen consumed per unit area ; k_n = the rate constant ; and n = the exponent of oxidation law.

- At low temperatures, the reaction between the metal and oxygen is located in the oxide film surface. The oxidation process is characterized by interstitial diffusion of metal atoms within the oxide film. The oxidation kinetic law of metal is exponential (n = 0):

  $$\log a = k_0 t + c_0 \quad (1\text{-}3)$$

- As the temperature increases, the gas diffuses to the metal. In this case, the oxide formed is more porous, yet still considered as protective due to no subsequent ignition. This oxygen consumption is mathematically expressed as the parabolic oxidation kinetics law (n = 2):

$$a^2 = k_2 t + c_2 \quad (1\text{-}4)$$

- For higher temperatures, the oxidation is characterized by a direct action of the oxygen to form a porous oxide. The scheme of the reaction corresponds to a law where the consumption of oxygen is linear with time (n = 1):

$$a_1 = k_1 t + c_1 \quad (1\text{-}5)$$

In fact, the ignition process depends on the quality of the oxide layer formed during the oxidation period. This means that the temperature is sufficiently high for breaking the metal protective layer. The influence of the surface temperature on the characteristics of the oxidation of a metal is therefore undeniable.

The ignition is triggered by a localized heating on the metal surface, which will effectively speed up the exothermic oxidation reaction. Two mechanisms of ignition are proposed by Mellor and Reynold:

1) Mellor's ignition theory [4]

In the case of metal-oxygen reaction without formation of a condensed phase, the variation of energy released by the chemical reaction $\dot{q}_c$ and losses by conduction and radiation $\dot{q}_p$ depend on the surface temperature T_s represented in figure 2.

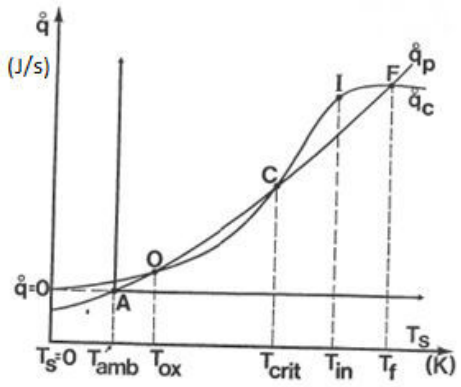

Figure 1-1. The ignition curve of metal ($\boldsymbol{T_{amb}}$ = ambient temperature, $\boldsymbol{T_{ox}}$ = metal oxide temperature, $\boldsymbol{T_{crit}}$ = critical temperature, $\boldsymbol{T_{in}}$ = ignition temperature and $\boldsymbol{T_f}$ = flame temperature) [4]

The evolution of $\dot{q}_c$ with T_s is slow at the beginning, then fast (the curve passes through an inflection point C) and again slow. It represents the evolution of an initial slow oxidation reaction, which accelerates until the ignition, and then slowly reaches a limit when the reactants are consumed. The shape of this curve could be explained as $\dot{q}_c$ is a function of Arrhenius term. On the contrary, the energy released in all range of temperature studied, symbolized by $\dot{q}_p$, is an increasing function of the temperature.

Three particular points, of which gain and loss are equal (point O, C, and F) can be distinguished on the graph. Only points corresponding to T_{ox} et $T_f$temperatures are stables. At the unstable equilibrium point T_{crit}, a slight increase in temperature provokes an increase of heat production which quickly brings the system to the stable point T_f. In the case of a slight decrease in temperature, on the contrary, the system will cool down to the stable oxidation T_{ox} point of the

metal in solid phase. Furthermore, a change in the concentration of reactants results in a gain curve shift to the left (increase of reaction rate) or right (decrease of reaction rate), leading toward or away of T_{crit} and T_{ox} and therefore greater ease or difficulty of ignition at low temperature.

2) Reynolds' ignition theory [5]

Reynolds identified the sequential steps that lead to the ignition of the metals and deduced three phenomena that can limit ignition: oxygen transport to the surface, its incorporation to the surface (oxide), and the diffusion of ions in the oxide. In his model, he assumes that the diffusion is the limiting phenomenon. He studied the evolution of the surface temperature of a metal sample, using the energy equation as follows:

$$\frac{C}{S}\frac{dT_s}{dt} = \underbrace{\dot{q}_c}_{\text{heat released by reaction}} - \underbrace{h_c(T_s - T_g)}_{\text{energy loss by convection}} - \underbrace{\varepsilon\sigma\,(T_s^4 - T_r^4)}_{\text{energy loss by radiation}} \qquad (1\text{-}6)$$

Heat losses by conduction in the metal are neglected; all the metal is assumed to be at the same temperature. In this mathematical expression, the terms used have the following meanings:

$\dot{q}_c$ = heat flux released by the chemical reaction, occurs at the surface, J/sec.m^2
S = surface of the sample, m^2
C = overall heat capacity of the sample, J/K
h_c = heat transfer coefficient by convection, J/s. m^2.K
T_s = surface temperature, K
T_g = gas temperature, K
ε = the surface emissivity coefficient
σ = constant of Stefan-Boltzman, 57.6 x 10^{-9} J/m^2.s.K^4
T_r = the radiation effective temperature to the environment, K

This equation calculates the ignition temperature T_{in} according to the rate constant A and the activation energy E_a of the oxidation reaction $M_x + \frac{y}{2}O_2 \rightarrow M_xO_y$ where M is the metal and x, y are the stoichiometric coefficients of the reaction. Ignition occurs when the amount of heat released by the oxidation reaction exceeds the heat losses from the system. Mathematically, the ignition condition corresponds to:

$$\frac{d}{dT_s}\left(\frac{C}{S}\frac{dT_s}{dt}\right) = 0 \qquad (1\text{-}7)$$

$$\frac{d\dot{q}_c}{dT_s} - h_c - 4\,\varepsilon\,\sigma T_s^3 = 0 \qquad (1\text{-}8)$$

The flow released by the chemical reaction on the surface, if a linear kinetic law of oxidation is considered, can be put in the form:

$$\dot{q}_c = A\,\dot{Q}\,e^{-E/RT_s} \qquad (1\text{-}9)$$

where E = activation energy, A = frequency factor, Q = heat of reaction.

By substitution of equation (9) to (8) and for $T_s = T_{in}$, the ignition temperature T_{in} is then given by the relationship:

$$e^{-E/RT_{in}} = \frac{h_c R}{A\,Q\,E}\,T_{in}^2 + 4\,\frac{\varepsilon\,\sigma R}{A\,Q\,E}\,T_{in}^5 \qquad (1\text{-}10)$$

This equality is represented graphically by the intersection of the curves where the ignition temperature can then be identified (cf. figure 3):

$$e^{-E/RT_s} = \frac{h_c}{A\,Q\,E}\,R\,T_s^2 + 4\,\frac{\varepsilon\,\sigma}{A\,Q\,E}\,R\,T_s^5$$

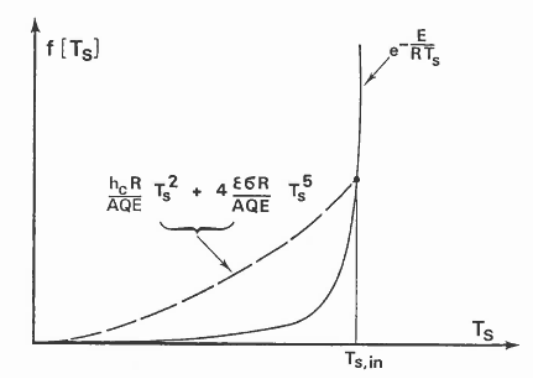

Figure 1-2. The determination of ignition temperature [4]

Taking the balance of energy absorbed (either linear or parabolic) and released (radiative and convective), the equation 10 is then reformulated into:

$$e^{-\frac{1}{T^*}} = \frac{(T^*)^5}{\eta^*} + (T^*)^2 \qquad (1\text{-}11)$$

with

$$T^* = \frac{T_{in}\,R}{E_a}\;;\;\eta^* = \frac{A\,Q}{4\,\sigma\,\varepsilon\,n}\left(\frac{R}{E_a}\right)^4\left(\frac{\gamma}{\delta\rho}\right)^{n-1}\;;\;h^* = \frac{h}{A\,Q}\frac{E_a}{R}\left(\frac{\delta\rho}{\gamma}\right)^{n-1}$$

The parameters γ, δ and ρ, represent, the coefficient of the oxide mass on the mass of oxygen required for its formation, the thickness of the initial oxide layer, and the density of the oxide respectively, allowing to take account of oxide characteristics in the calculation. It is valid for both linear growth ($n = 1$) and for a parabolic oxide growth ($n = 2$). By plotting $T^* = log\,\eta$, the calculation results give a fairly good agreement with the experimental results of Reynolds when the convection is ignored ($h^* = 0$).

B. Sodium ignition

Determining a sodium ignition temperature is difficult due to the multiplicity of the parameters this value is related to, such as the purity of the metal and the oxidizing gases, the process followed (the significant influence of the nature -protective or porous- of the oxide layer formed during the slow oxidation period). Theoretically, the ignition can occur whenever the transition temperature is exceeded. This latter is close to 150^{0}C according to Touzain [4].

1) Reaction with solid sodium

A piece of freshly cut sodium will react firstly with the molecules of water (moisture) contained in the air. Since sodium is highly reactive, it will capture the water vapor, thus the first observed reaction is a surface reaction between sodium and water in gaseous form. This sodium / water reaction provides hydrogen gas and sodium hydroxide (NaOH) more commonly known as soda. Although it is more stable than sodium, it is also a product which reacts with air and particularly in contact with the carbon dioxide present in the air to form sodium carbonates (Na_2CO_3 and / or $NaHCO_3$) afterwards. These carbonates are white solid crystals. This explains the color change of the sodium on the surface from gray to white. When this carbonate film is formed, it creates a real barrier between the sodium and the air humidity. Then the moisture has to diffuse through this carbonate film. These diffusion processes are very long and depend in particular on the thickness of the diffusion layer and moisture content. The evolution of the sodium-air reactions can be described by a sequence of steps presented in figure 1-3.

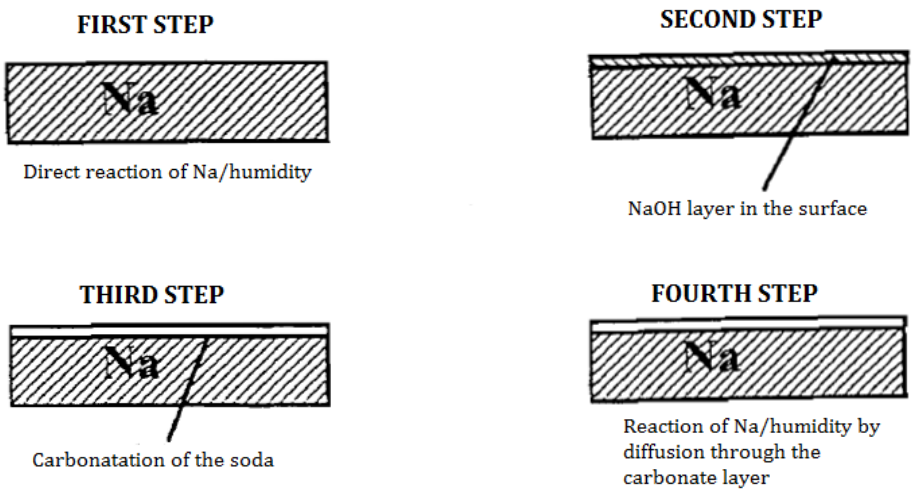

Figure1-3. Description of different stages of sodium-air reaction [6]

2) Reaction with liquid sodium

The most commonly determined experimental minimum ignition temperature of a pool sodium in the presence of air is about 215 ± 4⁰C [7]. According to Malet [7], at lower temperatures, like most metals, only a slow oxidation phenomenon that takes place. Just before ignition, in this case at 210⁰C, the oxidation law $a^n = k\,t$ is (c.f. figure 1-4):

- first mixed (n = 1.53), there is a superposition of a parabolic diffusion regime (n = 2) and a linear reaction regime (n = 1), the corresponding rate constant is found to be $k = 1{,}49.10^{-9}\ mol^{\frac{3}{2}}s^{-1}$,
- then linear ($n = 1, k = 8{,}7.10^{-8}\ mol.s^{-1}$) with disappearance of diffusion regime.

This slow oxidation period was also demonstrated at temperatures above ignition, as observed in the experiment of D. An et al. (cf. figure 7) [8]. This oxidation phenomenon is always preceded by the formation of nodules that takes place during the induction period, incorporated as an ignition delay.

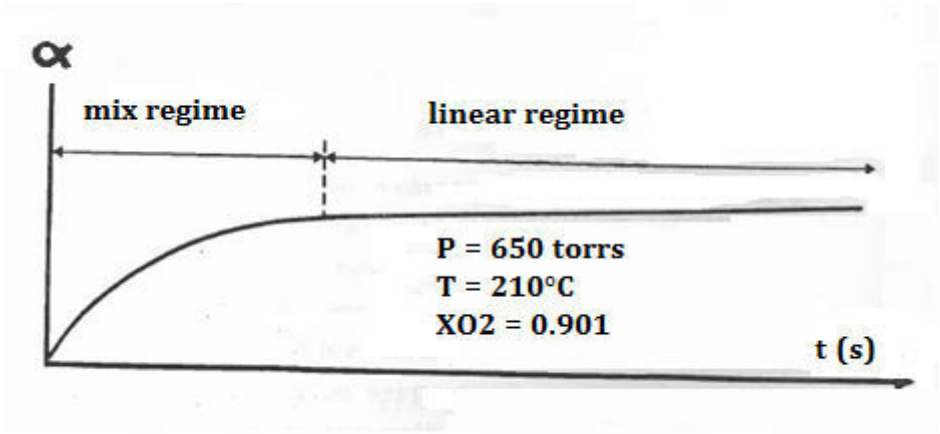

Figure 1-4. Slow oxidation under the ignition temperature [7]

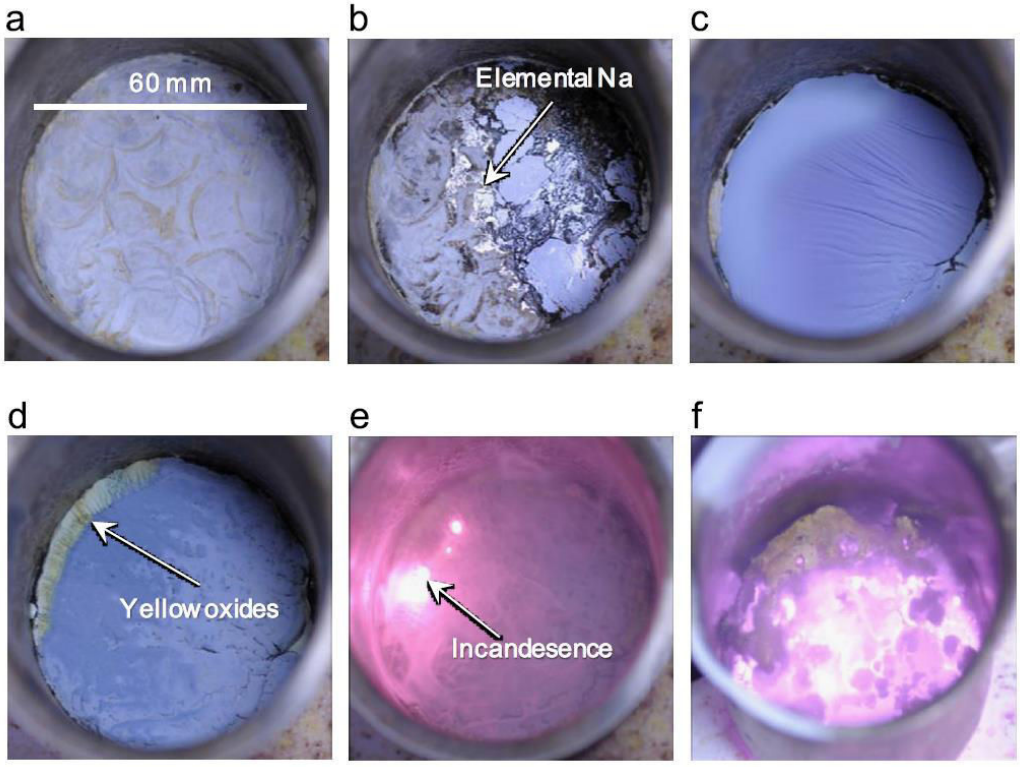

Figure 1-5. Images of 40 g sodium burned in a 250 ml beaker [8].
Time zero is the beginning of heating: (a) 100^{0}C, 6 min (apparition of Na_2O, Na_2O_2 and NaOH); (b) 285^{0}C, 17 min (nodulation → ignition at 290^{0}C) ; (c) 292^{0}C, 17.2 min (wrinkles appear when the oxide layer covers the surface) ; (d) 346^{0}C, 17,8 min (presence of Na_2O_2) ; (e) 385^{0}C, 17,8 min (vapor phase reaction as indicated by the light emission); (f) 443^{0}C, 29 min (combustion of pool sodium).

According to Malet [7], the nodules appear as spherules or needles. This phenomenon always precedes combustion and leads to the formation of a gray-blue mass. To the naked eye this mass may:

- either appear to be compact, in this case the final residue of combustion is very hard and formed below a total pressure (P_s),
- or have a granular structure which is friable and arborescent and formed above P_s.

The curve $\alpha = f\ (time)$ in the figure 1-6 shows an accelerated period corresponding to the nodulation. This period corresponds to a parabolic law of the form:

$$\alpha = Bt^2 \qquad (1\text{-}12)$$

wherein B is a nodulation factor. A parametric study performed by Malet [7] of this period also showed that it varied with the total pressure P of the system, the mole fraction of oxygen in the oxidizer XO_2 in the gas mixture and the initial temperature of sodium T_{Na}.

- If P varies (fixed XO_2 and T_{Na}): the delay is shorter when the pressure is getting higher. Below a certain pressure P_i, the nodulation will not lead to ignition and sodium will not burn.
- If XO_2 varies (fixed P and T_{Na}): the delay decreases according to an exponential law when the oxygen fraction increases.
- If T varies (fixed P and XO_2): the delay increases exponentially with the decrease of temperature.

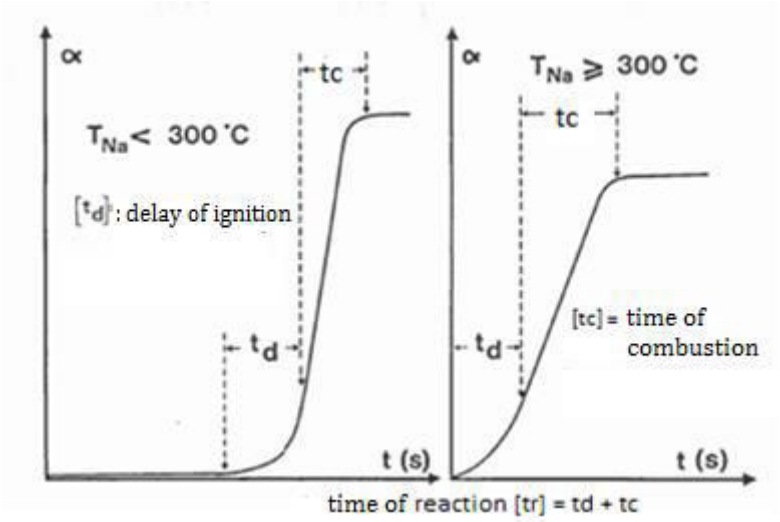

Figure 1-6. The rate (α) of the oxygen consummation over time [7]

Casselman [9] tried to understand the mechanism of nodules formation and ignition by performing a thermal mapping of the surface using an infrared camera. From these measurements, an interpretation of phenomena has been proposed. The preferential oxidation of certain particular lattice sites (non-uniformity of the thickness of the oxide layer) corresponds to an exothermic reaction, which provokes a local temperature increase at the metal surface. The nodule is identified as a metal droplet covered with an oxide film, as illustrated in figure 1-7, an experience where high saturated vapor pressure and temperature conditions favor the establishment of a strong reaction in vapor phase between sodium and oxygen, leading to ignition. Once the sodium ignites, a strong reaction period begins and oxygen consumption law exponent α becomes linear (right side of figure 1-6 that corresponds to the combustion time t_c).

The flammability limit expressed as a percentage of oxygen is relatively low, being between 0.01 and 0.03 mole fraction of oxygen. Table 1-1 below reports the ignition temperatures as a function of the molar fraction of oxygen.

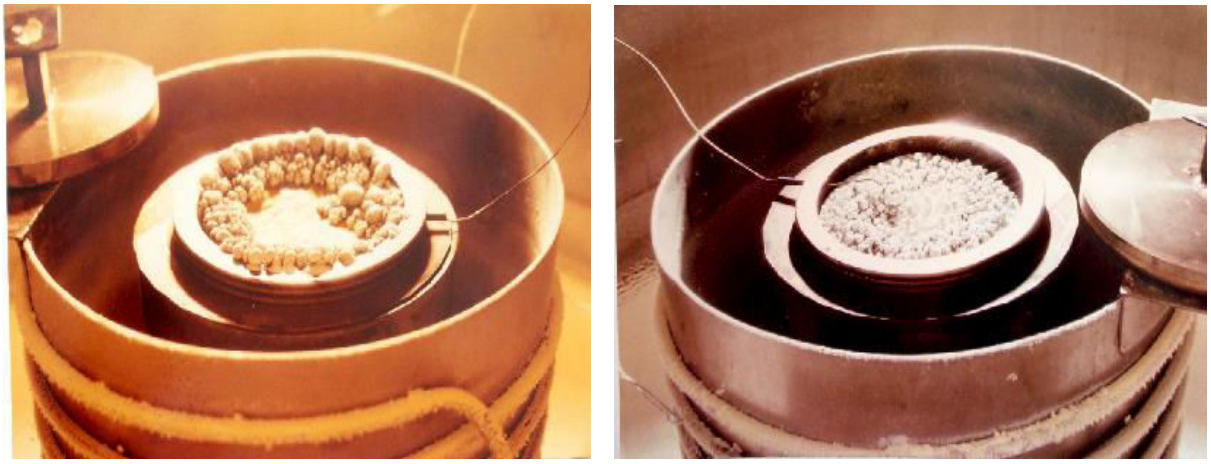

Figure 1-7. The nodulation without ignition at XO_2 = 0.05 : left T = 292°C and right T = 332°C [9]

Table 1-1. The ignition temperature as the function of oxygen molar fraction [10]

Molar fraction	0.050	0.075	0.100	0.150	0.21
Ignition temperature (^{0}C)	344	252	228	220	205

The ignition mechanism based on the oxygen concentration and temperature is shown schematically in figure 1-8.

The sodium ignition temperatures recorded in the literature (from 120^{0}C to 470^{0}C) are summarized in table 1-2. The different results are reported from different authors. It appears that sodium sample, in the presence of preheated fuel mixture, ignited at a higher temperature than the same sample heated under vacuum or inert atmosphere. It can be assumed that during the heating phase, the protective oxide layer formed from the lower temperatures is thick enough to slow down the ignition process. On the contrary, in the case of preheating in the absence of oxidizing gas, there is less amount of protective oxide. Therefore, the diffusion of oxygen to the metal is faster, which then causes an acceleration of the oxidation reaction and therefore results in a lower auto-ignition temperature.

The ignition temperature of an immobile sodium pool is also greater than for the agitated one. Indeed, agitations cause a disruption of the oxide film, the metal appears unprotected and hence allows a direct attack by oxygen, so that the ignition occurs at lower temperatures. The purity of the oxidant mixture is a parameter that also should not be forgotten. The high value of 320°C by Newman corresponds to a measurement performed under humid atmosphere in the presence of carbon dioxide. In this case, there is a formation of a sodium carbonate and sodium hydroxide layer at the surface of the pool that protects the metal until the melting of the latter is attained.

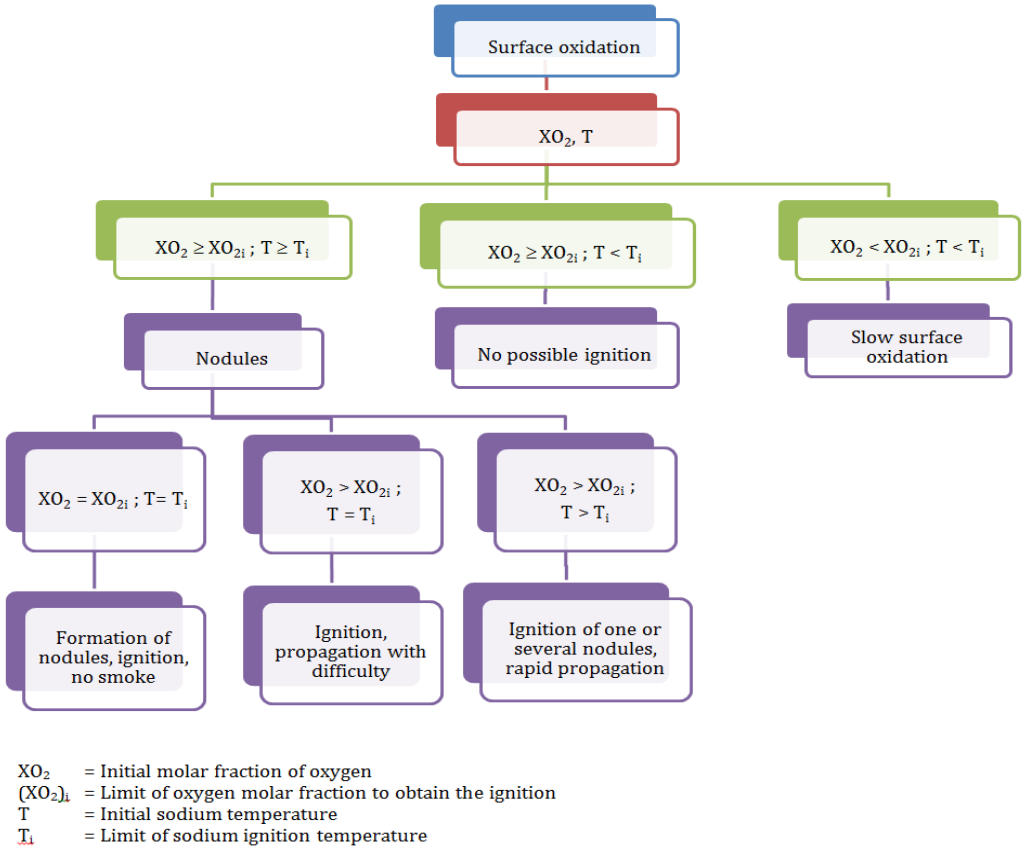

Figure 1-8. The mechanism of sodium ignition [11]

Table 1-2. Summary of sodium ignition temperatures [10]

Authors	Sodium ignition temperature			
	Droplets	**Agitated pool**	**Immobile pool**	**Preheated sodium with oxidizer**
MALET • Experimental • Theory			215°C 197-199-220°C	
REYNOLDS (Theory)			210°C	
LEMARCHAND-JACOB			209°C	
REUILLON			220°C	
GROSSE-CONWAY			118°C	
CORNEC-SANNIER			160°C	
LONGTON			260°C	
NEWMAN		150°C	320°C	
GRACIE-DROHER	120°C	204°C	288°C	
RICHARD	200°C			280°C
TOUZAIN			150°C	280°C
COWEN-VICKERS	133-138°C 120°C (pure Na)		260°C	440-470°C
CASSELMAN			205°C	

1.1.2 The combustion of sodium

A. Theories related to the combustion

The study of metal combustion is complex because it is the result of numerous chemical and physical processes (mass and heat transfers). The initiation of a combustion reaction is localized on the surface of metal (preliminary oxidation period). If the reaction rate is accelerated up to a certain critical value, the heat generated by the oxidation can cause ignition of the metal (earlier phase discussed above) and lead to combustion either in the vapor phase or on the surface metal. It is therefore possible to describe the combustion steps of metal.

Glassman [3] proposed general remarks related to the metal combustion, previously investigated by Grosse and Conway, based on thermodynamic and physical properties of metals and their oxides, as well as available data on chemical reactions involved in combustion:

- The combustion temperature is limited by the boiling point of the formed metal oxide.
- If the oxide boiling point is higher than that of the metal, the combustion occurs in the gas phase; if it is smaller, the combustion occurs on the surface.
- The radiative losses are likely to play an important role in metal combustion.
- The phenomenon driving the ignition can be completely different from the one driving the combustion in stationary regime.

In reality, gaseous phase combustion not only depends on the boiling point of the oxide. It may be prevented by the formation of a protective oxide layer, the decrease of temperature by heat losses, or both combined. Brzutowski and Glassman [3], then, proposed to include the thermal and radiative losses in the above criteria:

- If the losses are such that the oxide remains in the solid phase, the combustion is limited by diffusion through the latter, and the combustion rate will slightly increase.
- If the losses allow the oxide to melt, the burning rate will be limited by diffusion through the liquid oxide layer but the oxide layer will thicken more or less depending on temperature.
- If the liquid oxide dissociates, the reaction will be limited only by the rate of dissociation reaction and the removal of the oxide.

Markstein [4][12] established a classification of combustion methods, depending on the value of the reaction temperature T_r, the metal boiling temperature T_m, and the oxide boiling temperature T_o, and concluded the following three possibilities (c.f. figure 1-9):

- $T_r < T_m$ and T_o : slow oxidation (previously described in 1.1.1). An oxide layer is formed on the surface of the metal. If the oxide is porous, oxygen goes to metal. If it is protective, oxygen stops at the surface.
- $T_r \cong T_o < T_m$ (oxide is more volatile than metal): combustion the surface. It is a heterogeneous reaction.
- $T_m < T_r < T_o$ (metal is more volatile than oxide): combustion in the vapor phase. The reaction is homogeneous and produces less volatile oxides whose formation may easily happened outside of the flame zone (the flame temperature is considered to be the same as the oxide boiling temperature).

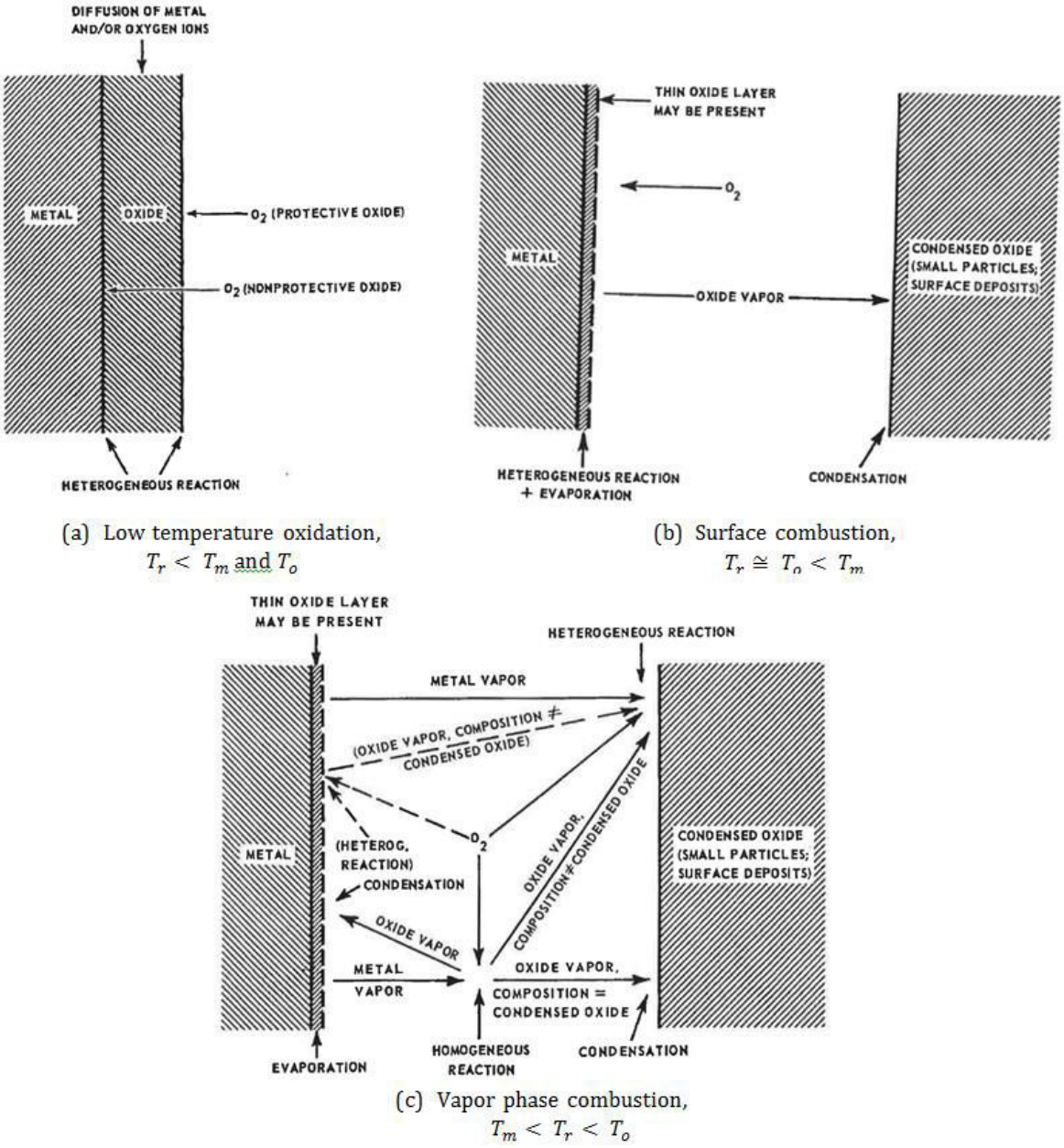

Figure 1-9. The three types of combustion according to Markstein [4]

B. Sodium combustion

A sodium fire have differences compared to other types of conventional fires. Several highlighted differences are summarized in table 1-3 below. The burning rate of the sodium is slower compared to kerosene with a much lower flame height, although its flame temperature is slightly higher than kerosene. The radiant heat flux from a sodium fire is much less intense than that arising from burning carbonaceous materials. Its heat of combustion is four times less than that of petrol with 11.3 x 10^6 and 47.8 x 10^6 J/kg respectively[13]. It produces aerosols in the form of sodium oxides. There is no risk of propagation due to the nature of the combustion products, and its burning intensity is 10 times less than that of kerosene.

Table 1-3. The comparison between sodium and conventional fire (kerosene) [14]

Data	Sodium	Kerosene
Combustion rate ($kg.m^{-2}.h^{-1}$)	25 (average) ; 36 (initial fire) ; 40 (for the safety calculation)	72 – 288 (depend on the ventilation condition)
Flame height	1 cm , whatever is the dimension of the pool	3 m for the fire of 1 m^2 surface
Flame temperature (^0C)	1350	1200 -1300
Heat transfer	No direct radiation (a fire of 2 m^2 can be approached up to 50 cm of the foyer)	Important radiation (difficulty to approach the fire)
Chemical reaction	Na_2O et Na_2O_2 by nucleation process	H_2O, H_2, CO, CO_2, and different fuel gases by chain reactions
Risks related to the combustion product	Chemical effect, no propagation	Explosion and propagation
Burning intensity (kW/m^2)	100	1000

Sodium combustion may occur on the surface and in the vapor phase [4]:

- In a pressure range between P_i (lower pressure limit below which there is no combustion) and P_s (upper limit pressure), the combustion reaction, proven by the presence of a blue flame (emission characteristic of molecular sodium Na_2) and the formation of peroxide Na_2O_2 is located at the surface. The presence of peroxide confirms the superficial reaction, because Na_2O_2 that can decompose at 280°C (melting temperature of 675°C) is more volatile than the metal. Under these conditions, this interpretation of combustion method applies to the second case of Markstein's model ($T_o < T_m$). The residue of the blue combustion is more compact and its surface has a lunar landscape.
- Above the P_s pressure, the flame becomes yellow (characteristic emission of gaseous atomic sodium), and happens in vapor phase. The yellow flame temperature (1350^0C) is measured experimentally to be between T_m (881°C) and T_o (1600°C). Na_2O may be present in the gas phase, in which the combustion provides sufficient energy to the surface to vaporize the metal and maintain the reaction. On the contrary, Na_2O_2 is revealed to be present in the residual crust and aerosols after combustion. The yellow combustion residue is friable and arborescent.

The sodium combustion is a complex phenomenon, which increases the difficulties of the case studies, notably in identifying among the different processes those that mainly control the reaction. On the basis of the combustion product distribution (40% of the sodium in aerosol form, 60% as surface residues) it may be assumed that sodium pool combustion involves a double mechanism: a vapor phase combustion process with a superficial combustion process simultaneously. The mechanism may be schematically represented in the following way (cf. figure 1-10): the sodium evaporates and diffuses through the region between the pool and the flame; the sodium monoxide formed in the flame is entrained away from the reaction area and is transformed into sodium peroxide. A fraction of these aerosols may be redeposited on the liquid layer, but the quantity of surface residues can only be explained by oxygen diffusion through the

flame area and by a surface reaction between the oxygen gas and the liquid sodium. Thus, the different processes that can play a role in the combustion process of pool sodium fire are:

- The chemical process
  - The formation of Na_2O and Na_2O_2, found at the surface once the burning is complete,
  - The formation of Na_2O in the flame zone,
  - The formation of Na_2O_2 in the form of aerosol in the air above the flame zone.

  The reactions are described as follow (for 1 mole):

  $$Na_{(g)} + \frac{1}{4}O_{2\,(g)} \rightarrow \frac{1}{2}Na_2O_{(s)}\ ;\ \Delta H_{773} = -311\ kJ.mole^{-1} \quad (1\text{-}12)$$

  $$Na_2O_{(s)} + \frac{1}{2}O_{2\,(g)} \rightarrow Na_2O_{2(s)}\ ;\ \Delta H_{773} = -92\ kJ.mole^{-1} \quad (1\text{-}13)$$

  In the flame zone, only the monoxide formed is stable (since the flame temperature is 1350°C and the peroxide decomposes at 657°C). However, once out of the flame zone, Na_2O aerosols dispersed in the gas phase will continue to react with available oxygen to form sodium peroxide. It is therefore considered (if the oxygen supply is not limited) that the combustion product found in the atmosphere outside the room consists essentially of peroxide Na_2O_2. Therefore, in most cases the combustion reaction is assumed to be complete and is written:

  $$Na_{(g)} + \frac{1}{2}O_{2\,(g)} \rightarrow \frac{1}{2}Na_2O_{2(s)}\ ;\ \Delta H_{773} = -357\ kJ.mole^{-1} \quad (1\text{-}14)$$

  The formation of sodium superoxide, NaO_2, is also possible on a chemical balance: $Na_{(g)} + \frac{1}{2}O_{2\,(g)} \rightarrow \frac{1}{2}NaO_{2(s)}$ in conditions of large excess and high pressure of oxygen. That is why this reaction is not adopted in the description of the sodium combustion under air atmosphere.

- The physical process
  - The evaporation of metal,
  - The diffusion of oxygen,
  - The diffusion of sodium in the gaseous state through the flame zone,
  - The formation and growth, likely due to a phenomenon of nucleation and condensation of Na_2O particles in the flame zone,
  - The transport by convection of oxidized particles outside the flame zone,
  - Precipitation of certain oxidized particles in the hot flame zone to the colder surface.
  - Heat exchange between the heat producing source and different receiving elements: the metal itself, the support structures, the surrounding atmosphere charged with aerosols, the containment walls.

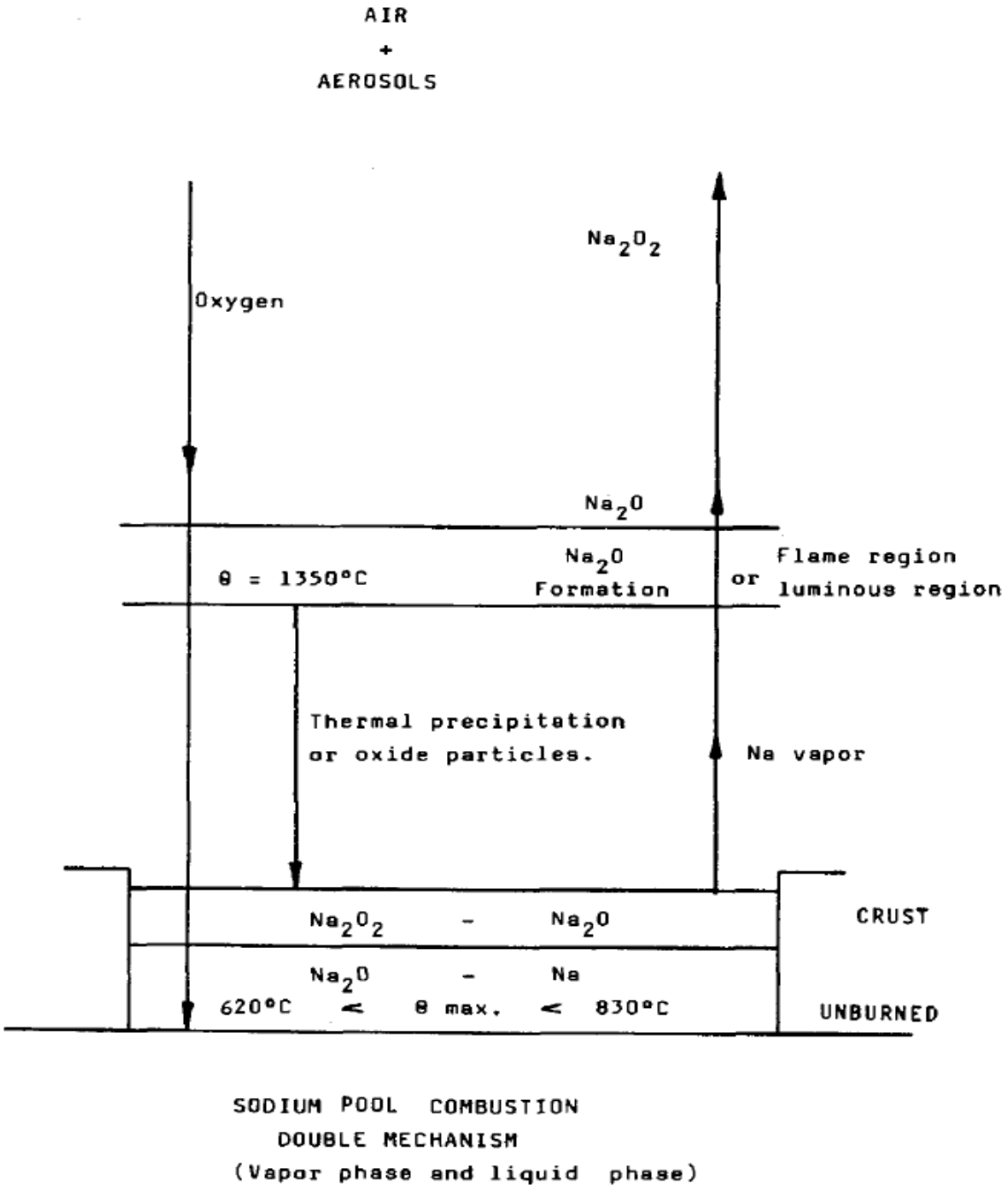

Figure 1-10. Scheme of the combustion process of a pool sodium fire [5]

Several sodium fire experimental tests were carried out to understand the mechanism of each type of fire. Our focus is on pool fires. The available results are taken:

- in Cadarache; with enclosures of 4.4 m^3 (VEGA, CASTOR, POLLUX ...), 22 m^3 (EBCOS program), 400 m^3 (CASSANDRE program LUCIFER, EFNA, SATAN ...), 3600 m^3 in Esmeralda (ESM I.1 tests and I. 2),
- in Karlsruhe; with FAUNA installation (220 m^3).

Table 1-4. The summary of tests results conducted for sodium pool fire [10], [15]

Test	Volume of the enclosure, m^3	Containment	Surface, m^2	Initial T of Na (^0C)	Average rate of combustion ($kg.m^{-2}.h^{-1}$)
EBCOS	4.4	Close	0.125	500	38.4
DRAC	400	-	10	200	17.7
LUCIFER					
• 1	400	-	2	250	17.1
• 4	400	-	2	140	18.5
• 5	400	-	2	840	17.9
CASSANDRE	400	Close	1	500	36
CASSANDRE	400	Close	10	500	28
ESMERALDA					
• ESM I.1	3600	Close	10	500	24
• ESM I.2	3600	Close + O_2	50	500	20
• ESM III.2.2.M	3600	Ventilated	19.5	345	30
• ESM III.2.2.R	3600	Ventilated	14	200	15
• ESM III.1.2	3600	Ventilated	15.7	200	25
• ESM VI.1	2000	Open	20	550	32
• ESM VI.2	2000	Open	20	550	35
• ESM VI.3	2000	Open	30	550	33
• ESM V.1	3600	-	1.3	550	4.5
• ESM V.2	3600	-	2.6	550	4.5

Table 1-4 summarized the results of the entire test conducted. Sodium combustion rate appears to vary from 4.5 to 60 $kg.m^{-2}.h^{-1}$. The trend of the average combustion rate decrease as the combustion surface increase is observed. For a surface of 0.125 m^2 in a confined space, the average burning rate was 38.4 $kg.m^{-2}.h^{-1}$. It decreased to 36 $kg.m^{-2}.h^{-1}$ when the surface changed to 1 m^2 and was further lowered to 24 and 20 $kg.m^{-2}.h^{-1}$ for 10 and 50 m^2 surfaces respectively. The convective motions that prevent the diffusion of oxygen in the center of sodium over a large pool area were certainly the cause. The sodium initial temperature appears to have an influence on the type of combustion. When it is in the order of 500 ° C, the vapor phase combustion process is the one most likely established. On the other hand the combustion at the surface remained predominant, with some outbreaks occurring randomly, for the initial temperature of 200°C. From the results of ESMERALDA tests particularly during ESM I.2 test, the amount of sodium burned and found in aerosols is 45% maximum of the burned mass. Aerosols consist of sodium peroxide, sodium oxide and sodium hydroxide. The sodium residue combustion consists essentially of sodium monoxide with a small amount of peroxide. At the end of combustion, the percentage of sodium burned in the form of peroxide is 52% on average [15].

1.1.3 The extinction of sodium

A. Theories related to the extinction

There are 7 methods in extinguishing a fire [16]: isolate the oxidant (1) and / or the fuel (2), cooling the oxidant (3) and / or the gas phase (4), inhibiting the homogeneous chemical reaction (5) and / or heterogeneous (6), and blow the flame away (7). Considering the flame as a reaction

zone, two aspects have to be considered: (i) the rate at which it is fed by reactants, let call a characteristic or diffusion time τ_r, and (ii) a strength of the chemistry to consume them, called the characteristic chemical reaction time τ_c. In combustion, the Damköhler number, D, compares these both time scales and, for that reason, it is one of the most integral non-dimensional groups. If D is large, it means that the chemistry has always the time to fully consume the fresh mixture and turn it into equilibrium. Real flames or combustion are usually close to this state. During extinction, however, the fuel burning rate gradually decreases until a critical low value of the Damköhler number, which corresponds to a rapid extinction of the flame, is reached.

A variety of Damköhler numbers can be defined for different reacting flows. It can either be based on flow time:

$$\tau_r = \frac{l}{v} \tag{1-15}$$

where l is a characteristic length and v a representative velocity, or on a diffusion time:

$$\tau_r = \frac{l^2}{d} \tag{1-16}$$

where d is an appropriate diffusion coefficient. The decision to use equation 1-15 or 1-16 will depend on whether the major transport process into the reaction region during extinction is convective or diffusive, respectively.

Sodium fire is considered as a diffusion flame (non-premixed system) since the oxygen in the atmosphere is separated initially from the sodium. As a result, the inter diffusion of fuel and oxidizer is the essential transport process that occurs during the flow process of combustion, thus equation 1-16 is preferred. However, it is unclear whether the value of d should represent an overall fuel-oxidizer, fuel-product or oxidizer-product diffusion coefficient. Nevertheless, studies showed[16] that fuel-product and oxidizer-product diffusion coefficients often increase in a laminar diffusion flame. Hence, the quantity d should represent a diffusion coefficient for penetration of important reactants into flames.

Further ambiguity also arises from various possible selections of the chemical time, τ_c. It might be based on any of the many elementary kinetic steps that occur in the combustion reaction. A simplification by a one-step overall process has been chosen in the combustion research. Equation 1-17 below represents an approximation of a complicated chemical kinetic scheme, where the constants$A$, E, m, and n must be determined empirically. It should be emphasized that values of the constants depend not only on the nature of the fuel but also on the flame condition (non-premixed or premixed). Although well-established values for the constants frequently are not available, the result of the approximation with this equation has generally been found to be good for hydrocarbon fires with $m = n = 1$, $E = 167.472$ kJ.mole^{-1} and $A = 10^{13}$ cm^{3}g^{-1}.s^{-1}.

$$w = c_F^n c_O^m A exp\left(-\frac{E}{RT}\right) \tag{1-17}$$

w = the rate of fuel consumption in the gas phase flame (g/cm^3.s),
c_F = the local fuel concentration (g/cm^3),
c_o = the local oxidizer concentration (g/cm^3),
n = overall reaction order with respect to fuel,
m = overall reaction order with respect to oxidizer,
E = the activation energy (J/mole),

R = the universal gas constant (J/mole.K),
T = the local temperature (K),
A = the pre-exponential constant $(g/cm^3)^{1-m-n}.sec^{-1}$.

By simply dividing the density ρ by w in the gas-phase reaction zone; τ_c can be obtained:

$$\tau_c = \frac{\rho}{w} = \rho c_F^{-n} c_O^{-m} A^{-1} \exp\left(\frac{E}{RT}\right) \quad (1\text{-}18)$$

From the equation (16) and (20), the Damköhler number can be written as follows:

$$D = \left(\frac{l^2}{\rho d}\right) c_F^n c_O^m A \exp\left(\frac{E}{RT}\right) \quad (1\text{-}19)$$

Some quantities in this equation, especially c_F, c_O, and T, vary considerably from one point to another in the fire. Therefore, the quantity D, defined in equation (1-19) is variable. In order to obtain a constant value, it is necessary to select specific positions at which the variables are evaluated. Two positions are worthy of consideration. One is in the center of the flame, for example a maximum temperature position. The value of the constant D obtained if c_F, c_O and T are all evaluated at such position is designated by D_a.

From an operational point of view, it is more desirable to define a particular Damköhler number in terms of limit values, because these can sometimes be obtained more easily. Therefore, in a second approach, the quantities c_F and T can be measured in the gas at a point on the fuel surface, while c_O can be evaluated in the ambient air. The constant value resulting for D will be referred as D_b.

The fire behavior depends on the value of D_a. If a flow pattern is defined and the boundary conditions are specified, then the main properties of a fire, such as the maximum temperature in the flow field can be calculated as a function of D_a. A typical result of this type for a simple particular system is shown in figure 1-11.

For a low activation energy E of the chemical reaction, the maximum temperature dependence in the flow field with the number of Damköhler is represented by a monotonic function that goes from the lowest temperature at zero Damköhler number to an adiabatic flame temperature of infinite Damköhler number [17]. The "nearly frozen" part of the curve describes a system without combustion; along this line an observer would say that the fire is out. The "nearly equilibrium" of the curve describes a vigorous combustion system. Ignition and extinction occur along the intermediate portion of the curve.

The relation between D_b and D_a can be deduced from a simple physical reasoning. If E is large, the most important factor in the equation (19) is $\exp(-E/RT)$. The relationship between D_a and D_b is approximately:

$$D_b \approx D_a \, exp\left(\frac{E}{RT_a} - \frac{E}{RT_b}\right) \quad (1\text{-}20)$$

where T_a is the flame temperature and T_b is the limit temperature (at the surface of the fuel).

In the case of high activation energy and of adiabatic flame temperatures than the limit temperature, the curve develops a S-shape as that shown in figure 1-12. The ignition conditions

are clearly defined as the position of the vertical tangent at low temperature and the conditions of extinction by the vertical tangent at high temperature [17]. The lower branch represents an extinction state and the upper branch represents a combustion state. However, the middle branch is unstable and the observation of this branch is not necessary. Only the states of combustion and suppression are observed.

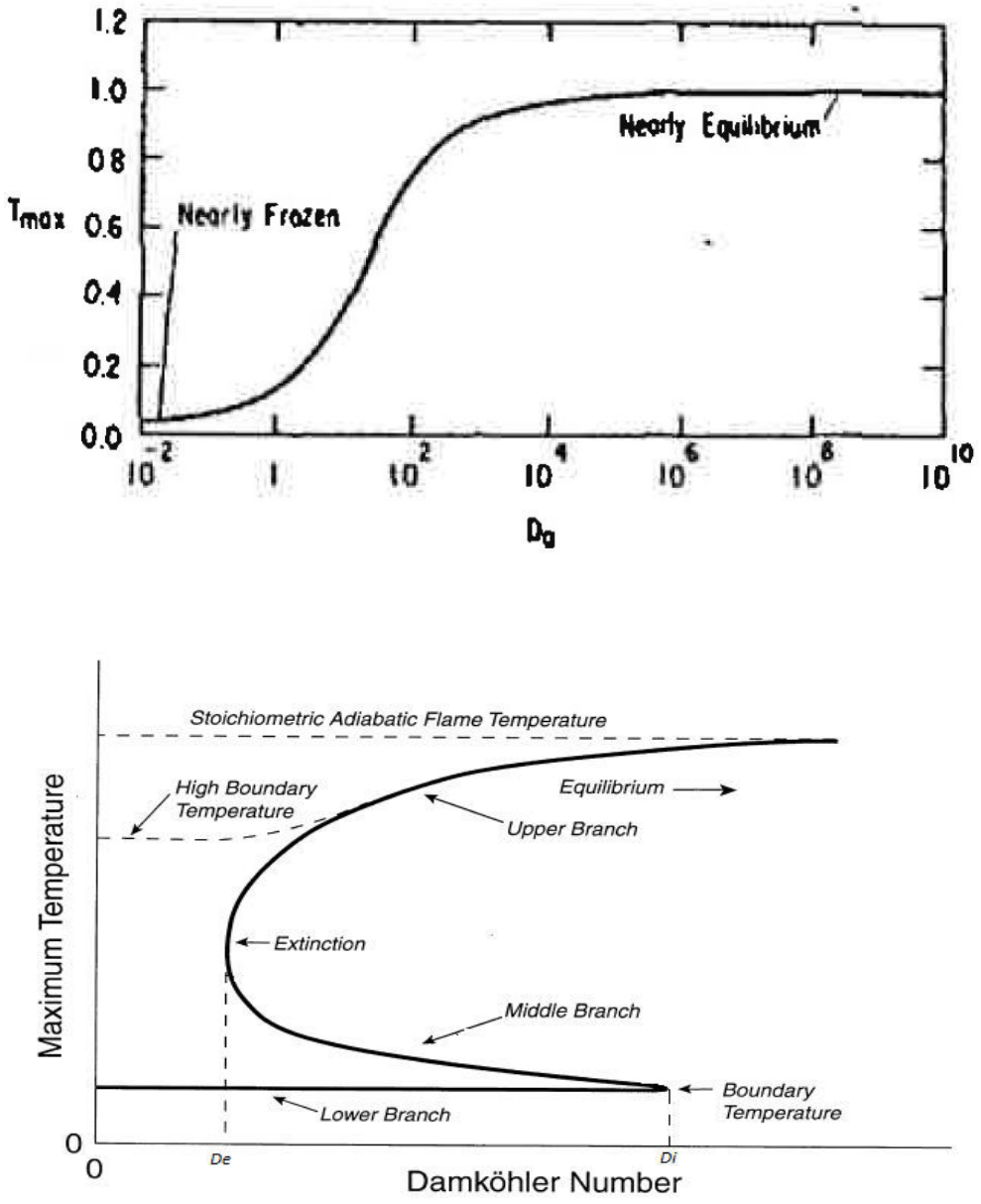

Figure 1-11. Variation of non-dimensional maximum temperature with the boundary Damkohler number, D_b [18]

If, for a combustion system, the D_b value is lowered below the extinction value D_e, it will then join the lower branch, which means the fire is extinguished. The fact that $E\ /\ RT$ is large in practice has been used as the basis of asymptotic methods to obtain simple and reasonably general expressions of D_e. An approximate version of the asymptotic theory results is:

$$D_e = k\left[\frac{RC_pT_{af}^2}{EQ_F}\right]^3 exp\left(\frac{E}{RT_{af}} - \frac{E}{RT_b}\right) \quad (1\text{-}21)$$

where C_p is the average specific heat at a constant pressure for gas, Q_F is the heat released in the combustion reaction in the gas phase per unit mass of consummated fuel, and T_{af} is the flame temperature for an infinite Damköhler number, generally very close to the adiabatic flame temperature. The rate coefficient k depends on the system being studied, but generally its value is in the order of 10^{-3}. Thus, the extinction is reached when $D_b < D_e$, or by combining equations 19 and 21 the equation becomes:

$$\left(\frac{l^2}{\rho d}\right) c_{Fb}^n c_{Ob}^m A \exp\left(\frac{E}{RT_{af}}\right) < k\left[\frac{RC_p T_{af}^2}{EQ_F}\right]^3 \quad (1\text{-}22)$$

The suppression is considered effective not only if the fire is extinguished, but also a further re-ignition cannot occur. If, for a system on the first branch, the value of D_b is high above D_i, then the only solution available is on the third leg, a combustion state. The re-ignition occurs when D_b exceeds the D_i ignition value. Therefore, to allow the extinction, it is necessary to have D_b has not only to be less smaller than D_e, but also at a smaller temperature. Equation (1-22), then, can be used to determine the most significant method of extinction. The combustion isolation of the flame reduces c_{Ob}; the fuel isolation reduces c_{Fb}; the chemical reaction kinetics slow down can reduce A (and/or E); the flame or oxidizer cool down reduce T_{af}, which is effective because the exponential factor is dominant; while the flame blow increase the convection velocity v, which is equivalent to increase D in equation (1-21).

However, the correlation between present day extinguishment methods and the Damköhler criterion is only qualitative. In order to quantitatively know the relation of the extinction with the Damköhler numbers, one must know all quantities in equation (23). Lecoustre et al. [19] made a prediction of the extinction of diffusion flame at different pressures using the code S3D of Direct Numerical Simulation (DNS). They performed a validation of the model calculation from the criterion of Damköhler flame extinction. However they have not calculated D_e as a criterion for extinction. Instead, they calculated the evolution of the Damköhler number following the increase in temperature. A high Damköhler number corresponds to a stable flame, while a smaller value of the Damköhler number correspond to a condition close to extinction. In this case, extinction is defined when $D < 1$.

B. Sodium fire extinction

Sodium ignition is a phenomenon that can occur even if the sodium is at relatively low temperature when it is in contact with oxygen. The combustion kinetics analyses highlighted the important role of an evaporation-diffusion processes in combustion [5]. Therefore, isolating the fuel from oxidant is essential to achieve a complete extinction.

The separation of fuel and oxidizer is used in the following means of action:

- Sodium leak traps
  They consist essentially of a sodium recovery tank and a lid provided with movable flaps allowing the passage of sodium while avoiding the diffusion of oxygen over the sodium pool collected. This system is able to limit the combustion.
- Extinguishing powders
  The powder used to extinguish a sodium fire should have the following criteria:
  - Chemical compatibility with the metal fire to be extinguished,
  - Capable to cease the combustion,

- Large heat capacity,
- Inflammability and stability,
- Absence of the extinguisher corrosion and toxicity or the decomposition of by-product,
- Low density.

Our study concerns the utilization of extinguishing powders. More detailed information about the commercial extinguishing powders will be presented in the next part.

1.2 Literature review of the extinguishing powders

The extinguishing powders could act on a metal fire following 3 modes of extinction that can possibly be applied on a metal fire [5]:

- **Extinction by cooling the metal fuel**
  The projection of a certain quantity of extinguishing powder to the metal fuel will cool the latter, thus decreasing the kinetics of combustion or even bringing down its temperature below the ignition point. This method depends on the heat capacity and the thermal conductivity of the powder. However, the cooling effect does not seem to have a significant impact for the extinction, even if it favors the process, due to the unproved relation between heat capacity and thermal conductivity towards the extinction capability. One exception is graphite, which is recognized to have an efficient extinction capacity considering its high coefficient of thermal conductivity.

- **Extinction by suffocation**
  This method consists in blocking the oxygen access to the metal or on the contrary preventing the metal vapor from contacting the oxygen. It is a simple process because it involves neither the physical modification nor the chemical process of the powder. Although it is not an essential process for extinguishing a fire, it highly contributes to the extinction considering that the shape of powder grains (i.e. spherical shape being the best) ensures sufficient compact distribution over the metal.

- **Extinction by formation of a continuous insulating layer**
  The formation of an insulating layer allows the total separation of metal from oxygen. This can be attained by the melting of the powder in contact with the hot metal. Accordingly, extinguishing powders which composition corresponds to an eutectic, hence having a low melting temperature, are of particular interest. The melting is an interesting phenomenon not only because it creates a liquid insulating layer, but also because it simultaneously absorbs the heat necessary to reach the melting. Thus, this method is a combination of the two methods of extinction previously described. Furthermore, it is worth noting that other parameters which are more difficult to control in order to cover the metal surface, like the viscosity as well as the density, are also playing an important role on the efficiency of extinction.

There are two categories of powders that can be used for extinguishing a sodium fire, that have been tested [19, 20]:

- *Non fusible powders* (T_f > 600°C, superior to the maximum temperature of sodium used in the reactor ≈ 550°C)
  The extinction process consists of covering the sodium pool with a layer that is sufficiently thick to isolate properly the sodium from the oxygen (extinction by suffocation). Even though, frequent re-ignitions can be observed with several powders. In these cases, the liquid metal returns back to the surface and newly inflames in contact with air. Thus, the powders need to have certain physical criteria, such as a bulk density inferior to liquid sodium as well as being fluid enough to be spread easily and homogeneously on the surface, and being of sufficiently small particle size to prevent the sodium to arise back to the surface. Likewise, the powders should not contain any component inducing corrosion, exothermic reaction, or forming harmful products. For that reason, among the commercial powders tested, the silica and phosphate based powders have been excluded for the extinction of sodium fire.

- *Fusible powders* (T_f < 600°C)
  They consist of powder mixtures having a composition such that the melting temperature is about or lower than 500°C. By virtue of these properties, the powder forms a sealed pasty film on the surface of the sodium. If one of the components contains a small amount of hydration water, it can play a double role. On one hand, it reacts at the interface to form a sodium hydroxide film (as the result of a small reaction of crystallized water with sodium at low temperature, no presence of hydrogen detected throughout the tests), which is a powerful agent for extinction. On the other hand, water removal favors an agglomeration of components to form an isolating compact layer at the surface of the metal. The Marcalina powder is one of the fusible powders devoted to sodium fire.

A review of the available commercial extinguishing powders dedicated to the metal fires will be presented so that the components, compositions, and efficiency of these powders in extinguishing a sodium fire can be compared. Around 20 patents will be discussed based on their basic component used as the extinguishing powders.

1.2.1 Graphite based powders

The first graphite based extinguishing powder was developed in 1944 by the Dow Chemical Company. It consists essentially of granular carbon with 0.5 - 3% weight of a semi-liquid high flash point organic substance, such as heavy mineral oil, that should be chemically unreactive with the burning metal. The graphite particles were preferably finer than 2380 microns (8 meshes) and at least 50% coarser than 74 microns (200 meshes) to allow free flowing and prevent packing or caking. These components were mixed with such thoroughness that the liquid coats the individual particles of the graphite. The slow evaporation of heavy oil lets the vapors formed fill the space between graphite particles and excluding air from the fire. These vapors were present in such small amount that although they are flammable, they do not form a sustained flame over the surface of graphite. No secondary fires were observed when it was spread over a light metal fire, such as magnesium. Yet, the application on a fire by a scoop or shovel made it less practical and safe [21].

Ansul Chemical Company powder formulated the Lith X powder, comprising 93% weight of electro furnace graphite, 5% of Attapulgus clay or magnesium silicate as an anticaking agent, and

2% of bulky magnesium stearate as water repelling agent. As opposed to the previous powder, it is dischargeable as a stream from an extinguisher under pressure. It has a particle size range such that it will pass through a 20 mesh sieve and no more than about 25% will pass through 325 mesh sieve. When applied to a sodium fire, a few cracks of graphite were seen on the surface [22].

Carbon microsphere having a 50 to 100 microns size formed by heating a styrene divinyl benzene resin beads at a temperature of about 850°C in a flowing nitrogen over a period of 48 hours was the product invention of [23]. It contains less than 10% of organic compounds. It could be projected from a conventional powder extinguisher canister with flow and projection qualities close to those of a liquid. It was claimed to be successfully applied on a sodium fire due to its capability in covering the metal surface and conducting heat away from the metal.

Graphex ($C_{6.23}H_{0.82}O_{0.71}S_{0.09}X_x$), developed by CECA S.A. and le groupe Carbone Lorraine, was a complex of 10% sulfuric acid exfoliated graphite. Immediate extinction was accomplished during the application of 500 g of product on 1 kg of sodium(R^1 =0.5). The exfoliated graphite layer that formed “in situ” at the molten metal surface did not flow away and provided isolation. The required amount of product was substantially slight, depending only on the surface of the metal, and not on their volume. The product could preferably be conditioned as granules, bars, and foils. Besides, it can be preserved both in small bags disposed within the sodium reception chambers in case of accidental pouring or in blocks (coated or uncoated) serving as construction elements of receptacles. Still, it was only reliable when applied on high sodium temperature started at 620°C [2, 23]. This powder could not extinguish the sodium fire during accident in Almeria solar plant [14].

1.2.2 Chloride based powders

The Ansul Chemical Company produced a powder based on 65 - 95% weight of sodium chloride (NaCl) as an inert salt, 1 – 20% copolymer of vinylidene chloride and acrylonitrile as a binding agent, 1 – 10% of fuller’s earth as an absorbent, 1 – 3% of magnesium stearate as a water repellant agent, and 0 – 5% of tricalcium phosphate as a flowing agent. It could be employed at a considerable distance from a fire through a pipe or hose in a controlled stream. Though, the utilization by shoveling or pouring from a pail was also possible if desired [25].

The powder mixture of NaCl and anhydrous $CaCl_2$ (30 – 70% mol) with an adjuvant as additives, i.e. polysiloxane, silane, metal stearate, fine silica, talc, alumina, or graphite, was created by Nippon Dry Chemical Co. Ltd. It was found to be effective for quenching Na, Mg, Al, Li fires [26].

Commercial chloride based powders were among others Met-L-X (NaCl and $Ca_3(PO_4)_2$), Pyromet ($(NH_4)_2H(PO_4)$ and NaCl), T.E.C/Tri Eutectic Chloride (KCl 29%w, NaCl 29%w, and $BaCl_2$ 51%w; T_f = 544,6°C) [5], as well as Totalit M_2 (85% of pulverized NaCl coated with the organic product used as a fluidizing agent). It has a relatively good performance of extinction with R = 2.3 (T_{Na} = 580°C). The stabilization of the oxygen partial pressure and the decreasing temperature of sodium demonstrated a successful extinction. However, the increase of the gas temperature that happened simultaneously with the oxygen consumption evidenced that there was a secondary

[1] R = Weight ratio of powder used to sodium

reaction, which was apparently due to the emission of cyanide resulting from the reaction of sodium with the contained organic product [24]. Moreover NaCl, such as reported in [4], found to provoke fast rates of stress corrosion induced by chloride in the austenitic stainless steel during the high operating temperatures, so its utilization is no longer suggested.

1.2.3 Phosphate based powders

A dry free flowing phosphate based powder was composed primarily of 79% weight of monoammonium phosphate, 15% of 200 meshes (74 microns) magnesium carbonate (magnesite), 5% of precipitated tri calcium phosphate, 300 meshes (40 microns) of 0.4% silica as a water repellant agent, and 0.6% of dimethyl diethoxysilane (silicone) used as flowing agent. A chemical reaction took place between the monoammonium phosphate and magnesium carbonate releasing carbon dioxide, water, and forming the corresponding ammonium-metal-phosphate. The latter with some excess of unreacted monoammonium phosphate melted on the hot burning surfaces producing an adherent foamy mass which smothered the fire. The fire extinguishing action of the phosphate and magnesium carbonate combination was substantially greater than either one alone. Thus, a synergistic action made these compositions being an efficient fire extinguisher for combatting all types or classes of fires [27].

Perrefite-Auby Society invented a phosphate-resin based powder in 1972. The melting of polyamide resin gave the immediate formation of a tight carbon-like crust stopping the fire on the burning metal. Monoammonium phosphate, ammonium sulfate, and fluidizing agent's mixture allowed a gas release to promote a foaming carbon crust. Urea and azodicarbonamide added reinforced the foam and pore production in the crust. The complete extinction was observed within 6 seconds wherein 30 g of powder (of the best composition) were used for extinguishing 300 g of sodium fire (R = 0.1) [28]. Although this powder seemed to be potentially very interesting, the phosphate based powders basically contain phosphor, which in humid condition can produce the toxic phosphine (PH_3) [24].

1.2.4 Inorganic based powders

These inorganic powders developed by Minnesota Mining and Manufacturing Company [29] contain a minor amount of finely divided stable metallophile (i.e carbon, silicon carbide or zirconium boride) of no more than 100 microns particle size, associated with a major amount of a small size stable glass or ceramic bubbles having a lesser specific gravity and also not reacting violently with the metal. One lb. of sodium was melted in a 10-inch steel frying pan, ignited and allowed to burn for 6 minutes. To the fire was then applied 0.5 lb of a mixture of 80% 40-micron glass bubbles and 20% 0.1-0.5 micron silicon carbide. The fire was considered to be extinguished after around 20 minutes (R=0.5)[29].

1.2.5 Organic based powders

MgA powder is composed mainly of organic products. Therefore, it could lead to all the risks of subsequent secondary fires during the decomposition of the product [5].

1.2.6 Silica based powders

Vermiculite was an exfoliated mica ($(MgCa)_{0.7}(MgFe^{3+}Al)_6(AlSi)_8O_{20}(OH)4.8H_2O$) based powder obtained by heating to form a product of very low bulk density (around 0.08). 4 kg of vermiculite were needed to quench 10 kg of sodium (R=0.4; T_{Na} = 610°C). The extinction was achieved despite of the reaction that occurred during the powder spreading. In fact vermiculite large particles made the sodium to impregnate the powder, thus they were found to be in a huge division state after combustion. The intervention was also difficult due to the pyrophoric combustion residue. Another test was also conducted for suppressing 184 kg of sodium in a 400 m^3 container. This time, 24 kg of vermiculite was needed. However, a brutal rise of pressure was observed (from 12 to 132 mbar) along with a temperature elevation from 590 to 680°C)[24].

Perlite is constituted of a high proportion of silicon dioxide/silica (SiO_2). When contacting with sodium, the molecular chain released the silica and gave a sodium-silica reaction [24]. Perlite was also found to be the major component, preferably around the composition 99 – 55% by weight, in the extinguishing powder developed in [30] besides mono- and di-ammonium phosphate. The mixtures of silica with aluminum oxide were also found to be efficient in suppressing fire [26]. However, the silica based powders were suggested to be excluded from the powders used for sodium fires as this component reacts with the sodium as soon as 200°C to form sodium oxide and silicate through an exothermic reaction [24].

1.2.7 Boron based powders

A boron oxide (B_2O_3) based powder was developed in Japan by Shin-Etsu Handotai Company in 1989 [31]. It comprises 90% by weight of B_2O_3 with a water content not exceeding 2% and has a particle diameter ranging from 5 to 1000 µm. A small amount of inert inorganic powder, such talc, clay, mica, feldspar, calcium orthophosphate and graphite, was added to improve the flowability. It was also suggested that a material having a relatively low melting point and capable of being eutectically melted with boron oxide could be combined to enhance the suffocating and cooling effects of boron oxide. These materials included sodium chloride, potassium chloride, anhydrous sodium carbonate, magnesium carbonate, anhydrous sodium tetraborate, etc. Upon the contact with sodium fire or in the vicinity of the burning material, the boron oxide would melt above 450°C and the particles started to be sintered together to form a crust. When melting took place, the particles were coalesced and then vitrified to form a glassy transparent layer. Considering the high viscosity of the molten B_2O_3, this layer was free from flowing down even at such a high temperature (exceeding 1100°C) to serve as a complete air-shielding layer. The boiling point of boron oxide is as high as 2250°C so that the loss of molten B_2O_3 by vaporization was negligibly small. In addition, its heat of melting was as large as 316.7 J/g, which was also significant to intensify the cooling effect in the fire extinguishment since it absorbed the heat of combustion from the burning material to lessen the violence of fire. Around 9 – 11g of powders were needed to blow out 5 g of sodium fire (R = 2.2). Yet, the effectiveness was not remarkable. Besides, it is a hygroscopic compound that returns to boric acid by absorbing moisture in the atmospheric air.

1.2.8 Carbonate based powders

Carbonate based powders were developed as an alternative to chloride based powders. One of these powders contain 75-94% weight of sodium carbonate (Na_2CO_3), 1-5% of metal stearate (water repellant agent), 2-10% of attapulgus clay (fluidizing agent), and 3-15% of polyamide resin (crusting agent). The crust formed isolated the molten metal from the atmosphere. It would not have any serious toxicological effect. It might be applied either by a pressurized fire extinguisher from a safe distance or gently deposited over the metal surface by a shovel [32]. Even so, 37 kg of this powder were needed to extinguish a fire of 10 kg of sodium at 593°C (R > 3.7). Furthermore, the extinction was only temporary [24].

Ansul Na-X was another commercial powder based on pulverized sodium carbonate coated with stearates and nylon. Not only 23 kg of powders were not enough to suppress a 10 kg of sodium fire at 580°C (R > 2.3), but also the organic products contained in the powder were inflamed causing the sodium to rise upon the surface of the powder, which made it even worse [24].

1.2.9 Eutectic mixture based powders

The influence of hydration water contained in the alkali metal salts on the mechanism of methane flame inhibition was also studied by Birchall [33]. The efficiency of a powder in extinguishing flame appears to be dependent on the surface area of solid presented to the flame as results suggested that the high efficiency of certain alkali salts was due to their decomposition in the flame to give a solid reaction product having a large specific surface. In fact, alkali salt hydrate represented sixtyfold increase in specific surface compared to the anhydrous ones having little change during treatment at high temperature. Therefore, substances which when heated underwent reactions of the type

$$Solid\ I \rightarrow solid\ II + gas$$

in which solid II is finely particulate, might be potentially effective as a flame-inhibiting agents. He, then, showed that substances decomposing at low temperature are more effective than thermally stable substances. It was illustrated by the behavior of anhydrous sodium carbonate that shown no presence of cavity, zone in which combustion was inhibited, compared to small cavity produced by sodium carbonate decahydrate. In the case of potassium oxalate hydrate, a high flame current and a large cavity resulted as soon as the pellet touched the flame. The current and cavity then declined rapidly as the pellet surface became coated with the relatively inactive potassium carbonate. Furthermore, the high extinguishing efficiency of certain alkali-metal salts would be due to the decomposition in the flame of relatively large particles, with the formation of submicron particles of a solid decomposition product. For example, 1.2g of 44µ K_2CO_3 was required to extinguish a CO diffusion flame corresponding to a powder surface area of about 700 cm^2, while the weight of 44µ $K_2CO_3.H_2O$ required was 0.1g, given 0.075g of K_2CO_3 on decomposition corresponds to a particle size of about 2µ [33]. Hence, the efficiency of an alkali salt in extinguishing a flame according to [33] would depend on the following:

- The change in surface area accompanying the reaction, solid (I) → solid (II) + gas.
- The chemical nature of the secondary particles.

- The particle size that determine a residence time in the flame sufficient enough to allow the decomposition of the original solid within the flame.

The effect of heat absorbed from the combustion system when it undergoes its endothermic decomposition has been studied in [32, 33]. Magnesium hydroxide is used as a flame retardant in polymeric materials, of which the water vapor release during the decomposition dilutes the combustion gases and the magnesium oxide layer generated during the breakdown could act as a protective char in the condensed phase.

In her thesis, Reuillon [5] developed a powder mixture comprising at least two salts of alkali metals, in proportions such as to obtain a composition having a melting point lower than the temperature of the liquid metal to be extinguished. Among the powders tested were binary eutectics (Na_2CO_3-Li_2CO_3, Li_2CO_3-K_2CO_3, LiCl-Li_2CO_3, NaCl-Na_2CO_3), ternary eutectics (KCl-NaCl-$BaCl_2$, K_2CO_3-Na_2CO_3-Li_2CO_3), quaternary eutectics (Na_2CO_3-$BaCO_3$-$BaCl_2$-NaCl), two quaternary eutectics (KCl-NaCl-K_2CO_3-Na_2CO_3) and five quaternary eutectics (KCl-NaCl-K_2MoO_4-Na_2MoO_4). Moreover, one of the salts should contain hydration water. The advantage of using a water containing powder was studied [5] in the case of the NaCl/Na_2CO_3 powder. The anhydrous salt, eutectic mixture NaCl/Na_2CO_3 showed no significant capacity of extinction. The same salt when tested with mixtures in identical proportions identical to that of the eutectic with a variable moisture content, became much more effective, especially when the water content was 10 to 12%, which is slightly less than the corresponding water content of sodium carbonate monohydrate (14.5% water in pure $Na_2CO_3.H_2O$). However, moisture content higher than that of carbonate monohydrate provoked reignition. Furthermore, the agglomeration phenomenon which is deleterious to transport the product might occur for such high water content compositions [20].

The eutectic based mixture that finally demonstrated the best efficiency along with the capacity of extinction for the sodium fire was the binary eutectic mixture of Li_2CO_3-$Na_2CO_3.H_2O$ associated with graphite [34, 35]. This powder was then commercialized as Marcalina, which will be discussed more into details in the next part (§1.3).

1.2.10 Bicarbonate based powders

Bi-ex was a manufactured product composed of sodium bicarbonate ($NaHCO_3$) coated with an organic product as a fluidizing agent [24]. 47 kg of powder were needed to extinguish 10 kg of sodium at 585°C (R=4.7). The chromatography analysis observed the presence of hydrogen according to these reactions:

- Thermal decomposition of $NaHCO_3$ releasing H_2O

$$2\,NaHCO_3 \rightarrow CO_2 + H_2O + Na_2CO_3$$

$$Na + H_2O \rightarrow NaOH + \frac{1}{2}H_2$$

- Metal-acid reactions transforming bicarbonate into carbonate

$$NaHCO_3 + Na \rightarrow Na_2CO_3 + \frac{1}{2}H_2$$

$$H_2 + \frac{1}{2}O_2 \rightarrow H_2O$$

1.3 The physicochemical characteristics of Marcalina: literature background

Marcalina is an extinguishing powder dedicated to metal fires, specifically recommended for sodium, potassium, or mixture of both fires. The absence of toxicity and secondary reactions give it additional value as an extinguisher. It was developed as a result of joint research between CNRS and CEA subjected to a French [37] and an international patent [36]. While, the manufacturing and marketing license was granted by French Society for the Patents Management on Nuclear Application (BREVATOME) to CACI.

1.3.1 Physicochemical characteristics of Marcalina

The theoretical compositions (in weight) of Marcalina are as follows [38]:

- Na_2CO_3 : 43.2% ± 2%
- Li_2CO_3 : 43% ± 2%
- Graphite : 9% ± 1%
- H_2O : 4.8% (cannot be superior to 5.4% ± 1%)

Graphite is considered to be chemically inert (up to high temperatures) and anti-hygroscopic. It has a low density and a good thermal conductivity. It plays especially a fluidizing role and eliminates the need for coating the powder with products that could alter its effectiveness and quality. Thanks to its lubricating properties, it allows, at one hand, facilitate the flow of the powder mixture during spreading and, at the other hand obtain a suitable viscosity thus giving a sufficiently rigid coverage to ensure the permanence of its protective nature [5]. Moreover, the reaction between graphite and sodium occurs only at 900^0C to give sodium acetylide Na_2C_2.

The proportion of carbonates close to the eutectic is suspected to facilitate the melting at low temperature. Nevertheless, the different melting temperatures are found to be contradictory one to another. Eitel et al. in [39] found that the double salt was detected with a congruent decomposition temperature of 510°C. Janz et al. [40] considered that this carbonate system has a simple eutectic type at the 52 mole% of Li_2CO_3 – 48 mole% of Na_2CO_3 at 500°C with congruently melting compound as can be seen in figure (1-13a). As opposed to Janz et al., Cairns et al. [41] found, in a very careful thermogravimetric study, an incongruently melting compound: $LiNaCO_3$ that decomposes at 500.757 ± 0.005°C. In this case an incongruent eutectic was found

at 53.30 mole% of Li_2CO_3, composed of $LiNaCO_3$ and Li_2CO_3 melting at 499.754 ± 0.057°C (cf. figure 1-13b). $LiNaCO_3$ crystal was produced by seeded growth from a melt containing 53 mole% of Li_2CO_3 and 47 mole% of Na_2CO_3 in [42]. Two phase transitions were observed: the high temperature (β-γ) phase transition identified at 360°C and the (α-β) phase transition observed at 175°C. The phase diagram was constructed using differential thermal analysis varied from 46-60% moles as seen in figure 1-13c. They found the incongruent melting of eutectic in the composition of 55 mole% Li_2CO_3 and 45 mole% Na_2CO_3 at 485°C. They were able to grow the single crystal of $LiNaCO_3$ from the melt composition within a range of 50.5%-54.5% moles of Li_2CO_3. Therefore, several tests with different proportion of carbonate mixtures will be conducted to verify the eutectic melting temperature.

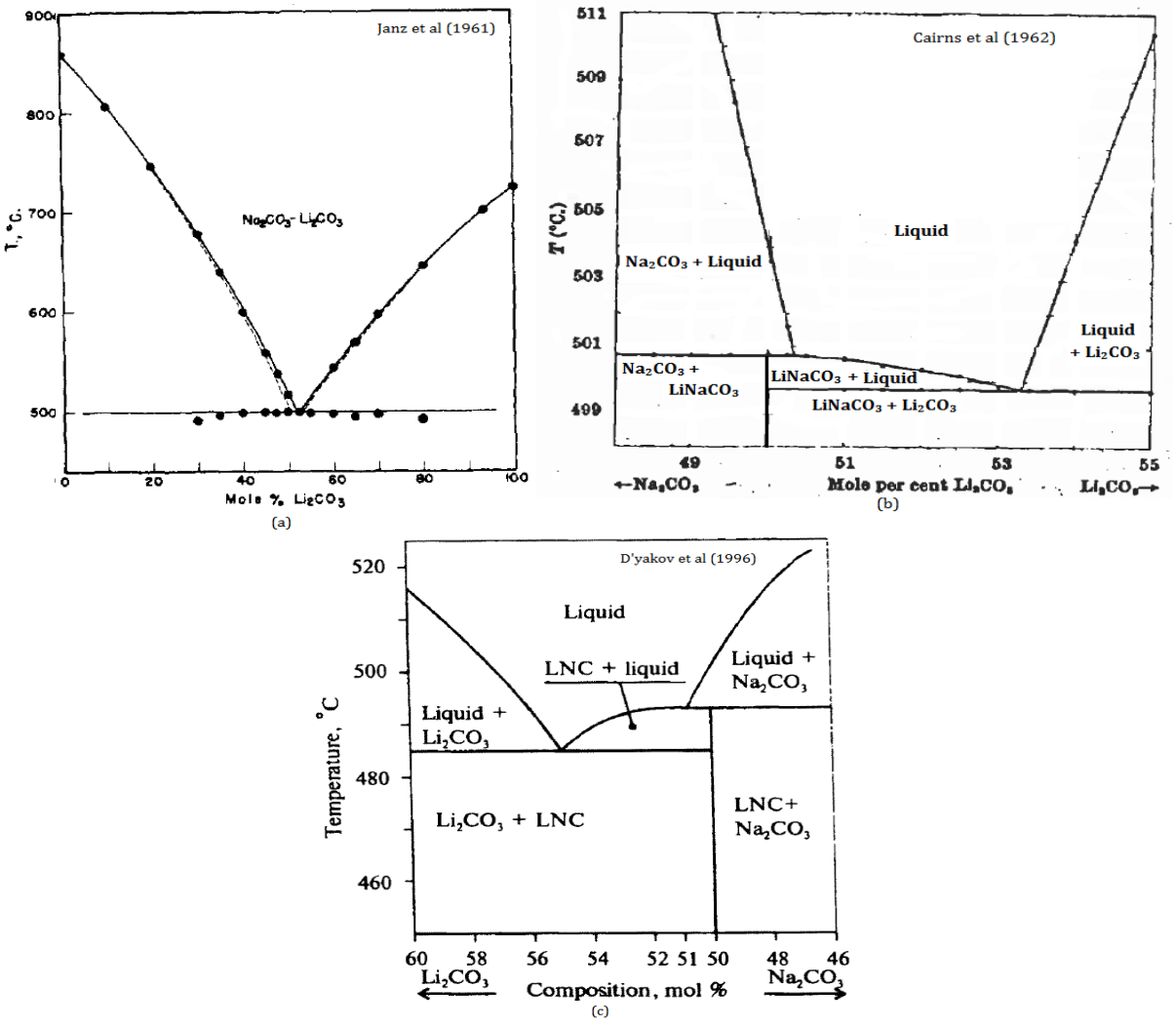

Figure 1-12. The literature review of Na_2CO_3 – Li_2CO_3 system phase diagram

The study of M. Reuillon [5] revealed that water contents slightly lower than the corresponding carbonate monohydrate (14.5%) was favorable to extinction. Indeed, with mixtures contained 10% or 12% water, no sodium reignition occurred after spreading, or only a few weak re-ignitions. On the contrary, with the mixtures of 14.5% and 15% water, the re-ignitions appeared

to be more frequent. Based on the results obtained for the powder batches ordered on 1981, the water content was varied between 4.4% - 7.3%. Therefore, the chemical analysis is important to the quality control of powder [38]:

- Humidity control : passage of a certain quantity of powder to the stove for 24 hours at 120°C,
- Graphite filtration : dissolution by 1M of sulfuric acid (H_2SO_4) with a filtration on 10µ Millipore filter, rinsing using ethanol, drying the residue in the stove for 1h at 80°C, followed by weighing the graphite as the residue,
- Na and Li sampling : dilution of the filtrate pursued by analysis using absorption atomic spectroscopy.

The density measurements were done using a volumenometer. The results were as follows [38]:

- Bulk density : 0.40 ± 0.05 kg/m^3
- Tapped density : 0.65 ± 0.05 kg/m^3

The true density of the powder has been also measured by a pycnometer with isopropyl alcohol. The average value was 2.145 g/cm^3.

According to M. Reuillon [5] the particle size distribution (psd) of the powder need to be taken into consideration. Most of the powders employed have an average psd between 40-80 µm that favors a good fluidity. In her studies, she particularly used a psd of less than or equal to 160 µm, that was chosen based on the recovered quality of the commercial powders of similar psd.

The particle sizes of the commercial Marcalina powders were classified in terms of mesh size ASTM NF X 11-501 (1970) within the range 63 – 600 µm. About 0.05% of the powder had 600 microns size, 50% of had particle sizes larger than 75 microns, and around 85% have 63 microns size [43]. The psd test using Coulter-Counter[2] method performed in 1978 showed a particle median diameter of 23 microns. However, for the powder received in 1981, the diameter was found to be 7 microns. Moreover, the presences of really hard agglomerates were hardly observed in large dimensions of 10-15 mm or sometimes even more. These agglomerates were found especially after several weeks or months of storage in the 9L extinguisher and 1100 L storage truck that belongs to FLS Cadarache. Hence, it appeared that the physical characteristics of powders were not constant throughout time, which most possibly happened because of either the lack of homogeneity or a difference in the production method [44].

1.3.2 Transport properties of Marcalina

The slope of the repose angle (α) and the flow angle (β) was measured to be 49° and 86° respectively. When the powders are stored during a sufficiently long time, it tends to be easily packed, which then alters its flowability. Nevertheless, it could be fluidized and so be

[2] Coulter-Counter method is particle size and number determination method using the variation of electrolyte resistance due to the particle suspension in the passage of a calibrated orifice. In this case, the diameter of orifice used was 50µm and water was added with sodium chloride as electrolyte.

transported pneumatically using argon or azote as a carrier gas. The period of fluidization varied upon the capacity of different powder containers. For the powders stored in 9, 20, and 40 L, 1 year storage did not modify the physicochemical properties of the powders. Fluidization of the powder is required after 1 year of storage for the powder extinguisher of 70, 150, and 320 L capacities. Similar recommendations are for the capacities of 500 to 2000 L. The frequency of fluidization was suggested to be around 6 months for the capacities of more than 2000 L [45].

Test facilities dedicated to study the pneumatic transport of the powder were developed. These facilities included the elements to ensure the following functions [45]:

- powder storage,
- fluidization,
- suspension, dosage, and introduction of the powder in the transport circuit,
- pneumatic transport,
- powder spreading by fix and/or mobile device.

In order to assure the pneumatic transport, it is essential to maintain enough flow rates in the pipe so that the powder deposit during transport could be avoided. This flow rate can be obtained by giving a suitable diameter, involving a sufficient gas flow and pressure to overcome the pressure drop. The latter depend not only the pipe route but also on the amount of material introduced into the pipe relative to the amount of carrier gas.

Two types of powder spreading devices were designed to assure the separation of powder and gas served as handling at the outlet of transport pipe: fix and mobile spreader. The fix spreader comprises of three concentric conical pieces placed at different heights, in the axis of the conveying duct. It is mostly used for direct applications upright on the sodium pool. Meanwhile, the mobile spreader is dedicated to apply powder in difficult places to reach such as under or above the sodium pipes. This spreader can equip 9 L, 20 L or 40 L and suitable to apply the powder horizontally. Either one or both of these spreaders can be used on a fixed pipeline or at the end of a mobile launcher. Its use will depend on the needs of the operator. Due to the importance of physical properties in the powder handling, transport, and storage, the physical analyses are also conducted in this study.

1.3.3 Role of physicochemical properties to the extinction

According to Reuillon [8, 44], Marcalina has a lower density (in a solid form) than sodium, thus lighter and also immiscible at the sodium surface. Its small quantity of hydration water (contained in the form of sodium carbonate monohydrate) reacts with sodium oxides and sodium at low temperature to form a thin film of sodium hydroxide at the interface between the sodium and the powder. However, the quantity of water reacting with sodium is still small enough so that the presence of hydrogen was not detected in the tests. At high temperature, the melting of carbonates is attained, forming a pasty (due to graphite incorporation), uniform, and continuous film suitable to separate the liquid sodium and the surrounding air. It has an insulating effect, as it opposes to the diffusion of oxygen and sodium vapor. Based on the observation of combustion residue after test, Reuillon [5] proposed the hypothesis of the extinction mechanism based on the presence of two crusts, as shown in figure 1-13 below.

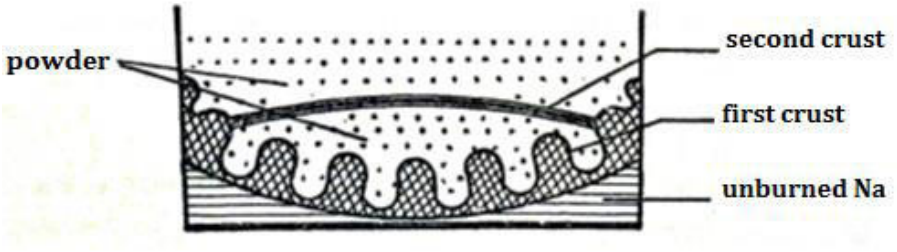

Figure 1-13. Diagram of the crusts observed after the extinction test [5]

The first crust might be hypothetically identified as the film of sodium hydroxide, which formed rapidly due to the reaction of sodium-hydration water, allowing for the isolation of sodium surface at low temperature. When the temperature rose, the total or partial melting of the mineral salt mixture at this first crust provides additional protection against attack by oxygen. The second crust, consisting of a stack of sheets, is considered to be a mixture of molten salts in which the graphite is inserted intimately, playing the role of binder. This last crust prevents the diffusion of oxygen to sodium. It is an additional asset for the isolation of metal and oxidizer [5].

A study conducted by Desremeaux et al. [46] also shown that Marcalina could be used in the potassium fire as like NaK fire. The calorimetry thermogram Marcalina-NaK and Marcalina-K shows no noticeable reaction, particularly regarding the reaction $8C + K \rightarrow KC_8$, probably because of the low proportion of graphite in the powder (9%).

1.3.4 Test results

Several tests have been conducted to evaluate the extinguishing capacity of Marcalina [45]. For small scale sodium fires (10 g of Na), 5 g of powder (R = 0.5) were needed for sodium fires at temperatures of 550°C, 301°C, and 275°C. Therefore, it could be used to extinguish a sodium fire at low and high temperature. For sodium at 596°C burned on a surface of 0.2 m^2, the extinction was found to occur after 15 minutes of spreading 6 kg of powder, with no re-ignition. 260 kg of sodium pool fire at a temperature of 600°C with a thickness of 16.1 cm on a surface of 2 m^2 was successfully blocked with 100 kg of spilled powder. During 30 minutes after spreading, no re-ignition was observed. Additional 5 kg of powder easily suppressed the re-ignition points appeared afterwards (R = 0.4). The re-ignition happened because of the contraction of the sodium during its cooling that initiated the movement of the pool surface. It eventually cracked the melted powder bed due to its difference in dilatation coefficient difference with sodium. Thus, these phenomena suggested that a control would be necessary until the sodium is completely cooled. Another test was conducted in a confined atmosphere of a 400 m^3 container, in which 200 kg of sodium at 550°C was spilled over a 2 m^2 tray. 100 kg of powder (8 cm of thickness) were capable of simultaneously decrease the temperature of sodium and gas, the pressure, as well as the oxygen consumption taken as the extinction parameter (R = 0.5).

In addition, Marcalina is capable of extinguishing other types of metal fires. 130 g of powder have completely suppress a 200 g potassium fire, 80 g are needed for a 100 g calcium fire with the maximum temperature of 1020°C, and only 35 g were required to attain a complete

suppression of a 90 g magnesium fire at 800°C. Furthermore, it is capable of quenching a hydrocarbon fire. 1.5 kg of powders have turned off 20 liters gasoline fuel and 10 liters fuel oil fires [36].

In order it properly works, the powder must be poured over the free surface (either vertical or horizontal) of the burning metal, in such a way that the latter is separated from the ambient air, by using a specially designed equipment capable of maintaining its initial characteristics, obtaining the thickness and quantities necessary for extinction, as well as utilizing the minimum quantities of carrier gas. This equipment can be fixed (for major sodium user facilities), mobile (for large capacities), or manual with conventional fire extinguisher.

Several questions arise about the behavior of the powder to optimize its operation. The aging, especially with a high intake of water can alter its composition and could affect its effectiveness to extinguish the fire. In addition, the powder extinguishing mechanism is not yet precisely defined, notably for the role of each component to extinguish the fire. It is part of this thesis scheme, thus these problematics will be studied and discussed.

1.4 Literature review on grinding/milling technique during powder fabrication: mechanochemical reaction

CACI, the manufacturer of Marcalina, has ceased its activity nowadays. Several batches of powder in stock may (or not?) assure the safety aspect during the sodium utilization. In view of the research development program for ASTRID project, high quantity of sodium will cause the increasing demand of Marcalina. Therefore, the anticipation of powder shortage needs to be taken into account promptly to secure the safety aspect of the project.

Marcalina has a relatively fine particles as what have been described in §1.3.1. A fine milling method is a prerequisite to obtain such range of particle sizes and homogenizing the powder mixture. Indeed, milling is not only capable of creating particles of a certain size, but also increasing the surface area and the proportion of high activity regions at the surface [47].

Reuillon [5] used ball mill to obtain the eutectic carbonate mixture powder with a dominant size of 45µm. The high energy release during ball-powder collisions leads to various phenomena in the solids including defects in the crystal structure, amorphization, decrease of particle size, plastic and elastic deformation of particles, increase of specific surface area of the powders, polymorphic transitions, and even so chemical reactions [48]. In that respect, milling may be described as a mechanochemical treatment, the change of reactivity as mechanical activation while reaction induced by mechanical energy as mechanochemical reaction. The mechanochemical reactions during the milling process take place without any external supply of thermal energy. Thanks to these mechanisms, reactions generally observed at high temperature can occur even at low temperature in a ball mill with no external heating needed [49]. In this case, the ball mill is considered as a chemical reactor in which a wide range of chemical reactions can be mechanically initiated.

"Mechanochemistry is a science dealing with the chemical and physicochemical changes induced in substances as a result of applied mechanical energy." The most common way is via ball-particle collisions in a milling device often referred as the "high-energy milling" technique [47]. In this technique, a powder or mixture of powders is typically milled in liquid-free conditions; under such circumstances, a larger amount of the kinetic energy of a moving ball inside a grinding bowl is transferred to the powder particles during collisions. Here, the form of mechanical activation plays an important role. There are 4 types of main stress that can be applied (cf. fig. 1-15): compression, shear (attrition), impact (stroke), and impact (collision).

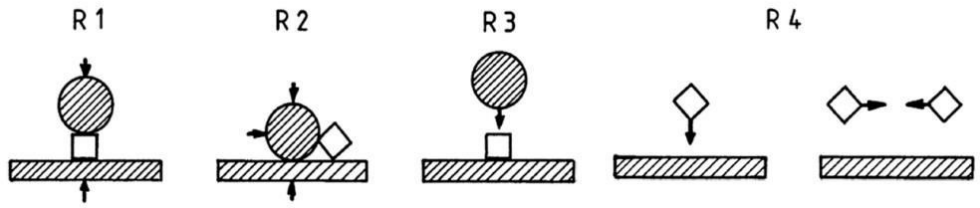

Figure 1-14. Main stress types in mills, R1 – compression, R2 – shear (attrition), R3 - impact (stroke), R4 – impact (collision), *circle* – mass of milling media, *square* – mass of material charge, *rectangle* – mass of mill wall [47]

The planetary ball mill is one of the most used particularly for research purposes. It employs the principle of centrifugal acceleration instead of gravitational. Two types of rotations produced the characteristic ball motion (cf. fig. 1-16):

- rotation of the grinding bowl around its center,
- rotation of the supporting disc to which the bowls are attached: the two rotational senses are opposite.

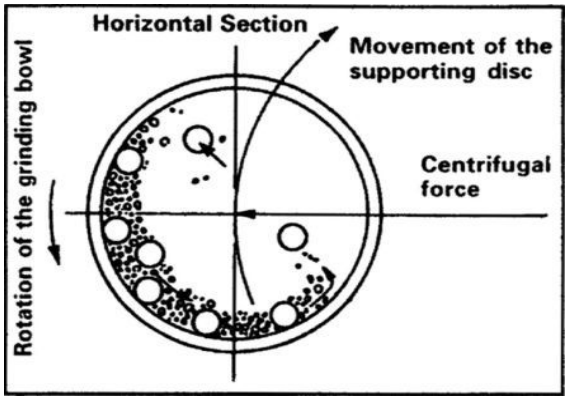

Figure 1-15. Movements of working parts and balls in a planetary mill [47]

There are several variables influencing the milling process [47]. The *type of mill* chosen will affect the stress mechanism, the feed size, and also the product size distribution. The *material used for the milling media* is important due to impact of the milling balls on the inner walls of the milling chamber. Generally, high density and larger balls give better results because of high impact forces on the powders. The balls also need to be denser than the material to be milled. The *Ball-to-Powder Ratio* (BPR or charge ratio) represents the weight ratio of the milling balls to

the powder charge. Regarding the *filling of the milling chamber*, in general, about 50% of the space is left empty in order to maintain enough space for the balls and the powder particles to move around freely in the milling chamber. The *milling atmosphere* is essential to minimize the product contamination. The *milling speed* will influence progressively the intensity of milling as well as the temperature inside the milling chamber. The longer *milling time* might increase the level of contamination.

Several phenomena might happen during the milling process [47]. As the particle size decreased, the surface area will become larger and facilitates the formation of new surfaces. These may contribute to the powder *contamination*. During high-energy milling, the size of crystals decreases to some critical values, followed by the crystals deformation, and subsequently *amorphization*. The particle size reduction is frequently become complicated due to the particle size enlargement where smaller particles are put together to form larger entities (*agglomeration*). Two kinds of temperature effects during milling are usually taken into account: local temperature pulses due to ball collisions and the overall temperature in a vial. During the milling process part of the milled powder is attached to the vial walls and other part is attached to the balls. The remaining part is in a free state moving in the volume of the milling chamber. All these parts have different temperatures. The temperature of the powder influences the diffusivity and defect concentration in the powder thus influencing the phase transformations induced by milling. The highest temperature obtained with the smaller bowl using a Fritsch P-5 planetary mill was 327°C at 318 rpm. A decrease of the temperature is expected at very high speeds, as the balls stay attached to the container wall for too long, reducing both heating and efficiency of milling [47]. The temperature of the milling balls of a water-cooled AGO-2 planetary mill measured by Kwon et al showed that the ball temperatures over 600°C were reached when running the mill for 20 min at the highest intensity setting. An additional temperature range of 50-300°C may be added to give the highest local temperature due to the impulsive temperature increase of the powder compressed between the colliding milling tools [50]. The theoretical calculations related to kinetic energy during milling are presented in Annexe (A.1).

Several examples of the mechanochemical reactions have been given in literature [51]. Apparently, the *polymorphous transformation of crystalline to amorphous phase* may increase as the milling intensity increases and decrease as the temperature increases. A *synthesis of high temperature compounds*, such as carbides TiC, VC, Cr_3C_2, may be performed up to typically 24h of milling instead of produced at the temperature range of 1400-2300°C. A *synthesis of multi component complex compounds*, such as $Pb(Zn_xMg_{1-x})_{1/3}Nb_{2/3}O_3$, may be obtained by soft-mechanochemical procedure of PbO, $Mg(OH)_2$, Nb_2O_5, and $2Zn(OH)_2.H_2O$ in a multi ring type mill up to 3 h. It can also cause *decomposition* ($CuCO_3.Cu(OH)_2 \rightarrow 2CuO + CO_2 + H_2O$) as well as *displacement* ($2CuO + Ti \rightarrow 2Cu + TiO_2$) *reaction*.

Still, because of a great number factors affecting mechanochemical treatment, the influence of milling parameters on the mechanochemical reactions is insufficiently explained. Due to the predominantly experimental application, an essential question still arises whether it is possible to prescribe the milling conditions in advance for the attainment of a desired structure or product of mechanochemical treatment.

CONCLUSION

This chapter provided the literature review related to the sodium ignition, combustion, extinction, and grinding. Sodium ignition is mostly preceded by oxidation phase, followed by the presence of several nodulations until the combustion phase is established. In order to assure a complete extinction of a sodium fire, it must be isolated from oxygen. An extinguishing powder, known as Marcalina, was developed by CEA. It consists of a graphite mixture with lithium carbonate and sodium carbonate monohydrate in close eutectic proportion. It appears that it is capable of extinguishing the sodium fire at low and high temperature, thanks to its properties. The physicochemical properties of this powder taken from literature were also presented in this chapter and will be useful as guidance to the physicochemical analyses demonstrates in the next chapter. At last, the brief description relative to the mechanochemical reaction, phenomenon that might happen during grinding, is also introduced.

BIBLIOGRAPHY OF CHAPTER I

[1] Thierry Bonhomme, "Maitrise risque sodium," presented at the Cours No. 219 Ecole du Sodium et Metaux Liquids (ESML), CEA Cadarache, Mar-2013.

[2] J. P. Sarrut, "Method of extinguishing metal fires," US Patent 4,177,152, Dec-1979.

[3] M. Muller, "Etude du processus d'initiation par laser de la combustion d'un alliage métallique sous atmosphère d'oxygène.," École Nationale Supérieure De Mécanique et d'Aéronautique, 2013.

[4] M. Reuillon, "Etude thermodynamique et expérimentale des réactions intervenant dans la combustion du sodium," Université d'Orleans, 1984.

[5] Reuillon M., "Etude de la combustion du sodium et de l'extinction de ses feux par les substances pulvérisees: Role des additifs," L'Université d'Orleans, France, 1976.

[6] G. Rodriguez and J. Desremaux, "Physico-chimie du sodium." Centre d'Etudes de Cadarache, 13-Nov-1997.

[7] J. C. Malet, "Contribution à l'étude des processus d'inflammation et de combustion de métaux alcalins liquides en lit.," Université d'Orléans, 1972.

[8] D. An, P. B. Sunderland, and D. P. Lathrop, "Suppression of sodium fires with liquid nitrogen," *Fire Saf. J.*, vol. 58, pp. 204–207, May 2013.

[9] C. Casselman., "Etude des processus conduisant à l'inflammation et à la combustion d'une nappe de sodium liquide.," Université de Provence., 1978.

[10] J.C. Malet, "Les feux de sodium : Synthèse des résultats." Document CEA, 1990.

[11] C. Casselman., *Ignition of a liquid sodium pool.* 1979.

[12] G. . Markstein, "Heterogeneous reaction processes in metal combustion," presented at the XIth Symposium (International) on Combustion, Pittsburg, Pensylvenia, 1967, pp. 219–234.

[13] G. Bulmer and A. M. . Fire E, "Fire safety considerations related to the usage of sodium," presented at the I.Chem.E Symposium Series, London, 1972, vol. No.33.

[14] JC. Malet., "Les feux de sodium (transparents)." Document CEA, DRN/DER/STPI Ecole du Sodium.

[15] JC Malet, "Ignition and combustion of sodium – Fire consequences – Extinguishment and prevention." Document CEA/IPSN, IPSN/DRS/LEMFF/CEA Cadarache, 1980.

[16] F. A. Williams, "A unified view of fire suppression," *J. Fire Flammabl.*, vol. 5, pp. 54–63, 1974.

[17] A. Linan, "The asymptotic structure of counterflow diffusion flames for large activation energies," *Acta Astronaut.*, vol. 1, pp. 1007–1039, 1973.

[18] F. A. Williams, "Progress in knowledge of flamelet structures and extinction," *Prog. Energy Combust. Sci.*, vol. 26, pp. 657–682, 2000.

[19] V. R. Lecoustre, P. G. Arias, S. Roy et al., "Direct numerical simulations of diffusion flame extinction at different pressures," *8th US Natl. Combust. Meet.*, 2013.

[20] L. Felician, N; Simon, "Marcalina: Bilan bibliographique et caractérisation de produits disponibles," Document Technique DEN DEN/CAD/DTN/STPA/LIPC/2012-012.

[21] T. Richard, "Extinguishing light metal fires," US Patent 2,346,627, Apr-1944.

[22] William R. Warnock,, "Fire extinguisher compositions for metal fires," US 790045, 21-May-1963.

[23] Charles R. Schmitt, "Extinguishant for metal fires," US Patent 3840075, Oct-1974.

[24] Bailly J., "Extinction des feux de sodium: Choix initial du type de poudre utilisee sur la base d'essais de laboratoire." 1990.

[25] William R. Warnock, Menominee, Mich, "Extinguishing agent for combustible metals," US Patent 2937990, 24-May-1960.

[26] Jeong, Ji Young; Jeong, K. C.; Kim, B. H.; Kim, T. J.; Choi, J. H.;, "Analysis of patents on extinguishing agent for sodium fires," KAERI/AR-624/2002.

[27] Z. J. Lobos, "Dry chemical fire extinguisher composition," US Patent 3,172,852, Mar-1965.

[28] Edgar CHahvekilian, Robert Peteri, et André Hennequart, "Composition extinctrice pour feux de métaux," FR 2102424, 13-Mar-1972.

[29] LeRoy J. Leeper, St. Paul Park, and Gunther H., "Fire extinguishing," US Patent 3475332, 28-Oct-1969.
[30] R. A. Porter, "Fire extinguishing composition," US Patent 5,626,787, May-1997.
[31] H. Yamaguchi, "Method for fire extinguishment of hardly extinguishable dangerous material," European Patent 0323350, 07-May-1989.
[32] J. F. Riley and E. E. Stauffer, "Extinguishing agent for combustible metal fires," US Patent No. 3985658, 12-Oct-1976.
[33] J. D. Birchall, "On the mechanism of flame inhibition by alkali metal salts," *Combust. Flame*, vol. 14, no. 1, pp. 85 – 95, 1970.
[34] J. Formosa, J. M. Chimenos, A. M. Lacasta, and L. Haurie, "Thermal study of low-grade magnesium hydroxide used as fire retardant and in passive fire protection," *Thermochim. Acta*, vol. 515, no. 1–2, pp. 43–50, Mar. 2011.
[35] K. Kuang, X. Huang, and G. Liao, "A comparison between superfine magnesium hydroxide powders and commercial dry powders on fire suppression effectiveness," *Process Saf. Environ. Prot.*, vol. 86, no. 3, pp. 182–188, May 2008.
[36] M. Reuillon *et al.*, "Powder for extinguishing fires of liquid substances or of a mixture of liquid substances," US Patent 4,149,976, Apr-1979.
[37] Reuillon M. , Mellottee H. , Devillers B. , Alfille L.,Duco J. , Fruchard Y. , Malet J.C. , et Chappellier A., "Procédé et poudre pour l'extinction des feux de métaux liquides," 75 36225, 03-Mar-1978.
[38] CACI, "Fiche technique de controle de la fabrication, condition de stockage, controle de reception de la poudre Marcalina." 22-Jan-1982.
[39] W. Eitel and W. Skaliks, "Über einige Doppelcarbonate der Alkalien und Erdalkalien," *Z. Für Anorg. Allg. Chem.*, vol. 183, no. 1, pp. 263–286, Oct. 1929.
[40] G. J. JANZ and M. R. LORENZ, "Solid-Liquid Phase Equilibria for Mixtures of Lithium, Sodium, and Potassium Carbonates," *J. Chem. Amp Eng. Data*, vol. 6, no. 3, pp. 321–323, 1961.
[41] E. J. Cairns and D. I. MacDONALD, "Sensitive Thermal Analysis Establishing Formation of the Incongruently Melting Compound LiNaCO3," *Nature*, vol. 194, no. 4827, pp. 441–442, May 1962.
[42] V. A. D'yakov, C. A. Ebbers, M. V. Pchelkin, and V. I. Pryalkin, "Lithium sodium carbonate: A new nonlinear-optics crystal," *J. Russ. Laser Res.*, vol. 17, no. 5, pp. 489–494, Sep. 1996.
[43] "La poudre Marcalina : Caracteristiques physiques, stockage et fluidisation, transport pneumatique, epandage," Rapport DSN/SRS/SESTR 80/44 11.
[44] Société NEU, "Etude du compprtement de la poudre extinctrice de feux de sodium (Marcalina) et de sa tenue dans le temps sous l'action de la fluidisation et de la pression dans un réservoir: Compte rendu d'essai 81 EC 35.M." 1981.
[45] Bailly J., "Extinction des feux de sodium: Mise en ouvre de la poudre extinctrice Marcalina." 18-Oct-1990.
[46] J. Desremeaux, M. Rodriguez, S. Trambaud., "Compatibilité de la poudre extinctrice Marcalina avec le sodium, le potassium, et l'alliage NaK-56." 2000.
[47] P. Baláž, "High-Energy Milling," in *Mechanochemistry in Nanoscience and Minerals Engineering*, Springer Berlin Heidelberg, 2008, pp. 103–132.
[48] T. Rojac, P. Šegedin, and M. Kosec, *Using Infrared Spectroscopy to Identify New Amorphous Phases - A Case Study of Carbonato Complex Formed by Mechanochemical Processing, Infrared Spectroscopy - Materials Science, Engineering and Technology*, Prof. Theophanides Theophile (Ed.). 2012.
[49] J. Coreño A., O. Coreño A., J. J. Cruz R., and C. Rodríguez C., "Mechanochemical synthesis of nanocrystalline carbonate-substituted hydroxyapatite," *Opt. Mater.*, vol. 27, no. 7, pp. 1281–1285, Apr. 2005.
[50] L. Takacs and J. S. McHenry, "Temperature of the milling balls in shaker and planetary mills," *J. Mater. Sci.*, vol. 41, no. 16, pp. 5246–5249, May 2006.
[51] A. M. Spasic and J.-P. Hsu, *Finely Dispersed Particles: Micro-, Nano-, and Atto-Engineering*. CRC Press, 2005.

CHAPTER II
Materials and methods

This chapter deals with the materials and methods used in the experiments, which includes four studies related to: the physicochemical characterizations, the powder aging, the powder production, and the extinction. It also covers the physicochemical properties results followed by discussions related to the study.

The characterization analysis of powders were focused on three powders chosen among the powders available stored in different places and conditions [1]. They will be referred as powders A, B, and C. The choice has been made based on the difference of compositions observed in these powders.

Concerning the method of fabrication, the original materials listed in the patents relative to Marcalina were used, which includes lithium carbonate (Li_2CO_3), sodium carbonate monohydrate ($Na_2CO_3.H_2O$), graphite (C), as well as anhydrous sodium carbonate (Na_2CO_3) [2,3].

2.1. Chemical composition of the powders

The chemical properties are the primary criteria in controlling the quality of the powder. Besides using the same method as what previously used by the producer (see §1.3.1), the coupling of thermo-gravimetric analysis and micro gas chromatography as well as the x-ray diffraction analysis are developed in this study. These analyses are expected to produce more elaborated results of chemical characterization in terms of identifying the evolution of composition with time. Moreover, the physical properties are also measured in order to evaluate their impact on the powder extinguishing performance during their utilization. Indeed, the particle size will affect the flow behavior. Thus, these informations will help to determine the appropriate method of powder spreading for later employment.

2.1.1 Chemical characterizations methods and results

A. <u>Thermo-Gravimetric Analysis (TGA) coupled with micro Gas Chromatography (µ-GC)</u>

Thermo-Gravimetric Analysis was performed by using a Mettler Toledo TGA/SVTA/851e to measure the sample weight change in a furnace. The temperature was programmed for heating under 50 ml/min dry air from the ambient temperature up to 200^{0}C with 1^{0}C/min heating rate and a plateau of 60 or 240 minutes, finished by cooling under 50 mL/min argon flow (measurement accuracy ± 1 µg). A coupled analysis was realized by connecting the gas outlet of the TGA to the gas inlet of a µ-GC SRA3000. The latter has been calibrated with a precision of ±2% and its detection limit is 20 ppm. This analyze allows us to relate the sample weight loss observed by TGA to the gases released during heating as monitored by µ-GC. Very small samples are used in this analysis (about 70 mg). The TGA thermogram results (weight loss as a function of time and/or temperature) were obtained from STARe software provided by Mettler Toledo. Meanwhile, the Microsoft Excel assisted Soprane software was used to obtain the quantity of gas measured by µGC in which the gas concentration release throughout time was plotted.

Figure 2-1 shows the concentration release of CO_2 as a function of the temperature. CO_2 was released within the same temperature range at which the weight losses are observed in the TGA

analysis. The weight loss (Δm) from the TGA analysis for the three powders A, B and C is presented in figure 2-2. Powder A has the lowest weight loss while powders B and C have the highest loss. Powder A released a very low quantity of CO_2 compared to powder B and C. Even though powder B has the highest weight loss among these powders, it has a twice smaller amount of CO_2 released than powder C. CO_2 was the only gas detected by µGC during the heating cycle. Table 2-1 summarizes the result of TGA and µGC analysis.

Table 2-1. TGA and µGC analyses of powders A, B and C

Sample	Δwt (%)	T range (°C)	CO_2 concentration (mol.g^{-1})
Powder A	4.8	50 – 110	2.0×10^{-5}
Powder B	11.8	50 – 100	3.9×10^{-4}
Powder C	11.8	50 – 100	6.8×10^{-4}

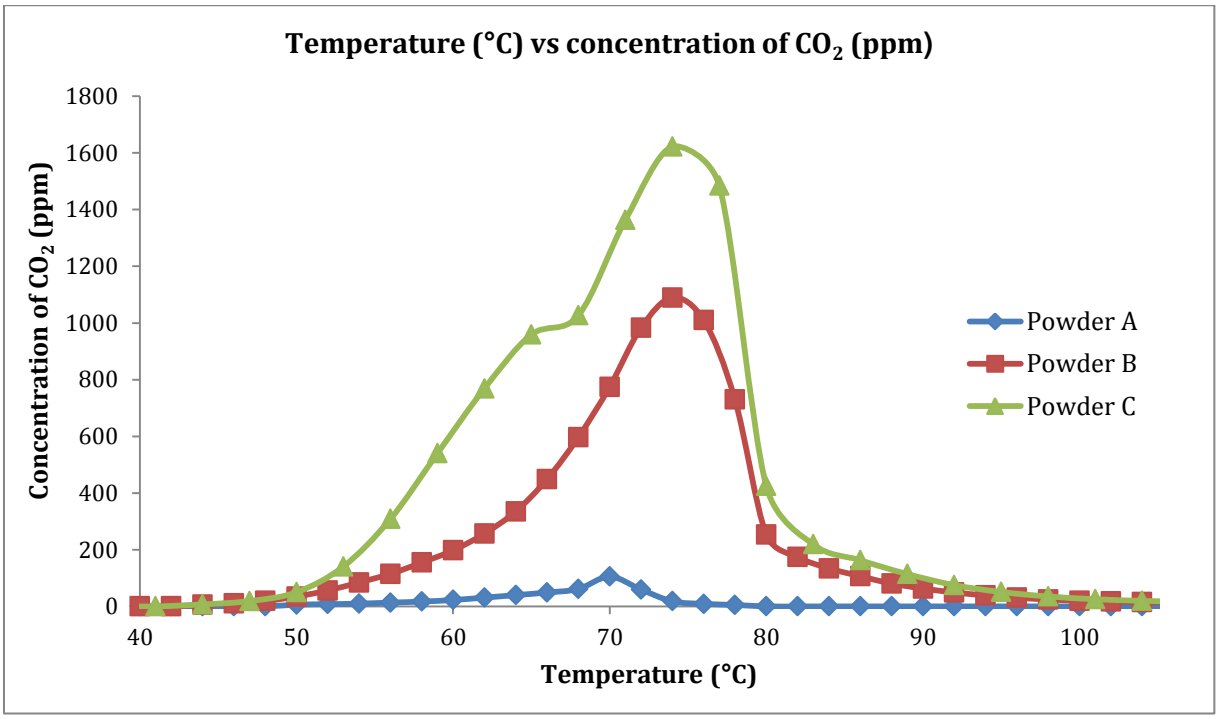

Figure 2-1. The plot of CO_2 concentration released vs temperature

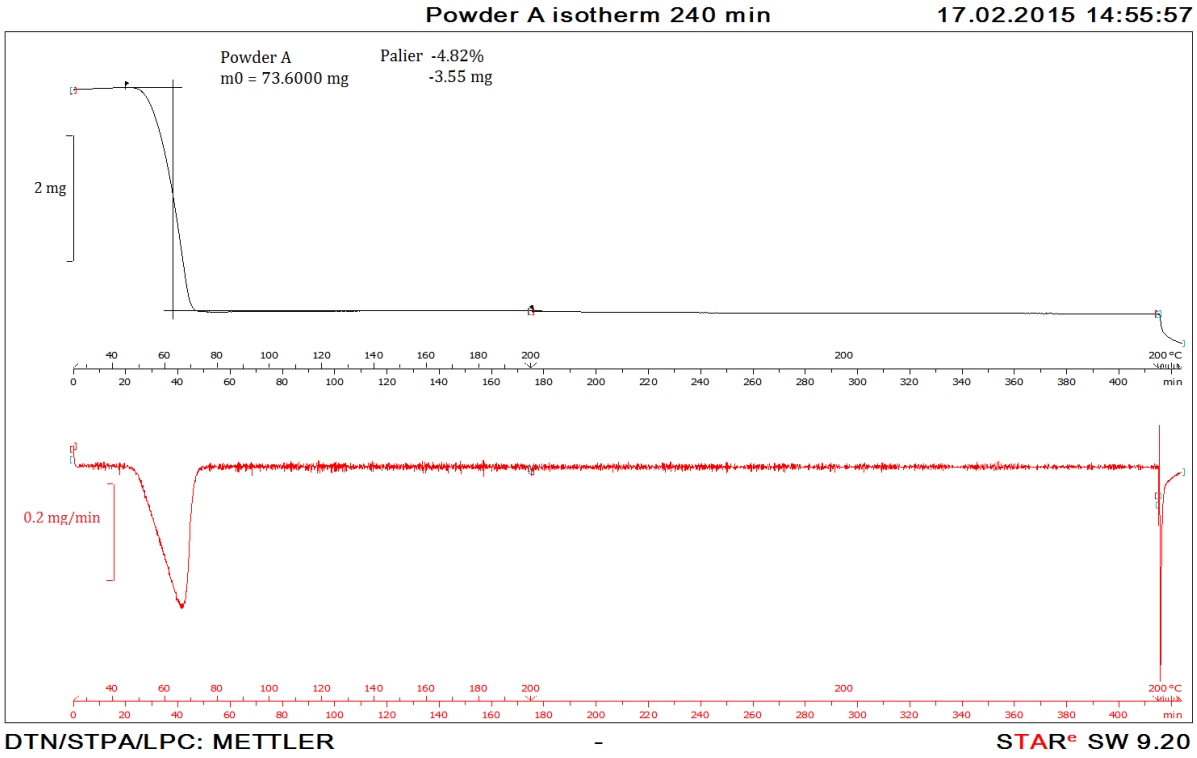

(a)

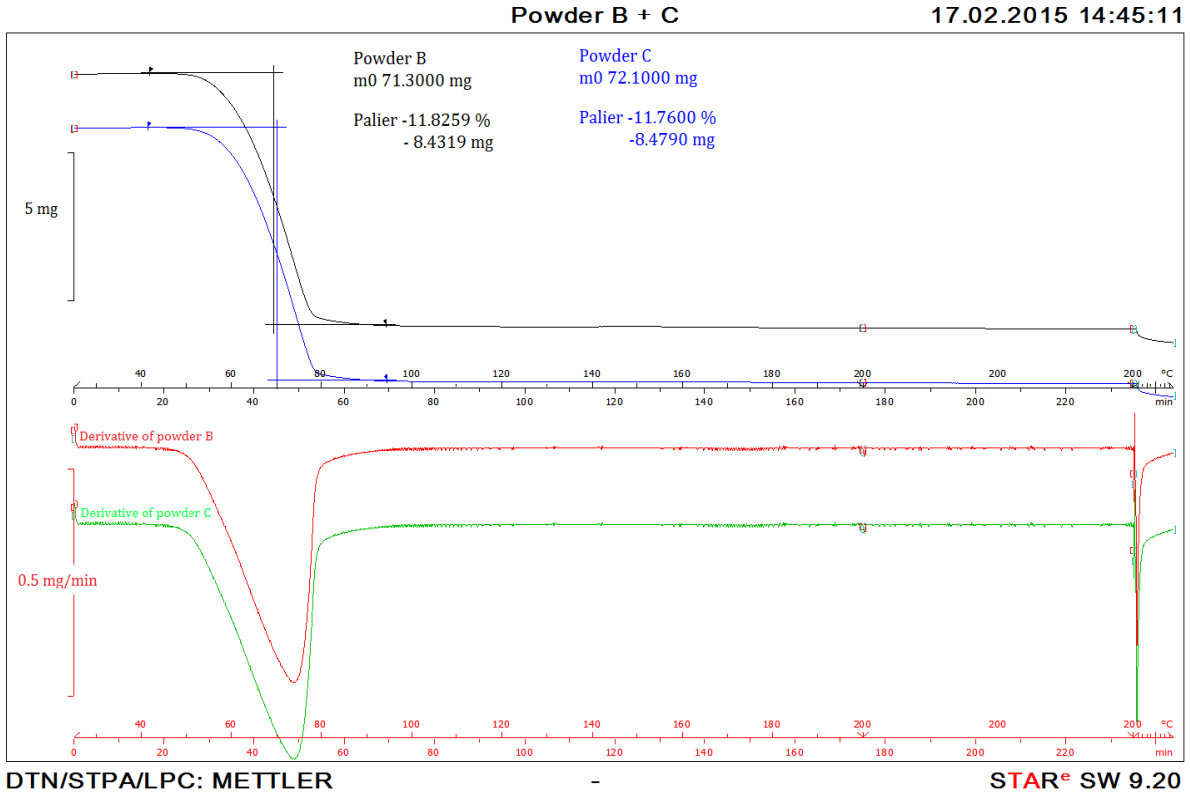

(b)

Figure 2-2. Thermogram of (a) Powder A and (b) Powders B and C

B. X-Ray Diffraction (XRD)

The XRD analysis was carried out to complement the results of TGA and µGC analyses since it allows the identification of the components of the powder. The tests were conducted with a Siemens Bruker D5000, in the 12^0 to 80° of 2Θ angle range (between incident and scattered beam), with a 0.02° angular step and 4s/step. Figure 2-3 displayed the peaks identified for the 3 powders. Since the most interesting major peaks were observed in low angular domains, the results of high ones were then omitted.

XRD Bruker EVA software was used to analyze qualitatively the results by identifying phases in a specimen in comparison with standard patterns (i.e. data collected or calculated by someone else). The semi quantitative analysis approach was performed in order to estimate the proportions of different phases using the Reference Intensity Ratio (RIR) methods. It is based on the comparison of the intensity for peaks hkl in different phases (i.e. phases α and β) according to the equation:

$$\frac{I_{(hkl)\alpha}}{I_{(hkl)\beta}} = k\frac{X_\alpha}{X_\beta} \quad (2\text{-}1)$$

where α is the phase to be determined, β is the standard phase, and k is the calibration constant derived from a plot of $\frac{I_{(hkl)\alpha}}{I_{(hkl)\beta}}$ vs $\frac{X_\alpha}{X_\beta}$, and X represents the mass fraction for both phases. In this method, the k value is taken for corundum as the β phase in a 50:50 mixture with the α phase where $I_{(hkl)}$ is defined as the 100% line for both phases, which are published for many phases in the Powder Diffraction File (PDF) contained in the software. In the PDF card, this is defined as $k = \frac{I}{I_c}$, the reference intensity ratio for a 50:50 mixture of each phases and corundum. Thus, with $\frac{I_{(hkl)\alpha}}{I_c} = k\frac{X_\alpha}{X_c}$ and $\frac{I_{(hkl)\beta}}{I_c} = k\frac{X_\beta}{X_c}$ the equation (2-1) is then modified into:

$$\frac{I_{(hkl)\alpha}}{I_{(hkl)\beta}} = \frac{(\frac{I}{I_c})_\alpha . X_\alpha}{(\frac{I}{I_c})_\beta . X_\beta} \quad (2\text{-}2)$$

However, it should be noted that the use of published I/I_c values for quantitative analysis might fall short because of problems with preferred orientation, heterogeneity of mixing, and variable crystallinity.

Five components were detected: sodium carbonate monohydrate ($Na_2CO_3.H_2O$), lithium carbonate (Li_2CO_3), graphite, lithium sodium carbonate ($LiNaCO_3$) and trona ($Na_2CO_3.NaHCO_3.2H_2O$). These later two compounds were not mentioned in the patents [2,3], thus becoming the components to be more thoroughly studied. The strongest peaks of $LiNaCO_3$ were observed in powder A. They are much lower for powder C, while they are almost undetected in powder B. On the other hand, trona was not observed in powder A, contrarily to strong peaks identified in both powders B and C. The least quantity of $Na_2CO_3.H_2O$ is detected in powder C.

The results of semi quantitative (SQ) XRD analyses are summarized in table 2-2. The highest quantity of $LiNaCO_3$ was found in powder A with 42 wt%, while nothing was detected in powder B. Meanwhile, trona was found to be at its lowest content in powder A, and to be quite dominant in powders B and C with 31 wt% and 39 wt%, respectively. The lamellar nature of graphite

crystals causes imprecision in the results due to the preferred orientation. Nevertheless, SQ analysis is able to estimate the order of magnitude of the compositions.

Table 2-2. SQ XRD analysis results for powders A, B, and C

Samples	Composition (wt%)				
	$Na_2CO_3.H_2O$	Li_2CO_3	$LiNaCO_3$	Trona	Graphite
Powder A	23	27	42	1	7
Powder B	34	31	0	31	4
Powder C	8	24	29	39	1

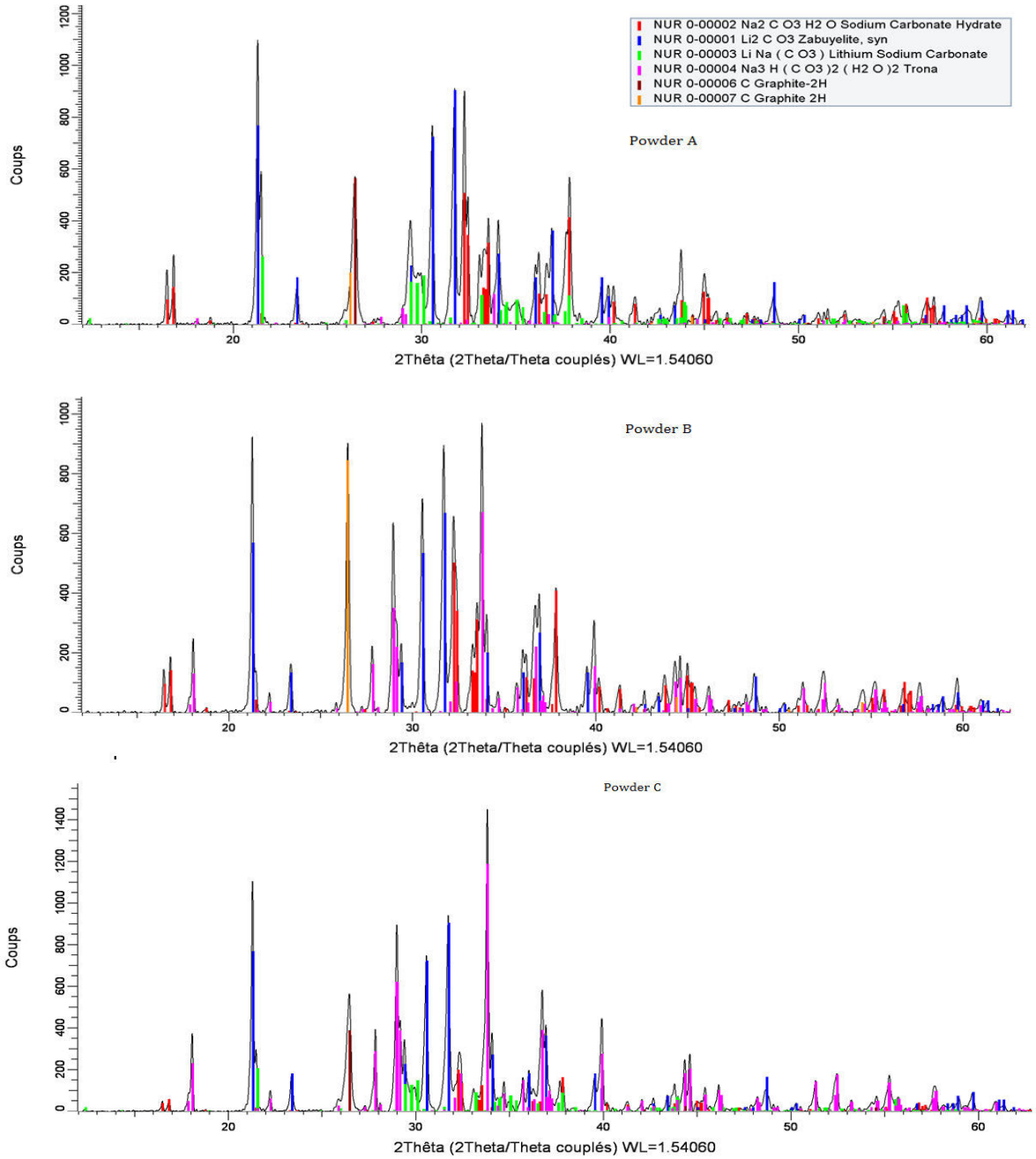

Figure 2-3. XRD diagrams for powder A, powder B, and powder C

C. Graphite filtration and Atomic Absorption Spectroscopy (AAS)

The graphite filtration and AAS were conducted to calculate the elemental composition of the powders. Previously, the powders must be dehydrated to dose the water and CO_2 content. The results of the weight loss were consistent with the TGA analyses, although 20% difference (TGA-µGC vs furnace) of the H_2O and CO_2 content is to be noted for the powder C.

1M sulfuric acid was used to dissolve the sample afterwards. Filtration was performed using 10µm of Millipore filter followed by washing the residue with demineralized water and drying in an oven for 2 hours at 100^{0}C. The dry residue of graphite was then weighed in an analytical balance Mettler Toledo AG 204 (precision ± 0.1 mg). The result shows that powder A has 8.6 wt% of graphite, which is close to the specification. On the contrary, powder B and C have both smaller contents with 7.2 wt% and 6.3 wt% respectively. It should be noted that the quantity of graphite might only have experience a slight evolution during aging, however the content might evolve as the weight changes following the composition (more or less H_2O and CO_2 contained in the form of $Na_2CO_3.H_2O$ and trona). As for powder C, the bad quality of acid used might have altered the result of filtration inducing a quite significant difference. Therefore, the quality of acid is an important factor to achieve a good filtration.

An AAS type 110/220 Varian equipped with hallow cathode lamps and two burners (N_2O/Air-C_2H_2 and Air-C_2H_2) was used. This analysis allows the dosage of sodium and lithium concentrations in the filtrate recovered from the filtration. The latter was diluted 25 times for analyzing the sodium and 10 times for the lithium. A range of standards for sodium and lithium was prepared in the concentration of 25, 50, 75, and 100 mg/l. A 5 mA current lamp under air-C_2H_2 fuel was fixed as working condition. The wavelength and slit width was set at 330.2 nm and 0.5 nm respectively for the sodium; meanwhile they were 323.3 nm and 0.2 nm respectively for the lithium. Regarding the interference in air-acetylene flame, lithium ionization is appreciable and it is necessary to match all solutions with respect to easily ionized elements, such as Na, which is partially ionized.

Table 2-3 summarizes the results of the graphite filtration and AAS analyses (yielding the concentrations of sodium and lithium in the filtrate solution) for the three powders. The combination of the TGA/µGC, graphite filtration, and AAS analyses allows the calculation of the powder composition that will be detailed in the discussion. It will be compared to the XRD semi-quantitative analysis. These results will be used to finally calculate the composition of each powders, of which a systematic error of calculation may be identified (details can be seen in 2.2.1 and 2.2.2).

Table 2-3. Graphite filtration and AAS analysis results for powders A, B, and C

Samples	m initial (m_0) (g)	Δm (TGA) (%w)	m H_2O + m CO_2 (furnace) (g; %w)	m graphite (g)	C Na ($g.l^{-1}$)	mol Na ($x10^{-2}$)	C Li ($g.l^{-1}$)	mol Li ($x10^{-2}$)	Molar ratio of Li/Na
Powder A	2.0	4.82	0.10 [4.8%]	0.18 [8.6%]	1.50	1.64 ± 0.08	0.67	2.40 ± 0.12	1.46
Powder B	2.3	11.9	0.28 [12%]	0.17 [7.2%]	1.38	1.50 ± 0.08	0.57	2.07 ± 0.10	1.38
Powder C	2.1	11.8	0.31 [15%]	0.13 [6.3%]	1.79	1.95 ± 0.10	0.78	2.78 ± 0.14	1.43

D. Differential Scanning Calorimetry (DSC)

A Mettler Toledo DSC 1 has been used to detect phase transformation (melting and crystallization) of the powders. The powder was put in an inconel crucible then heated from 25 to 600°C at a rate of 2°C/minute followed by cooling until it reached the room temperature using nitrogen as the carrier gas. The DSC thermogram, representing endothermic and exothermic energy variation as a function of time and/or temperature, was collected from STARe software.

Figure 2-4 presents the comparison chart of the thermal decomposition of the three powders. During heating, large endothermic peaks were observed at 80-90°C and 499.0±0.5°C. The powders having higher quantities of trona decompose at a slightly higher temperature (around 90°C) for powders B and C than powder A (at 80°C), and absorb about twice more energy. During cooling, an exothermic peak was observed at around 488°C for these three powders. The difference in temperature obtained between heating is due to the lesser accuracy in temperature determination during cooling. Table 2-4 gives the summary of the DSC results. The discussion will develop more information about the interpretation of the results.

Table 2-4. Summary of the DSC results for powders A, B, and C

Samples	Initial weight (g)	Heating			Cooling		
		Energy (kJ.mol^{-1}H_2O)[1] (kJ.mol^{-1}$LiNaCO_3$)[2]	Onset T (°C)	Peak T (°C)	Energy (kJ.mol^{-1}$LiNaCO_3$)	Onset T (°C)	Peak T (°C)
Powder A	5.2 x 10^{-3}	- 2.6 (1) - 21.8 (2)	65.5 (1) 496.9 (2)	81 (1) 498.9 (2)	18.2	488.5	487.6
Powder B	7.1 x 10^{-3}	- 5.4 (1) - 18.9 (2)	72.4 (1) 496.7 (2)	90.6 (1) 499.4 (2)	19.3	481.9	488.3
Powder C	8.4 x 10^{-3}	- 6.2 (1) - 22.8 (2)	73 (1) 496 (2)	92.6 (1) 498.5 (2)	15.3	493.1	488.4

*) (1) First peak observed during heating; (2) Second peak observed during heating

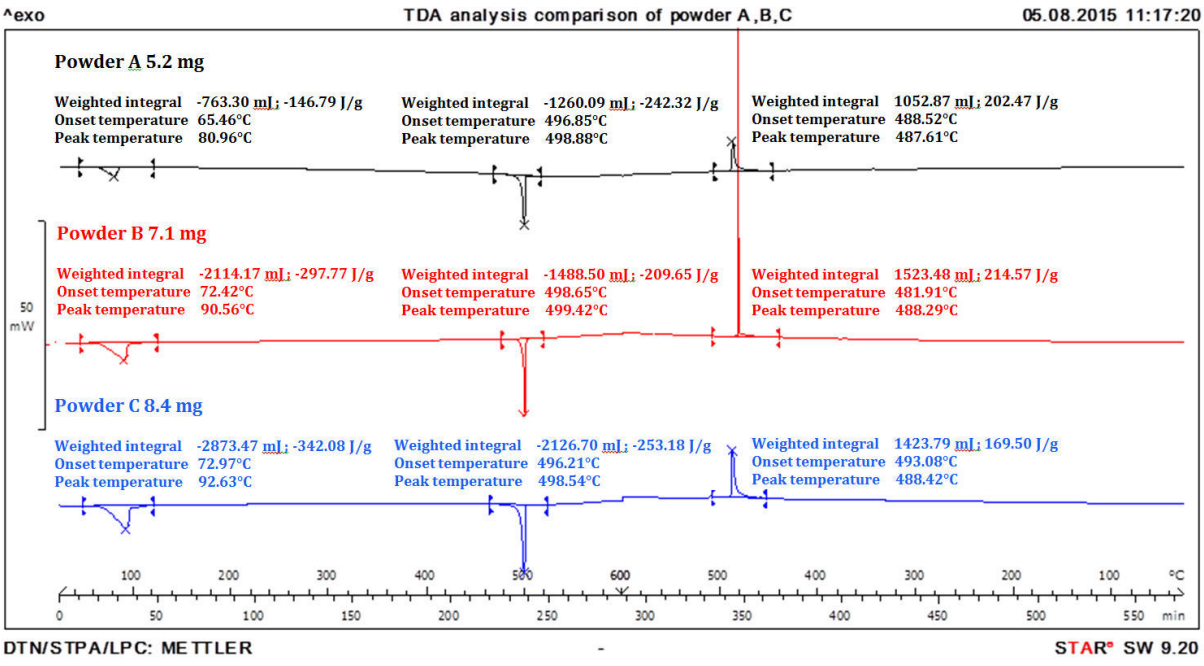

Figure 2-4. DSC chart results for Powder A, Powder B, and Powder C

2.1.2 Discussions

2.1. <u>Calculation methods</u>

The XRD is a valuable analysis integrated to the new characterization method compared to the former one. It highlights the presence of trona and $LiNaCO_3$, two compounds that were not mentioned either in the patents [2][3] or in the Reuillon's thesis [4]:

- Trona or sodium sesquicarbonate ($Na_2CO_3.NaHCO_3.2H_2O$)

Trona is in fact relatively abundant in nature. It is a natural ore composed of 46.53w% of sodium carbonate (Na_2CO_3), 34.82w% sodium bicarbonate ($NaHCO_3$), 14.92w% of hydrated water and 3.73w% of impurities (such as Na_2SO_4, insoluble, and others)[5]. It is known to be stable to up to 57°C under dry conditions. A single stage decomposition into sodium carbonate occurs at a temperature range of 77-214°C under N_2 atmosphere according to reaction (2-3)[6].

$$2(Na_2CO_3.NaHCO_3.2H_2O)_{(s)} \xrightarrow{\Delta H} 3Na_2CO_{3_{(s)}} + 5H_2O + CO_2 \uparrow ; 29.65\% \text{ loss} \qquad (2\text{-}3)$$

$$\Delta H_{R,\,298.15\,K} = 133.39 \text{ kJ.mole}^{-1}$$

The thermodynamic calculation of the reaction using HSC Chemistry[1] confirmed that the reaction is spontaneous above 105°C with $\Delta G_{200°C} = -89.8\ kJ$.

At intermediate temperatures, within 112-147°C, under CO_2 atmosphere, sodium carbonate monohydrate ($Na_2CO_3.H_2O$) and wegscheiderite ($Na_2CO_3.3NaHCO_3$) are formed as intermediates (cf. reaction 2-4). They then decompose according to reactions 2-5 and 2-6 respectively[7].

$$3\ (Na_2CO_3.NaHCO_3.2H_2O) \xrightarrow{\Delta H} Na_2CO_3.3NaHCO_{3.} + 2\ Na_2CO_3.H_2O + 4\ H_2O \qquad (2\text{-}4)$$

leading to 10.62 wt.% loss by H_2O release,

$$2\ Na_2CO_3.H_2O \rightarrow 2\ Na_2CO_3 + 2\ H_2O \qquad (2\text{-}5)$$

leading to 5.31 wt.% loss by H_2O release,

$$Na_2CO_3.3NaHCO_3 \rightarrow 2.5\ Na_2CO_3 + 1.5\ H_2O + 1.5\ CO_2 \qquad (2\text{-}6)$$

leading to 13.70 wt.% loss by H_2O and CO_2 release.

As reactions (2-4) and (2-5) have only water as product, CO_2 will behave as an inert gas in reducing the partial pressure of humidity over the solid, thus reaction shifts to the right. For the decomposition of wegscheiderite (reaction 2-6), CO_2 will delay the reaction. This delay breaks down at 157°C, since at this temperature the overall reaction ceases to be multi-stage to become single stage (reaction 2-3). However, its delay relative to nitrogen atmosphere condition showed that a reaction involving carbon dioxide, such as wegscheiderite decomposition, is rate controlling [6].

[1] HSC (H, S, and Cp) Chemistry is thermochemical software designed for various kinds of chemical reactions and equilibria calculations as well as process simulation.

At the same time $Na_2CO_3.H_2O$ decomposes at the temperature range of 63-127°C as confirmed in [8] and is proven to be a spontaneous reaction at above 85°C as calculated by HSC. Therefore, the first peak observed during heating in the DSC can be attributed to the heat release during the decomposition of both $Na_2CO_3.H_2O$ and trona contained in the powder since it shows the same temperature range. Moreover, the weight loss observed in TGA as well as the CO_2 concentration detected in µGC appears to be in the same temperature range as DSC.

Based on trona reaction of decomposition (cf. reaction 2-3), we might suppose that its formation from Na_2CO_3 and/or $Na_2CO_3.H_2O$ depend on the influence of humidity and CO_2 during storage. Therefore, an assumption has been made that trona is a product of aging, a hypothesis that will be validated by the aging experiments developed and discussed in chapter 3.1.

- Lithium sodium carbonate ($LiNaCO_3$)

$LiNaCO_3$ crystal was discovered from the phase diagram study of lithium carbonate and sodium carbonate. Several phase diagrams have been presented in §1.3.2. Indeed, the experiment result of its formation conducted in DSC (figure 2-5) with a mixture of 50:50 mole% of Li_2CO_3 and Na_2CO_3 shows the endothermic peak at 499 ± 0.5°C, which is consistent with diagram of Cairns et al [9]. Thus, this diagram is chosen as our guidance of information related to $LiNaCO_3$ formation later on. The enthalpy of melting is measured to be $\Delta H_m = 11.1\ kJ.mol^{-1}$ with the specific heat of $c_p = 2.1\ kJ.(mol.°C)^{-1}$. Figure 2-6 compares the XRD analysis of lithium and sodium carbonate composition (a) before and (b) after heating and cooling treatment in DSC. It can be seen that both presents different profiles.

It is shown in the DSC analysis of powders A, B, and C (cf. figure 2-4) that the second peak observed during heating may correspond to the melting point of eutectic as indicated by Cairns et al. However, the XRD result of powder B having no more $LiNaCO_3$ still have the melting temperature close to the other two powders. This confirms that the eutectic is formed even with separate grains of Na_2CO_3 and Li_2CO_3.

Nevertheless, its existence in the mixture might be related to the production method of the powder (whether it is produced by melting at high temperature or other methods?), which is unfortunately not known ever since the discontinued activity of the producer. Therefore, a study of the grinding effect to the mixture of Na_2CO_3/Li_2CO_3 and/or $Na_2CO_3.H_2O/Li_2CO_3$ was then performed and discussion around this aspect will be more developed in chapter 3.2 to elaborate this possibility. On the contrary, the aging may provoke its decomposition as will be thoroughly discussed in the aging experiments (chapter 3.1).

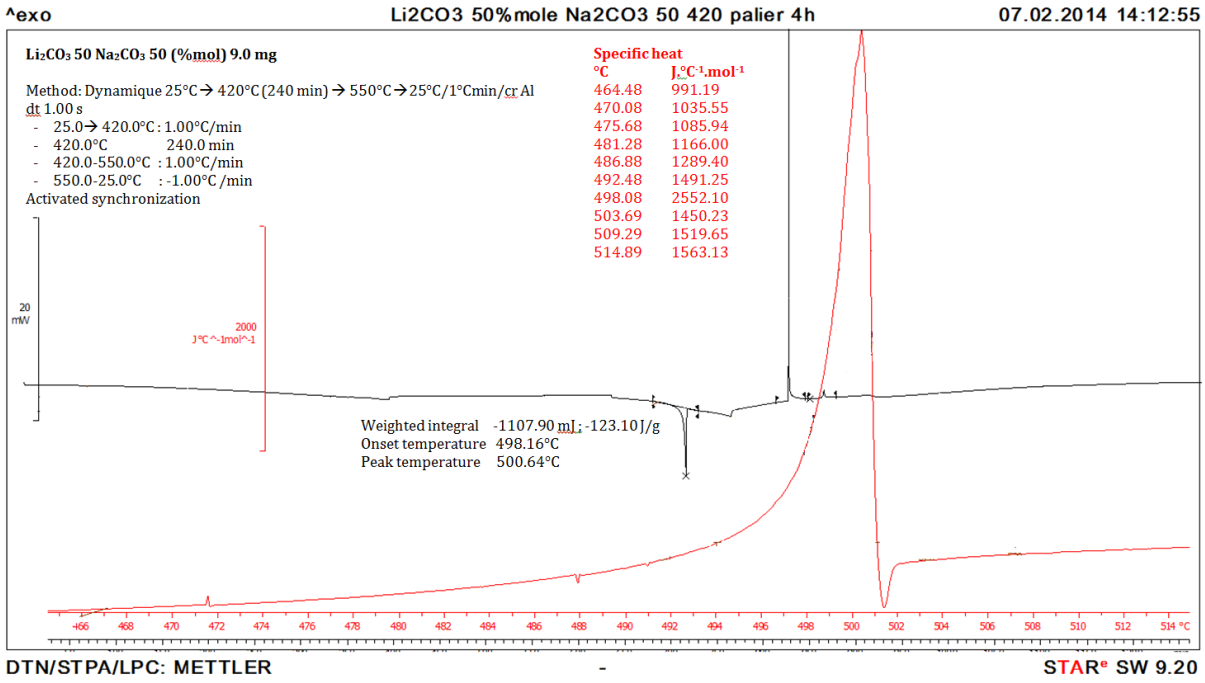

Figure 2-5. Thermogram of Li_2CO_3 and Na_2CO_3 mixture (50 mol% proportion) after treatment in DSC

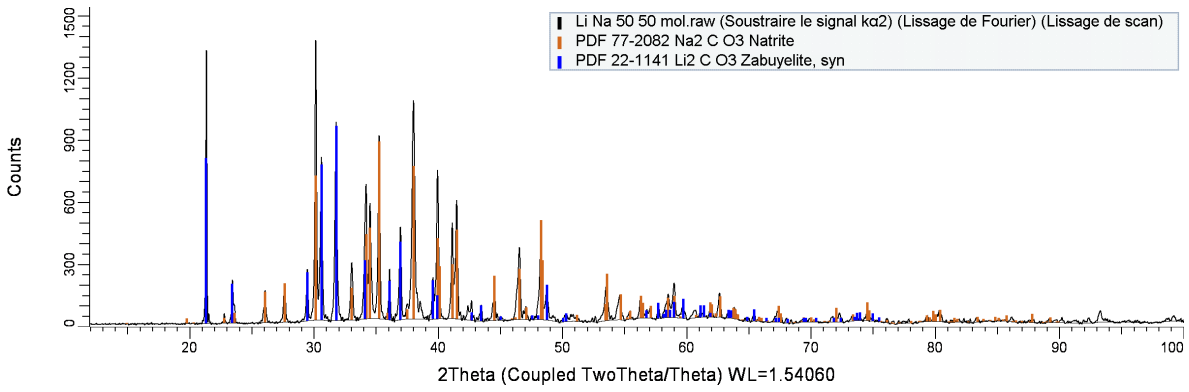

(a)

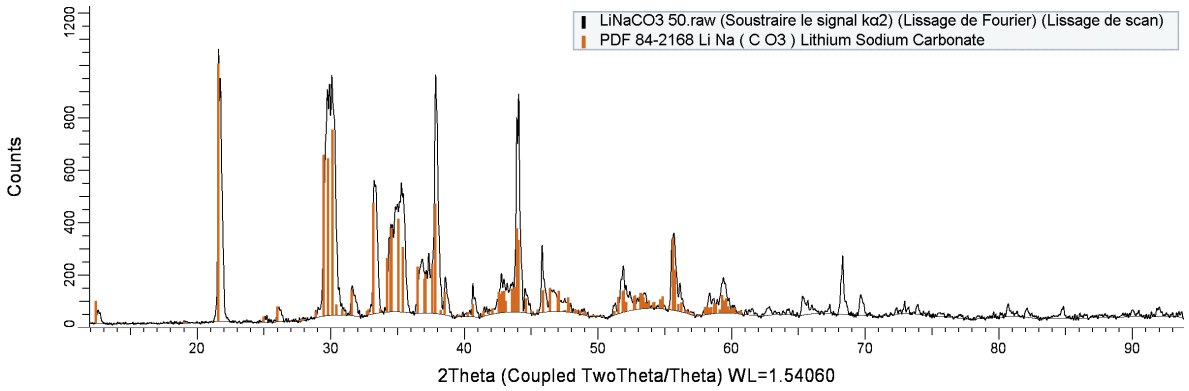

(b)

Figure 2-6. XRD profile (a) before DSC and (b) after DSC

Table 2-5 give summaries of the powders A, B, and C composition based on the semi quantitative of XRD. It must be underlined that due to the presence of graphite, which might alter the accuracy of measurement, the value detected for other components have been normalized. 9w% of graphite is then imposed to the system. Only powder A has a water content that is still in the range of specification, while powder B and C have four times amount higher than that of powder A. The only source of Marcalina composition can be obtained from its patent [2,3], in which Reuillon stated that 9w% of graphite mixed with 48w% and 43w% of sodium carbonate monohydrate and lithium carbonate respectively present the best performance of extinguishing sodium fire. It corresponds to 7%w of hydration water contained in the powder. The manufacturer, CACI, then determined the range of specification (in terms of quality control perspective) that depends on the water quantity from 4.8 – 5.4 (±1)w%. However, as the information of the composition is taken from the results of analytical composition providing separately the water content from sodium carbonate, the initial quantity is likely questionable. Nevertheless, if the water content is assumed to be in the form of hydration water contained in sodium carbonate, the quantity of minimum and maximum specification can be predicted with 21w% and 38w% of $Na_2CO_3.H_2O$ respectively.

Table 2-5. Summary of Marcalina composition from the literature and semi quantitative XRD results

Samples	**Composition (wt%)**					
	$Na_2CO_3.H_2O$	**Li_2CO_3**	**$LiNaCO_3$**	**Trona**	**Graphite**	**$H_2O_{[hyd]}$**
Marcalina [2,3]	48	43	0	0	9	7
Marcalina (spec min)	21	70	0	0	9	4.8
Marcalina (spec max)	44	47	0	0	9	6.4
Powder A (SQ-DRX)	23	26	41	1	9	6.1
Powder B (SQ-DRX)	32	29	0	30	9	25.4
Powder C (SQ-DRX)	7	22	26	36	9	23.0

The results of the physicochemical analyses previously conducted allowed the determination of the powder composition qualitatively and quantitatively (although in the latter case, hypotheses are necessary to conduct the calculation). Qualitatively, 2 types of powders could be distinguished from all samples that have been analyzed:

- The powder "in specification" (the least transformed powder or closest to original): high quantity of $LiNaCO_3$ and low quantity of trona (e.g. powder A),
- The powder "off specification" (the most transformed powder): low quantity of $LiNaCO_3$ and high quantity of trona (e.g. powders B and C)

The transformation of the powders is called aging as it is caused by more or less long time exposure in ambient conditions, but it does not anticipate on the extinguishing capacities of the powder, which is studied in a following chapter.

Quantitatively, two hypothesis were taken into account according to the nature of water present in the mixture: (1) hydration water and (2) free (not chemically bounded to other compounds) water.

First hypothesis: water is only present in the hydrated compound (sodium carbonate and trona).

The TGA analysis allowed us to study the decomposition of the powder up to 200°C. Reaction (2-3) and (2-5) described the thermal decomposition of trona and $Na_2CO_3.H_2O$, respectively. They both decomposed into Na_2CO_3, so the final composition in carbonates remains unchanged. However, the µGC could detect the release of CO_2 which can be used to distinguish and quantify the presence of these two compounds.

From the results of µGC analyses, the molar quantity of trôna and its related released water could be obtained based on the quantity of CO_2 detected (1 mole of CO_2 → 2 moles of trôna → 5 moles of $[H_2O]_{trona}$ cf. reaction 2-3). As the weight loss provided by TGA corresponds to the quantity of CO_2 and H_2O contained in the powder, the molar quantities of trôna and $Na_2CO_3.H_2O$ can be obtained as follows:

$$\Delta m = m\,CO_2 + m\,H_2O\ total \tag{2-7}$$

$$\Delta m = m\,CO_2 + m\,[H_2O]_{Na2CO3.H2O} + m\,[H_2O]_{trona} \tag{2-8}$$

Introducing: $x = mole\ trona$, $y = mole\ Na_2CO_3.H_2O$

$$\Delta m = \left(\frac{1}{2}x\,MCO_2\right) + \left(y + \frac{5}{2}x\right)MH_2O \tag{2-9}$$

$$y = \frac{1}{MH_2O}\left[\Delta m - \left(\frac{1}{2}MCO_2 + \frac{5}{2}MH_2O\right)x\right] \tag{2-10}$$

where M represents the molar mass of the compounds. x is obtained from CO_2 measurements and then y can be deduced from the total mass loss according to (2-10).

AAS analysis completed the results with the quantities of sodium and lithium. The equations (2-11) to (2-15) described the details of the calculation in order to obtain the molar quantities of Li_2CO_3 and Na_2CO_3.

$$mole\ Na = 2\ mole\ [Na]_{Na2CO3.H2O} + mole[Na]_{LiNaCO3} + 3\ mole[Na]_{trona} \tag{2-11}$$

$$\text{mole Li} = 2\ \text{mole}\ [Li]_{Li2CO3} + \text{mole}\ [Li]_{LiNaCO3} \tag{2-12}$$

Introducing: $p = mole\ LiNaCO_3$, $l = mole\ Li_2CO_3$

$$mole\ Na = 2y + p + 3x \quad \Leftrightarrow\ p = mole\ Na\ - 2y - 3x \tag{2-13}$$

$$mole\ Li = 2l + p \quad \_ \tag{2-14}$$

$$mole\ Na - mole\ Li\ = 2y - 2l + 3x \Leftrightarrow\ l = y + \frac{3}{2}x - \frac{1}{2}mole\ Na + \frac{1}{2}mole\ Li \tag{2-15}$$

Second hypothesis: No $LiNaCO_3$ is present; hence, the powder is highly hydrated and free water is taken into consideration.

A slight change is taken into account in the calculation, as the equations (2-7) and (2-8) are no more valuable, the molar quantities of Na_2CO_3 and Li_2CO_3 are obtained from the results of AAS analysis (this becomes possible as no more $LiNaCO_3$ is postulated).

$$mole\ Na = 2\ y + 3\ x \tag{2-16}$$

y = (mole Na – 3 mole $[Na]_{trona}$)/2 (2-17)

$$mole\ Li = 2\ l \tag{2-18}$$

$$l = mole\ Li\ /2 \tag{2-19}$$

For the results of TGA and µGC, free water is added into the equation (2-810) as follows:

$$\Delta m =\ m\ CO_2 + m\ [H_2O]_{\ Na2CO3.H2O} + m\ [H_2O]_{\ trona} + m\ [H_2O]_{\ lfree} \tag{2-20}$$

Knowing always x from the CO_2 release and y from equation (2-17), the quantity of free water is easily obtained from equation (2-20).

These calculations were applied to quantify the composition of the powders. Table 2-6 summarizes the results of the calculations and the comparison with the normalized SQ XRD.

Table 2-6. Summary of the composition calculations for the analyzed samples

No.	Samples	$Na_2CO_3.H_2O$ (%w)	Li_2CO_3 (%w)	$LiNaCO_3$ (%w)	Trôna (%w)	Graphite (%w)	Free water (%w)	Calculation method
1.	Powder A	31	33	26	1	9	0	Hypothesis 1
	Powder A	25	29	45	1	0	0	SQ XRD no graphite
	Powder A	23	26	41	1	9	0	Normalized SQ XRD
2.	Powder B	29	38	0	20	8	4	Hypothesis 2
	Powder B	36	32	0	33	0	0	SQ XRD no graphite
	Powder B	32	29	0	30	9	0	Normalized SQ XRD
3.	Powder C	16	35	18	26	5	0	Hypothesis 1
	Powder C	8	24	29	39	0	0	SQ XRD no graphite
	Powder C	7	22	26	36	9	0	Normalized SQ XRD

The results obtained from these two methods of analysis (XRD and chemistry analysis) exhibits differences. A normalization of values resulted from SQ-XRD analysis is needed because of the imprecision of the results due to the planar layered structure of graphite, which affects the measure of the peak intensity (preferential orientations) in the XRD analysis. Therefore, they are normalized by artificially adding 9wt% of graphite with the assumption that graphite is the

component least influenced by aging. Even so, large differences were still identified because the lack of precision notably for the semi quantitative XRD analysis that depend mostly on the I/I_{cor} coefficient of the chosen phases. Thus, the results of SQ XRD can only be used to determine the order of magnitude of the composition. More precise results could possibly be obtained by quantitative analysis by fitting the peak with the Rietvield method. Considering this, it is assumed that the best precision is obtained with chemical analysis.

2.2. Accuracy of calculations

Four indicators of error are established to verify the accuracy of calculation:

- $\alpha = \left|\frac{\Delta w_{TGA} - \Delta w_{furnace}}{\Delta w_{furnace}}\right| x100\%$
- $\beta = \left|\frac{wt\%\ of\ graphite\ filtered - 9\ wt\%\ (theoretical\ value\ in\ the\ patent)}{9\ wt\%}\right| x100\%$
- $\gamma = \left|\frac{molar\frac{Li}{Na}ratio\ obtained\ from\ AAS - 1.43\ (theoretical\ molar\ \frac{Li}{Na}ratio\ in\ the\ patent)}{1.43}\right| x100\%$
- $\delta = \left|\frac{calculated\ total\ weight\ from\ chemical\ analysis - initial\ weight\ (before\ AAS\ analysis)}{initial\ weight}\right| x100\%$

The parameters α, β, γ involve the possible first source of errors obtained from dosing the quantity of H_2O and CO_2 (in ATG-µGC/furnace), graphite (filtration), and sodium-lithium (AAS) respectively. Meanwhile, parameter δ represents the difference of calculated weight (obtained from each analysis) compared to the initial weight of powder, which depends on the precision of each analysis method that are related one to another.

However, each parameter α, β, γ presents certain limits towards δ as follows:

- Parameter α only takes into account the quantity of H_2O and CO_2, which is then used to determine the quantity of trona using the molar ratio of the reaction 2-6 (1 mole of CO_2 = 2 moles of trona). Since the total Na (measured by AAS) is then distributed between trona, hydrated sodium carbonate and $LiNaCO_3$, this parameter does not affect the calculated total weight. Thus, high error in α may not give any influence to δ.
- Parameter β influences the dosing of Na and Li contained in the filtrate during AAS analysis. Hence, bad filtration step may alter the total weight calculated (thus affecting δ value).
- Parameter γ calculates the value of molar ratio (whether or not it is far from 1.43), while the concentration values are the ones that count in δ. One can have the same ratio but completely different concentration values. Hence, a good value of γ may not cause high error in δ.

Overall, parameters α, β, γ may indicate high errors, but give good results in δ. The above parameters have a limitation as it is not able to estimate the molar ratio of trona and sodium carbonate monohydrate. Besides, reducing δ also requires the improvement of Li and Na dosing in AAS. Hence, it is suggested that all four indicators present satisfactory results to obtain good composition in each powders. The uncertainty parameters for powders A, B, and C are reported

in table 2-7. It appears that only powder A has small error as it, indeed, has the least transformation than powders B and C.

Table 2-7. Summary of the parameter of errors for the analyzed samples

Error	Powder A	Powder B	Powder C
α	0.1%	0.7%	20.5%
β	4.3 ± 0.1%	19.9 ± 0.2%	29.5 ± 0.3%
γ	2.2 ± 0.1%	3.4 ± 0.1%	0.2 ± 0.1%
δ	0.2%	14.5%	18.5%

2.2. *Physical properties analyses methods and results*

The physical properties are indispensable information in terms of the employability of these powders as an extinguishing agent. As differences of colors are observed in several samples, ranging from dark to light grey, the evolution of physical properties during aging might be interested notably to understand its impact on the flowability.

2.2.1 Scanning Electron Microscopy (SEM)

Two SEMs were used to analyze the microstructure of the powders. An Environmental SEM Philips XL30 ESEM FEG equipped with Field Emission Gun (FEG) in a controlled pressure chamber has been used to characterize the size of the particles. The powder samples were deposited on a cylindrical support of 1 cm diameter via a double sided carbon tape. A SEM EVO MIS HD Carl Zeiss with LaB6 as filament in vacuum condition is also used to observe the microstructure of powders exposed in aging experiments.

Figure 2-7 displays the different microstructures of these powders at two similar magnifications observed with Environmental SEM. Powder A is constituted of regularly shaped rod-like particles (5µm length), which coexist with larger particles of 20µm length. On the other hand, powder B is made of much bigger particles with 100µm irregular shapes (with agglomerated needle shape particles). Powder C looks more similar to powder A, although most of its needle shape particles appeared to be broken when compared to powder A.

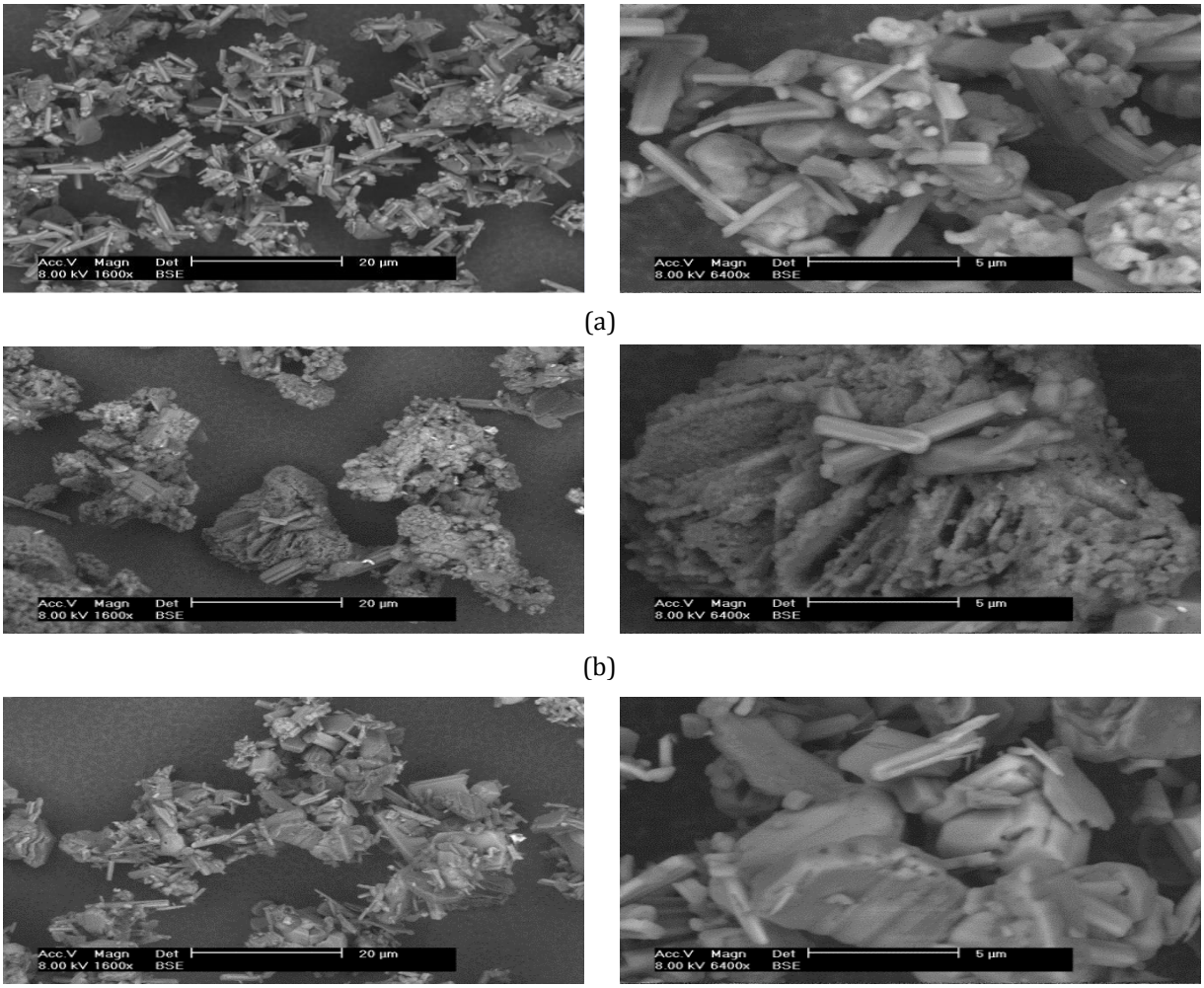

Figure 2-7. SEM images of (a) Powder A (b) Powder B (c) Powder C with 1600x (left) and 6400x (right) magnifications

2.2.2 LASER particle size analysis

The particle size distribution of the powder was determined using LASER diffraction equipment from Malvern model Mastersizer 2000. The size distribution is inferred from the interaction of a set of particles and the incident LASER beam by analyzing the beam diffraction spot. It measures the angular variation of the scattered light intensity when the beam passes through a sample of the dispersed particles. Large particles scatter light at small angles relative to the beam and with high intensity, while the smaller particles scatter light at higher angles and smaller intensity. The dry method was used, in which the powder is conveyed in the measuring cell by means of compressed air within the pressure range from 1.5 to 3.5 bars.

For powder A, a pressure of 3.5 bar was applied and the particle median diameter (D_{v50}) was found to be 5.62 µm with monomodal distributions. The pressure was varied from 1.5, 2.5, and 3.5 bars for powders B and C. A slight particle enlargement was observed in powder C with 7.43 µm (monomodal distribution) with respect to powder A, while particles B were found to be six

times bigger than powder A with an average size of 30.3 µm and a multimodal distribution. The summary of the particle size analysis results is reported in table 2-8.

Table 2-8. LASER particle size analysis results

No.	Samples	Pressure (bar)	D_{v50}[a] (µm)	Distributions
1.	Powder A	3.5	5.6	Monomodal
2.	Powder B	1.5	28.9	Monomodal
		2.5	29.9	Multimodal
		3.5	30.3	
3.	Powder C	1.5	8.2	Monomodal
		2.5	7.6	
		3.5	7.4	

[a] D_{v50} is the median particle size in volume distribution that splits the distribution with half above and half below this diameter.

2.2.3 Volumenometer

The packed densities were measured by a volumenometer Erweka. A known mass of powder was introduced into a graduated test tube of 250 cm^3 and the bulk volume was recorded after certain number of standard taps (400 taps). Based on these results, the Carr Index (CI) representing the indicator of flowability and the Hausner Ratio (HR) as the compressibility index can be evaluated. Both indexes should be defined from the results of bulk and tapped density measurement. Generally, the free flowing powders have low CI (<15%) and low HR (<1). On the contrary, cohesive powders exhibit higher compressibility, thus having a higher CI (>25%) and higher HR (>1.4) [10].

The summary of the tapped and bulk densities as well as the calculated Carr and Hausner indexes of the powders are listed in table 2-9. This index is used to categorize the powders based on their flow behavior. Powders A and C have similar tapped and bulk densities, while their values are doubled for powder B. Based on the Carr Index, these three powders are comprised in the moderate flow category, whereas the Hausner Index considers them as slightly compressible and cohesive. These results are in contradictory with those obtained from FT4 rheometry, which shown a cohesive characteristics for powder A, C and easier flowability for powder B. This can be explained by an agglomeration phenomenon that happened more easily for powder A and C during tapping, thus allowing the particles to occupy a bigger volume and to be less dense than in powder B.

Table 2-9. The summary of the volumenometer analysis results

Sample	Tapped density ($g.mL^{-1}$)	Bulk density ($g.mL^{-1}$)	I_C[1]	I_H[2]
Powder A	0.38	0.32	0.16	1.19
Powder B	0.69	0.54	0.22	1.28
Powder C	0.37	0.30	0.21	1.26

[1] Carr Index : $I_C = \frac{\rho_{tap} - \rho_{bulk}}{\rho_{tap}} = \frac{\rho_\infty - \rho_0}{\rho_\infty}$ (2-21)

[2] Hausner Index : $I_H = \frac{\rho_{tap}}{\rho_{bulk}} = \frac{\rho_\infty}{\rho_0} \geq 1$ (2-22)

2.2.4 Helium pycnometer

The particle's true densities were measured by a helium pycnometer AccuPyc 1330 of Micromeritics. It consists of 2 cells: calibrated volumes V_1 (the powder cell) and V_2 (expansion cell) connected by a valve. Both cells were initially at the atmospheric pressure P_A and an ambient temperature T_A. The volume cell V_1 was then charged by a superior pressure P_1. When the communicating valve was opened, the gas permeated the cell volume V_2 which causes a pressure drop to a value of P_2. As a result, the true density can be obtained by the powder mass ratio between the powder placed on V_1 and the volume calculated by the apparatus.

The true particle density represents the ratio of the weight over the volume of the grains. The results for the three powders are of the same value with 2.2 g.mL^{-1}. Using equation (2-23), the bulk porosity of the powders can be calculated. Powder A and C are composed of 86% of porosity, to be compared with the less porous powder B with 75% porosity.

$$\rho_{bulk} = \rho_{true}(1 - \varepsilon) \quad (2\text{-}23)$$

2.2.5 FT4 powder rheometry flow test

As the powder will be spread on the sodium fire, the flowability will be an interesting property to be studied. An FT4 powder rheometer from Freeman Technology (Gloucestershire, UK) is designed to characterize the rheology or flow properties of the powders. It measures the resistance of the powder to flow in motion. A precision blade, or impeller, is rotated and moved downwards and upwards through the powder to establish a precise flow pattern causing particles to interact, or flow relative to one another (see figure 2-8). The rotational and vertical resistances experienced by the blade represent the difficulty of this relative particle movement, or the bulk flow properties, which are measured in the form of torque and force respectively. Both signals are represented as a Total Flow Energy, which is the energy required to move the blade through the sample from the top to the bottom of the powder column. Although due to the constant change of both values, it is necessary to calculate the energy for each small distance travelled, known as the Energy Gradient expressed in mJ/mm.

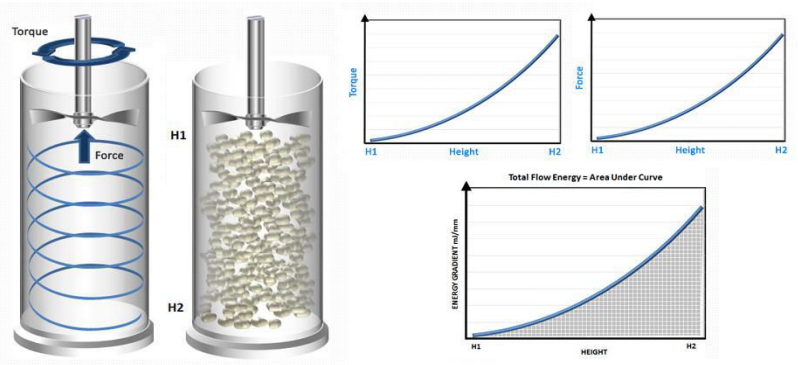

Figure 2-8. The basic principle of flow measurement in FT4 powder rheometer

There are two types of flow pattern that are typically employed for quantifying flowability (cf. figure 2-9):

- Forced (confined) flow

It measures the powder's flowability when forced to flow. The powder is confined by the closed bottom end of the test vessel. This property is defined as the Basic Flowability Energy (BFE) and is measured during the downward blade movement.

- Low stress (unconfined) flow

It measures the powder's flowability when unconfined. The resistance to flow is measured as the blade crosses from the bottom of the vessel to the top. As there is no solid surface at the top of the vessel preventing the powder from dilating and moving upwards, the powder is unconfined during this test. This property is defined as the Specific Energy (SE).

The regimes of confined and unconfined flow are very different and so it is important, when correlating data with process performance, to identify which regime is most representative of the process being considered.

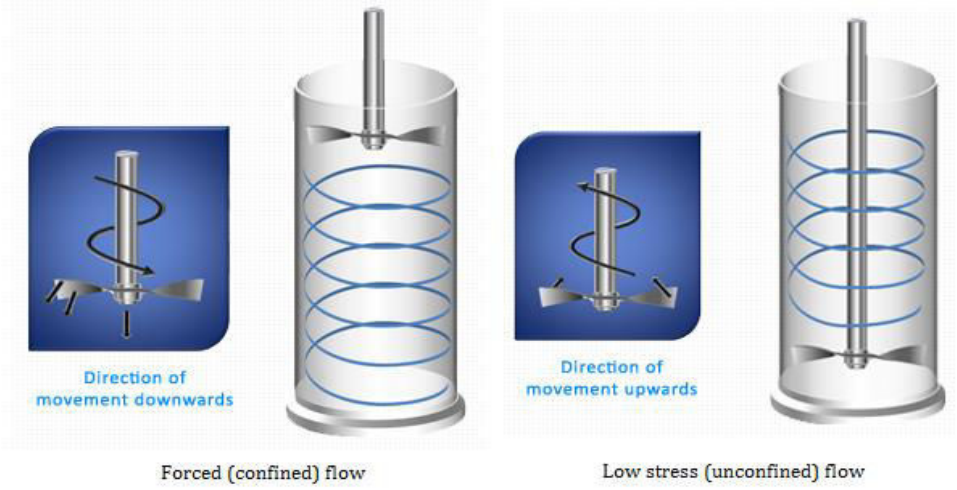

Figure 2-9. Two types of flow pattern employed in FT4 powder rheometer

Basically a *conditioning cycle* (see figure 2-10) is usually completed prior to every test in order to remove the variability introduced by the operator during loading of the sample, and any residual compaction from previous tests (except if a consolidated sample is intentionally being evaluated). The process involves gentle displacement of the whole sample in order to loosen and slightly aerate the powder. The aim is to disturb and gently drop each particle in order to construct a homogenously packed powder bed, removing any pre-compaction or excess air and ensuring the results from the following test are independent of how the operator handles the powder and places it into the testing vessel.

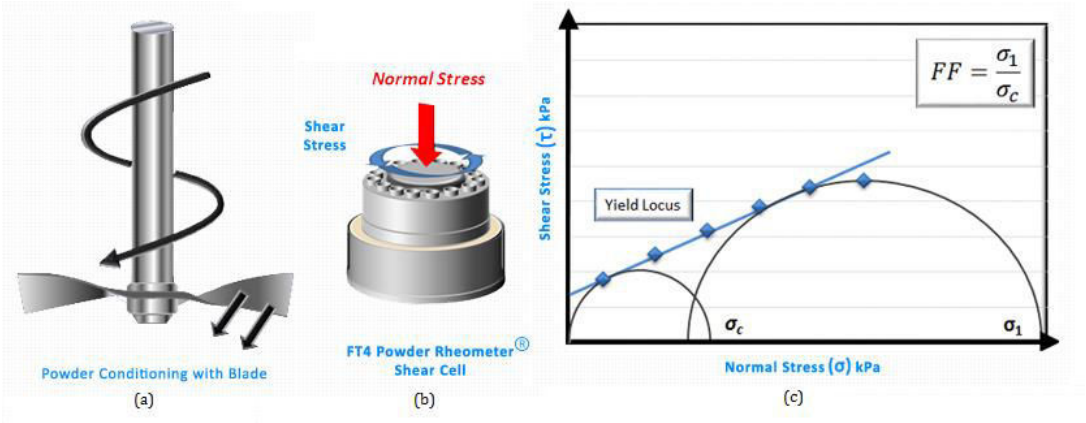

Figure 2-10. (a) The powder conditioning cycle with blade, (b) the FT4 powder rheometer shear cell, (c) the yield locus plot

The FT4 also includes a Shear Cell accessory to perform a shear testing, which is a fairly static test, measuring the powder's behavior as its transitions from no-flow to flow. It always characterizes the powder in a consolidated state. It is ideally suited to predicting powder behavior in process operations where the powder is consolidated and where flow rates are low and/or sporadic.

Shear cell test was conducted at very small speeds, in which a shear (or horizontal) force is applied to an upper layer of powder whilst the adjacent lower layer is prevented from moving (or vice versa). The force is increasing but no relative movement at the shear plane occurs until the shear force is sufficiently high to overcome the powder's shear strength, at which point the powder bed 'yields' and the upper layer of powder slips against the lower. Figure 2-10 showed the shear cell design used in FT4 powder rheometer. Several shear tests were carried out at different levels of normal stress. The data produced represent the relationship between shear stress and normal stress, which can be plotted to define the powder's Yield Locus (cf. figure 2-10). In simple terms, the higher the shear stress for a given normal stress, the less likely it is that the powder will yield and begin to flow when confined under a similar consolidation stress in a hopper or other vessel. For each sample, the yield locus were obtained for 2, 4, 8, and 16 kPa values of normal stress and each were analyzed using Mohr stress circle analysis to obtain the values of unconfined yield strength (f_c) and major principle stress (σ_1) plotted on a graph afterwards. The set of yield locus determined for different consolidation allows us to obtain the flow function whose index can determine the flowability type of the powder according to the Jenike classification (cf. table 2-10).

Table 2-10. Jenike classification of powder flowability by flow index (i) [11]

Flowability	No flow	Cohesive	Easy flow	Free flow
Flow index (i)	<2	<4	<10	>10

An example of a typical yield locus of powder A for 2kPa is presented in figure 2-11. The yield locus was fitted by the Warren Spring equation $(\frac{\tau}{C})^n = \sigma + T/T$ where n (shear index) is a measure of curvature of the yield locus. From each yield locus, the following two quantities were estimated by two specific Mohr circles: the unconfined yield strength (UYS) and the major consolidating stress (MCS). A solver was used to fit, by iteration, the data points to the Warren Spring equation and to construct the Mohr circles tangent to the yield locus. The same type of calculation is conducted for the other consolidating stresses. The UYS and MCS obtained from each consolidating stress can be used to trace the flow function, which is a plot of UYS versus MCS. It produces the stress needed to make an arch collapse or to make the material flow. The inverse of its slope is the flow index (i) which is used as an index of the flowability of a powder according to the Jenike's classification (cf. table 2-10)[11].

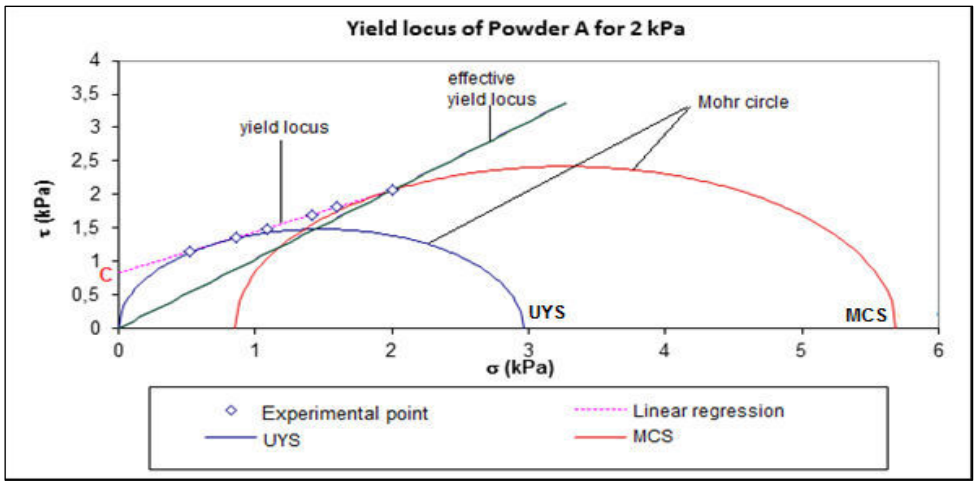

Figure 2-11. Yield locus of powder A for 2 kPa

Typical flow functions for powder A, B, and C are presented in figure 2-12. It shows that powder A has a cohesive characteristic in 2 kPa. The higher the consolidating stress applied, the less cohesive it would become. Nevertheless, the powder would still be categorized as a cohesive powder at high stress value. It turned out that at higher stresses, powder C has the same tendency as powder A to be cohesive, while powder B is capable to flow easily. Thus, the results are in a good agreement with the particle size measurements.

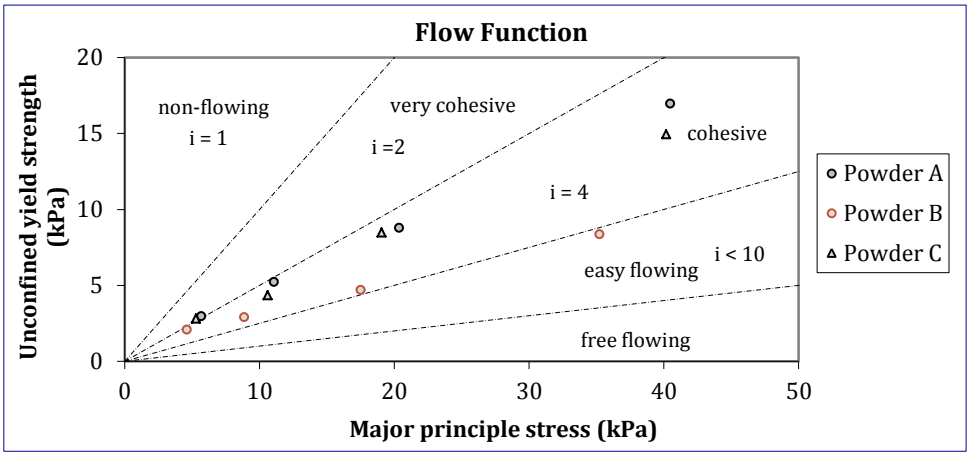

Figure 2-12. Summary of powder's flow function

2.2.6 *Dynamic Vapor Sorption (DVS)*

DVS is a gravimetric technique in which a powder sample is subjected to varying conditions of air humidity and temperature. The temperature of analysis was set at 25°C. Humidity was varied between 0 to 90% in 10% increments for adsorption cycle continued by desorption cycle started from 90 to 0% humidity with the same increments. The criteria of the equilibrium were calculated in the function of mass introduced with the sensibility of 5 micrograms for the balance. The period fixed for each plateau was between 10 minutes (min) to 360 minutes (max).

This analysis permits to obtain a first estimate of weight gains at different humidity conditions which may be representative of different storage conditions. These three powders start to gain weight under 78.5%RH during the adsorption cycle. Powder A exhibits the largest weight change with 44.6%, while both powders B and C gain less than half of it with 20.4% and 14.6%, respectively. The desorption cycle of the products demonstrates the recrystallization as powder A turns into two separate products with a distinguishable color difference. The same behavior is also observed for powders B and C. Figures 2-13 – 2-15 present the results of DVS isotherm chart for powders A, B, and C. The hysteresis demonstrated in the figure represents the stability of the sample towards the fluctuation of humidity. This hysteresis might be corresponds to the passage of sodium carbonate monohydrate to decahydrate starts at 70%RH in ambient temperature. Thus, it relates to the stability of the sample. The narrower is the hysteresis, the more stable is the sample. These powders showed that they are less stable in the conditions of more than 50%RH, although it seems that powder A is more sensitive even at lower humidity (<50%RH) as the desorption cycle showed that a slight water uptake (≈ 2w%) is still observed.

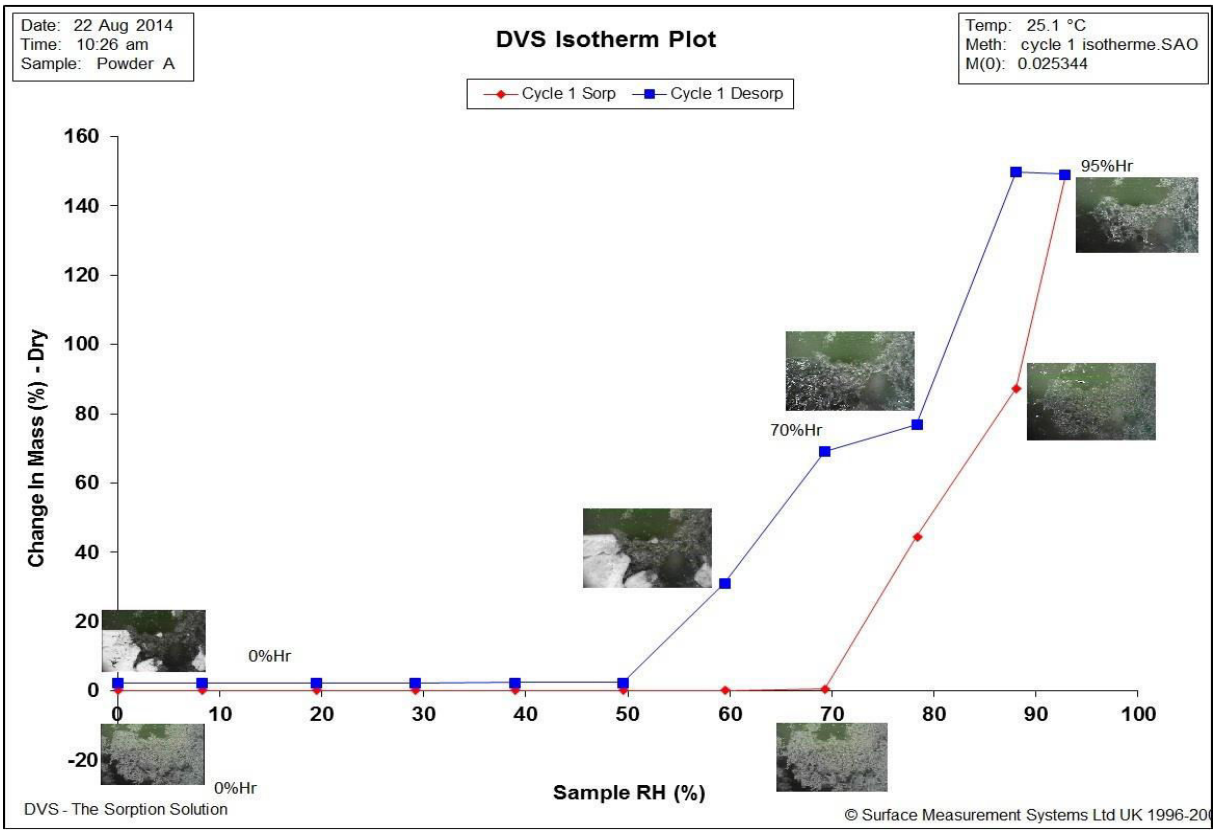

Figure 2-13. DVS isotherm chart plot for powder A

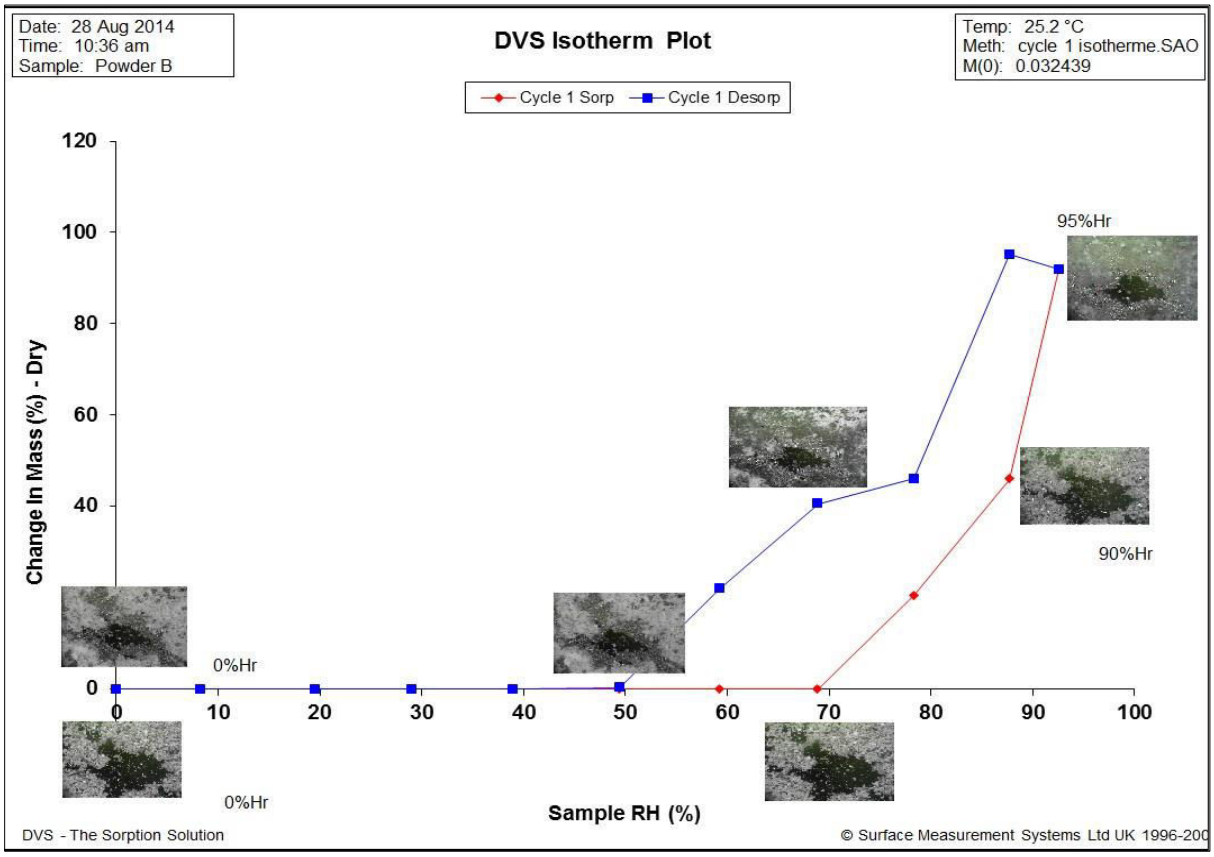

Figure 2-14. DVS isotherm chart plot for powder B

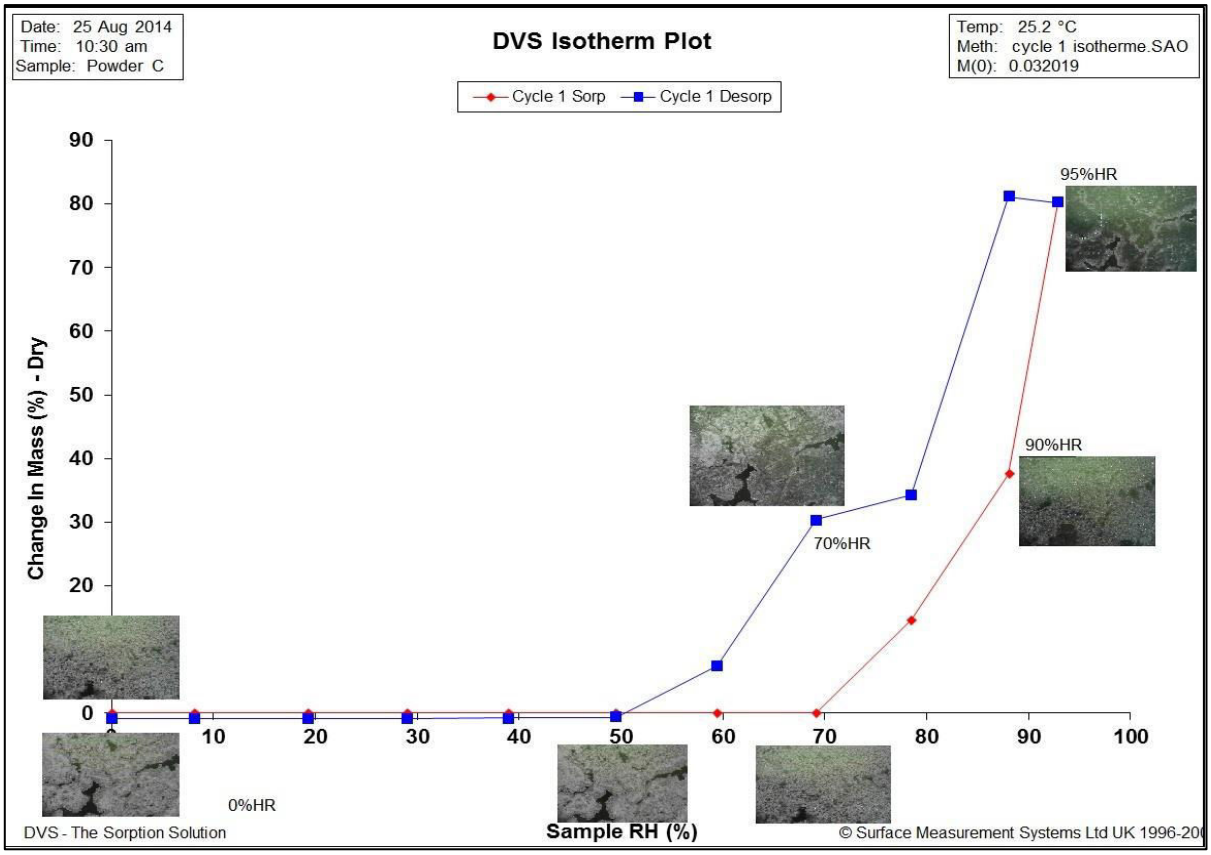

Figure 2-15. DVS isotherm chart plot for powder C

2.3. *Methods of aging, production and extinction analysis*

2.3.1 Study of aging

The chemical analyses highlight the presence of trona and $LiNaCO_3$, two compounds that were not mentioned either in the patents [2,3] or in the Reuillon's thesis [4]. A study to understand the origin and/or decomposition of both components during aging is then developed. A comprehension of the aging mechanism is expected based on this study to understand the variation of composition observed in powders A, B, and C.

Considering that the powder is initially composed of sodium carbonate monohydrate ($Na_2CO_3.H_2O$) and lithium carbonate (Li_2CO_3) in the patent, $Na_2CO_3.H_2O$ is then taken as the pure sample of interest. Lithium sodium carbonate ($LiNaCO_3$), however, is supposed to be part of the initial composition of powder since the literature study indicates that it can only be formed during fusion of sodium and lithium carbonates at high temperature. Moreover, powder whose water content is higher than that of specification has lesser quantity of $LiNaCO_3$. Therefore, it is also become the object of observation. Furthermore, as powder A is the only sample whose water content is still in the range of specification, it is chosen as the referent Marcalina sample.

$Na_2CO_3.H_2O$ of Sigma Aldrich with ≥ 99.5% purity was used. As $LiNaCO_3$ is not commercially available, it was produced by heating the sodium carbonate (Na_2CO_3) and lithium carbonate (Li_2CO_3) in 50:50 molar proportions at 600°C until the salts melted. The melt was allowed to cool

slowly within the furnace down to room temperature where it was left until the following day. Then, it was slowly reheated to 420°C, hold at that temperature for 4-5 h, and again cooled to room temperature in the furnace, as proposed in [12].

Six desiccators equipped with saturated saline solutions were prepared to store the samples listed in table 2-11. Three solutions were employed in order to control the relative humidity at low (8%, KOH), moderate (33%, $MgCl_2$) and high (75%, NaCl) values. Besides humidity, the role of ambient carbon dioxide was also studied. Therefore two conditioning methods (with and without the air passage) were applied (cf. figure 2-16). XRD analysis was conducted to understand the evolution of powder compositions. The experiments were realized in the span of 8 months.

Table 2-11. Samples and conditions of the aging experiments

Samples	**Low humidity**		**Moderate humidity**		**High humidity**	
	Without CO_2	With CO_2	Without CO_2	With CO_2	Without CO_2	With CO_2
$LiNaCO_3$	x	x	x		x	x
$Na_2CO_3.H_2O$	x	x		x	x	x
Powder A	x	x		x	x	x

Figure 2-16. The storage conditioning setups of the aging experiments without the air passage (left) and with the air (CO_2) passage (right)

2.3.2 Study of production method

The quality of powder currently in stock regarding their extinction capacity is still questionable and part of the objective of this thesis. Still, the information related to their fabrication is essential so that the prevention of sodium fires remain ensured in the future. Indeed, after the cease activity of CACI, the knowledge deprivation of how to reproduce Marcalina is one of several issues to be answered nowadays. On this regard, the study is focused on the grinding technique since it is not only able to decrease the particle size, but also ensure the powder homogenization.

The original materials listed in the patents relative to Marcalina were used, which includes lithium carbonate (Li_2CO_3), sodium carbonate monohydrate ($Na_2CO_3.H_2O$), graphite (C), as well as anhydrous sodium carbonate (Na_2CO_3)[2,3].

Two types of grinding apparatus were used: automated mortar grinder and planetary ball mill. These grinders are chosen in order to compare the composition of product after grinding with different type of grinder (thus, different technique/mechanism). This information will be useful to consider the choice of grinder in the industrial application perspective.

- *Automated mortar grinder* [13]

The Retsch RM100 mortar grinder comminutes, mixes, and homogenizes the samples by pressure and frictional forces. The scraper slows the motion about 50% and feeds the material into the area between the mortar and pestle. This force feed ensures that the entire sample is continuously subjected to the grinding, homogenization process, and is also mixed thoroughly. The necessary grinding process is achieved by weighing of the pestle itself combining with the adjustable spring pressure acting on its axes.

- *Planetary ball mill* [14]

The planetary ball mill Fritsch Pulverisette 6 mono mill classic line was used as another grinding process. The grinding bowls, which are mounted on the main rotating sun disk, rotate in the opposite direction around the center of this disk. Due to this movement, the sample is comminuted very effectively and fast by impact, shearing, and friction forces resulting from ball-to-ball and ball-to-wall collisions. With the planetary movement, the grinding bowl filling is subjected not only to the force of gravity, as in the case with conventional ball mills, but centrifugal and coriolis (inertial) forces further increase the kinetic energy of the grinding parts. Zirconium oxide balls were used as the grinding sets for this experiment. The rotational speed was varied among 100, 200, 300, 400, 500, and 600 rpm during each 1h milling with pause of 10 minutes for each 15 minutes and reserve mode (allowing the mill to change its direction of rotation, thus improve the sample homogeneity).

2.1.3 Study of extinction

Powders A, B, and C are used as the Marcalina powder samples of interest. Besides these powders, synthetic powders of different chemical compositions were prepared for the extinction tests. Details of the latter as well as the choice of their compositions will be explained in chapter 4. The raw materials were first milled in the planetary ball mill then sieved using Fritsch Analysette Pro 3 Sieve Shakers: only the particles with a size ≤ 63 µm were used. This particular size range was taken in order to produce a synthetic powder as representative as possible of Marcalina (see § 1.3.1). The sieved materials were then mixed in a Turbula T2F, commercialized by WAB society, to get homogenized final samples. Turbula is a reversing mixer based on the combination of three movements: translation, rotation and inversion. This combination results in a three-dimensional movement close to a chaotic one and allows obtaining homogeneous mixtures rapidly in many industrial cases. Each sample produced was analyzed by XRD to verify the composition.

The Chris(X)ti-Na, short from eXtinction Na, test device is a facility that is dedicated to study the extinguishing properties of the powders in a small sodium pool fire [15]. Figure 2-19 (a) shows the sketch of the test facility, while (b) shows the real facility with magnification on sodium container and powder spreader. It is located in a 168 m^3 installation equipped with high air flow ventilation (5,400 m^3/h) to extract the caustic smokes produced as the results of combustion.

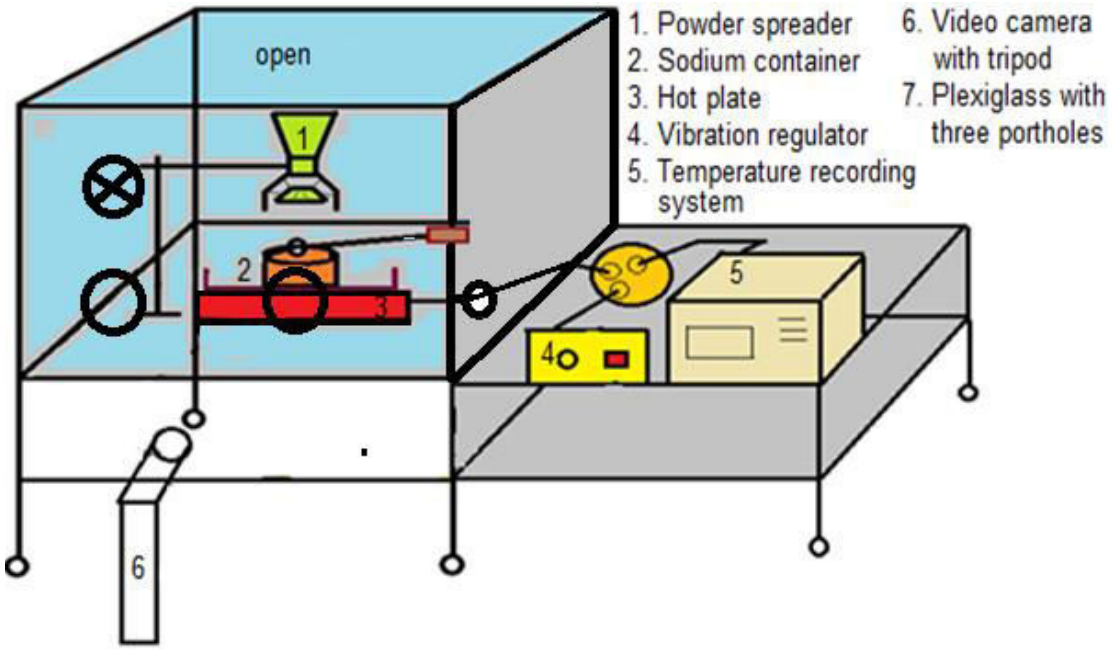

(a)

(b)

Figure 2-17. The Chris(X)ti-Na test facility (a) diagram (b) reality

The Chris(X)ti-Na experimental setup consists of a metallic table equipped with a powder spreader device, which is placed above a 78.5 cm^3 stainless steel crucible (as a sodium container heated with an electrical hot plate) and the measurements devices. The sodium is conserved in a sealed insulated stainless steel container where temperature can be raised up to 500°C using an electric hotplate. Fire extinction is observed by the temperature measurements and by video recording of the experiment. Four thermocouples are installed inside the sodium container at different important locations: inside the sodium, at the sodium pool surface, in the flame and the powder. The position of the thermocouples is detailed in figure 2-21. Ten grams of sodium are used in each experiment, having 0.7 cm of height. Two spreading methods were studied with the help of two powder spreader devices: (a) the powder vibrator and (b) the powder trap, for two different ways of spreading: gradually and instantaneously. Both methods are shown in figure 2 -22 (a) and (b) respectively. The vibrator sieves allow the powder to be spread continuously, thus the observation of the influence of chemical properties can be achieved in a slower and precise way, as for which the vibration can be stopped whenever the extinction is achieved. Meanwhile the trap door (in a form of a manually mobile blade) allow powder to be spread once all of sudden in which the same quantity of powders (5 g) would be maintained on each test, hence the efficiency of the powders can be compared.

The sodium was put in a stainless steel container wrapped by the heat insulator in order to prevent the heat losses. The container was connected to a stainless steel cone, through which an inert gas was introduced in order to prevent sodium oxidation. Furthermore, a container lid was placed onto the ensemble preventing the direct contact with oxygen during heating by a hotplate. As soon as the sodium temperature attained 450°C, the aspiration system was started and the inert gas circulation was stopped. The container lid was then removed, allowing a direct contact of liquid sodium with the oxygen. Even if there was a sodium oxide layer observed on the surface of liquid sodium, the fire took place in a few seconds. After the sodium fire has established (sodium temperature around 540°C), the powder in the reservoir located above the sodium container was spread. In case of continuous powder spreading, a vibration regulator allowed us to control the spreading rate between 4.5-5.5 Hz. The hotplate was unplugged to prevent the renewal of heat source. The vibration was stopped when no more flames were observed. The mass of powder loss (that either fell outside of the container or remained in the sieves) was noted. The difference between the initial mass of powders stored on the reservoir with the one lost during the experiment indicated the mass of the powder used to extinguish the sodium fire. Meanwhile in the case of direct spreading, the powder directly fall at once in the receptacle. 5 grams of each powder samples were used to extinguish 10 grams of sodium whether or not the extinction is obtained. The combustion residue was then cooled down to room temperature for sampling. The sequence of the experiments was recorded by a video camera. Test personnels were protected by Nomex© gowns, fire-resistant gloves, and full face shields.

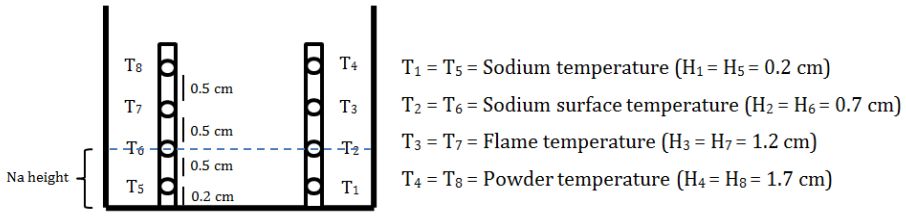

Figure 2-18. The position of thermocouples inside the sodium receptacle

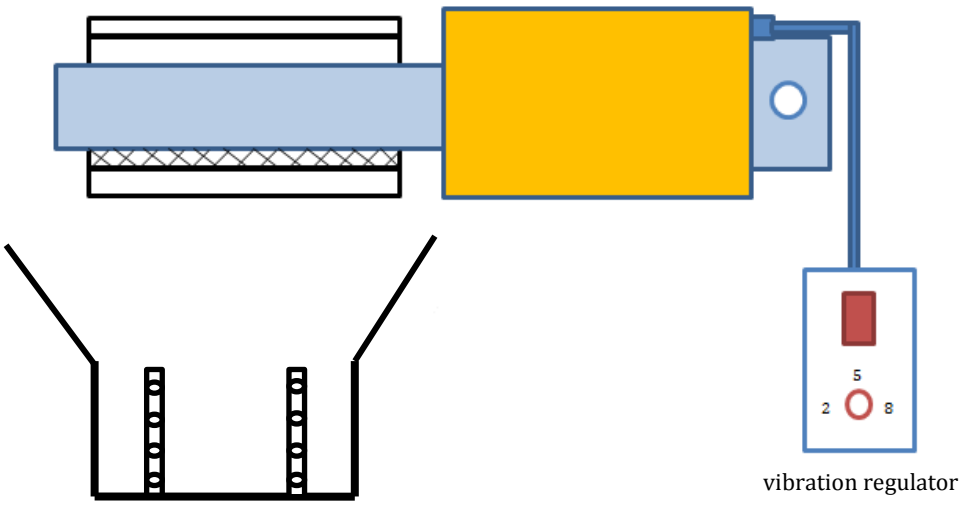

(a-1)

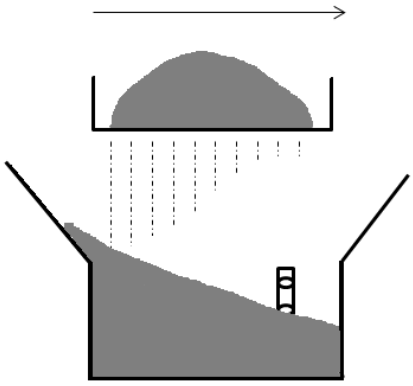

The translation movement of the vibration starts from the left to right. The faster vibration was setting, the faster will be the movement. Thus the profile of powder distribution on the receptacle will be more homogenous. However, it should be noted that, the vibration setting must not exceed the intensity of 5.5 Hz to make sure the sieve keeps steady in place and prevents the risk of powder blows up from the sieve during the experiment. The profile on the left shows the powder distribution that is generally produced during the experiment. The powder distributes more dominantly in the left side than in the right. The experiment were conducted using mostly 5 Hz of vibration intensity. Fortunately the cone barrier placed in the receptacle allows some powders that remain in the cone to slip down to the receptacle, thus covering up some uncovered spaces with the powder.

(a-2)

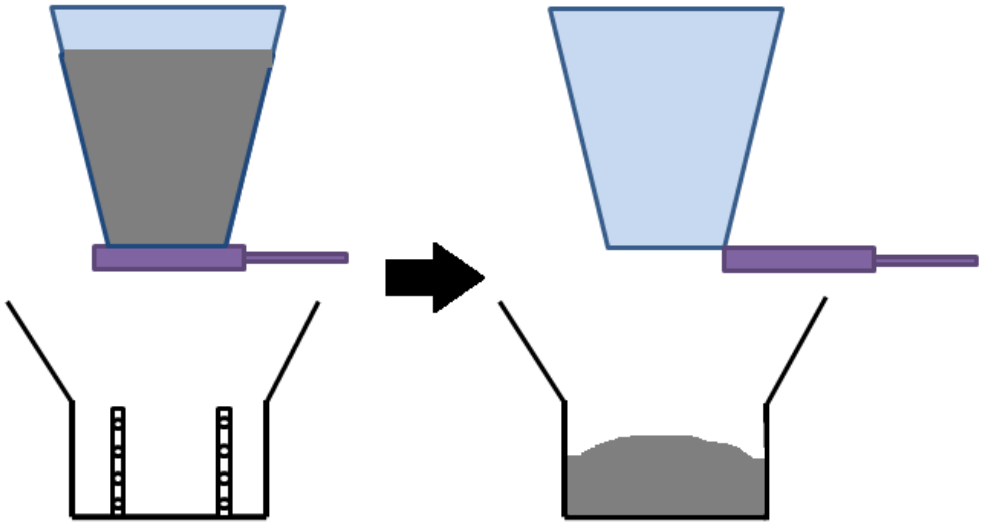

before spreading

after spreading

(b)

Figure 2-19. (a-1) The system of powder spreading with vibration (gradually spreading), (a-2) Profile of powder distribution in the sodium receptacle after spreading, and (b) The system of sudden spreading using powder trapdoor

CONCLUSION

The physicochemical analysis of three Marcalina samples (powders A, B, and C) have been conducted and detailed in this chapter. Table 2-12 provided the summary of the results. These results emphasize the presence of trona and $LiNaCO_3$. Study related to the aging of powder discussed in the next chapter will give the explanation about the fluctuation of composition observed in each powder. Meanwhile, the effect of grinding during the fabrication is also examined so as to give insights on the powder fabrication.

Table 2-12. Summary of the physicochemical results of powder A, B, and C

Characteristics	Powder A	Powder B	Powder C
Physical observations (color)	Dark grey	Light grey	Dark grey
Microstructure (SEM)	Regular shaped of 5µm length rod-like shape, coexist with larger particles of 20µm length	Irregular shaped of 100µm particles (with agglomerated needle shape particles)	Similar to powder A
Particle size	5.6µm	30.3µm	7.4µm
ρ_{true}	2.2 g.mL^{-1}	2.2 g.mL^{-1}	2.2 g.mL^{-1}
Porosity	86%	75%	86%
Carr Index (CI)	0.16	0.22	0.21
Hausner Index (HI)	1.19	1.28	1.28
FT4 powder rheometry flow test	Cohesive (++)	Cohesive (-) ≈ easy flow	Cohesive (+)
DVS weight gain @78.5%RH	44.6% Slight sensitive to the low RH (<50%) Not stable at >50%RH	20.4% Relatively stable at low RH (<50%RH) Not stable at >50%RH	14.6% Relatively stable at low RH (<50%RH) Not stable at >50%RH
Chemical composition			
- **$Na_2CO_3.H_2O$ (%w)**	31	29	16
- **Li_2CO_3 (%w)**	33	38	35
- **$LiNaCO_3$ (%w)**	26	0	18
- **Trona (%w)**	1	20	26
- **Graphite (%w)**	9	8	5
- **Free water (%w)**	0	4	0

BIBLIOGRAPHY OF CHAPTER II

[1] N. Kusumanindyah, L. Brissonneau, T. Gilardi, H. Berthiaux, and C. Gatumel, "Study of the physicochemical properties and the aging phenomena of an extinguishing powder for sodium fire," *Récents Prog. En Génie Procédés*, no. 107, 2015.

[2] Reuillon M. , Mellottee H. , Devillers B. , Alfille L.,Duco J. , Fruchard Y. , Malet J.C. , et Chappellier A., "Procédé et poudre pour l'extinction des feux de métaux liquides," 75 36225, 03-Mar-1978.

[3] M. Reuillon *et al.*, "Powder for extinguishing fires of liquid substances or of a mixture of liquid substances," US Patent 4,149,976, Apr-1979.

[4] M. Reuillon, "Etude de la combustion du sodium et de l'extinction de ses feux par les substances pulvérisées, rôle des additifs.," Université d'Orléans, 1976.

[5] A. Ekmekyapar, H. Erşahan, and S. Yapıcı, "Nonisothermal Decomposition Kinetics of Trona," *Ind. Eng. Chem. Res.*, vol. 35, no. 1, pp. 258–262, 1996.

[6] M. C. Ball, C. M. Snelling, A. N. Strachan, and R. M. Strachan, "Thermal decomposition of solid sodium sesquicarbonate, Na2CO3· NaHCO3· 2H2O," *J Chem Soc Faraday Trans*, vol. 88, no. 4, pp. 631–636, 1992.

[7] R. S. Gärtner and G.-J. Witkamp, "Mixed solvent reactive recrystallization of trona (sodium sesqui-carbonate) into soda (sodium carbonate anhydrate)," *Hydrometallurgy*, vol. 88, no. 1–4, pp. 75–91, Aug. 2007.

[8] Matthew C. Ball, Christine M. Snelling and Alec N. Stracha, "Dehydration of sodium carbonate mnohydrate," *J Chem Soc Faraday Trans*, vol. 81, pp. 1761–1766, 1985.

[9] Cairns E.J. and MacDonald D. I., "Sensitive thermal analysis establishing formation of the incongruently melting compound LiNaCO3," *Nature*, pp. 441–442, 1962.

[10] R. Carr, "Evaluating flow properties of solids," vol. 72, pp. 163–168, 1965.

[11] E. Teunou, J. . Fitzpatrick, and E. Synnott, "Characterisation of food powder flowability," *J. Food Eng.*, vol. 39, pp. 31–37, 1999.

[12] A. N. Khlapova and V. M. Elenevekaja, "The lithium carbonate - sodium carbonate systeme," *Russian Journal of Inorganic Chemistry*, pp. 610 – 613, 1968.

[13] Retsch, *Retsch Mortar Grinder RM 200*. .

[14] Fritsch, "Operating instructions planetary mono mill PULVERISETTE 6 classic line." .

[15] N. Kusumanindyah, L. Brissonneau, T. Gilardi, C. Gatumel, and H. Berthiaux, "Study of the aging impact on the extinction efficiency of an extinguishing powder for sodium fire," *Chem. Eng. Trans.*, vol. 48, 2016.

CHAPTER III
Study of the aging and production method of the powder

The results of physicochemical analyses presented in the previous chapter highlight the presence of trona and $LiNaCO_3$, two compounds that are not stated in the patent. These compounds are found to be present in variable proportions in each sample. The aging experiments were then conducted to identify the mechanism of chemical evolution that happened to the Marcalina in different storage conditions. The influence of relative humidity and ambient carbon dioxide was studied by applying two different conditioning methods (cf. figure 2-16). As explained at the end of the previous chapter, sodium carbonate monohydrate, LiNaCO3, and powder A were chosen as the sample of interest. Powder A was selected as the referent Marcalina sample because its water content was still in the range of specification indicated by the producer (cf. §1.3.1), while the two others (pure $Na_2CO_3.H_2O$ and $LiNaCO_3$) were chosen because they were the most likely to undergo any chemical transformation under air storage.

This chapter is dedicated to discuss the presence of trona and $LiNaCO_3$ in the mixture. The results of the experimental study will provide worthy informations, especially related to the storage condition and the production method of the powder.

Meanwhile, the presence of $LiNaCO_3$ was questionable as whether or not it might be produced intentionally during the production process. As it can only be formed at high temperatures, the study of its presence will be of a valuable insight for the fabrication method, which is unknown ever since the cease activity of CACI. A grinding/milling process is surely an essential part of the production, since it allows the particle size reduction and maintains the homogeneity of the powder at the same time. The mechanochemical reaction during the milling process is then suspected to produce $LiNaCO_3$ as a by-product of carbonate mixtures grinding. In grinding conditions, the $LiNaCO_3$ formation could occur at ambient temperature in a ball mill with no external heating needed. In this case, the ball mill is considered as a chemical reactor in which a wide range of chemical reactions can be mechanically initiated.

3.1 The results and discussions of aging experiments

The detail of experimental materials and methods used are described in §2.3.1. XRD analyses were conducted to understand the evolution of powder compositions. The samplings were taken during the 8 months of observation. However, the experiments results present certain obscurity, especially for $LiNaCO_3$ and $Na_2CO_3.H_2O$ samples. The results of these pure samples are unlikely comparable to what obtained in powder A due to the difference of particle sizes. Therefore, the results of powder A will be more thoroughly discussed. All XRD diagrams of aging are reported in appendix A.2.

Figure 3-1 shows the results of the semi quantitative XRD analyses for the composition evolution of powder A during 8 months in the 75% HR with air passage condition. The amount of trona increases and the amount of $LiNaCO_3$ decreases with time. $LiNaCO_3$ turns almost completely into $Na_2CO_3.H_2O$, Li_2CO_3 and few trôna after two months. $LiNaCO_3$ is no longer observable after 8 months of aging in this condition. Between the second and the fourth month, the $Na_2CO_3.H_2O$ turns completely into trôna.

As illustrated in figure 3-2, in the absence of CO_2, $LiNaCO_3$ is completely decomposed after two months to $Na_2CO_3.H_2O$, Li_2CO_3 and few $Na_2CO_3.7H_2O$. No trona is observed at this time. At longer times, trona and $Na_2CO_3.7H_2O$ content built up at the expense of $Na_2CO_3.H_2O$. The latter appears to increase at the expense of $Na_2CO_3.7H_2O$, although it is questionable (considering the presence of trona), if air tight conditions were conserved in the last months.

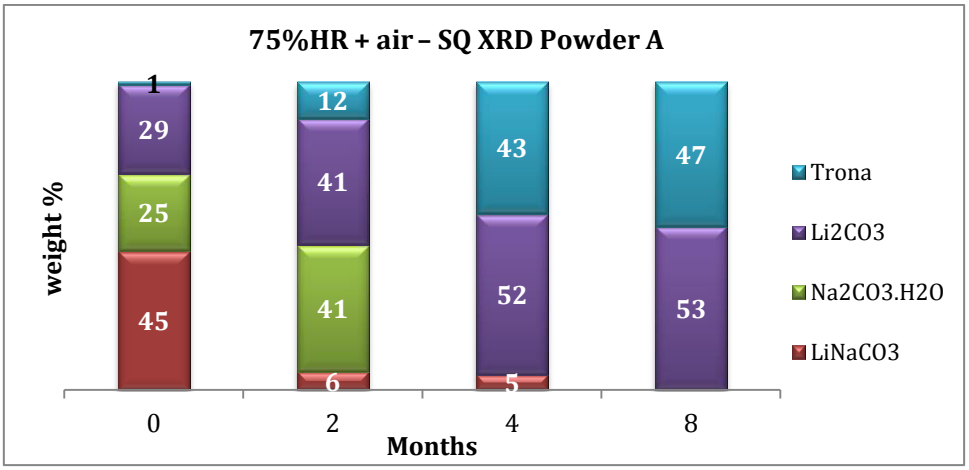

Figure 3-1. Semi quantitative XRD results for powder A in the 75% RH with air passage condition

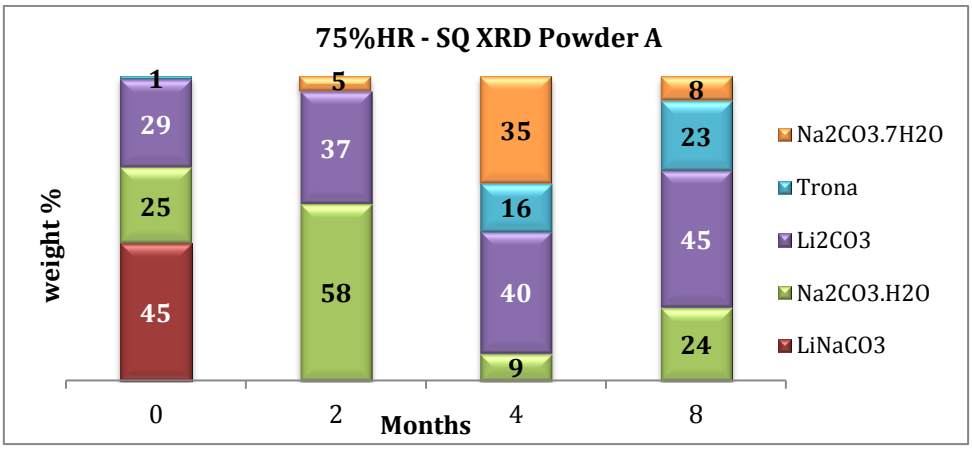

Figure 3-2. The results of semi quantitative XRD for powder A in the condition of 75% RH without air passage

In less humid air conditions, the kinetics of $LiNaCO_3$ decomposition and trona formation are much slower. Thus, it should be of interest to question the limit conditions, relative to the humidity levels and presence of CO_2, in which both reactions are thermodynamically possible. Figure 3-3 and 3-4 details the XRD results for the sample conserved in 32%HR and 8%HR respectively in open condition in which the evolution of composition can be observed over time.

The slight 10 wt% decrease of $LiNaCO_3$ and 9 wt% increase of $Na_2CO_3.H_2O$ due to the decomposition of $LiNaCO_3$ were observed under sealed condition at 8%RH after eight months (cf. figure 3-5). Logically, this should be followed by a simultaneous increase amount of Li_2CO_3, which is not the case. It might be due to the SQ-XRD uncertainty. Still, it demonstrates that $LiNaCO_3$ decomposed more rapidly without the presence of CO_2 based on

comparison results of sample conserved in sealed and open conditions at low humidity (8%RH).

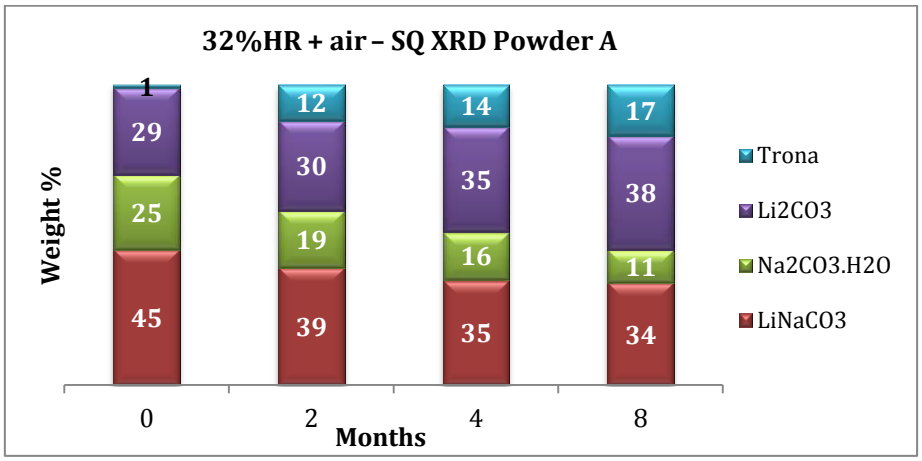

Figure 3-3. Semi quantitative XRD results for powder A in the 32% RH with air passage (open condition)

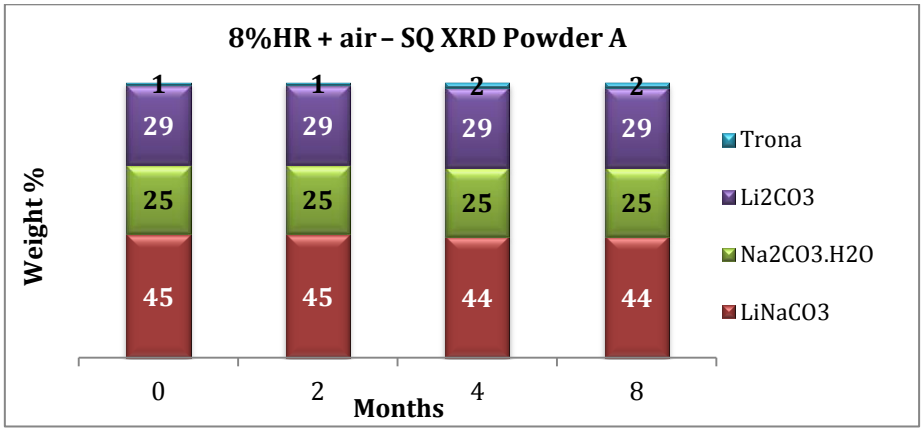

Figure 3-4. Semi quantitative XRD results for powder A in the 8% RH with air passage (open condition)

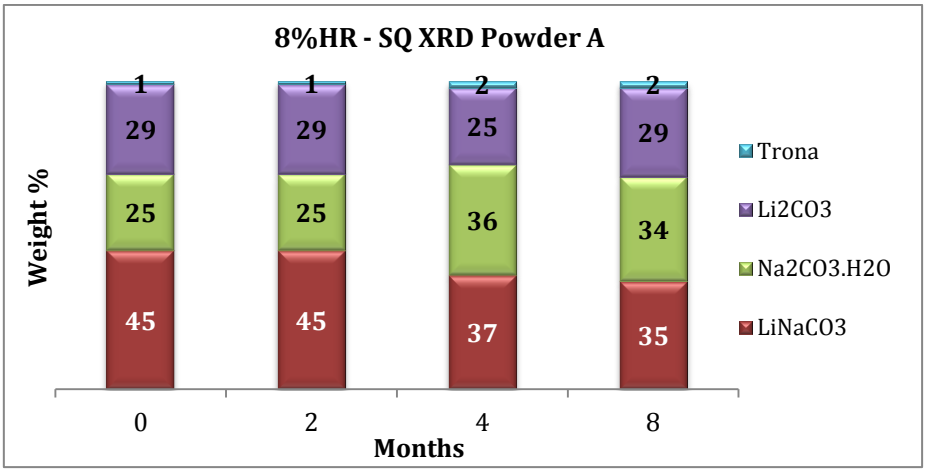

Figure 3-5. The results of semi quantitative XRD for powder A in the condition of 8% RH without air passage (closed condition)

The comparison of the composition variation for powder A at the end of 8 months for the three RH conditions with or without air is shown in figures 3-6 and 3-7, respectively. In open conditions, the least presence of trona is found in the 8%RH condition with 2 wt%. Its quantity becomes 9 times and 24 times higher in the 32%RH+air and 75%RH+air conditions, respectively. Here, the trona increase correlates with the decrease of $LiNaCO_3$ and $Na_2CO_3.H_2O$. In case of the low 8% RH+air, its amount is relatively constant with only 1 wt% of increase at the end of 8 months. On the contrary, trona is much more difficult to form without the presence of CO_2 even at high humidity (75%RH).

Meanwhile, $LiNaCO_3$ was found to be fully decomposed and 23% of trona was formed during the 75%RH sealed condition. Once again, the presence of trona questioned the air tightness of the 75%RH conditions. It is also possible that 8%RH is not air tight either but that the transformation into trôna is much slower in this condition.

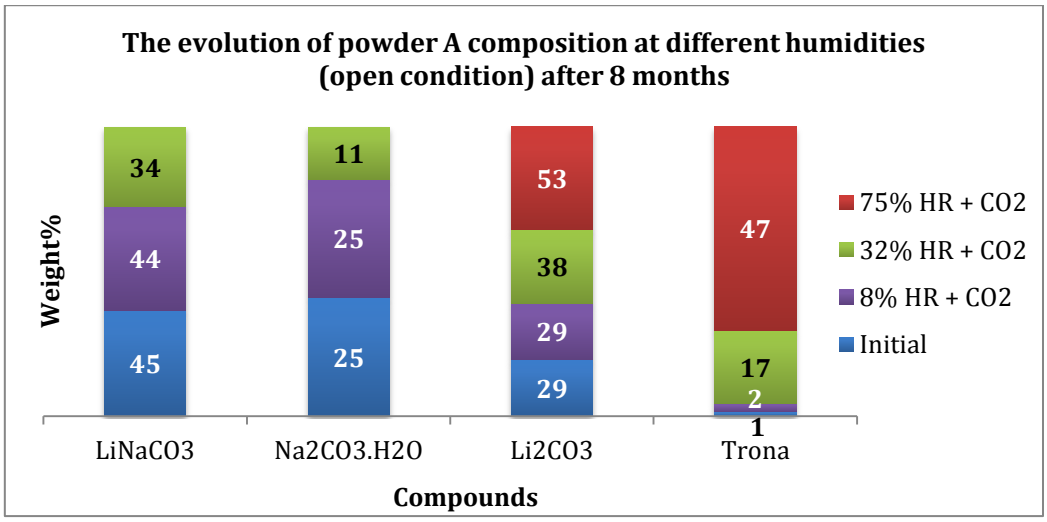

Figure 3-6. Comparison of the compositions variation of powder A at different humidity conditions with air passage (open condition) after 8 months

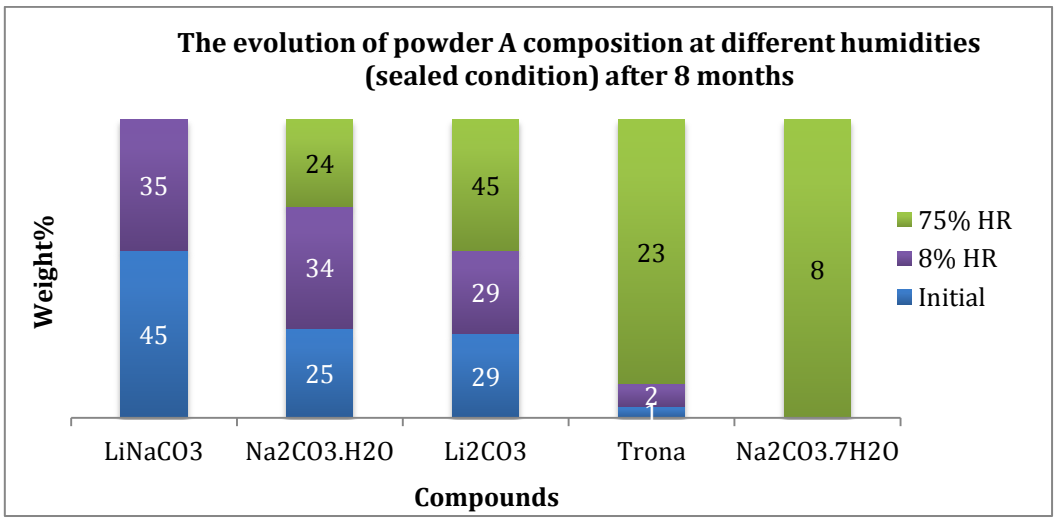

Figure 3-7. Comparison of the composition evolution of powder A at different humidity conditions and without air passage (sealed condition) after 8 months

The semi quantitative XRD data recapitulation for the aging of $LiNaCO_3$ and $Na_2CO_3.H_2O$ after 8 months is reported in Table 3-1. In the case of pure $LiNaCO_3$, the decomposition appears only in the condition of high humidity (RH=75%) where it partially transforms into $Na_2CO_3.H_2O$ and Li_2CO_3, whereas trona appears to be formed from $Na_2CO_3.H_2O$ samples exposed in open condition at all humidity levels. Even though, the influence of humidity on the formation of trona is hardly concluded due to the heterogeneity of particle sizes used for the initial samples.

Overall, it is difficult to compare the results of these pure samples with powder A considering the difference of particle sizes. Indeed, $Na_2CO_3.H_2O$ sample has 200µm (D_v50), which is 40x bigger than powder A (D_v50 = 5µm). The same problem is also encountered for $LiNaCO_3$, which has approximately 100µm particle size (SEM). Figure 3-8 below illustrate the microstructure of each sample emphasizing on their difference in particle sizes. This fact might explain the slower reaction kinetics of pure samples compared to what observed in powder A.

From the aging experiment results, we may conclude that:

- The presence of CO_2 favors the formation of trona.
- The higher humidity condition facilitates both the reaction formation of trona (with CO_2) or $Na_2CO_3.7H_2O$ (without CO_2) and decomposition of $LiNaCO_3$.

In addition, it appears that the particle sizes might influence the kinetics of both reactions. Having bigger particles, the results of $Na_2CO_3.H_2O$ and $LiNaCO_3$ pure samples after 8 months of aging showed a slower formation of trona and decomposition of $LiNaCO_3$ compared to powder A. This conclusion will be compared to the thermodynamic standpoint as thoroughly discussed in the next part.

Table 3-1. SQ-XRD data recapitulation for the aging of $LiNaCO_3$ and $Na_2CO_3.H_2O$ after 8 months in sealed (%HR) and open (%HR + CO_2) conditions

Samples	$Na_2CO_3.H_2O$	Li_2CO_3	$LiNaCO_3$	Trôna	$Na_2CO_3.7H_2O$
$LiNaCO_3$ 8%HR+CO_2	0	0	100	0	0
$LiNaCO_3$ 8%HR	0	0	100	0	0
$LiNaCO_3$ 32%HR	0	0	100	0	0
$LiNaCO_3$ 75%HR+CO_2	0	4	95	0	1
$LiNaCO_3$ 75%HR	20	9	70	0	3
$Na_2CO_3.H_2O$ 8%HR +CO_2	88	0	0	12	0
$Na_2CO_3.H_2O$ 8%HR	100	0	0	0	0
$Na_2CO_3.H_2O$ 32%HR+CO_2	78	0	0	22	0
$Na_2CO_3.H_2O$ 75%HR + CO_2	86	0	0	11	3
$Na_2CO_3.H_2O$ 75%HR	76	0	0	0	24

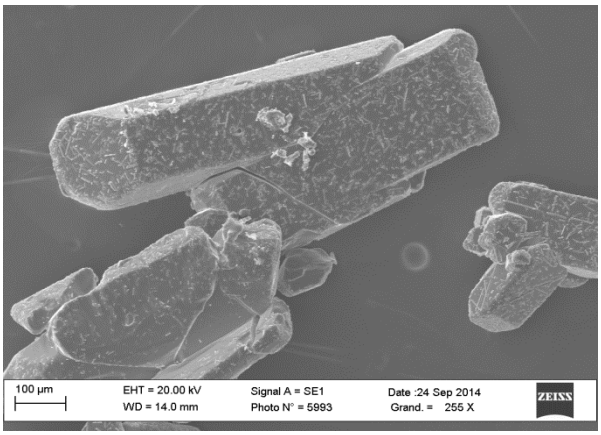

$Na_2CO_3.H_2O$ reference

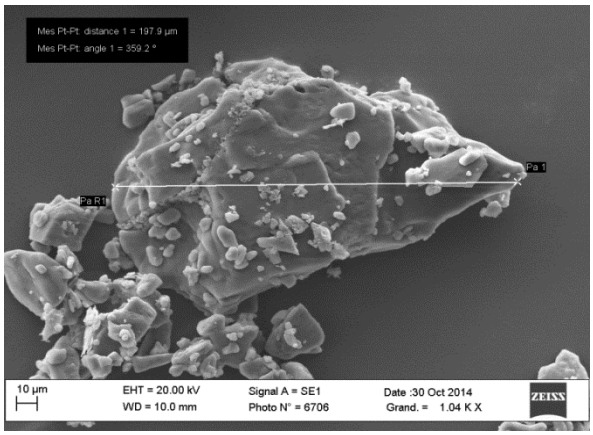

$LiNaCO_3$ reference

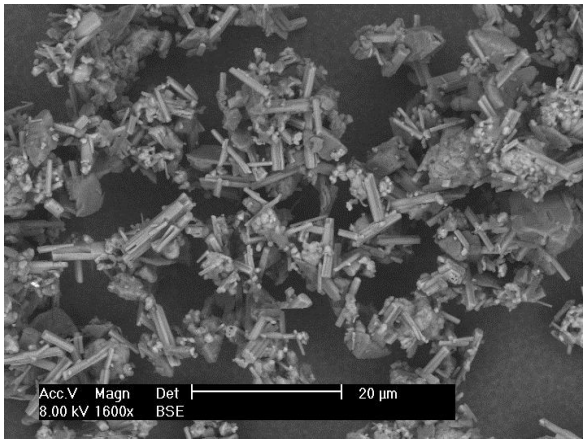

Powder A reference

Figure 3-8. The comparison of SEM image on powder reference sample used in the aging experiment

3.1.1 The production of trona

Sodium carbonate monohydrate is the most stable hydrated form of sodium carbonate as compared to the others (heptahydrate and decahydrate) in ambient conditions. However, in the excess presence of water vapor (high humidity) and carbon dioxide, it can be easily transformed into trona as can be seen by the results of XRD analyses after 8 months of aging. The chemical transformation happened as follows:

$$3\,Na_2CO_3.H_2O + 2\,H_2O + CO_2 \rightarrow 2\,[Na_2CO_3.NaHCO_3.2H_2O] \quad (3\text{-}1)$$

The thermodynamic calculation using HSC Chemistry confirms that it is, indeed, a spontaneous reaction at 25°C with $\Delta G_r = -45.1$ kJ and $K_{eq} = 8.08x10^7$ (cf. table 3-2). The reaction is highly unlikely above 105°C (as $\Delta G_r > 0$ indicates non spontaneous reaction).

Table 3-2. The thermodynamic calculation of reaction (3-1) over temperatures using HSC Chemistry at 1 atm

T (°C)	ΔH (kJ)	ΔS (J/K)	ΔG (kJ)	K	Log(K)
25	-191.1	-489.5	-45.1	8.1E+07	7.9
45	-191.11	-489.6	-35.3	6.4E+05	5.8
65	-191.2	-489.8	-25.6	8.9E+03	3.9
85	-191.2	-490	-15.8	1.2E+02	2.3
105	-191.3	-490.3	-6	6.6E+00	0.8
125	-191.5	-490.6	3. 9	3.1E-01	-0.5
145	-191.6	-490.9	13.7	2E-02	-1.7
165	-191.8	-491.3	23.5	1.6E-03	-2.8
185	-192	-491.7	33.3	1.6E-04	-3.8
200	-192.1	-492	40.7	3.2E-05	-4.5

Besides the experimental results of aging, the influence of $H_2O_{(g)}$ and $CO_{2(g)}$ at the ambient temperature was also studied thermodynamically based on the calculations using HSC Equilibrium module. It enables the calculation of multi-component equilibrium compositions in heterogeneous systems. The equilibrium composition is calculated using the GIBBS solver, which uses the Gibbs energy minimization method. The following results will describe the composition at equilibrium state at 25°C:

i. The influence of $H_2O_{(g)}$

Humidity plays an important role in the stability of sodium carbonate monohydrate. Figure 3-9 shows the calculation results of the equilibrium compositions with various moles of $Na_2CO_3.H_2O$ as the initial conditions. It starts to decompose into decahydrate ($Na_2CO_3.10H_2O$) at 50%RH with the least initial conditions (0.01 kmole) experience the most decomposition.

Meanwhile, heptahydrate seems to be not formed at these conditions. Indeed, heptahydrate is likely an unstable phase. It has 2 types of crystallographic structures; type “b” is stable between 32.02 and 35.27°C, while type “a” is metastable at any temperature. The latter even decomposes at 20°C in a few days to form poorly defined products, probably the monohydrate and/or decahydrate [1].

The aging experiment of $Na_2CO_3.H_2O$ sample showed no indication of the presence of decahydrate at 75%RH in sealed condition (see table 3-1). On the contrary, the presence of heptahydrate is observed in the sample of powder A conserved in a sealed condition (cf. figure 3-4). As what have been previously implied, the $Na_2CO_3.H_2O$ sample used in this experiment has bigger and irregular particle size distribution compare to powder A which has smaller and more regular particle with D_v 50 of 213.5µm and 5.6µm respectively. This might influence the kinetic of the reaction. In this case, the equilibrium condition might not yet be attained. Furthermore, the calculation also estimates around 7.5 wt% of decahydrate formation at equilibrium for 75%RH. Considering the presence of heptahydrate as the unstable composition, there might be not as much of decahydrate produced in reality, hence it should be too small to be detected in XRD analysis (with limit detection of ~3% in two phase mixture and 0.1µm < particle size < 40µm of powder specimen preparation).

ii. The influence of $CO_{2(g)}$

Figure 3-10 shows the influence of CO_2 on the equilibrium composition of sodium carbonate monohydrate at different humidity conditions. It appears that more trona or sodium sesquicarbonate are formed at the increasing of humidity (cf. figure 3-9a). 8.4 wt%, 18.2 wt%, and 30 wt% of trona were thermodynamically predicted to be formed at equilibrium at 8% RH, 32% RH, and 75% RH conditions respectively.

On the contrary, wegscheiderite or decimite ($Na_2CO_3.3NaHCO_3$) occurs to be slightly decreasing with the increase of RH (cf. figure 3-9b). 2.9 wt%, 2.7 wt%, and 2.3 wt% of wegscheiderite were formed at the increasing humidity. Consequently, its presence causes trona to decrease down to 2 wt%, 5.1 wt%, and 11.2 wt%. According to [2], wegscheiderite has been shown to be formed when sodium carbonate is heated in carbon dioxide-water vapor mixtures following this reaction that goes to completion at temperatures up to 368 K:

$$5Na_2CO_3 + 3H_2O + 3CO_2 \leftrightarrow 2(Na_2CO_3.3NaHCO_3) \quad (3\text{-}2)$$

However, monohydrate apparently reacts more quickly than the anhydrous compound to form wegscheiderite [2]:

$$5Na_2CO_3.H_2O + 3CO_2 \leftrightarrow 2(Na_2CO_3.3NaHCO_3) + 2H_2O \quad (3\text{-}3)$$

Nevertheless it is only an intermediate product of $NaHCO_3$ formation in the condition of CO_2 excess [2]:

$$Na_2CO_3.3NaHCO_3 + H_2O + CO_2 \leftrightarrow 5NaHCO_3 \quad (3\text{-}4)$$

Meanwhile, nahcolite ($NaHCO_3$) appears to be the most stable compound with 34.2 wt%, 36.4 wt%, and 38.4 wt% at 8% RH, 32% RH, and 75% RH conditions respectively as can be seen in figure 3-9c. This results is contradictory with the literature [3], that deals about the stability of sodium carbonates.

It should be emphasized that sometimes a substance is very stable thermodynamically, but its amount in experiments remains quite low. It is obviously due to kinetic reasons, which is certainly the case for the experiment. This is why, eliminating such a substance, which have been proven experimentally, in the calculations in order to simulate the kinetic (rate) phenomena is sometimes permitted (i.e. wegscheiderite and nahcolite are omitted in figure 3-10 (a)).

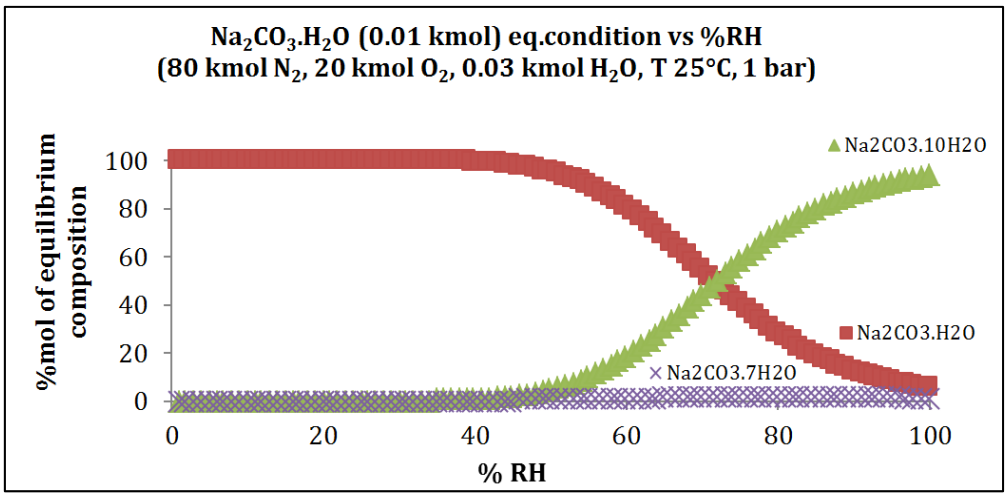

(a)

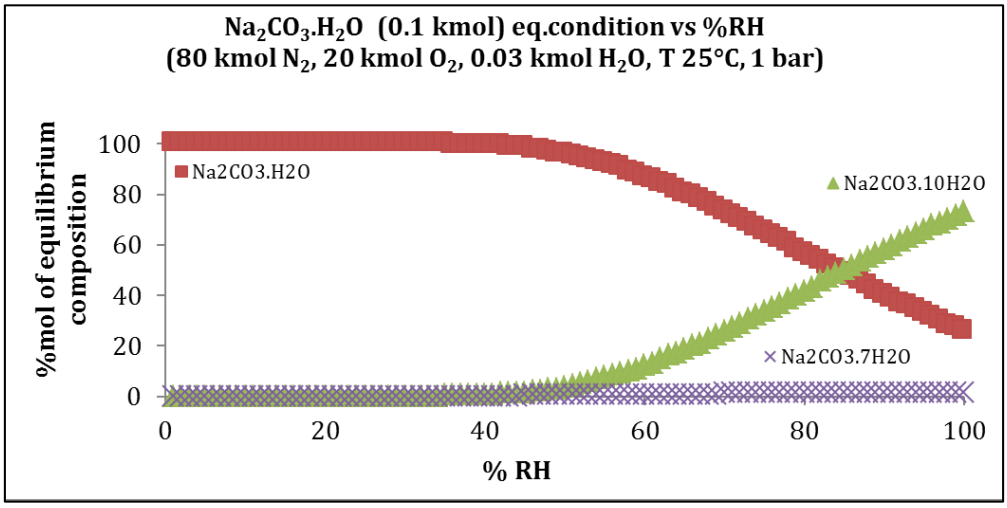

(b)

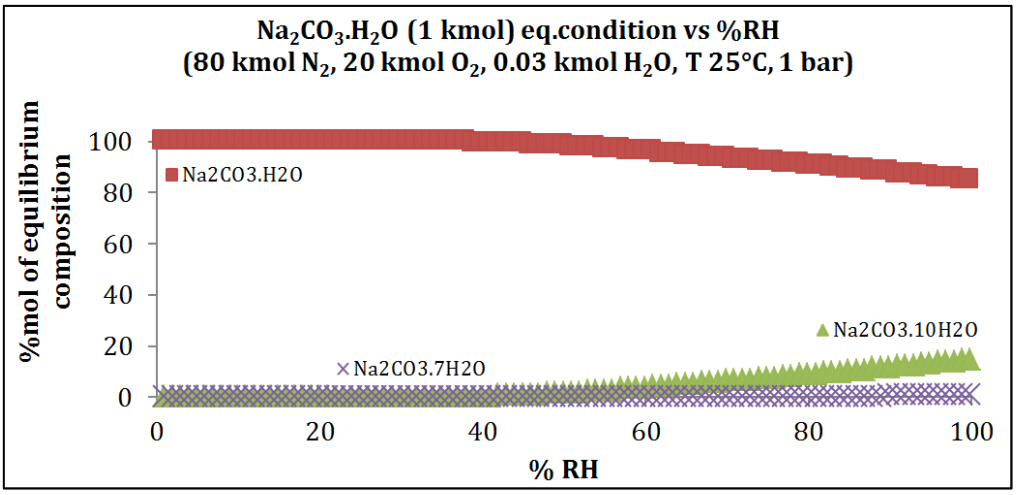

(c)

Figure 3-9. The influence of H_2O variation towards the equilibrium composition of (a) 0.01 kmol (b) 0.1 kmol (c) 1 kmol $Na_2CO_3.H_2O$ aging

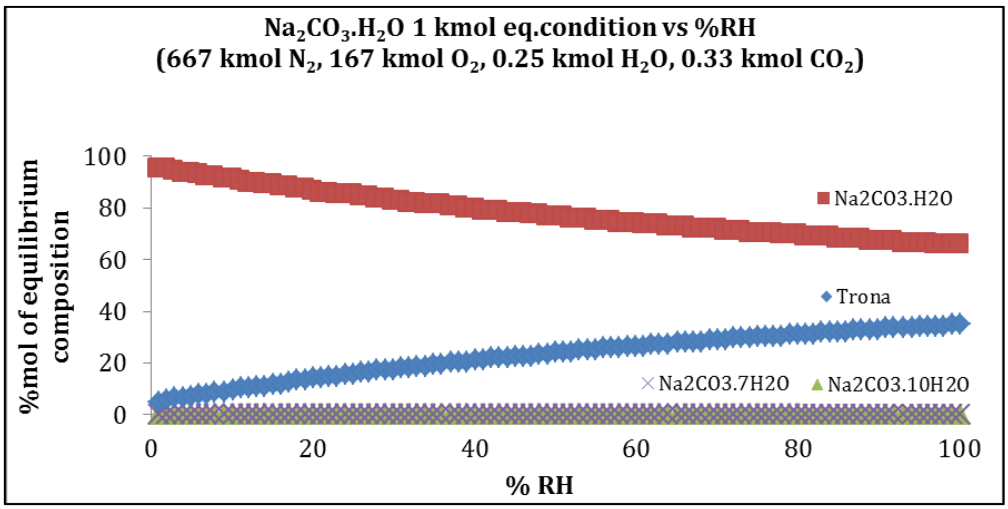

(a)

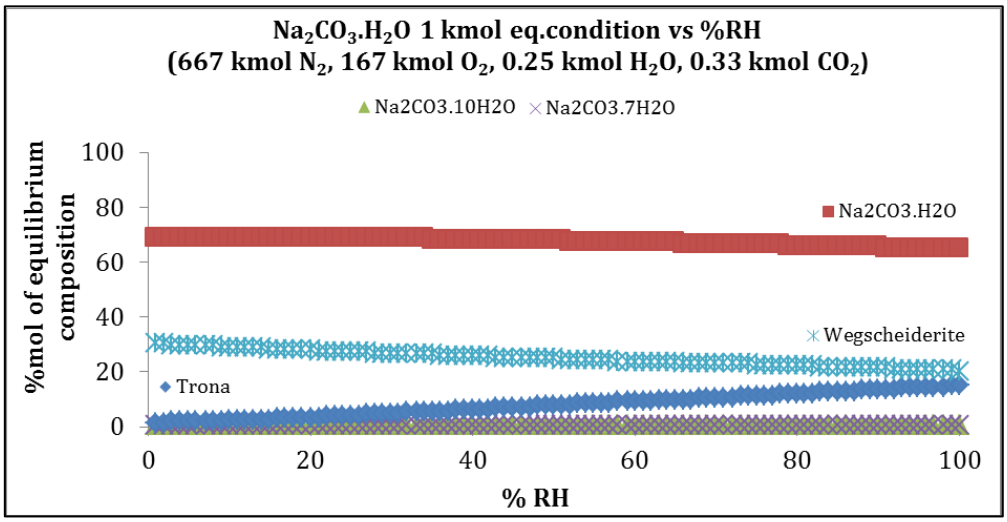

(b)

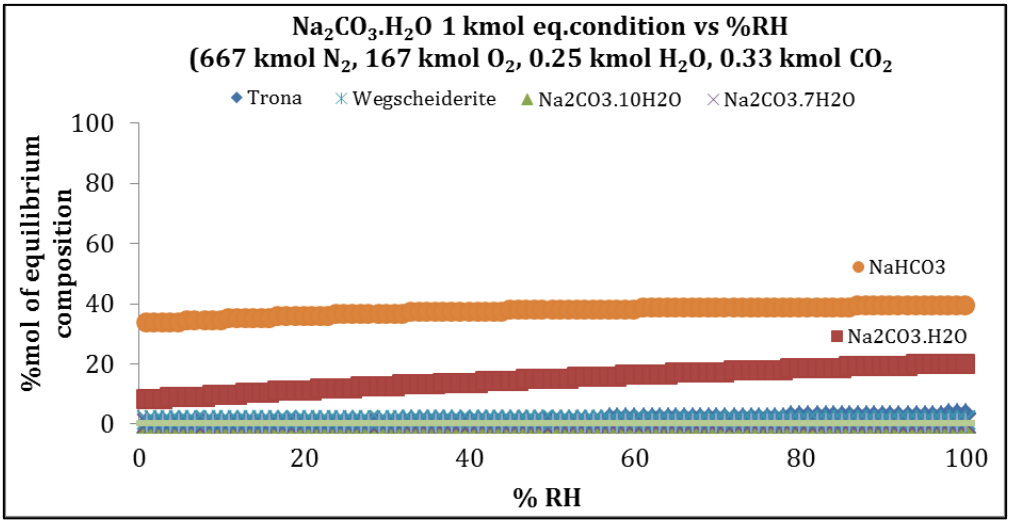

(c)

Figure 3-10. The influence of CO_2 towards the equilibrium composition of $Na_2CO_3.H_2O$ with the presence of (a) trona, (b) trona and wegscheiderite, (c) trona, wegscheiderite, and nahcolite

According to [3], almost all natural deposits of sodium carbonates consist either of trona or sodium bicarbonate ($NaHCO_{3(s)}$, nahcolite), since these are the crystal that are most likely to be formed from natural carbonate brines. Trona is the most common mineral due to two factors: the equilibrium between carbonate and bicarbonate in aqueous solution and its incongruent solubility. The equilibration occurs via the absorption/desorption of the atmospheric CO_2.

$$2HCO_{3(aq)}^{-} \overset{\Delta T}{\leftrightarrow} CO_{3(aq)}^{2-} + H_2O_{(l)} + CO_{2(g)} \quad (3\text{-}5)$$

This equilibrium shifts significantly with temperature. The decrease of temperature favors the formation of bicarbonate $NaHCO_3$. It is stable at atmospheric CO_2 partial pressure up to about 90°C. However the (evaporative) crystallization of nahcolite causes the brine to enrich rapidly in sodium carbonate. The amount of carbon dioxide available in the atmosphere is too low to allow the quantitative conversion of the excess carbonate into bicarbonate (cf. reaction 3-5) in competition with the natural evaporation rate. Therefore, the brine enriches in sodium carbonate until trôna becomes likely the stable solid phase. Moreover, nahcolite is formed where PCO_2 exceed at least 10 times that of atmosphere [4]. Since the crystallization of trôna, the same stoichiometric amounts of bicarbonate and carbonate are removed from solution and the brine composition stabilizes. As a result, nahcolite formation in the nature depends on a combination of lower temperatures, low alkalinity solutions (brines) and low evaporation rates. The equilibrium can theoretically be shifted further towards carbonate ion CO_3^{2-} by reducing the ambient carbon dioxide partial pressure and/or by further increase of the temperature. Intense carbon dioxide stripping (with only ppm-level in the strip gas phase) could allow crystallization of sodium carbonate monohydrate and complete conversion into a bicarbonate-free solid phase.

Neither wegscheiderite nor nahcolite were observed in the aging experiment of either $Na_2CO_3.H_2O$ pure sample or powder A conserved in open condition. Therefore in this case trôna is likely to be a stable solid phase with total decomposition of $Na_2CO_3.H_2O$ into trona observed during the experiment of powder A sample. The rate of its formation in the $Na_2CO_3.H_2O$ pure sample might be less than the one in powder A. Nevertheless, its formation is still observed in the 8 months of aging.

iii. Discussions

This calculation is in qualitative agreement with the aging mechanism proposed for the experiments which shows the major influence of CO_2 slightly rich condition (0.33 kmol – stoichiometrically corresponds to the reaction 3-1) in order to form trona. Besides, higher relative humidity seems to favors its formation. Without CO_2, sodium carbonate decahydrate begins to form at high RH conditions (>50%).

Both results are in qualitative accordance with the results of powder A. The formation of trona started to be observed at 32%RH, while the complete transformation is observed at 75%RH (cf. figure 3-1) with only trona and lithium carbonate as the remaining compounds. On the other hand, trona is more hardly formed in the sealed condition due to the lesser quantity of CO_2 (cf. figure 3-2). Hence, the formation of trona thermodynamically depends

not only on the presence of CO_2, but also on the humidity conditions that might affect the reaction kinetics. Although, it should be noted that thermodynamically $NaHCO_3$ is more stable than trona.

It is, unfortunately, more difficult to compare with the sample of pure monohydrate. Since it has 38 times bigger particle size than powder A, it becomes apparent that longer time will be needed to reach full transformation into trona. The irregularity of each sample particle size used in different RH for both open and sealed condition also makes the results harder to correlate (cf. table 3-1).

The SEM observations were also conducted in order to observe the physical difference of particles before and after aging. Before aging, monohydrate was composed of nonporous particles with several outgrowth crystals on the surface as can be seen in figure 3-11a. After 8 months of aging for the monohydrate sample conserved in 75%RH open condition following phenomena are observed:

- certain part of particle surface became more porous, with appearance of several outgrowth crystal from the porous surface as can be seen in figure 3-11b,
- the outgrowth crystal then appears to predominantly cover the surface of particles and the agglomeration of these crystals then formed newly smooth surface comparable to the shape of trona reference sample (cf. figure 3.11c).

On the contrary, the sample stored in 75%RH sealed condition shows different form (cf. figure 3.11d). It appears that the outgrowth crystals also appear more often than in the sample reference one. However, the crystals don't seem to be agglomerated on the surface contrarily to the sample conserved in open condition.

Therefore, the evolution of powder compound would be highly influenced by the storage conditions, notably with the presence of CO_2 and slightly humid conditions. The kinetics also depends on the particle size, of which study would be interested to improve the storage condition.

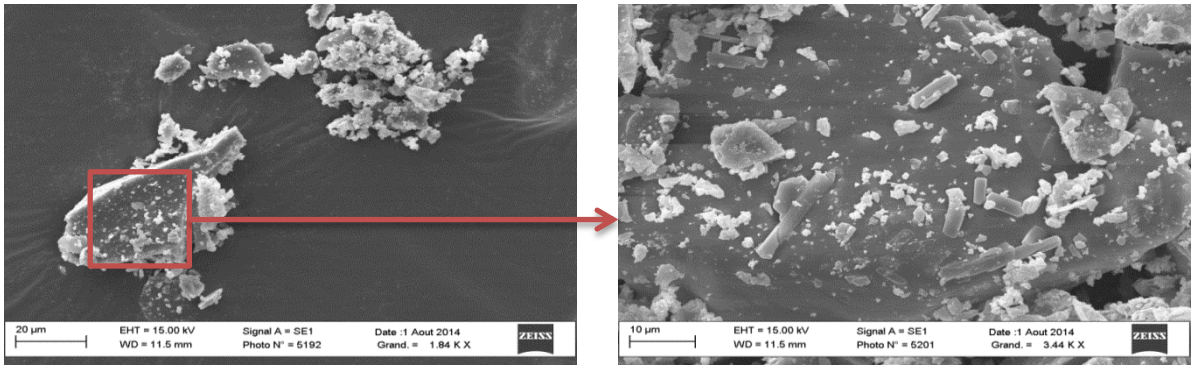

(a) $Na_2CO_3.H_2O$ reference

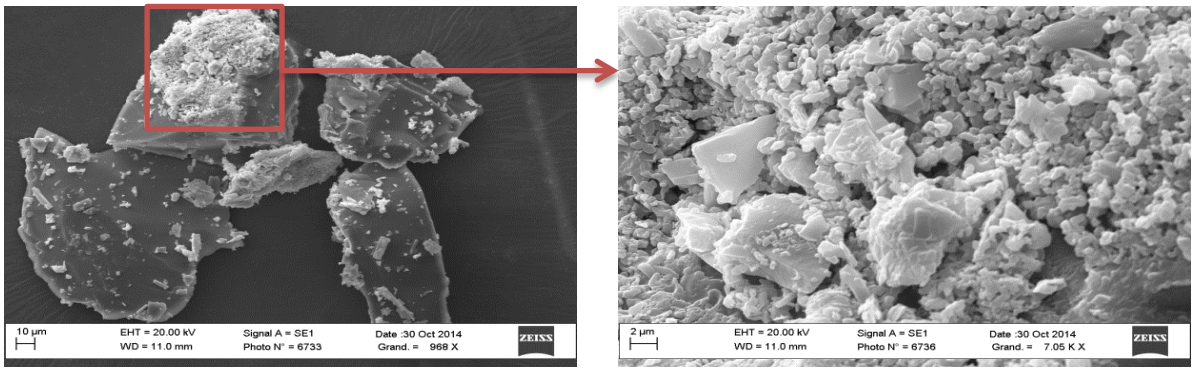

(b) $Na_2CO_3.H_2O$ reference sample conserved in open desiccator (presence of CO_2 & 75% RH) after 8 months

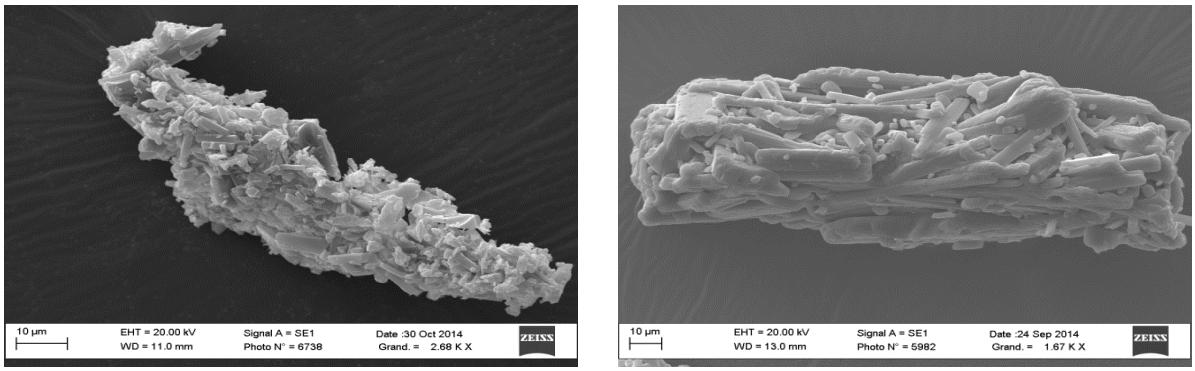

(c) $Na_2CO_3.H_2O$ reference sample conserved in open desiccator (presence of CO_2 &75% RH) after 8 months (left) vs trona reference (right)

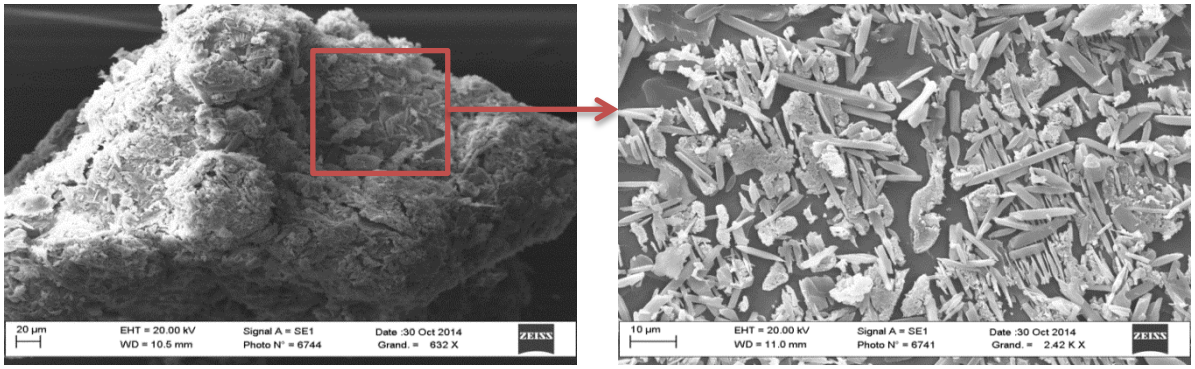

(d) $Na_2CO_3.H_2O$ reference sample conserved in sealed desiccator (without presence of CO_2 & 75% RH) after 8 months

Figure 3-11. SEM observation results of $Na_2CO_3.H_2O$ samples before and after 8 months of aging in both open and sealed storage conditions

3.1.2 The decomposition of $LiNaCO_3$

At present, $LiNaCO_3$ is known to be formed by heating the lithium carbonate and sodium carbonate (50:50 mol%) above the melting point 500°C. The results of aging showed that it could be transformed into $Na_2CO_3.H_2O$ and Li_2CO_3 in the presence of high humidity (see table 3-1) according to reaction (3-5), in the form of small crystals as in powder A or big crystals ($LiNaCO_3$ alone). It should be noted that the presence of CO_2 inhibits the reaction considering that no $Na_2CO_3.H_2O$ was detected in the aged samples of $LiNaCO_3$ (cf. table 3-1) in air conditions. Moreover, the decomposition reaction happened to be much slower for powder A under air (cf. figure 3-1) compared to the one conserved in the sealed condition. It could be assumed that CO_2 absorption on the surface competes with H_2O absorption and prevents the reaction of H_2O with the compound.

$$2\ LiNaCO_3 + H_2O \rightarrow Li_2CO_3 + Na_2CO_3.H_2O \qquad (3\text{-}6)$$

The SEM micrographics in figure 3-12 illustrate the morphology of the sample before and after aging under 75%HR in both open and sealed conditions. At the beginning, $LiNaCO_3$ is composed of non-porous crystals with superposed irregular shaped crystals at the surface (fig. 3-12 (a)). We observed that the surface of the sample conserved on sealed condition appears to be more porous with appearance of needle shape hydrated crystals (fig. 3-12(b)). These crystals can be hardly found in the aged sample conserved in open conditions (fig. 3-12(c)). A significant morphological transformation is not observed in this sample as compared to the reference ones.

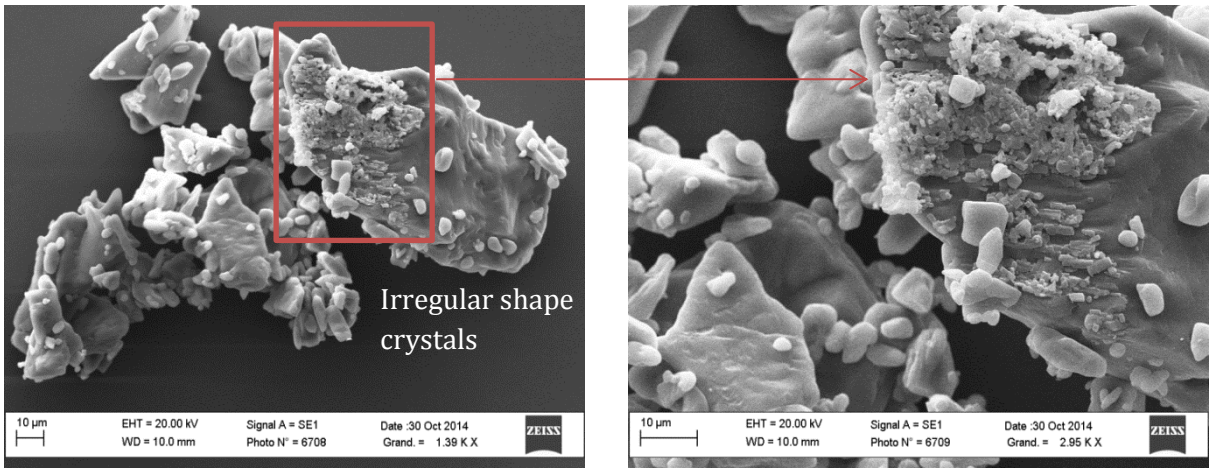

a) $LiNaCO_3$ reference

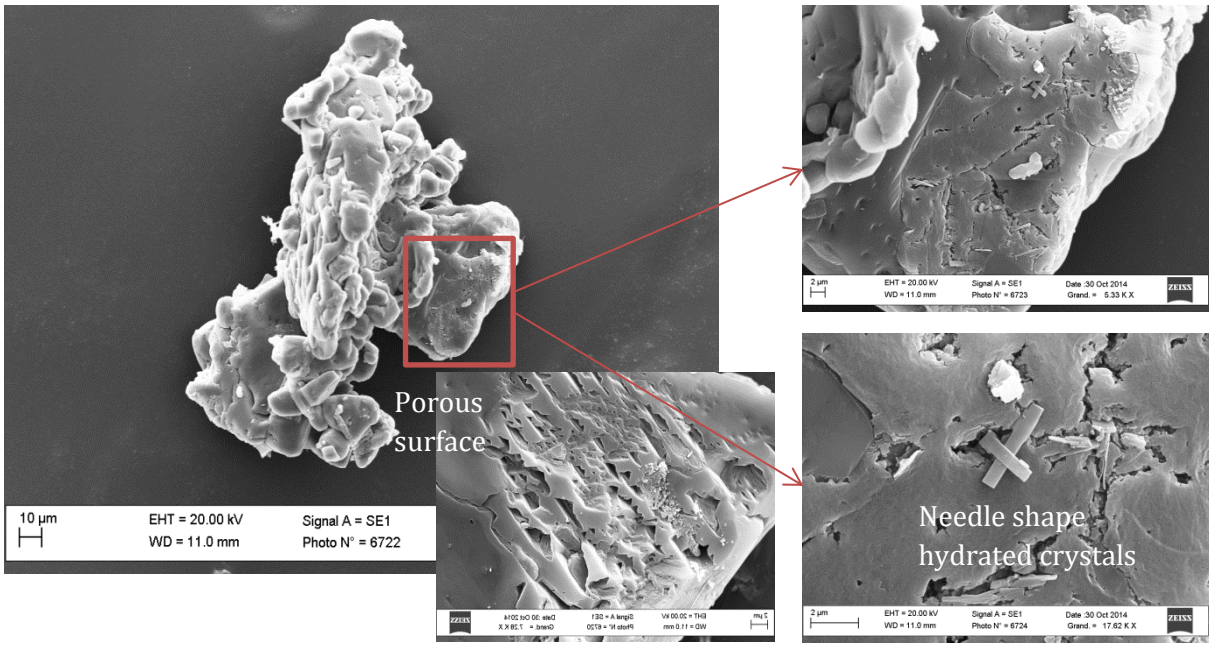

b) $LiNaCO_3$ reference sample conserved in sealed desiccator (without presence of CO_2) after 8 months

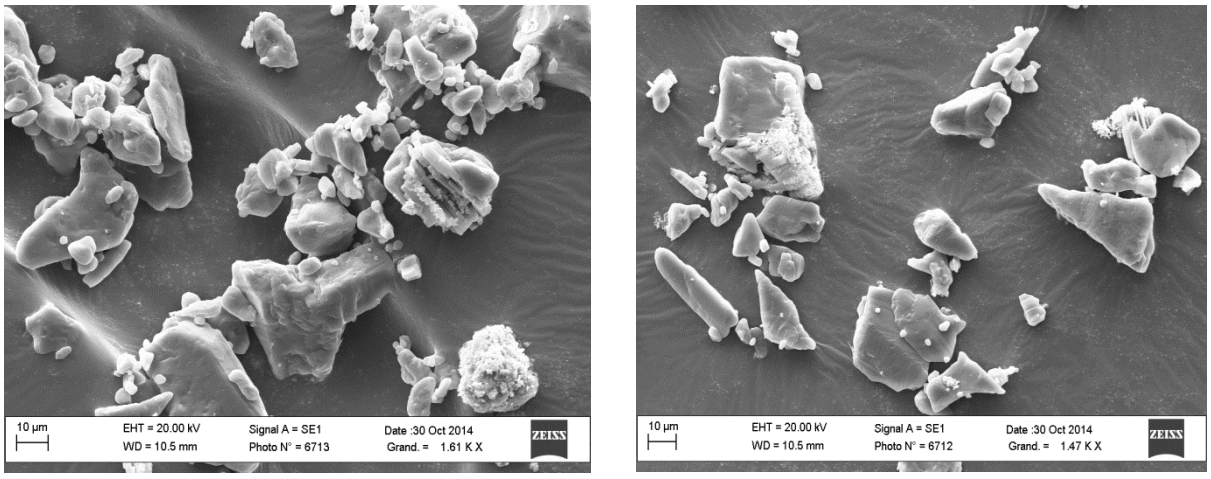

c) $LiNaCO_3$ reference sample conserved in open desiccator (presence of CO_2) after 8 months

Figure 3-12. The SEM observation results of $LiNaCO_3$ sample before (a) and after 8 months of aging (75%HR) in both sealed (b) and open (c) storage conditions

3.1.3 Discussion of the aging mechanism

The powder A sample, which is conserved in open condition, exhibits both the total production of trona and total decomposition of $LiNaCO_3$ after 8 months of aging under 75%RH. This means that both reactions (3-1) and (3-6) happened. They might happen simultaneously, although the kinetic of reactions is highly depending on the atmosphere condition (related to the presence of CO_2).

$$3\,Na_2CO_3.H_2O + 2\,H_2O + CO_2 \rightarrow 2\,[Na_2CO_3.NaHCO_3.2H_2O] \quad (3\text{-}1)$$

$$2\,LiNaCO_3 + H_2O \rightarrow Li_2CO_3 + Na_2CO_3.H_2O \quad (3\text{-}6)$$

Based on the above reactions, it is possible to predict the compositions of the powder at each step of aging as long as the initial compositions, the kinetics of reaction (relative to the presence of CO_2 and humidity level), and also the storage conditions are known. Table 3-3 confronts the results of the compositions predicted by each of the reactions (supposed to be complete) with the product compositions measured semi quantitatively using XRD. The products of each reaction (3-1), (3-6), and simultaneous reaction of (3-6 + 3-1) were first calculated based on their stoichiometry using the weight fraction (that converted into mole fraction) of powder A before aging as the initial composition:

- 0.13 mole of trona is produced from 0.19 mole of $Na_2CO_3.H_2O$ according to reaction (3-1),
- 0.23 mole of Li_2CO_3 and $Na_2CO_3.H_2O$ are produced from 0.46 mole of $LiNaCO_3$ according to reaction (3-6),
- 0.41 mole of $Na_2CO_3.H_2O$ and 0.58 mole of Li_2CO_3 are produced from 0.46 mole of $LiNaCO_3$ that experienced a complete transformation based on reaction (3-6). 0.28 mole of trona is then produced from the pursuit of reaction (3-1).

It appears that the XRD result overestimates the amount of Li_2CO_3 with 30% difference, while it underestimates the amount of trona with 20% difference. It must also be underlined that both of weight fractions were obtained by omitting the quantity of graphite. Still, it demonstrates the lack of precision of XRD analysis in terms of quantitative perspective.

Table 3-3. The aged powder A compositions predicted based on stoichiometry reaction vs SQ XRD

Samples	Weight %				Mole %			
	$Na_2CO_3.H_2O$	Li_2CO_3	$LiNaCO_3$	Trona	$Na_2CO_3.H_2O$	Li_2CO_3	$LiNaCO_3$	Trona
Powder A composition before aging (SQ XRD)	25	29	45	1	19	35	46	0
The aged powder A composition (after 8 months) according to chemical reaction stoichiometry								
rx. (3-1)	0	27	43	30	0	38	49	14
rx. (3-6)	54	45	0	1	41	58	0	32
rx. (3-6)+(3-1)	0	41	0	59	0	68	0	32
The aged powder A composition (after 8 months) obtained from SQ XRD								
	0	53	0	47	0	78	0	22

The same type of calculation was done using the initial composition of Marcalina powder as mention in the patent in order to estimate the composition of aged powder. The results showed that 58w%, 37w%, and 6w% of trona, Li_2CO_3, and graphite respectively are obtained for complete aging reactions (3-6 + 3-1). Hence, it contains of approximately 11.6w% of hydration water after complete aging.

SEM observations were also conducted to compare the crystal morphology of powder A before and after aging. The observation was delicate due to the variety of compounds which are not easy to distinguish by SEM (light elements are difficult to be identified by EDS) thus it is not included as part of the discussion. Nevertheless, the images taken from the DVS analysis could give some insights about the adsorption and recrystallization process during exposition in several humidity conditions. Moreover, it is worth noting that the carrier gas used during the DVS experiment was an inert gas, thus the influence of CO_2 cannot be studied here.

The adsorption-desorption cycle for NaCl has been studied in [5], which can be used as an approach to be applied in powder A. At low to medium relative humidity of about 10% RH, two dimensional lattice gases in the form of small bubble gas are formed on the surface of a crystal (fig. 3-13a). Following the increase of humidity level (20-60% RH), the water molecules begin to adsorb on adjacent sites. Water-water interactions then start to govern adsorption at 70% RH (fig. 3-13b), forming the multilayer liquid-like water film on the particle surface at 80% RH (fig. 3-13c). At the vapor pressure of 90% RH water molecules diffuse through the water-powder interface provoking the collapse of crystal lattice (fig. 3-13d). The powder attains the deliquescence phase where powder undergoes its gradual dissolution and liquefaction at 95% RH (fig. 3-13e), thus the Deliquescent Relative Humidity (DRH) for powder A would be 95% RH.

When such a system is submitted to an atmosphere of RH < DRH, water evaporates continuously. Recrystallization begins at sites whose free energy barrier is the lowest. Therefore, in case of only partial dissolution of larger crystal aggregates, crystal growth occurs at RH slightly smaller than DRH, which means at 90% RH (fig. 3-13f). Growth then begins with the re-appearance of crystal edges (fig. 3-13g) followed by bulk growth at 70%RH (fig. 3-13h), in which we observed the morphological changes, until all water is evaporated (fig. 3-13i). After the complete dissolution of small crystals is obtained, the critical supersaturation to form solid nuclei is reached only if enough water is evaporated (fig. 3-13j). Once solid nucleus is formed in a droplet, crystal growth will follow until total evaporation of water (fig. 3-13k).

The DVS result (figure 2-13) of powder A displays that it corresponds to multilayer adsorption (type II isotherm). However, considering the presence of hysteresis, it might be also correlated to the adsorption with a capillary condensation in a mesoporous medium (type IV isotherm). The type I hysteresis, H1, represented a branch of adsorption and desorption that almost parallel applied for an adsorbent with cylindrical pores distribution. The fact that the desorption curve is slightly over the adsorption curve (at the end of test) might indicate a kinetic problem due to the presence of micro pores or cumulative error (lots of points). Overall, the result of dynamic sorption method is coherent to the static one (aging experiment with saturated saline solution) with weight gain starts at 78.5% RH.

The XRD analysis of the sample before and after DVS (cf. fig. 3-14) showed that the $LiNaCO_3$ was fully decomposed after the recrystallization process. It appears to be fully transformed into Li_2CO_3 and $Na_2CO_3.H_2O$. No presence of higher hydrated carbonates might be due to the

recrystallization back to the low level of humidity. Moreover, the formation of trona didn't appear to happen. It is due to the fact that in order to form the trona, certain quantity of CO_2 is needed. In the DVS experiment, nitrogen was used as the carrier gas instead of air. Thus, the trona can not be formed.

- **Example of the aging mechanism: case for powders B and C**

Powders B and C were considered as the most transformed powders, as compared to powder A. Applying the aging mechanisms that have been previously discussed (and validated) for powder A, the aging of powders B and C can be estimated. Powder B happened to encounter both reactions (3-1) and (3-6) simultaneously (cf. table 2-6 or 2-12 for its composition). This is due to the fact that $LiNaCO_3$ appeared to be completely decomposed, while trona was produced in large quantities. On the contrary, powder C still has a significant quantity of $LiNaCO_3$. Hence, in this case the reaction (3-6) was more rate controlling than reaction (3-1). It could also be interpreted as an inhibition of the $LiNaCO_3$ decomposition due to CO_2 absorption as suggested from the aging experiments.

The DVS results (figure 2-14 and 2-15) of powders B and C respectively also display the same type of isotherm as powder A. The exposition of both powders in different humidities showed that they exhibit similar morphology after recrystallization (fig. 3-15 and 3-17). They both showed a different form compared to powder A, which is probably due to the lack of trona in powder A. The result of XRD analysis for powder B sample after DVS experiment shows only slight transformation of trona. Again, this result proves that CO_2 is needed in order to form trona.

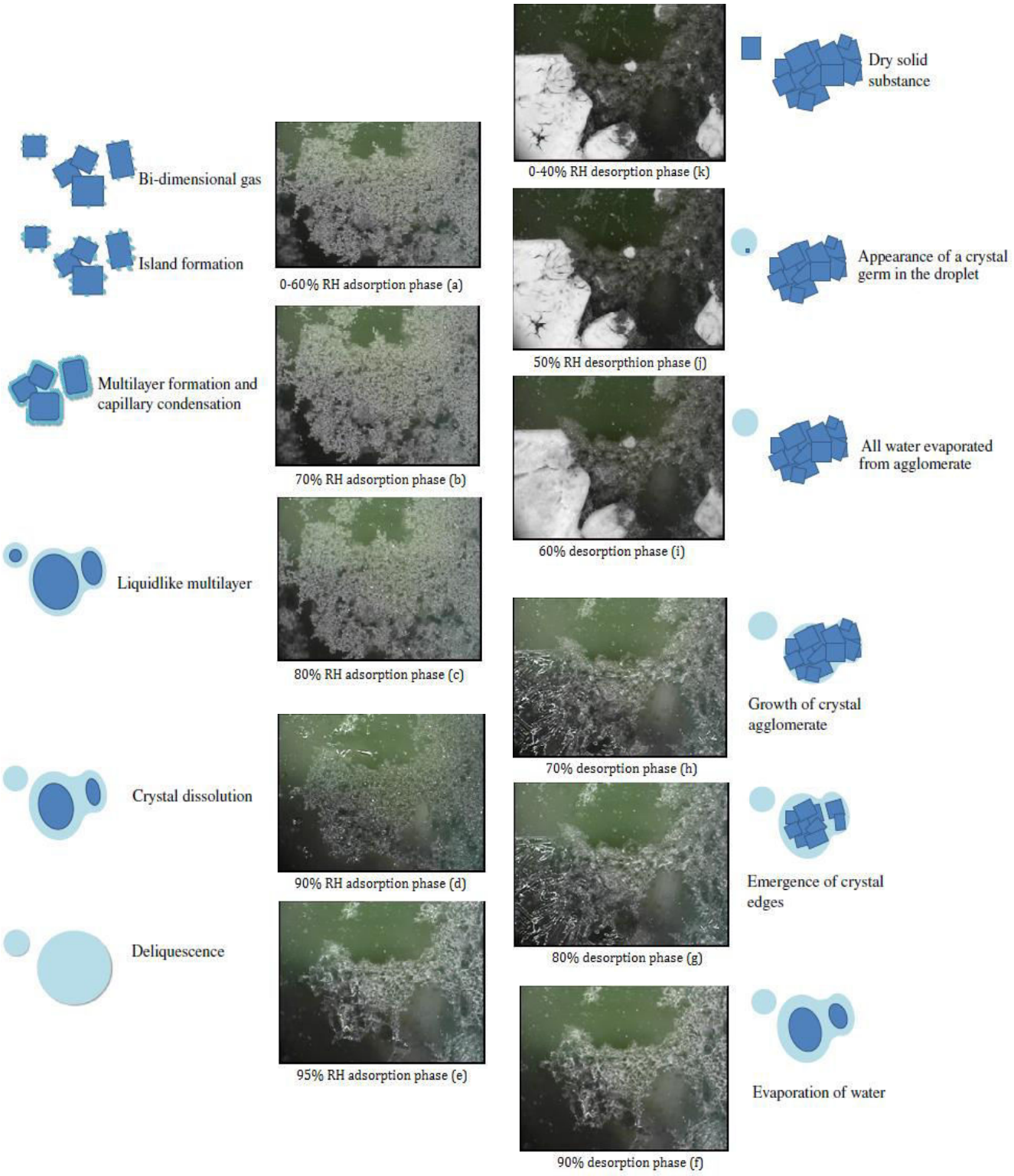

Figure 3-13. DVS observation results of powder A sample during adsorption – desorption cycle under different humidity

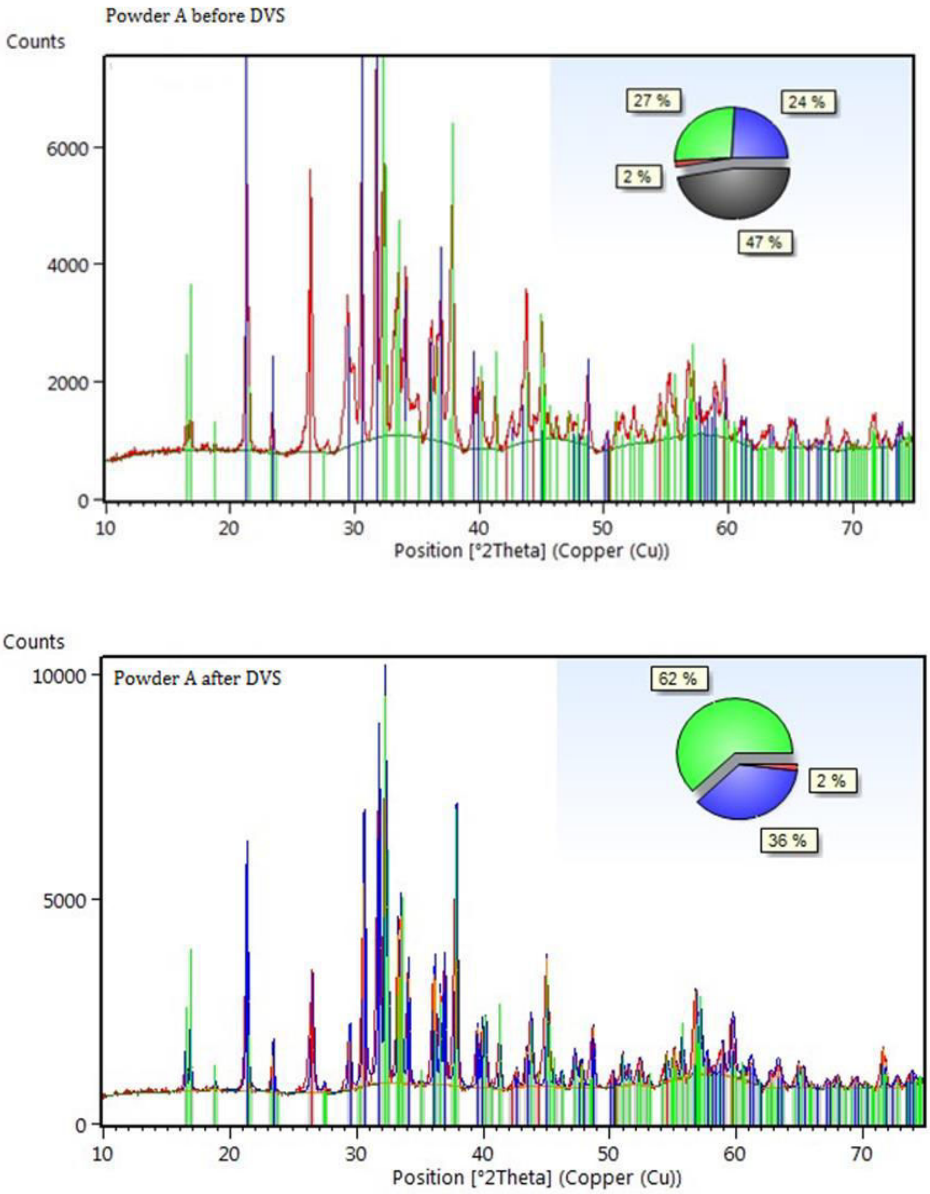

Samples	Compound	PDF Database	SQ XRD
Powder A before DVS	Lithium carbonate (Li_2CO_3)	00-022-1141	24%
	Sodium carbonate monohydrate ($Na_2CO_3.H_2O$)	01-076-0910	27%
	Carbon (C)	00-041-1487	2%
	Lithium sodium carbonate ($LiNaCO_3$)	01-084-2168	47%
Powder A after DVS	Lithium carbonate (Li_2CO_3)	00-022-1141	36%
	Sodium carbonate monohydrate ($Na_2CO_3.H_2O$)	01-076-0910	62%
	Carbon (C)	00-041-1487	2%

Figure 3-14. XRD analysis comparison of powder A sample before and after DVS analysis

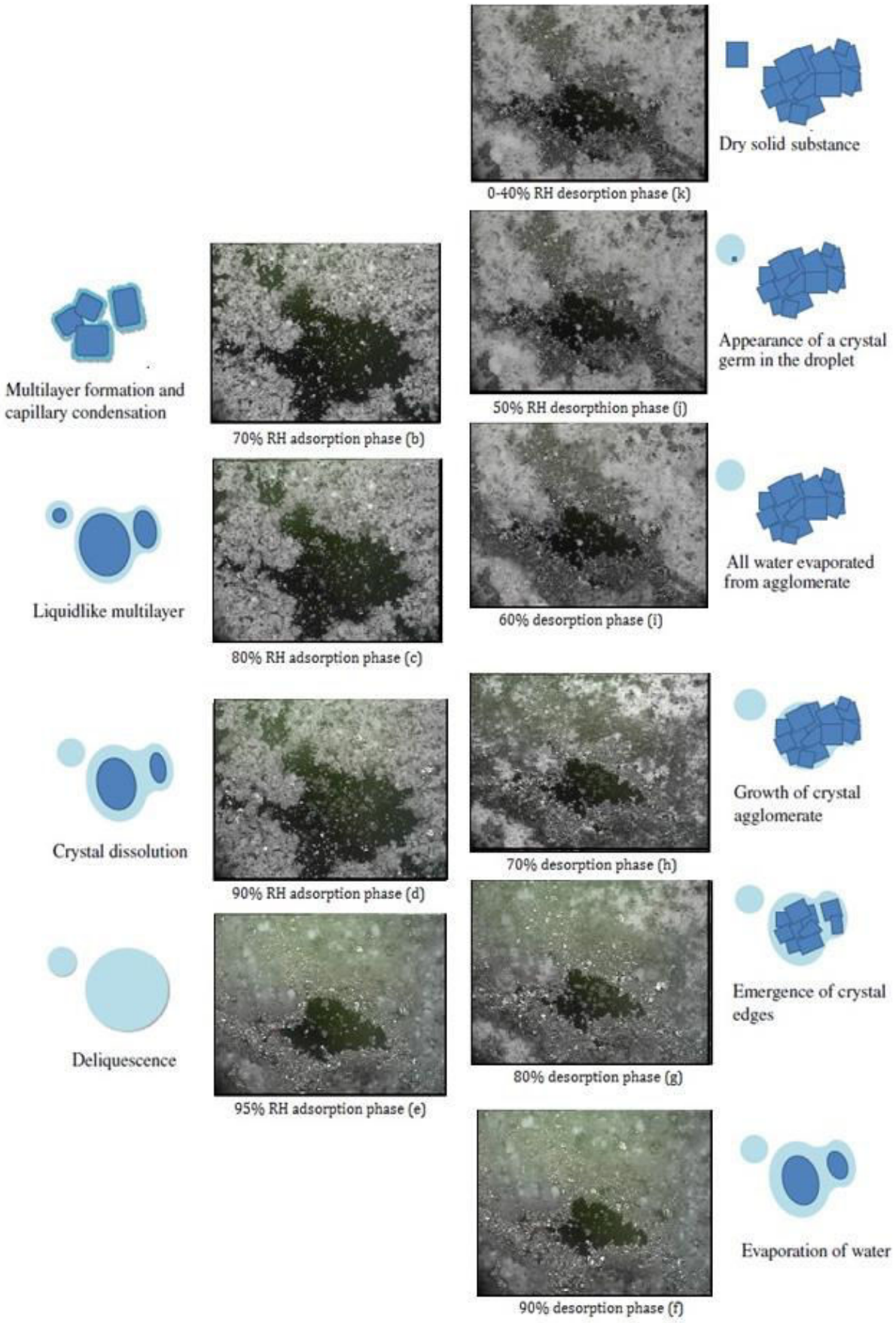

Figure 3-15. DVS observation results of powder B sample during adsorption – desorption cycle under different humidity

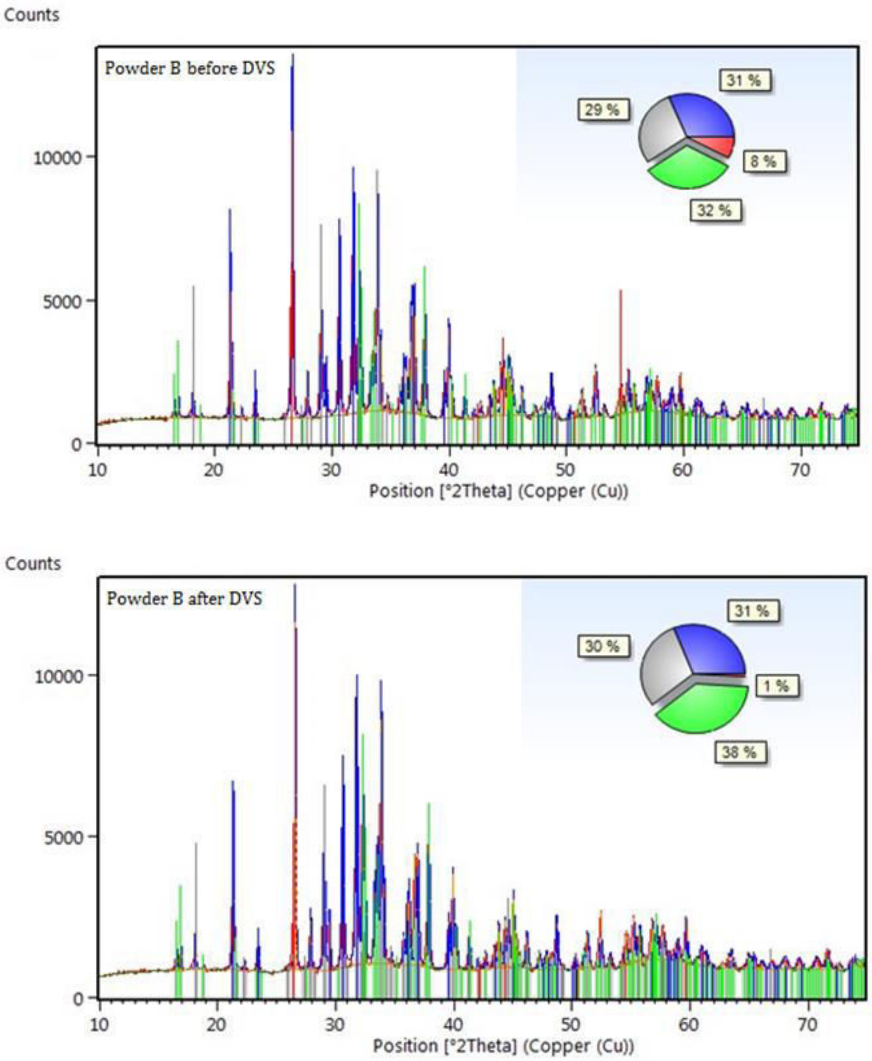

Samples	Compound	PDF Database	SQ XRD
Powder B before DVS	Lithium carbonate (Li_2CO_3)	00-022-1141	31%
	Sodium carbonate monohydrate ($Na_2CO_3.H_2O$)	01-076-0910	32%
	Carbon (C)	00-041-1487	8%
	Trona ($Na_2CO_3.NaHCO_3.2H_2O$)	00-029-1447	29%
Powder B after DVS	Lithium carbonate (Li_2CO_3)	00-022-1141	31%
	Sodium carbonate monohydrate ($Na_2CO_3.H_2O$)	01-076-0910	38%
	Carbon (C)	00-041-1487	2%
	Trona ($Na_2CO_3.NaHCO_3.2H_2O$)	00-029-1447	30%

Figure 3-16. XRD analysis comparison of powder B sample before and after DVS analysis

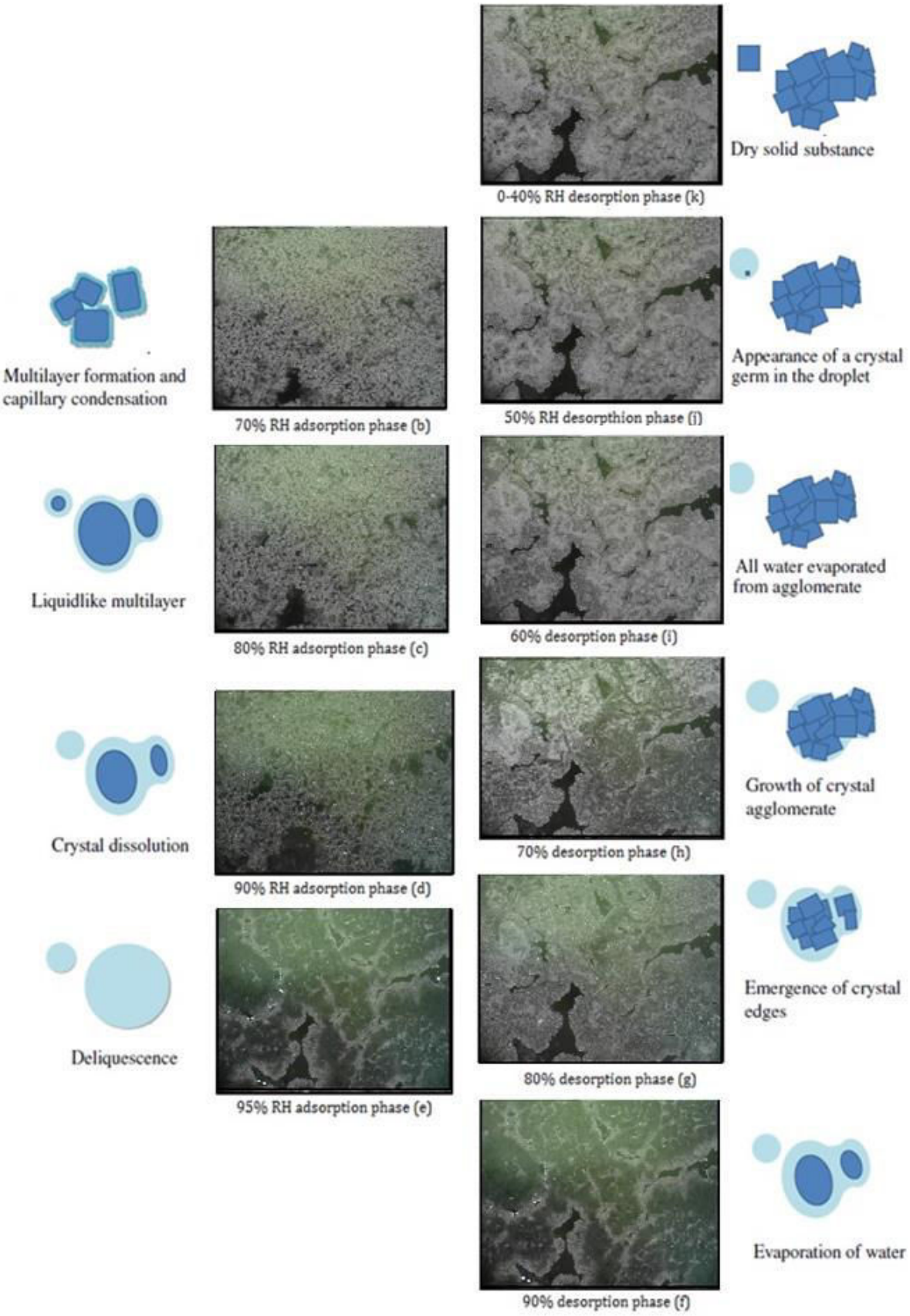

Figure 3-17. DVS observation results of powder C sample during adsorption – desorption cycle under different humidity

3.2 $LiNaCO_3$ as the byproduct during grinding/milling process

3.2.1 The results of grinding tests

This experimental result will confirm whether or not $LiNaCO_3$ is produced during the milling process. The formation of $LiNaCO_3$ can be calculated by stoichiometric approach using the sampling results taken on each milling and then analyzed by TGA. Figure 3-18 showed the process diagram of analysis adopted.

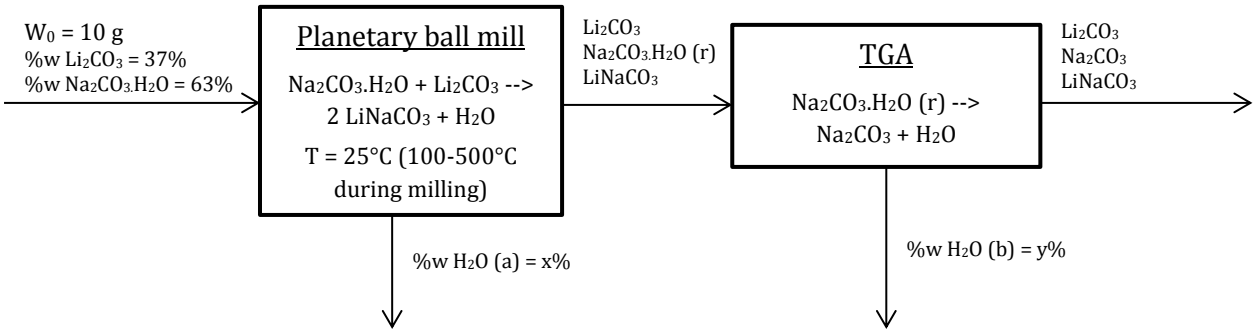

Figure 3-18. The process diagram of analysis in TGA for grinding samples

The TGA analysis allows the determination of the H_2O released (y%), which stoichiometrically corresponds to the quantity of the residual $Na_2CO_3.H_2O$ after milling process. Normalization of the result for 10 g of sample lead to the quantity of $Na_2CO_3.H_2O$ consumed (taken from $Na_2CO_3.H_2O$ initial - $Na_2CO_3.H_2O$ residue), which then permits to determine the quantity of $LiNaCO_3$ produced (mole of $LiNaCO_3$ = 2x mole of $Na_2CO_3.H_2O$ consumed). This method can be used as a comparative result to the semi quantitative XRD analysis obtained based on the difference of peak intensity. However, the results seem to always underestimate the ones from XRD. Since in this case the graphite (which often is the error source of analysis in XRD §3.3.2) is omitted, the XRD may provide better precision as compared to TGA (for which normalization is needed). The discussions will then pursuit the explanation about the formation of $LiNaCO_3$ during milling.

- *Automated mortar grinder*

3 types of samples have been milled as shown in table 3-4 below. The weight loss obtained from TGA is observed for each sampling time (1h). It may represent the residue of $Na_2CO_3.H_2O$ contained in the sample. $LiNaCO_3$ was shown to be present in the sample mixtures of Li_2CO_3 and $Na_2CO_3.H_2O$ (50:50 %mol) after 2h. Moreover the $LiNaCO_3$ XRD peaks are more significant after 3h of milling. However, this is not the case for mixtures of Li_2CO_3 and Na_2CO_3, for which no peak of $LiNaCO_3$ was observed after 3h of milling. A mixture of Li_2CO_3, $Na_2CO_3.H_2O$ and graphite also had the same result as the latter.

Table 3-4. The summary results of TGA and XRD analysis for samples obtained after milling in automated mortar grinder

No.	Sample	TGA (Δw=%)	XRD ($LiNaCO_3$)
1.	Li_2CO_3 + $Na_2CO_3.H_2O$ (50:50 %mol)	t = 0h --> 9% t = 1h --> 10% t = 2h --> 7% t = 3h --> 3%	t = 0h --> - t = 1h --> - t = 2h --> + t = 3h --> ++
2.	Li_2CO_3 + Na_2CO_3 (50:50 %mol)	- (after 3h)	- (after 3h)
3.	Li_2CO_3 + $Na_2CO_3.H_2O$ + C (43:48:9 %w)	n/a	- (after 2.5h)

- *Planetary ball mill*

Table 3-5 summarizes the results of TGA and XRD analysis for the samples obtained after milling under several operating conditions in the planetary ball mill. There are various interesting results worth discussed:

- Determination of the milling parameters:
  - Variation of rotation speed
    The highest $LiNaCO_3$ production was obtained at 600 rpm. This velocity, then, was used as a fix parameter to determine the other parameters (such as the number of balls, duration of milling, and weight of powder).
  - Variation of balls number
    The more balls are used, so does the formation of $LiNaCO_3$. Since the ball to powder ratio was needed to take into account, 30 balls were opted for 10 g of powder.
  - Variation of milling duration
    30, 40, and 50 balls were used with 15-60 minutes of milling duration, where samples were taken each 15 minutes. The results show that the longer is the milling time, the higher is the $LiNaCO_3$ formation. Duration of 60 minutes of milling was chosen with a pause of 10 minutes every 15 minutes of cycle.
  - Variation of the powder weight
    The increasing quantity of powder used (50 g instead of 10 g for the same parameter) neither significantly increased nor decreased the quantity of $LiNaCO_3$ produced. Therefore, 10 g of powder is maintained as the powder weight, considering the ball to powder ratio as one of the key parameter influencing the milling process [6].
- The milling of mixtures having graphite mixed together with Li_2CO_3 and $Na_2CO_3.H_2O$ produced no $LiNaCO_3$.
- The fact that $Na_2CO_3.H_2O$ milling didn't reduce the hydration water content in the compound.
- The grinding of mixtures of anhydrate carbonates showed full transformation into $LiNaCO_3$.
- The milling of mixtures having MoS_2 (as lubricant agent) mixed together with Li_2CO_3 and $Na_2CO_3.H_2O$ were able to produce 57% of $LiNaCO_3$. The lubricant has the small impact to the production of $LiNaCO_3$ (with 9% of decrease).

Table 3-5. The result summary of TGA and XRD analyses for samples obtained after milling in planetary ball mill

No.	Sample	Parameter		TGA	%w $LiNaCO_3$	
		Fix	Variable	(Δw=%)	Stoichiometry	XRD
1.	Li_2CO_3 + $Na_2CO_3.H_2O$ (50:50 %mol)	10 g 10 balls t = 1h	100 rpm 200 rpm 300 rpm 400 rpm 500 rpm 600 rpm	8.4% 9.1% 9.0% 8.9% 9.1% 8.0%	7.6% 0.6% 1.5% 2.6% 1.0% 11%	n/a n/a n/a n/a n/a n/a
2.	Li_2CO_3 + $Na_2CO_3.H_2O$ (50:50 %mol)	10 g 600 rpm t = 1h	15 balls 20 balls 30 balls	8.8% 7.9% 3.6%	3.5% 12% 55%	n/a n/a n/a
3.	Li_2CO_3 + $Na_2CO_3.H_2O$ (50:50 %mol)	10 g 600 rpm 30 balls	15 min 30 min 45 min 60 min	7.2% 5.4% 1.9% 3.6%	19% 38% 72% 55%	n/a 53% n/a 67%
4.	Li_2CO_3 + $Na_2CO_3.H_2O$ (50:50 %mol)	10 g 600 rpm 40 balls	15 min 30 min 45 min 60 min	6.8% 3.8% 2.4% 1.5%	23% 54% 68% 77%	n/a n/a n/a 86.4%
5.	Li_2CO_3 + $Na_2CO_3.H_2O$ (50:50 %mol)	10 g 600 rpm 50 balls	15 min 30 min 45 min 60 min	5.3% 1.8% 1.4% 1.7%	38% 74% 78% 75%	n/a n/a n/a 98%
6.	Li_2CO_3 + $Na_2CO_3.H_2O$ (50:50 %mol)	600 rpm 30 balls t = 1h	50 g	n/a	n/a	66%
7.	Li_2CO_3 + $Na_2CO_3.H_2O$ + C (43:48:9 %w)	10 g 600 rpm 30 balls t = 1h	-	n/a	n/a	0%
8.	$Na_2CO_3.H_2O$	10 g 600 rpm 30 balls	0 min 15 min 30 min 45 min 60 min	15.6% 14.5% 14.5% 14.6% 14.7%	n/a	n/a
9.	Li_2CO_3 + Na_2CO_3 (50:50 %mol)	10 g 600 rpm 30 balls t = 1h	-	n/a	n/a	100%
10.	Li_2CO_3 + $Na_2CO_3.H_2O$ + MoS_2 (43:48:9 %w)	10 g 600 rpm 30 balls t = 1h	-	n/a	n/a	57%

Note :

- n/a : analysis not conducted.
- %w $LiNaCO_3$ stoichiometry was obtained based on the results of %Δw of TGA deduced from this reaction: $Li_2CO_3 + Na_2CO_3.H_2O \rightarrow 2\ LiNaCO_3 + H_2O$.

3.2.2 Discussions

- *Formation of $LiNaCO_3$ by mechanochemical reactions of anhydrous sodium and lithium carbonate*

The experimental results above show that $LiNaCO_3$ can be produced by the mechanochemical reaction during milling process. For mixtures of anhydrous carbonates, the reaction happens as follows:

$$Li_2CO_3 + Na_2CO_3 \rightarrow 2\ LiNaCO_3 \qquad (3\text{-}7)$$

The mechanism of mechanochemical reaction between two constituents can be roughly explained in the following way [7]. Very intensive milling generates mechanical stresses in the particles. Fracture of these particles occurs thereby, creating clean surfaces since comminution and powders mixing in such a way enable very intimate contact between constituents. Highly disordered interfaces form in that way could be suitable nucleation sites for a new phase to form. Once the new phase is formed, reaction continues by permanent particle fracture which removes reaction product and creates new clean (fresh) surfaces. Hence, the reaction is not inhibited and persists until all reactants are consumed. Furthermore, the growth of the new phase is promoted by structural defects accumulated during milling as well as by local temperature rises appearing at the moment of ball impact. This may explain why $LiNaCO_3$ that conventionally need to be produced at around 500°C could be formed by mechanochemical reaction. However, as for the case of $Na_2CO_3.H_2O$, the fact that milling is not able to decrease the water quantity as measured in TGA (cf. table 3-6 no.8) proves that high temperature rises is not necessarily capable of release water contained in the hydrated form (as observed by TGA at 80°C). In this case, only the reduction of crystallite size probably occurs.

However, both mortar grinder and planetary ball mill showed contradictory results. $LiNaCO_3$ cannot be formed with mortar grinder from sodium carbonate anhydrate, contrarily to planetary ball mill, which for it occurred to be easier than from sodium carbonate hydrate. It might be due to the fact that mechanochemical treatment begins with a particle and crystallite refinement. In many instances, the first evidence of the reaction product do not appear before the critical crystallite size is reached [7]. Powders resulted from mortar grinder might have bigger crystallite size than that produced by planetary ball mill due to its lower performance. Therefore it is highly possible that in this case $LiNaCO_3$ has not been formed yet. Above all, the final product depends on the milling conditions; hence, different types of mill or the alteration of milling parameters may result in diverse reaction paths for mechanochemical reaction.

- *The role of water hydrate in the formation of $LiNaCO_3$*

The experimental results confirmed that $LiNaCO_3$ can also be produced from the mechanochemical reaction of lithium carbonate and sodium carbonate monohydrate according to this reaction:

$$Li_2CO_3 + Na_2CO_3.H_2O \rightarrow 2\ LiNaCO_3 + H_2O \qquad (3\text{-}8)$$

It appears that solids comprising oxygen and hydrogen, including solid acids and bases, acidic and basic salts, crystal hydrates, or the substances that react with each other releasing water, possess higher reactivity than anhydrous oxides. The hardness of these compounds is 3-4 times

smaller than that of anhydrous oxides that allows to decrease the level of mechanical loading and to pass to softer activation conditions [8]. A special domain dedicated to a novel approach involving these types of compounds is known as soft mechanochemistry.

The influence of water or hydroxyl groups on mechanochemical reactions (soft mechanochemical reactions) has been studied extensively by several authors [8]. Longo and Voght [8] synthesized $CaMg(CO_3)_2$ (dolomite) by activation of calcium or magnesium chlorides or sulphates with $Na_2CO_3.10H_2O$; these authors assumed that a rapid reaction was caused by local high solubility of components in thin films on the surfaces of ground material. Payakoff [8] carried out the synthesis of various oxalate complexes by mechanochemical activation of the solid oxalic acid with hydroxides and basic salts. In the studies of mechanochemical synthesis of hydroxyapatites from the mixtures of calcium orthophosphates and oxides, Chaikina [8] demonstrated that water molecules, being one of the structural components of the intermediate phase, stabilize it, making the rate of the formation of this phase dependent on the amount of bound water in the mixture. Boldyrev [80] also demonstrated that mechanochemical reactions of solids in the presence of water can be considered as hydrothermal ones. Hydrothermal, mechanochemical, and solid-phase syntheses of calcium silicate from anhydrous and hydrated oxides were compared. According to x-ray analysis, the interaction in the mixtures of anhydrous oxides under mechanochemical activation is not completed. However, the interaction of $Ca(OH)_2$ with $SiO_2.0.5H_2O$ is more intensive and able to produce hydro silicates, just like hydrothermal ones. Overall, mechanochemical reactions in a number of cases take place more rapidly in the mixtures of hydrated oxides than in the anhydrous oxides. Therefore, it is possible that in mortar grinder, $LiNaCO_3$ can be produced using $Na_2CO_3.H_2O$ as reactant but not for Na_2CO_3 anhydrous. It might be due to the fact that the presence of hydrate makes the formation of $LiNaCO_3$ less energetic than using anhydrous compound as a reactant.

- *The influence of graphite and MoS_2 during mechanochemical synthesis reaction*

Both in planetary ball mill and mortar grinder it was not possible to obtain $LiNaCO_3$ from graphite containing mixtures and more limited amounts with MoS_2. Both are solid lubricant that can limit the transfer of energy from the ball to the powder. It occurs that graphite is one type of surfactants that is usually used to obtain stabilization in high energy milling [6]. It is usually achieved by surrounding particles with a layer of substances which are sterically bulky such as polymers. These large adsorbates provide a steric barrier that prevents close contact of the fine particles. In this case, if a surfactant is added to water, its hydrocarbon chain tends to self-associate to minimize contact with water molecules. Moreover, the adsorption of surfactants results in a decrease of the surface energy of solids causing the decrease of their strength and resistance to mechanical effects. It should be noticed that a possible risk of explosion can also happen during the mechanochemical reaction involving graphite in the atmosphere; consequently inert atmosphere should be preferably chosen.

- *The energy calculation result for producing $LiNaCO_3$*

Table 3-6 summarized the parameters of calculation used to estimate the intensity involved during the production of $LiNaCO_3$ in a planetary ball mill Fritsch Pulverisette 6 using the equations reported in appendix (cf. A.1). The results of calculation of the energy involved during milling showed that the energy increases as the duration of milling increases, the number of balls increases, and the powder weight decreases (cf. table 3-7).

Table 3-6. The summary of parameter used during milling in planetary ball mill Fritsch Pulverisette 6

No.	Parameter	Value	Comment
1.	Vial		
	- D_v	0.076 m	The diameter of vial measured
	- H_v	0.06 m	The height of vial measured
2.	Ball		
	- d_b	0.01 m	The diameter of ball measured
	- n_b	30	The number of ball used
	- m_b (1 ball)	0.0299 g	The mass of ball
3.	$N_{b,v}$	$= \pi . D_v^2 . H_v / 4 d_b^2$ =272.19	The number of balls that can be contained in the vial
4.	$N_{b,s}$	$= \pi . (D_v - d_b) . H_v / 3 d_b^2$ = 41.47	The number of balls needed to cover one third of the inner surface wall
5.	ε	$= \ln(0.05) / \ln(\frac{N_{b,s}}{N_{b,v}})$ = 1.59	Parameter of ball diameter
6.	n_v	$= N_b / N_{b,v}$ = 0.11	Ratio of ball numbers to the total ball number contained in the vial
7.	φ_b	$= (1\text{-}n_v^{\varepsilon})$ = 0.97	Assumption taken for which until one third of the inner surface wall is not covered
8.	W_p	= 600 rpm = 62.83 rad/s	Absolute angular velocity of the plate
9.	W_v	= -1092 rpm = -114.35 rad/s	Absolute angular velocity of the vial (the negative sign signify the rotation opposite of the plate)
10.	r_{pv}	0.075 m	Radius plate - vial
11.	r_{vw}	0.038 m	Radius vial – wall
12.	V_b	$= \left[(W_p R_p)^2 + W_v^2 \left(R_v - \frac{d_b}{2} \right)^2 (1 - 2W_v / W_p) \right]^{1/2}$ = 9.40 m/s	The absolute velocity of the balls at the detachment point
14.	V_s	$= \left[(W_p R_p)^2 + W_v^2 \left(R_v - \frac{d_b}{2} \right)^2 2 W_p W_v R_p (R_v - \frac{d_b}{2}) \right]^{1/2}$ = 0.94 m/s	The absolute velocity with which the ball starts to move again with the vial
15.	E_b	$= \left(\frac{1}{2} \right) . m_b . V_b^2$ = 1.32 J	The kinetic energy when the ball is launched
16.	E_s	$= \left(\frac{1}{2} \right) . m_b . V_s^2$ = 0.01 J	The ball's residual energy
17.	ΔE_b	$= E_b - E_s$ = 1.31 J	The total energy released by the ball during the series of collision events
18.	$\Delta E_b{}^*$	$= \varphi_b . \Delta E_b$ = 1.27 J	The total energy released for total ball numbers used

Table 3-7. The relations of intensity consumed toward several variables applied in planetary ball mill at 600 rpm

Parameter	Variable	Intensity (kWh/g)	$LiNaCO_3$ produced (g)	Energy consumed (kWh)
30 balls 10g of $LiNaCO_3$	Time (min)			
	15	96	1.9	182.4
	30	191	3.8	725.8
	45	287	7.2	2066.4
	60	383	5.5	2106.5
1h of milling 10g of $LiNaCO_3$	Ball number			
	10	131	1.1	144.1
	30	383	7.2	2757.6
	40	501	7.7	3857.7
	50	613	7.5	4597.5
30 balls, 1 h of milling 10g of $LiNaCO_3$	Powder weight (g)			
	10	383	6.6	2527.8
	30	129	19.8	2554.2
	50	77	33	2541

The results obtained from the experiment of grinding showed that $LiNaCO_3$ is produced as a result of mechanochemical reaction during grinding. The energy consumed to produce $LiNaCO_3$ increases as the duration of milling and the number of balls use increase. 2.5MWh energy is consumed in order to produce around 6.6 g of $LiNaCO_3$ from 10 g of $Na_2CO_3.H_2O$ and Li_2CO_3 mixture (50 molar%).

Milling is certainly a process necessary in order to obtain a micro sized and homogenized powder as Marcalina. However, it is highly possible that $LiNaCO_3$ was formed unintentionally as the previous analysis conducted by the producer only control the water content and elementary composition (such as lithium, sodium, and carbon). Moreover, this component was only able to be detected by XRD, which is an improvement of analyses previously adopted. Whether it is necessary or not to form $LiNaCO_3$ to have good extinguishing properties as well as the influence of the presence of trona produced during storage towards the extinction will be discussed in the next chapter.

CONCLUSION

The experimental results of aging have demonstrated two different reactions that might happen simultaneously, whose reaction kinetics depends on the condition of storage:

- The high RH condition in the open atmosphere (presence of CO_2) promotes the formation of trona,
- The high RH condition in closed atmosphere (limited presence of CO_2) is favorable to the decomposition of $LiNaCO_3$.

Powder B happened to encounter both reactions, while the reaction decomposition of $LiNaCO_3$ in powder C is more reaction rate controlled. This might be due to the difference of storage conditions applied to both powders. It is suggested to control the humidity condition under 50% to prevent the reaction of aging. These two mechanisms allow us to estimate the composition of powder after aging if both reactions happened. The result showed that 58w% of trona might be formed which approximately corresponds to 11.6w% of hydration water.

Concerning $LiNaCO_3$, it appears to be produced by the mechanochemical reactions happening during the grinding process as what have been demonstrated in the grinding experiments. Indeed, the decrease of water content to the range of specification might be obtained if the composition was taken from the patent (7w% of hydration water). Furthermore, it is also possible that the producer might not suspect that the release of water content may also cause the formation of $LiNaCO_3$. Moreover, only XRD analysis is capable of detecting the presence of this compound and it is not the analytical method used at the years of production in order to control the quality of product.

The next part of the study will be focused on understanding the behavior of powders with different compositions on the extinction of sodium fires, notably related to the effect of aging towards the extinction capacity due to the presence of trona and the influence of $LiNaCO_3$, to evaluate the quality of extinction.

BIBLIOGRAPHY OF CHAPTER III

[1] C. G. Waterfield, R. G. Linford, B. B. Goalby, T. R. Bates, C. A. Elyard, and L. a. K. Staveley, "Thermodynamic investigation of disorder in the hydrates of sodium carbonate," *Trans. Faraday Soc.*, vol. 64, no. 0, pp. 868–874, Jan. 1968.

[2] Matthew C. Ball, Rosemary A. Clarke and Alec N. Strachan, "Investigation of the Formation of Wegscheiderite, Na2CO3.NaHCO3," *J Chem Soc Faraday Trans*, vol. 87, no. 22, pp. 3683–3686, 1991.

[3] R. S. Gärtner and G.-J. Witkamp, "Mixed solvent reactive recrystallization of trona (sodium sesqui-carbonate) into soda (sodium carbonate anhydrate)," *Hydrometallurgy*, vol. 88, no. 1–4, pp. 75–91, Aug. 2007.

[4] F. M. Doyle, "Crystallization and precipitation: Proceedings of the international symposium, Saskatoon, Saskatchewan, Canada, 5–7 October, 1987. Edited by G.L. Strathdee, M.O. Klein and L.A. Melis," *Can. J. Chem. Eng.*, vol. 67, no. 4, pp. 698–698, Aug. 1989.

[5] M. Langlet, M. Benali, I. Pezron, K. Saleh, P. Guigon, and L. Metlas-Komunjer, "Caking of sodium chloride: Role of ambient relative humidity in dissolution and recrystallization process," *Chem. Eng. Sci.*, vol. 86, pp. 78–86, Feb. 2013.

[6] P. Baláž, "High-Energy Milling," in *Mechanochemistry in Nanoscience and Minerals Engineering*, Springer Berlin Heidelberg, 2008, pp. 103–132.

[7] A. M. Spasic and J.-P. Hsu, *Finely Dispersed Particles: Micro-, Nano-, and Atto-Engineering*. CRC Press, 2005.

[8] E. Avvakumov, M. Senna, and N. Kosova, *Soft mechanochemical synthesis: A basics for new chemical technologies*. Kluwer Academic Publishers.

CHAPTER IV
Study on the extinction of sodium fire

This chapter is dedicated mainly to study the influence of the physicochemical properties previously discussed as regards to the extinction capacity of powders. Three samples of Marcalina powders (referred as powders A, B, and C) previously analyzed will be tested in the small sodium pool fire (10g) device. Afterwards, study will be more focused on understanding the influence of trona and $LiNaCO_3$ (related to the variation of hydration water content and the eutectic composition) on the capacity of extinction. Considering that it is difficult to discriminate their influence in such complex mixtures of several compounds, synthetic powders were produced with different compositions as reported in table 4-1. Each powder experienced the same method of fabrication as the one described in §2.3.3. Coupled TGA-µGC and XRD analyses of the synthetic powders are conducted in order to ensure the consistency of powder composition before each test.

Four distinguished groups of studies are chosen:

Firstly, the role of hydration water is studied based on the different proportions contained in pure components. Anhydrous sodium carbonate, sodium carbonate monohydrate, and trona were selected with 0 w%, 13.2 w%, and 18.1 w% of hydration water content respectively. The effect of sodium carbonate monohydrate and trona decomposition at relatively low temperature, followed by the high melting temperature of anhydrous sodium carbonate during the extinction will be investigated.

Secondly, the role of eutectic mixture with and without hydration water in sodium carbonate is the object of study. The composition of Marcalina as presented in the patent [1,2] is adopted. Hence, it represents 7w% and 0w% of hydration water content respectively. The effect of powder decomposition and its melting at relatively low temperature on the extinction will be observed.

Thirdly, the impact of hydration water content over and in the range of specification as recommended by CACI [3] is studied. The presence of trona with and without $LiNaCO_3$ in the mixture will be compared considering that it will influence the hydration water content to 5.6w% and 8.9w% respectively.

Finally, the influence of $LiNaCO_3$ during extinction is examined in order to understand the necessity of its existence in the mixture. The latter is still questionable, as $LiNaCO_3$ is a compound that melts at 500.6°C, while sodium and lithium carbonates decomposed at 498°C if sufficiently mixed in eutectic proportion. For that reason, pure $LiNaCO_3$ was mixed with 9w% of graphite. In addition, its presence in the mixture of Marcalina is studied with 2.9w% of hydration water. This study is essential in order to explain whether it might substantially improve the extinction quality or it will only contribute in reducing the content of hydration water (in the case of unintentional production during grinding).

Two experimental programs were developed and detailed in Table 4-2. The primary objective of this study is to understand the role of each chemical composition and physical property in order to propose an interpretation of the extinction mechanism of sodium fires. The difference between both programs is mostly related to the experimental setting (the sieve opening size and thermocouple placement), treatment of the extinction residue (air and inert), and the powder spreading method employed (continuous and direct). Continuous spreading is more representative of the real case of extinction using powder extinguishers, while direct spreading

gives insight into the role of chemical composition (omitting the physical properties that influence spreading performance) in the extinguishing process.

Table 4-1. Synthetic powders experimentally studied for sodium fire extinction

Samples	**Trona**	**$LiNaCO_3$**	**$Na_2CO_3.H_2O$**	**Li_2CO_3**	**Anhydrous Na_2CO_3**	**Graphite**	**%H_2O (hydrate)**	**Reason for the choice of compositions**
Powder I					91%	9%	0%	No H_2O, High melting temperature
Powder II			91%			9%	13.2%	Pure monohydrate, High melting temperature
Powder III	91%					9%	18.1%	Pure trona, High melting temperature
Powder IV			48%	43%		9%	7%	Monohydrate in Na/Li carbonate Low melting temperature
Powder V				43%	48%	9%	0%	Anhydrous Na/Li carbonate Low melting temperature
Powder VI	23%		30%	38%		9%	8.9%	Hydration water over the range of tolerance limit (4.8% and not over 5.4%±1%) Low melting temperature
Powder VII	6%	25%	30%	30%		9%	5.6%	Hydration water in the range of tolerance limit (4.8% and not over 5.4%±1%) Low melting temperature
Powder VIII		91%				9%	0%	Pure $LiNaCO_3$ Low melting temperature
Powder IX		50%	20%	21%		9%	2.9%	Hydration water under the range of tolerance limit (4.8% and not over 5.4%±1%) Low melting temperature

Table 4-2. Detail of experimental programs conducted for sodium fire extinction

	First test campaign (A)	Second test campaign (B)
Experimental period	11-12/2015	03-04/2016
Sample	Synthetic powders I - IX	- Powders A, B, C, - Synthetic powders II, IV, VII, IX
Spreading method	Continue spreading	Continuous spreading Direct spreading only for II, IV, VII, IX
Cooling method after extinction	Ambient air	Argon
Sampling of the extinction residue	Under the laboratory hood, ambient air	Inside laboratory glovebox Inert gas
Analytical method of the extinction residue	XRD	XRD and optical microscopy
Thermocouple's placement	Left and right	Right
Sieve size opening	2 superimposed sieves (1 mm + 0,85 mm) → caking problem	1 sieve of 1 mm → no caking problem, powder falls more rapidly

The entire experimental studies presented here were conducted in the Chris(X)ti-Na experimental facility (cf. 2.3.3). The chemical characterization of the extinction residue by XRD and optical microscopy were realized in the laboratory. The starting times for temperature and camera recordings are synchronized. The temperature profile recorded by thermocouples is associated with the phenomenon observed by video camera during the experiments, which are reported in the figures of result exploitation presented later on in this chapter.

The exploitation results are composed of two different steps, (i) combustion and (ii) extinction:

i. Combustion step

Generally, two types of sodium combustions are observed in the experiments, the combustion that is preceded by an oxidation phase (delay of ignition) as shown in figure 4-1 and the spontaneous combustion (without delay of ignition) as can be seen in figure 4-2. The difference in both phenomena is represented by temperature profile and video observation during the test. The difference in ignition delay is observed from the video and thermocouple recording. It is relatively short with an average of 2s on each test as observed in the video. However, the duration can be much significant as measured by thermocouples (i.e. 67s in figure 1). This is due to the preferential nodulation (ignition point) on the sodium surface that varied in each test. Depending on where it is located (whether or not it is near the thermocouple placement), the delay of temperature increase might vary. The sodium surface temperature measurement is represented by T_s as it is located at the sodium surface (cf. figure 4-1 and 4-2).

Taken the results presented in figure 4-1 as an example, after the lid opening, the nodules appeared at the middle of the sodium surface before a progressive and homogeneous propagation takes place at the sodium surface. Thus, the temperature doesn't increase immediately as the nodulation started rather far from the thermocouples. Shortly after the nodules started to spread, the temperatures began to increase.

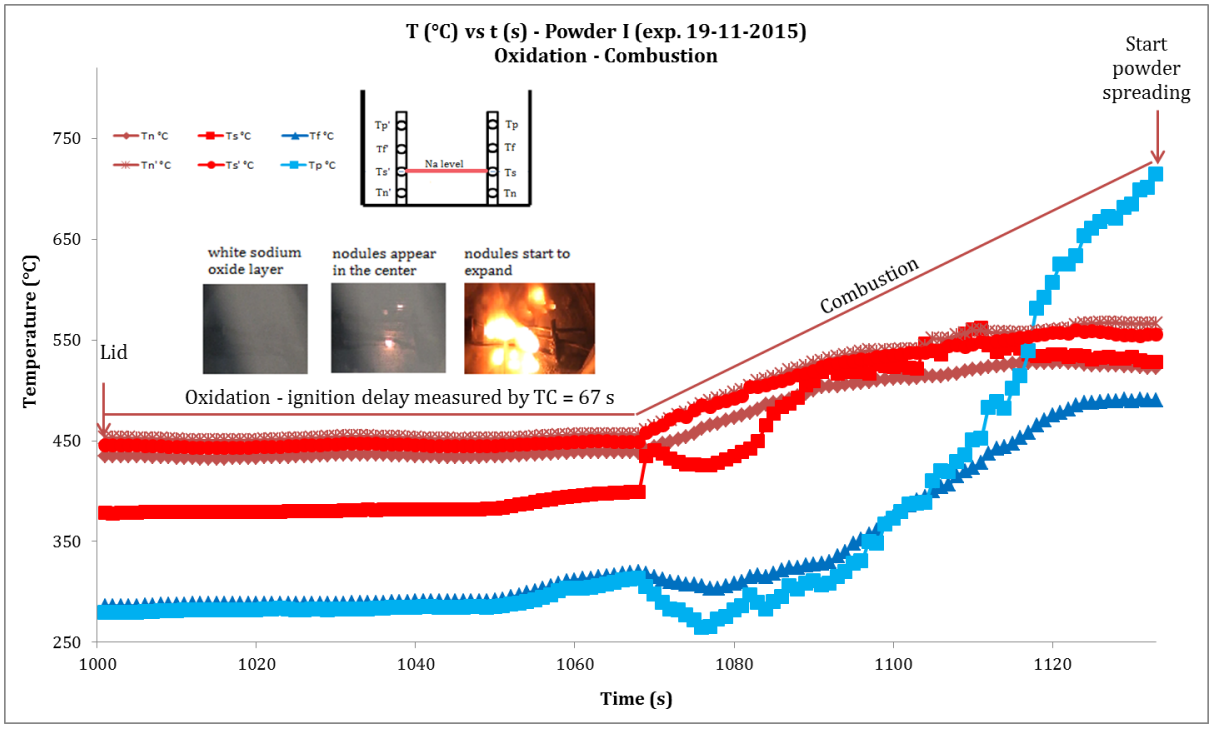

Figure 4-1. The temperature and video observations of the Chris(X)ti-Na experiment using powder I with continuous spreading during combustion with ignition delay

This is not the case for what is observed in figure 4-2. The nodules appeared near the thermocouples immediately after the lid opening. Hence, the increase of temperature is directly observed. However both cases showed temperature fluctuations that may represent the flame movements on the sodium surface, as mostly measured by T_f and T_p. In any case, these are phenomenon that cannot be controlled and that varied in each test. One of them might be observed in each combustion phase during experiment.

In both cases illustrated in the figures, the temperatures inside the sodium pool, T_n, and at the surface, T_s, slowly increase, while the thermocouples placed above it exhibit a faster temperature rise (in the range of 600-900°C). This indicates that the flames are located above the sodium surface. The temperature profiles and video observation during combustion for the other powders are reported in appendix (cf. A-3).

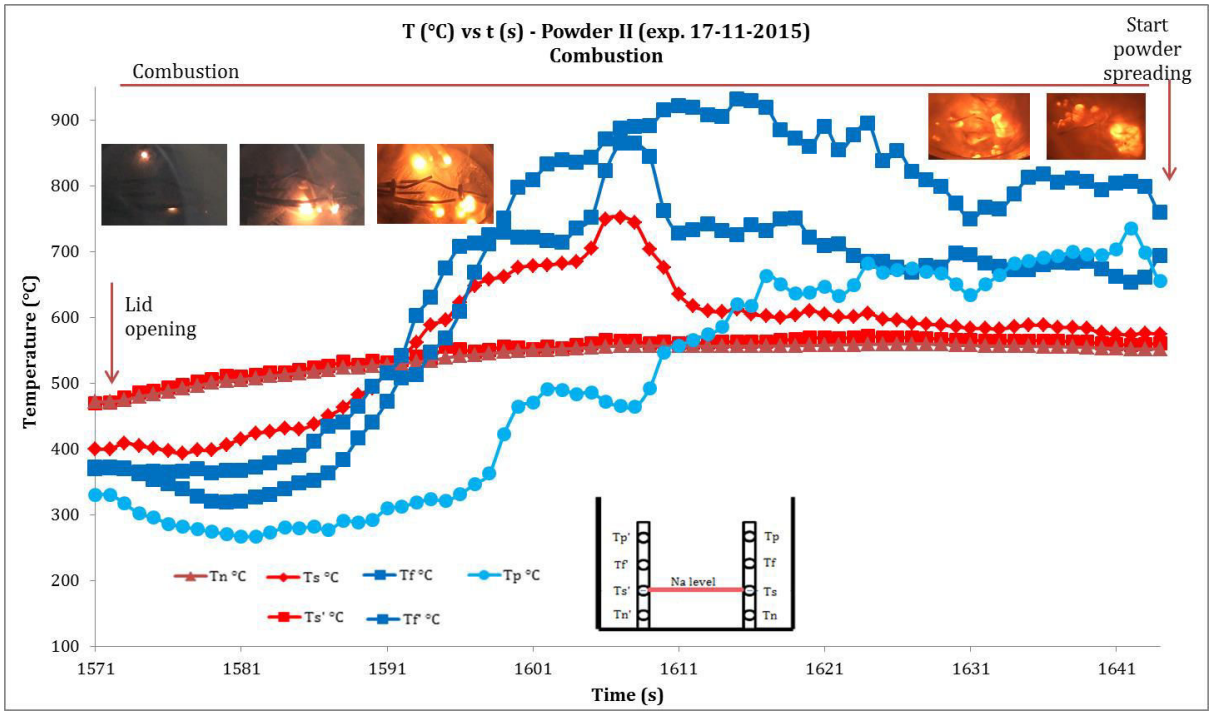

Figure 4-2. The temperature and video observations of the Chris(X)ti-Na experiment using powder II with continuous spreading during spontaneous combustion (without ignition delay)

ii. Extinction step

This process starts as soon as T_n and T_s reach a temperature around 500°C. This temperature is chosen as it represents the average sodium temperature operating condition in the reactor. Besides, this ensures that the temperature in which the spreading starts will always be the same for all tests. However, it must be emphasized that the flame temperatures indicated by both T_f and T_p before spreading might be different.

Several parameters are established to simplify the exploitation of results:

- All of thermocouples were immerged in the powder at the end of extinction.
- T_f and T_p are chosen as the best representation of the temperature profile indicating extinction (interpreted by the decrease of temperature), as they represented where the flames are located (above the sodium surface). The rate of temperature decrease and/or increase is calculated by dividing the temperature difference by the time.
- Both times at which the spreading is started and stopped are noted, allowing the synchronization between the temperature and video recordings.
- The extinction is considered to be achieved based on the absence of flame taken from visual observation using video camera. Overall, it is difficult to determine the extinction time, especially for the experiments with continuous spreading, as it highly depends on the homogeneity of the powder in covering the sodium surface, which is quite a challenge to control and maintain at each test. Nevertheless, the absence of flame marks the end of extinction as observed by video camera, and is considered to be sufficiently reliable in a practical point of view.

- The visual observation presented in each exploitation figure later on, approximately illustrates the phenomenon remarked between the start of powder spreading until the end of extinction. It might not represent what happens at the exact time and temperature.
- Certain temperature recordings might be disregarded in several cases, depending on whether or not the temperature represents the visual observation. For instance, in the case where the ignitions are still observed in the video due to the problem of homogeneity during powder spreading. Conversely, the data are kept if there is no indication of temperature increase simply because the reignition happened far from the thermocouple placement. Therefore, it is important to interpret the result of experiments based on several measurements and not judged by only one type of measure (video or temperature recording).
- The contribution of water to the extinction efficiency might be studied based on the quantity of water released. It can be calculated by multiplying the mass fraction of hydration water content in each powder by the quantity of powder used, which is measured, in each test.
- At last, general remarks of observation are summarized in the recap table provided for each group of study. The XRD diagrams of extinction residue are reported in appendix A-5.

4.1 Experimental results using Marcalina (Powders A, B, C)

Powders A, B, and C are tested in order to understand the effect of different compositions that were previously analyzed with regard to the extinction, in the continuous spreading test configuration. Powder A has the smallest content of trona, powder B does not contain $LiNaCO_3$, and powder C contains both trona and $LiNaCO_3$. All residues were cooled down with argon in a closed container. Table 4-3 summarizes the experimental results observed during extinction, completed with the XRD analysis of the residues.

Powder A is made of relatively fine particles. The temperature profile tends to decrease slowly at a rate of 0.3-0.4°C/s, as it struggles to melt at the sodium surface (cf. figure 4-3). A porous layer seems to be formed and several ignitions are observed under the crust. An intervention is needed to achieve a complete extinction. Even so, several ignition points still appear under the porous crust. 10.4 g of powder (0.5 g of water) are used to extinguish 10 g of sodium fire during 423 s. A small presence of NaOH was detected in the extinction residue.

A similar trend, but with a faster temperature decrease, is observed with powder B at an average rate of 6°C/s, as measured by T_f and T_p (cf. figure 4-4). Each decrease of temperature is mostly followed by temperature elevation at an average rate of 10°C/s. The final trend, leading to extinction, shows a fast temperature decrease with 9°C/s and temperature at the end of extinction is detected to be below the sodium surface temperature with 460°C and 390°C for T_f and T_p respectively. It has a better spreading performance as compared to powder A. Powder B melts easily at the sodium surface after the contact, thus complete extinction can be achieved. No high flame is observed during extinction. Both NaOH and $LiNaCO_3$ are detected in the residue. 8.5 g of powder B (0.7 g of water released), is needed to extinguish 10 g of sodium fire in 43 s.

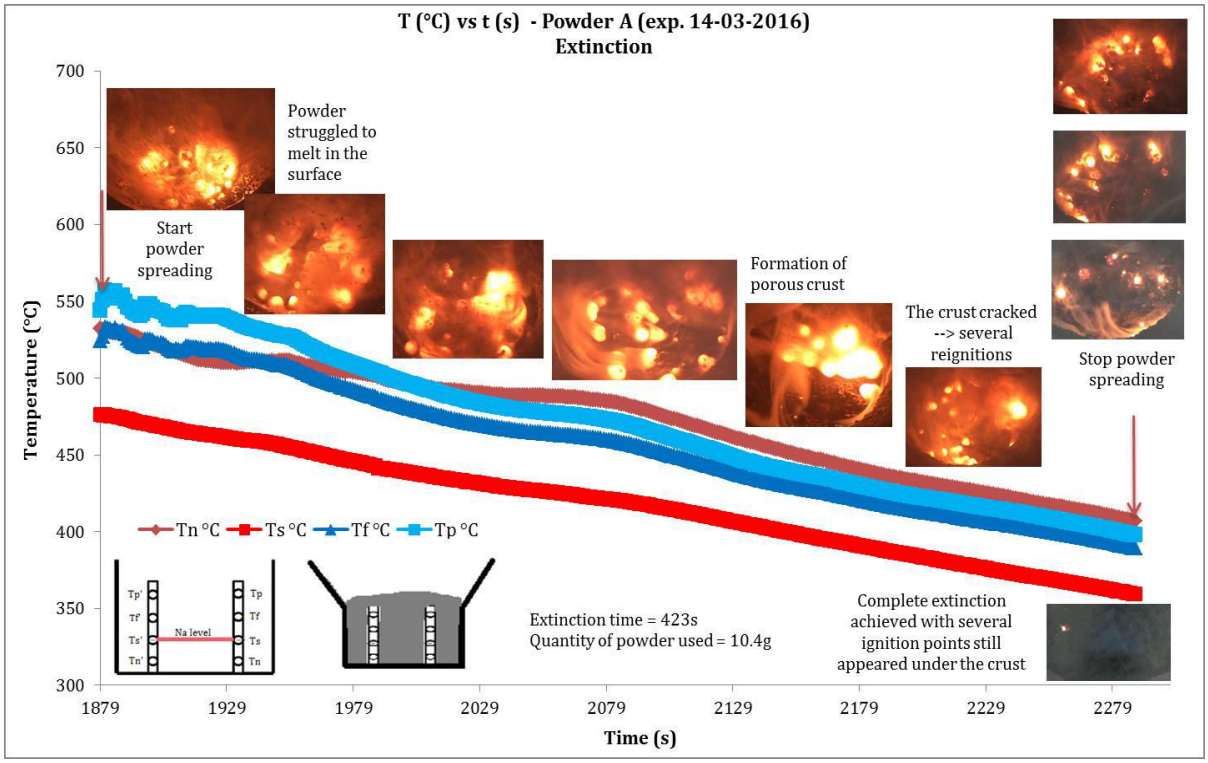

Figure 4-3. The temperature and video observations of the Chris(X)ti-Na experiment with continuous spreading during extinction using powder A

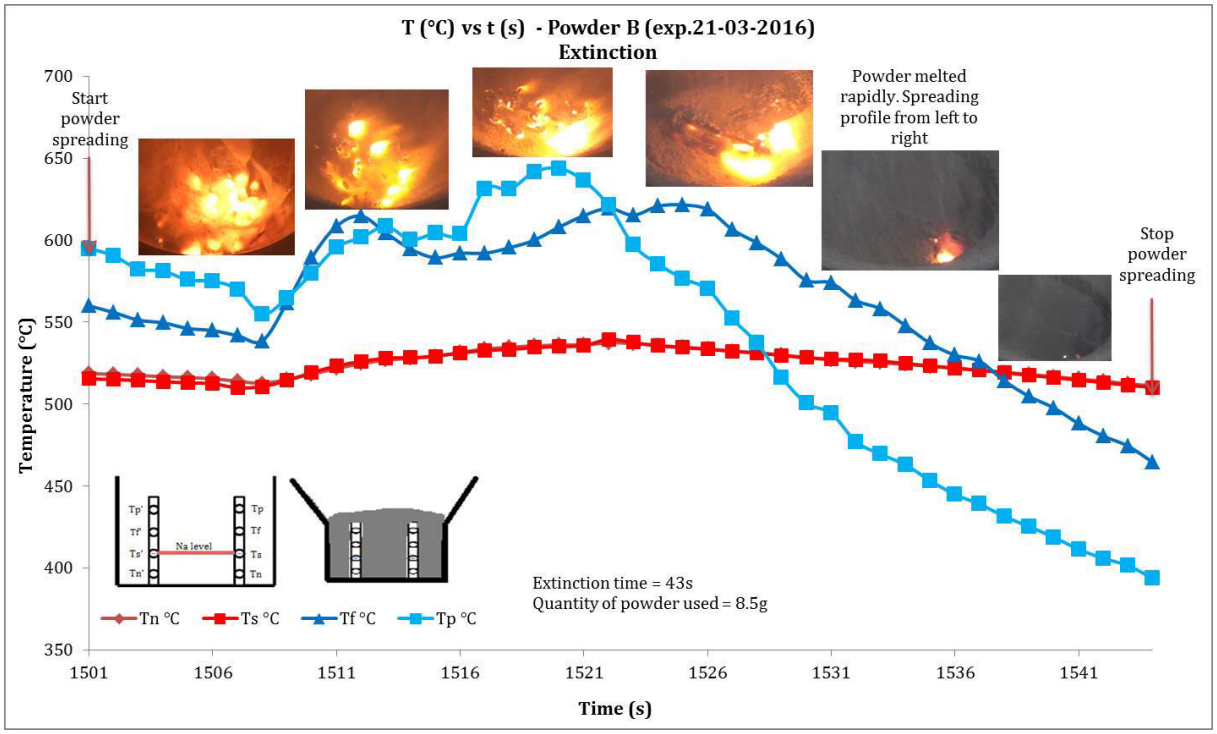

Figure 4-4. The temperature and video observations of the Chris(X)ti-Na experiment with continuous spreading during extinction using powder B

Although, it is made of the same fine particles as powder A, powder C doesn't seem to present any difficulty in melting at the sodium surface. T_f measures a moderate temperature rise of 4.8°C/s, followed by a rapid temperature drop (twice faster). At the same time, T_p records a temperature decrease at almost the same rate. The latter indicates the temperature of 350°C (cf. figure 4-5), which is the smallest temperature detected among the three powders at the end of extinction. More NaOH (as compared to powder A, but equivalent to powder B) is detected in the extinction residue. 6.2 g (0.5 g of water) are required to achieve a complete extinction for 78 s.

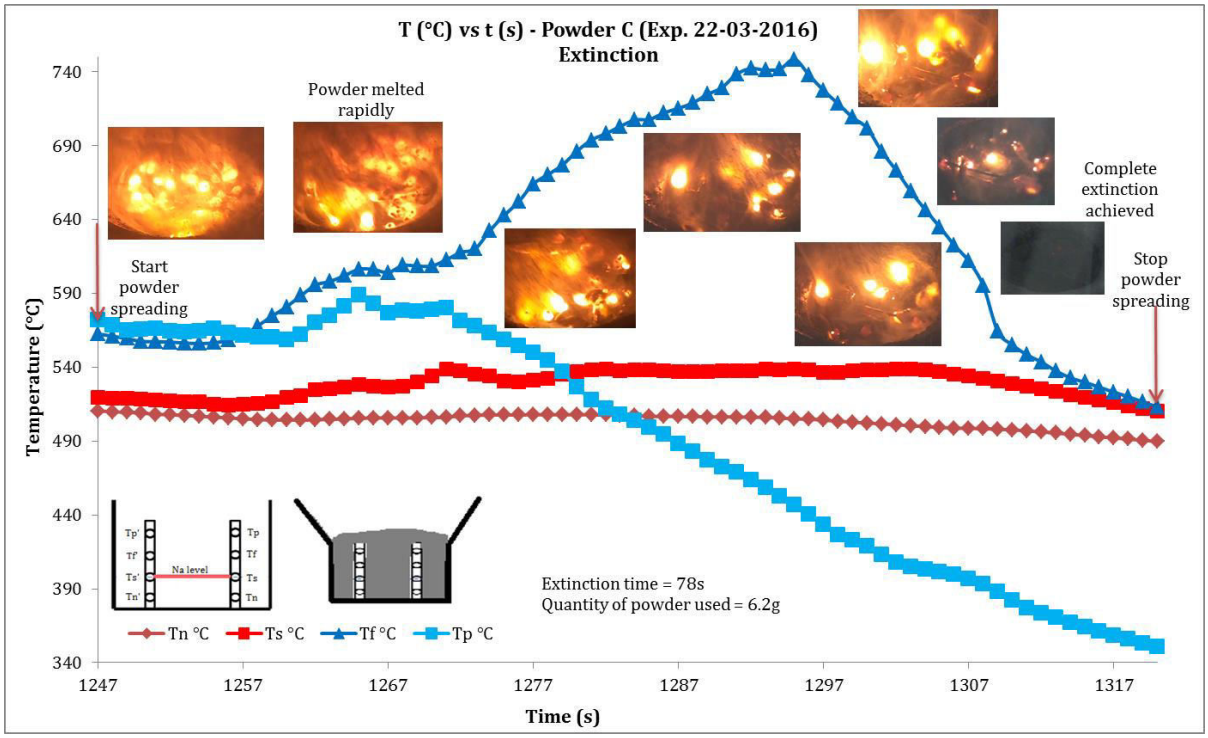

Figure 4-5. The temperature and video observations of the Chris(X)ti-Na experiment with continuous spreading during extinction using powder C

These tests demonstrate that the more hydration water is released into the sodium fire, the faster is the extinction (as shown in the test with powder B). The water released during extinction might eventually contribute to reduce the amount of powder employed to obtain the same complete extinction. Even if powders A and C release the same hydration water content, 4.2 g more of powder A is required to obtain the same extinction as for powder C, although several ignition points are still observed under the crust of powder A. Higher hydration water content also appears to improve the spreading performance considering that powder B (bigger particles) seems to have the best spreading performance and powder C has a better extinguishing performance than powder A.

Table 4-3. Summary of Chris(X)ti-Na experimental results using Marcalina powders A, B, and C with continuous spreading

Powder composition (w%)	Extinction time (s)	Powder quantity (g)	H_2O released (g)	XRD post test analysis	Thermocouples profile	Remarks
Powder A (4.7%w H_2O) Cooling residue with Ar $Na_2CO_3.H_2O$ 31% Li_2CO_3 33% $LiNaCO_3$ 26% Trona 1% Graphite 9%	423	10.4	0.5	NaOH + Na +	• T_n ↓ = 0.3°C/s • T_s ↓ = 0.3°C/s • T_f ↓ = 0.3°C/s • T_p ↓ = 0.4°C/s	• No caking problem in the sieve • Fine particles • Formation of porous layer → slow melting • O.I. (Operator Intervention) • No high flame observed • Complete extinction with several ignition points
Powder B (8.4%w H_2O) Cooling residue with Ar $Na_2CO_3.H_2O$ 29% Li_2CO_3 38% Trona 20% Graphite 8% Free water 4%	43	8.5	0.7	NaOH ++ LiNaCO3 +	• T_n=T_s= cst @510°C • T_f ↓ = 3°C/s, ↑ = 19°C/s, ↓ = 8.5°C/s, ↑ = 3.2°C/s, ↓ = 8.3°C/s • T_p ↓ = 5.7°C/s, ↑ = 7.4°C/s, ↓ = 10.4°C/s	• No caking problem in the sieve • Bigger particles than powder A • Progressive spreading from left to right • Rapid melting • No high flame observed • Complete extinction
Powder C (7.5 %w H_2O) Cooling residue with Ar $Na_2CO_3.H_2O$ 16% Li_2CO_3 35% $LiNaCO_3$18% Trona 26% Graphite 5%	78	6.2	0.5	NaOH ++ Na ++	• T_n = cst @ 505°C • T_s cst @ 510°C • T_f cst @ 550°C, ↑ = 4.8°C/s then ↓ = 9.4°C/s • T_p cst @ 570°C then ↓ = 4.7°C/s	• No caking problem in the sieve • Fine particles • Rapid melting • No high flame observed • Complete extinction

4.2 Experimental results using synthetic powders

4.2.1 Continuous spreading

A.1 *Role of hydration water*

Powders I, II, and III were made up from graphite mixed with anhydrous sodium carbonate, sodium carbonate monohydrate, and trona respectively. They present 0 w%, 13.2 w%, and 18.1 w% of hydration water contents respectively. Table 4-4 summarizes the experimental results observed during extinction and completed with the XRD analysis of the residues.

Powder I apparently struggles to melt at the sodium surface, as recorded by the temperature fluctuations during the first 70s observed by T_p. It is followed by a progressive temperature decrease at a 0.4°C/s rate. A total time of 295s is needed to spread the powder until the extinction is achieved with 8.6g of powder and intervention is required to cover reignition near the border. All of thermocouples indicate the same slow decreasing trend until spreading is stopped (cf. figure 4-6). A small presence of NaOH is detected in the extinction residue, which might be due to the reaction of unburnt sodium with air humidity during cooling down under air.

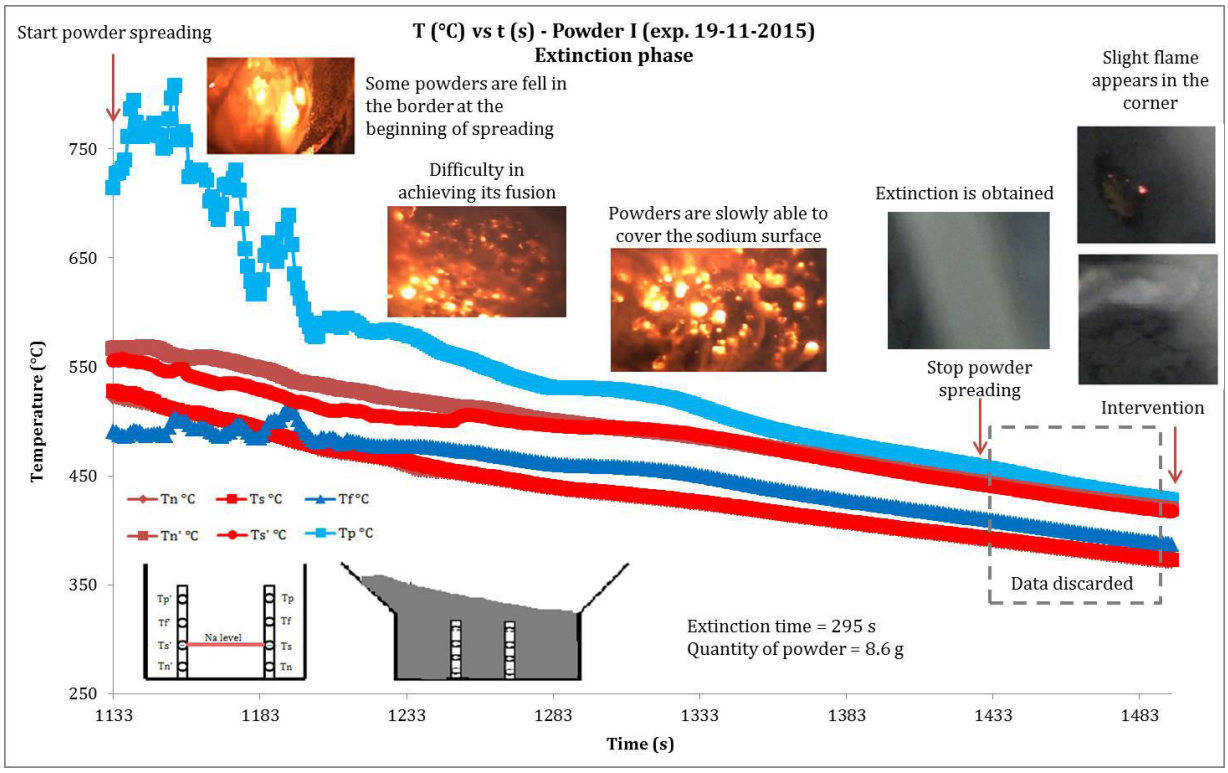

Figure 4-6. The temperature and video observations of the Chris(X)ti-Na experiment with continuous spreading during extinction using powder I

Contrarily to powder I, powders II and III experienced a rapid temperature decrease, registered by T_f and T_p, afterwards they experienced a rapid increase in temperature. T_p in the test using powder II (cf. figure 4-7) demonstrated a fast temperature rise with the average rate of 8.5°C/s for both tests conducted, followed by rate of temperature decrease twice faster at 20°C/s. Meanwhile, powder III shows a more constant temperature at around 510°C, before experiencing a slower temperature decrease at a rate of 15°C/s (cf. figure 4-8). The final T_p at the end of extinction is found to be at 200°C and 380°C for powders II and III respectively, both of which are smaller than those measured at the surface (T_s). For both powders, T_s displays a temperature rise of 6.5°C/s on the average before a decrease that leads to the complete extinction. A high flame of around 5 cm is detected and observed in the second test (IIB) with powder II during the fast powder spreading rate, which might have blown the fire. This phenomenon is not observed in the first test (IIA), as the spreading rate was smaller. A vapor phase flame circulates for 18s, causing a temperature rise close to 100°C, denoted by T_s in powder III. More details about the presence of flame during extinction will be provided in the "discussions" section. 5.5g of powder II (0.7g of water release) and 5.1g of powder III (0.9g of water release) are necessary to extinguish a sodium fire during 70s and 44s respectively. XRD analysis of the extinction residue shows higher peaks of sodium hydroxide (NaOH) in powders having higher quantities of hydration water as can be seen in table 4-4.

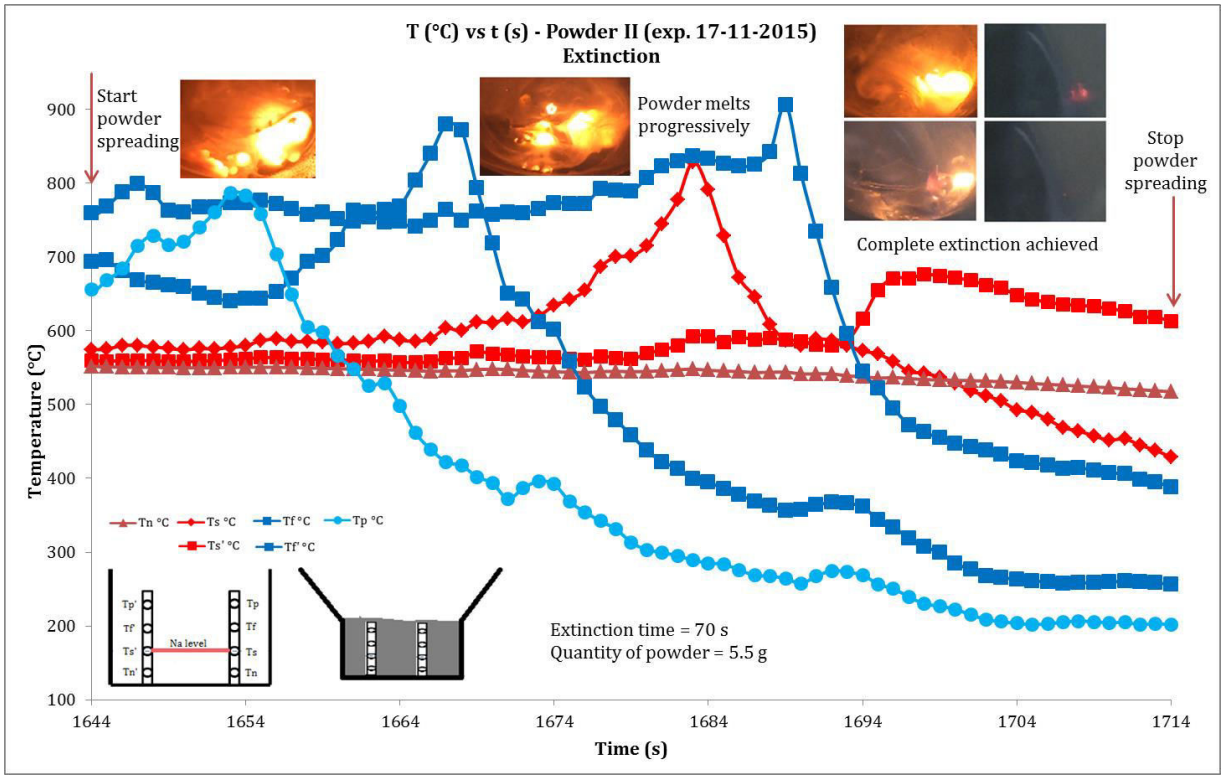

Figure 4-7. The temperature and video observations of the Chris(X)ti-Na experiment with continuous spreading during extinction using powder II

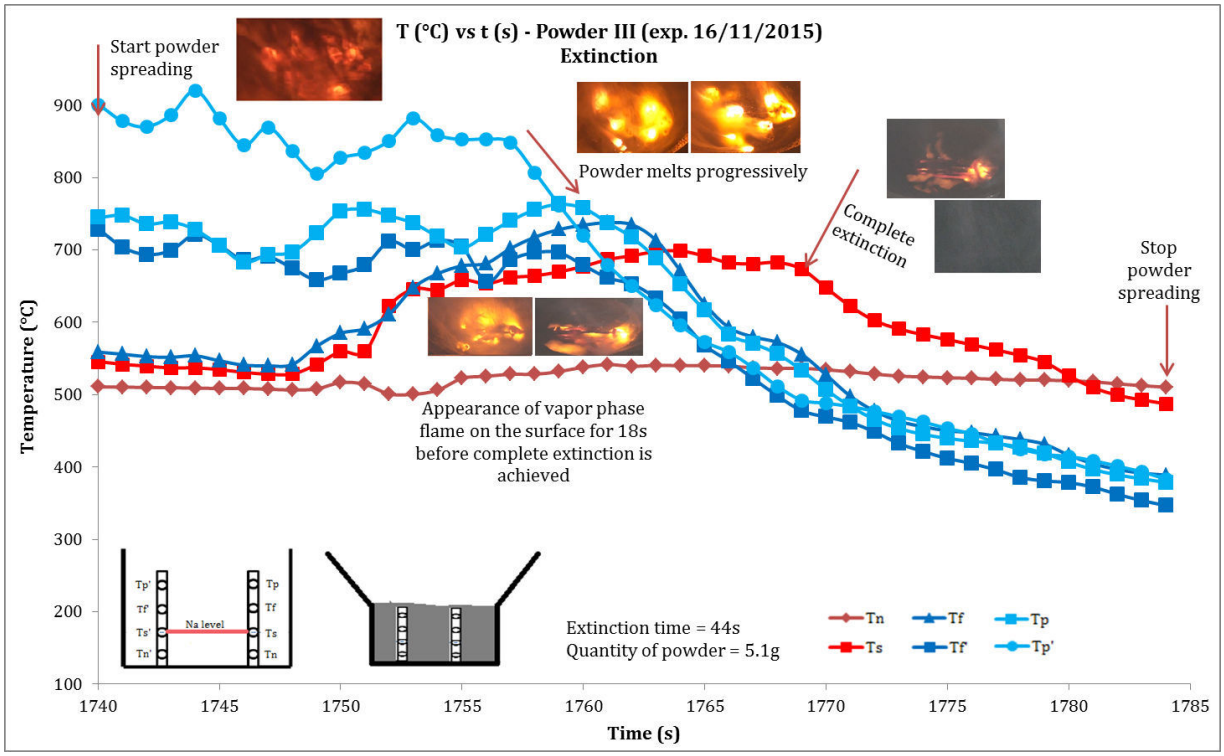

Figure 4-8. The temperature and video observations of the Chris(X)ti-Na experiment with continuous spreading during extinction using powder III

Overall, these tests displayed that both the quantity of powder used and the extinction time decrease as the content of hydration water increases. However, it is worth noting that the temperature at the sodium surface (T_s) and the one inside the sodium (T_n) stay constant at 530°C for powder containing hydration water. On the contrary, the one that contains no hydration water shows a progressive decrease of temperature. The explanation about these phenomena might indicate the difference of behavior of powders towards fire extinction, which might lead to the difference in the mechanism of extinction that will be discussed in section 4.3.

Table 4-4. Summary of Chris(X)ti-Na experimental results using synthetic powders I, II, and III with continuous spreading

Test	Study	Powder composition (w%)	Extinction time (s)	Powder quantity (g)	H_2O released (g)	XRD post test analysis	Temperature profile (°C/s)	Remarks
I A	**Role of hydrated water**	**Powder I** **(0% H_2O)** Na_2CO_3 91% Graphite 9%	295	8.6	0	NaOH +	• T_n =0.4°C/s • T_s =0.4°C/s • T_f = 0.3°C/s • T_p = fluctuations of T in the first 70s, followed by ΔT=0.6 °C/s	• Caking problem in the sieve • Bad spreading performance • Formation of porous layer → slow melting • No high flame • O.I . (Operator Intervention) • Unburnt Na is transformed into NaOH
II A		**Powder II** **(13.2% H_2O)** 1st test (A) $Na_2CO_3.H_2O$ 91% Graphite 9%	70	5.5	0.7	NaOH +++ Na ++	• T_n = cst at 550°C • T_s ↑ = 6.7°C/s then T_s ↓ =13.2°C/s • T_f ↑ = 3.3°C/s then ↓ = 20.7°C/s • T_p ↑ = 14.5°C/s then ↓ = 9.6°C/s	• Caking problem in the sieve • Better spreading performance • Rapid melting • No high flame • Complete extinction • Formation of NaOH during extinction
II B		**Powder II** **(13.2% H_2O)** 2nd test (B)	20	13.9	1.8	NaOH ++	• T_n = T_s = cst at 530°C • T_f slight ↓ = 2.2°C/s then rapid ↓ = 8.9°C/s • T_p slight ↑ = 2.5°C/s then 2x rapid ↓ = 30.3 and 22.2°C/s	• No caking problem • Fast spreading (notably near the left part) • Presence of high flame (H_2) ≈ 5 cm on the right • Fire blowout by fast spreading • Complete extinction • Formation of NaOH during extinction • Optical microscope observation reported in Appendix A-4
III A		**Powder III** **(18.1% H_2O)** Trona 91% Graphite 9%	44	5.1	0.9	NaOH ++++ Na +	• T_n = cst at 510°C • T_s ↑ = 6.3°C/s then ↓ =12.4°C/s • T_f ↑ = 13.8°C/s then ↓ = 16.2°C/s • T_p cst at 510°C then ↓ = 15.4°C/s	• Caking problem in the sieve • Best spreading performance • Presence of vapor phase flame for 18s around the Na surface • Rapid melting • Complete extinction • Formation of NaOH during extinction

A.2 *Role of eutectic mixture with and without hydration water in sodium carbonate*

Powder IV was prepared from graphite mixed with sodium carbonate monohydrate and lithium carbonate in the proportions proposed by Reuillon in the patents [1,2]. The same composition was also employed for powder V, with anhydrous sodium carbonate replacing monohydrate.

At the beginning of spreading (cf. figure 4-9), a lot of powder IV particles fall on the left side of the container. Powder then melts progressively from the left to the right side. The cone placed in the container helps the powder to glide and pushed it into the flame that mostly still appeared on the right side. T_p measure a fast temperature decrease at a 3.4°C/s rate after direct contact of powder with the flame. It is followed by a brief temperature rise at 14°C/s, before returning to another temperature decrease at 2.3°C/s. Meanwhile T_n, T_s, and T_f recorded a slow but continuous decrease of temperature. The complete extinction was obtained after 173 s of spreading with 7.3 g of powder (with 0.5g of water released).

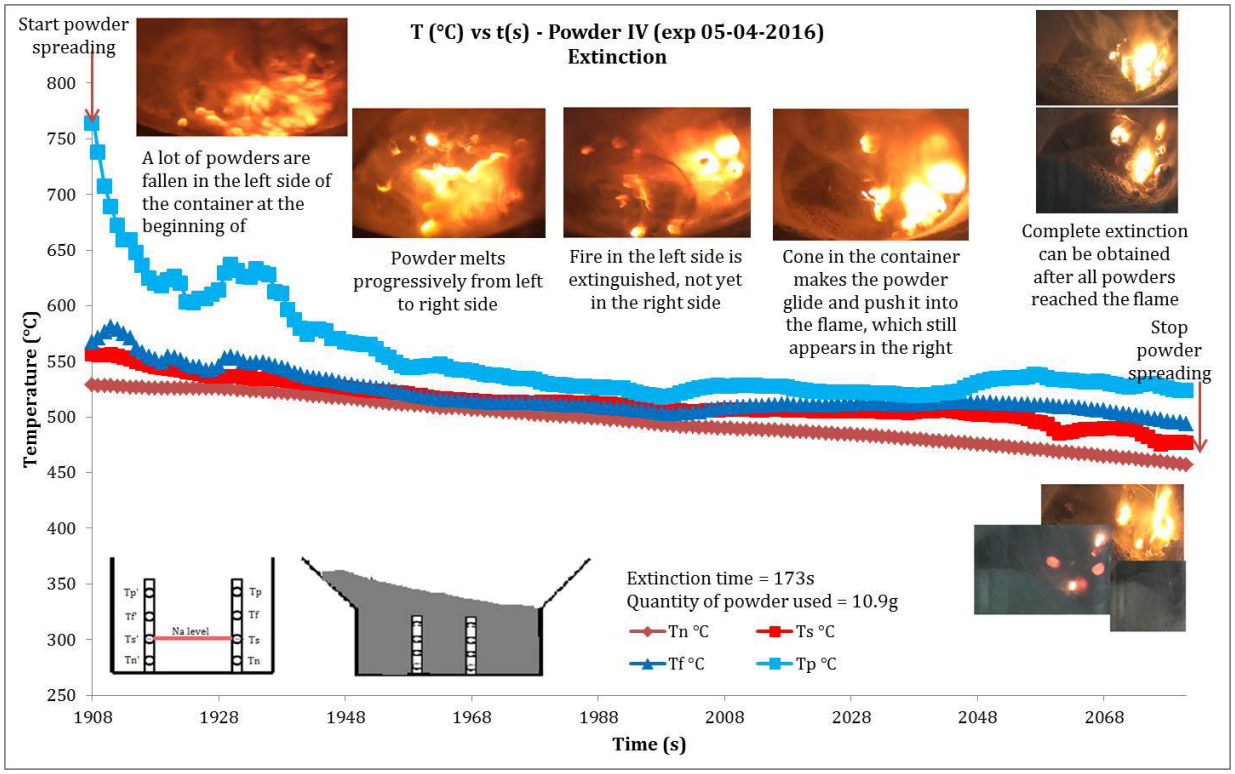

Figure 4-9. The temperature and video observations of the Chris(X)ti-Na experiment with continuous spreading during extinction using powder IV

Powder V (cf. figure 4-10) spreads heterogeneously at the sodium surface. It also encounters difficulty to melt at the sodium surface. As a consequence, the flame around half of the container can't be extinguished (temperature rise of 9.3°C/s). Hence, the operator intervention is needed to achieve complete extinction after 214 s of powder spreading where 7.8 g of powder is required. Even so, several ignition points are still appeared under the powder crust.

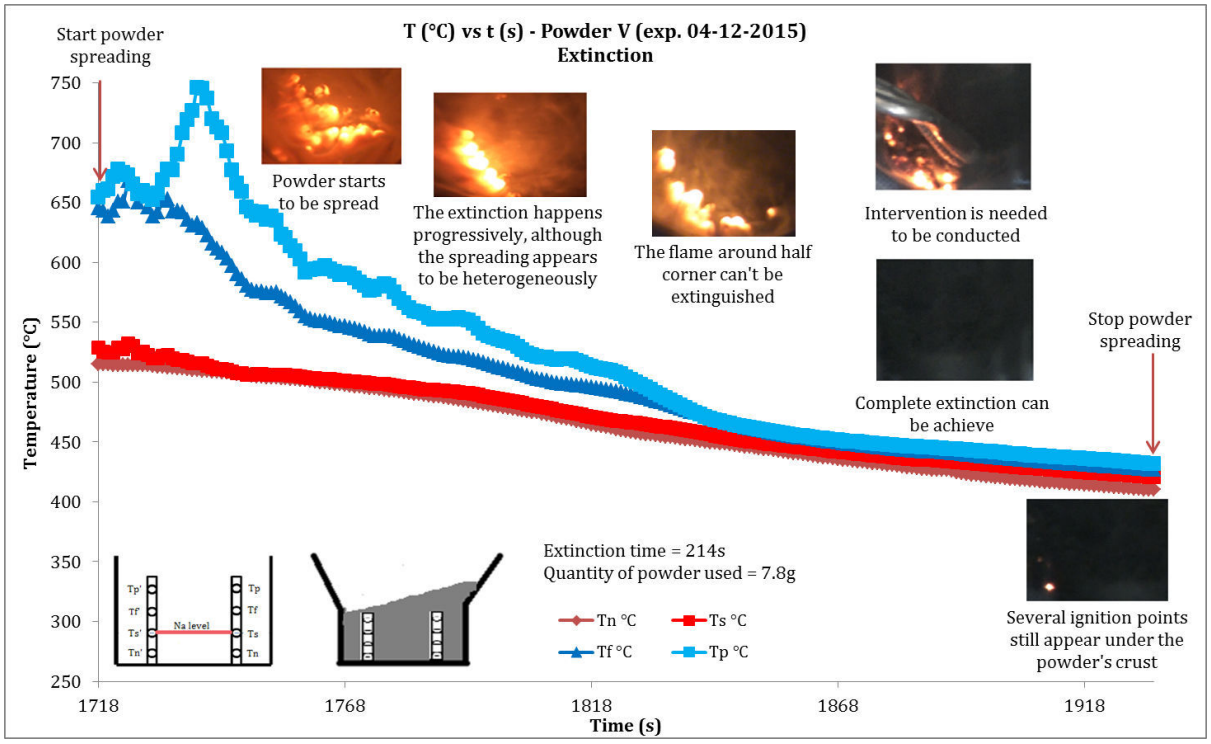

Figure 4-10. The temperature and video observations of the Chris(X)ti-Na experiment with continuous spreading during extinction using powder V

XRD analysis of the extinction residue shows the presence of sodium hydroxide (NaOH) peaks for powder IV and not for powder V. Meanwhile, the peaks of $LiNaCO_3$ also appear in the 1st test (IVA) of powder IV (cf. table 4-5), which not the case in the 2nd test (IVB).

The results of the tests once again show visually a better performance of the powder mixture containing hydrates. The time required to achieve a complete extinction appears to be shorten. It is worth mentioning that the temperature profile of T_p in the eutectic mixture with hydrated compound (powder IV) shows a decreasing trend rather than increasing at the beginning of powder-flame contact for those showed in the previous group of studies. This might be related to water content which is effectively smaller than that of powders II and III. This will be discussed more into details later on in this chapter.

Table 4-5. Summary of Chris(X)ti-Na experimental results using synthetic powders IV and V with continuous spreading

Test	Study	Powder composition (w%)	Extinction time (s)	Powder quantity (g)	H_2O released (g)	XRD posttest analysis	Temperature profile (°C/s)	Remarks
IV A	**Role of eutectic mixture with and without presence of hydration water in sodium carbonate**	**Powder IV (7% H_2O)** 1st test (A)* $Na_2CO_3.H_2O$ 48% Li_2CO_3 43% Graphite 9%	20	7.3	0.5	NaOH +++ LiNaCO3 +	• T_n cst at 480°C • T_s cst at 480°C/s then rapid ↓ = 39°C/s followed by slight ↑ = 7.3°C/s then ↓ until 448.7°C at the end of spreading • T_f fluctuations at 660°C then ↓ = 1.9°C/s followed by rapid ↑ = 10.3°C/s then ↓ = 2°C/s • T_p fluctuations at 770°C then ↓ = 3.4°C/s followed by rapid ↑ = 14.1°C/s then ↓ = 2.3°C/s	• No caking problem • Fast and homogeneous spreading • Rapid melting • Unburnt Na is transformed into NaOH • Complete extinction • Formation of NaOH during extinction
IV B		**Powder IV (7% H_2O)** 2nd test (B) Idem	173	10.9	0.8	NaOH + Na ++	• T_n slow ↓ = 0.4°C/s • T_s cst at 500°C • T_f fluctuations at 550°C then constant until 494.8°C at the end of spreading • T_p ↓ = 9.2°C/s then slight ↑ = 2°C/s followed by ↓ = 3.8°C/s until reach 523.8°C at the end of spreading	• No caking problem • Slower and homogeneous spreading • Complete extinction • Formation of NaOH during extinction
V A		**Powder V (0% H_2O)** 1st test Na_2CO_3 48% Li_2CO_3 43% Graphite 9%	214	7.8	0	NaOH ++ Na +	• T_n slow ↓ = 0.5°C/s • T_s slow ↓ = 0.5°C/s • T_f fluctuations at 650°C then ↓ = 1.6°C/s until 427.1°C at the end of spreading • T_p fluctuations at 650°C then ↑ = 9.3°C/s (due to the bad spreading performance) followed by ↓ = 2.7°C/s until 431.6°C at the end of spreading	• Caking problem in the sieve • Bad spreading performance • Formation of porous layer → slow melting • Unburnt Na is transformed into NaOH • Complete extinction after operator intervention

*) 1 sieve size of 1 mm

A.3 *Effect of trona without and with $LiNaCO_3$*

This part of the study is conducted for a mixture containing trona with $LiNaCO_3$ (powder VII) and without $LiNaCO_3$ (powder VI). Powder VI also represents the composition of Marcalina in aging conditions under the presence of hydration water superior to that of specifications (8.9w% of hydration water), while powder VII is still in the specified range (5.6w% of hydration water).

Powder VI (cf. figure 4-11) started to spread progressively from the left to the right side of the sodium container. It melts directly and formed a liquid layer that was able to prevent the Na-O_2 contact with a temperature decrease rate of 4.1°C/s. The brief increase of temperature at a 5°C/s rate was detected due to the presence of flame near the thermocouples, followed by a rapid temperature decrease (29°C/s). The operator intervention was needed to extinguish the flames located at the back side of container since the powder spread unevenly. Nevertheless, it does not influence the temperature recorded by thermocouples since the reignition flame is not located near the sensor. 9.8 g of powder VI (0.9 g of water released) is needed to extinguish the sodium fire for 130s.

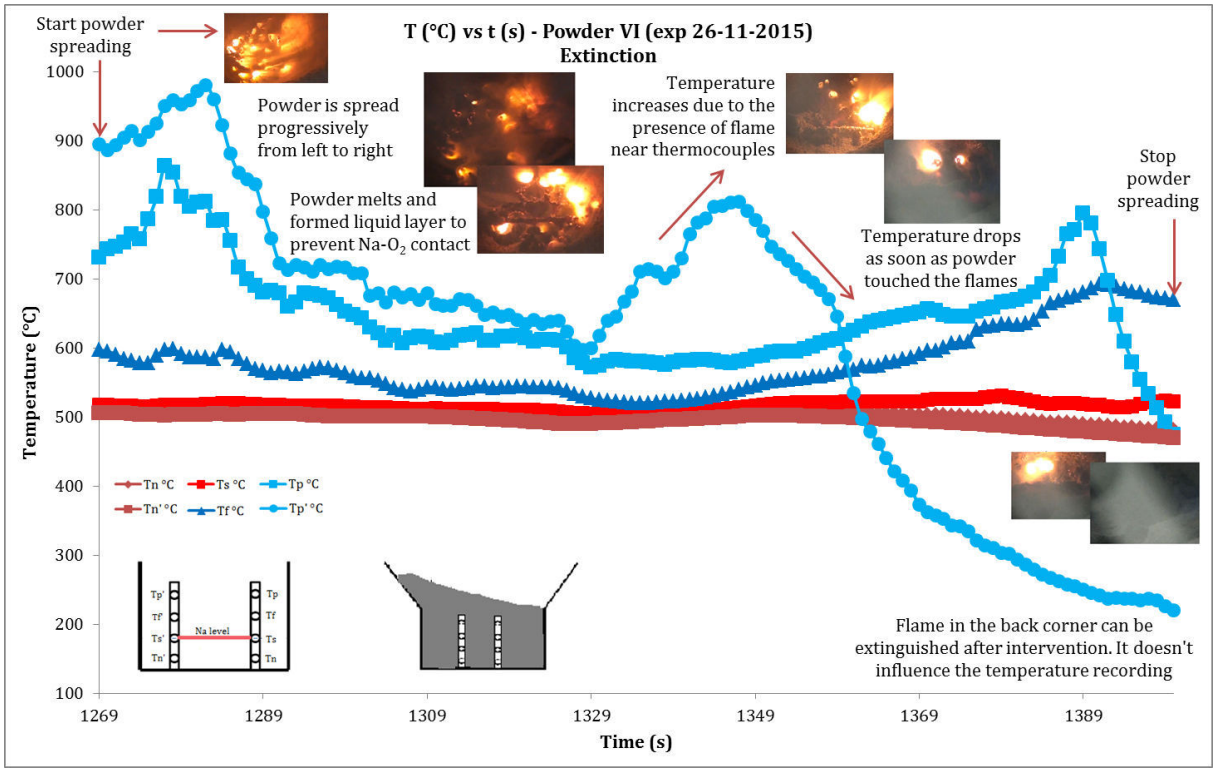

Figure 4-11. The temperature and video observations of the Chris(X)ti-Na experiment with continuous spreading during extinction using powder VI

The same trend of spreading is also observed in powder VII (cf. figure 4-12). It melts progressively from the left to the right. The temperature is decreased as soon as the powder reached the flame at a 17.2°C/s rate. The complete extinction is achieved after 37s of spreading

without operator intervention. 9.1g of powder is used to extinguish the sodium fire which corresponds to 0.5g of water released.

XRD analyses of the extinction residue show sodium hydroxide (NaOH) peaks in both powders VI and VII. The peaks of $LiNaCO_3$ are also detected in the tests with powder VII (cf. table 4-2).

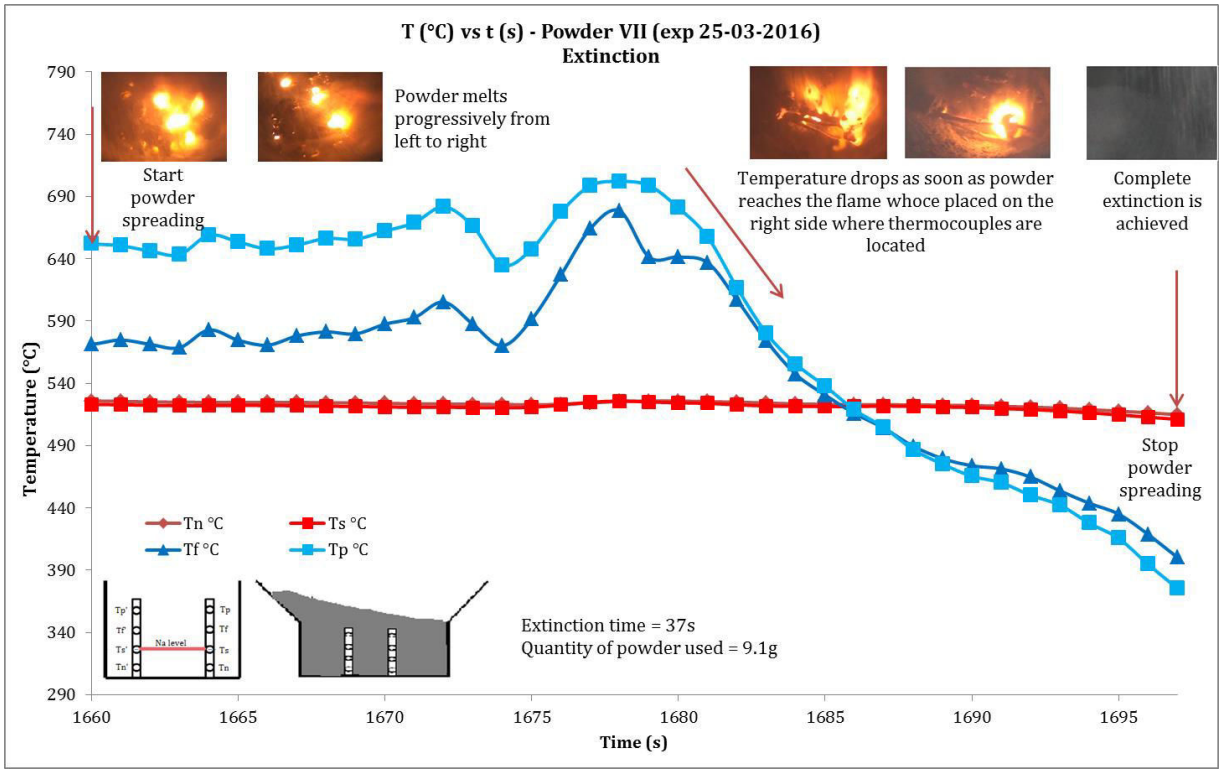

Figure 4-12. The temperature and video observations of the Chris(X)ti-Na experiment with continuous spreading during extinction using powder VII

These tests demonstrate that a high content of trona (consequently increasing the amount of hydration water) is not capable of improving the extinction capacity. On the contrary, a moderate content of $LiNaCO_3$ might give a better extinction performance in a higher sodium temperature. Nevertheless, the presence of trona doesn't diminish the extinction performance.

Table 4-6. Summary of Chris(X)ti-Na experimental results using synthetic powders VI and VII with continuous spreading

Test	Study	Powder composition (weight%)	Extinction time (s)	Powder quantity (g)	H_2O released (g)	XRD post test analysis	Thermocouples profile	Remarks
VI A	**Effect of trôna without and with presence of $LiNaCO_3$ (w% of hydration water over and in the range of specifica-tion)**	**Powder VI (8.9% H_2O)** 1st test (A) $Na_2CO_3.H_2O$ 30% Li_2CO_3 38% Trona 23% Graphite 9%	130	9.8	0.9	NaOH + Na +	• T_n cst at 518°C • T_s cst at 518°C • T_f cst at 520.5°C then ↑ = 2.4°C/s • T_p↑ = 16.6°C/s then ↓ = 4.1°C/s followed by ↑ = 5°C/s then rapid ↓ = 29°C/s	• No caking problem • Good spreading performance • Rapid melting • No high flash flame observed • Complete extinction (O.I) • Formation of NaOH during extinction
VII A		**Powder VII (5.6% H_2O)** 1st test (A) $Na_2CO_3.H_2O$ 30% Li_2CO_3 30% Trona 6% $LiNaCO_3$ 25% Graphite 9%	37	8.4	0.5	NaOH ++ *$LiNaCO_3$ +	Lack of thermocouples	• No caking problem • Good spreading performance • Rapid melting • No high flash flame observed • Formation of NaOH during extinction • Complete extinction
VII B		**Powder VII (5.6% H_2O)** 2nd test (B) Idem	37	9.1	0.5	NaOH + Na ++	• T_n cst at 510°C • T_s cst at 510°C • T_f cst at 600°C then ↑ = 27.1°C/s followed by rapid ↓ 14.6°C/s • T_p↑ = 16.8°C/s then ↓ = 17.2°C/s	• No caking problem • Good spreading performance • Rapid melting • No high flash flame observed • Formation of NaOH during extinction • Complete extinction

*) Uncertainty of the $LiNaCO_3$ formation during extinction due to its presence in the initial powder composition

A.4 *Effect of $LiNaCO_3$*

The effect of $LiNaCO_3$ was studied for two cases: $LiNaCO_3$ alone with graphite (powder VIII) and mixed with lithium carbonate and sodium carbonate monohydrate whose proportions give a hydration water content under the specification of Marcalina (powder IX).

Powder VIII (cf. figure 4-13), during the first 50s of spreading, a lot of powder remained at the edges. The powder has difficulties to melt at the sodium surface. The melting appears to happen slowly. A slow decrease of temperature was recorded at around 0.6°C/s. The complete extinction can be achieved although several ignition points still can be seen under the surface, thus an operator intervention was necessary. 10.3 g of powder is needed to extinguish the sodium fire for 430 s. NaOH is observed in the extinction residue.

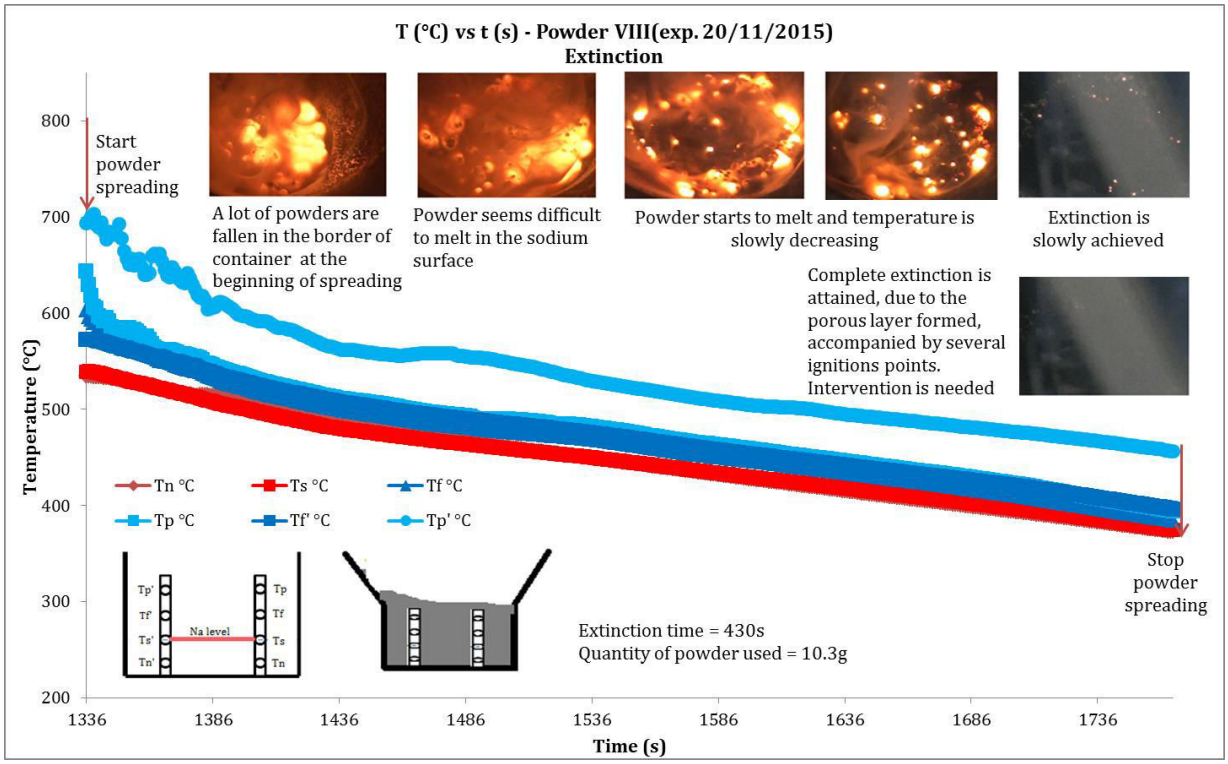

Figure 4-13. The temperature and video observations of the Chris(X)ti-Na experiment with continuous spreading during extinction using powder VIII

Powder IX (cf. figure 4-14), is spread progressively. The cone attached to the container allows powder to glide easily so that it was able to spread homogeneously on the surface. A slight temperature increase was followed by a progressive temperature loss. Powder was finally able to cover the entire surface. However, its struggle to melt at the sodium surface resulted in several re-ignitions. Hence an operator intervention is needed in order to obtain a complete extinction after 125s of spreading with 17.9 g of powder (0.5 g of water released). XRD analysis of the extinction residue shows a slight peak of NaOH in the experiment using powder IX (cf. table 4-7).

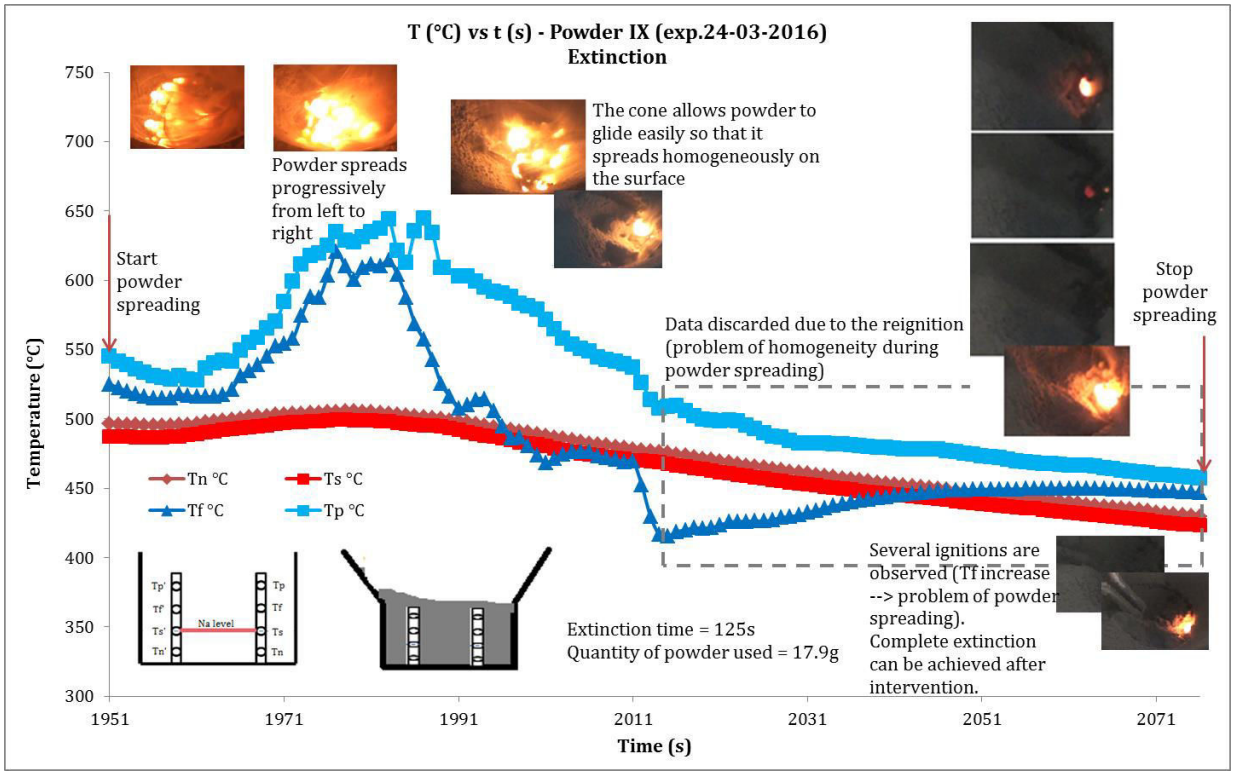

Figure 4-14. The temperature and video observations of the Chris(X)ti-Na experiment with continuous spreading during extinction using powder IX

These tests illustrated the importance of a sufficient water content to provide a rapid extinction. The melting of the $LiNaCO_3$ compound seems to happen slower than the ones containing hydration water.

Table 4-7. Summary of Chris(X)ti-Na experimental results using synthetic powders VIII and IX with continuous spreading

Test	Study	Powder composition (w%)	Extinction time (s)	Powder quantity (g)	H_2O released (g)	XRD post test analysis	Thermocouples profile	Remarks
VIII A	**Effect of $LiNaCO_3$**	**Powder VIII** **(0% H_2O)** 1st test (A) $LiNaCO_3$ 91% Graphite 9%	430	10.3	0	NaOH +	• $T_n = T_s \downarrow$ = 0.4°C/s • $T_f \downarrow$ = 0.5°C/s • $T_p \downarrow$ = 0.6°C/s	• No caking problem in the sieve • Bad spreading performance • Formation of porous layer → slow melting • NaOH is formed after test • Extinction with several reignition
IX A		**Powder IX** **(2.9% H_2O)** 1st test (A) $Na_2CO_3.H_2O$ 20% Li_2CO_3 21% $LiNaCO_3$ 50% Graphite 9%	690	17.5	0.5	NaOH ++ *$LiNaCO_3$ +	• T_n=$T_s \downarrow$= 0.3°C/s • Fluctuations T_f then ↓ = 2.3°C/s • Fluctuations T_p then rapid ↓ = 6.9°C/s followed by slight ↑ = 1.3°C/s then ↓ = 0.7°C/s and ↑ = 0.3°C/s	• No caking problem in the sieve • Progressive melting from left to right • Insufficient melting to extinguish the fire • No complete extinction → 2nd test needed
		Powder IX **(2.9% H_2O)** 2nd test (B) Idem	125	17.9	0.5	Na ++ LiNaCO3 +	• $T_n = T_s$ constant at 490°C then ↓ = 0.8°C/s • $T_f \uparrow$ = 2.8°C/s then ↓ = 6.4°C/s followed by ↑ = 0.5°C/s • $T_p \uparrow$ = 2.8°C/s then ↓ = 3.8°C/s constant until 457.4°C/s	• No caking problem in the sieve • Progressive melting from left to right • Insufficient melting to extinguish the fire • O.I. (Operator Intervention)

*) Uncertainty of the $LiNaCO_3$ formation during extinction due to its presence in the initial powder composition

4.2.2 Direct spreading

Powders II, IV, VII, IX were used to test the influence of spreading towards the extinction. These powders were chosen based on their variety of water content (sodium carbonate monohydrate and/or trona) and $LiNaCO_3$. In this case 5g of powder were used as the initial quantity to extinguish 10g of sodium pool fire. This value is obtained from the work of Reuillon [4], which led to the choice of Marcalina composition. The influence of spreading might be omitted in these tests, as the powder falls directly, using the trap opening, onto the fire. Therefore, the quantity of powder employed as well as the extinction time might be more accurate and then easier to be justified. In case of persistance of the fire, additional powder will be added through the cone.

With 13.2 w% of hydration water, no additional powder is needed to extinguish 10g of sodium fire. However, a high vigorous flame is observed at the moment the powder felt onto the fire, with 8.7°C/s increase rate of temperature as measured by T_f. It is then followed by a progressive melting of the powder, with 6.4°C/s rate of temperature decrease, above which a flame is present for around 47s. It also appeared that this powder is able to ensure the separation of sodium and air as the temperature inside and at the sodium surface stays relatively high (520°C). Furthermore, the sodium hydroxide appears to be a dominant compound in the extinction residue as detected by XRD.

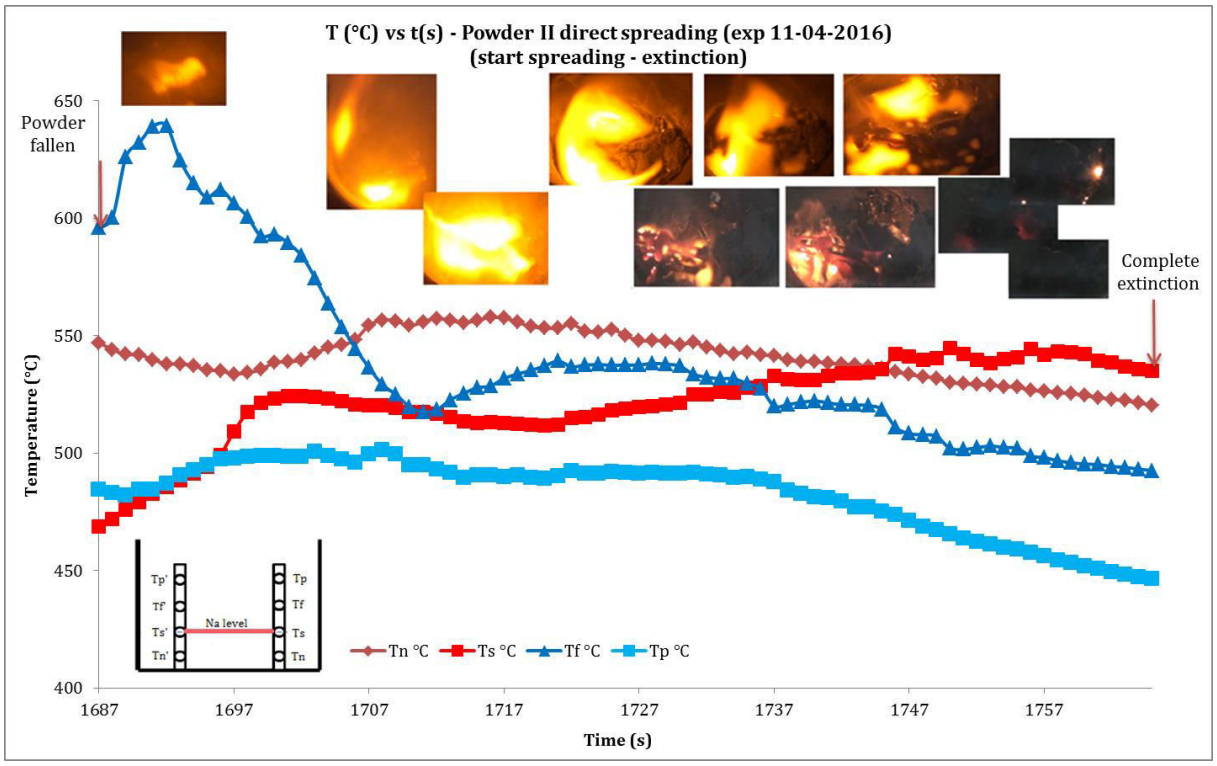

Figure 4-15. The temperature and video observations of the Chris(X)ti-Na experiment with direct spreading during extinction using powder II

1.8 g of additional powder IV (cf. figure 4-16) is needed, in complement to the 5 g of powder initially dropped, in order to achieve a complete extinction, although no high vigorous flame is observed in this case. The temperature profile shows a direct temperature decrease, as recorded by T_p with 5.4°C/s. It is followed by several temperature rises which then accompanied by a temperature decrease. A flame is observed for 20 s during powder melting as reignition is observed near the top front of container (t=1900 s). It is due to the lack of powder in this part (uneven distribution). Nevertheless, the flame is easily extinguished after supplementary powder is added. Not much of sodium hydroxide is detected by XRD as compared to the previous powder. $LiNaCO_3$ is present in the extinction residue.

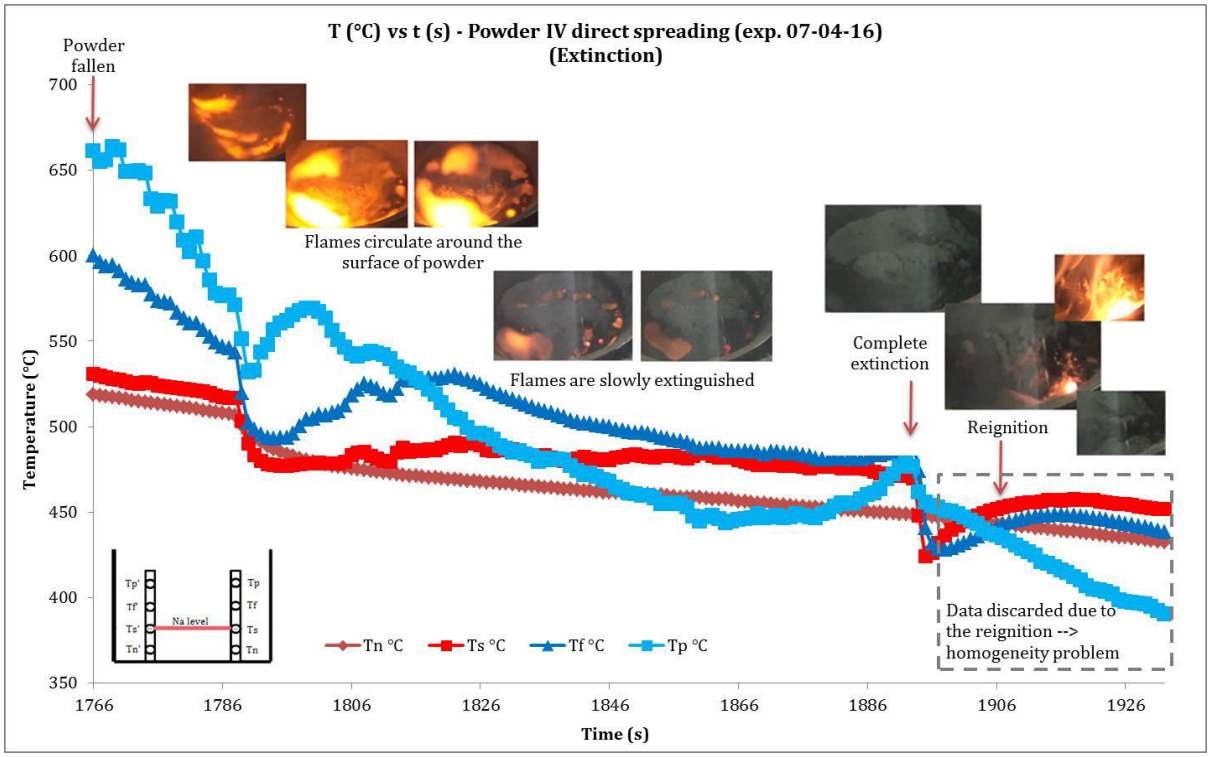

Figure 4-16. The temperature and video observations of the Chris(X)ti-Na experiment with direct spreading during extinction using powder IV

Powder VII (cf. figure 4-17) at the beginning seemed to be efficient for the extinction, with a slight temperature rise followed by rapid temperature decrease down to 430°C. However, reignition happened shortly afterwards, making 2.4 g of additional powder are necessary to attain a complete extinction. NaOH and $LiNaCO_3$ are detected by XRD in the residue.

Powder IX struggled to attain a complete extinction, even with 10 g used (5 itinial + 5 complementary). As it slowly melted on the sodium surface, the porous crust formed was not able to secure sodium from its contact with oxygen. Several temperature increases are observed by T_p followed by rapid decrease. No high vigorous flame was observed during the extinction. The same result of XRD as for powder VII is found here, as both NaOH and $LiNaCO_3$ are detected in the sample.

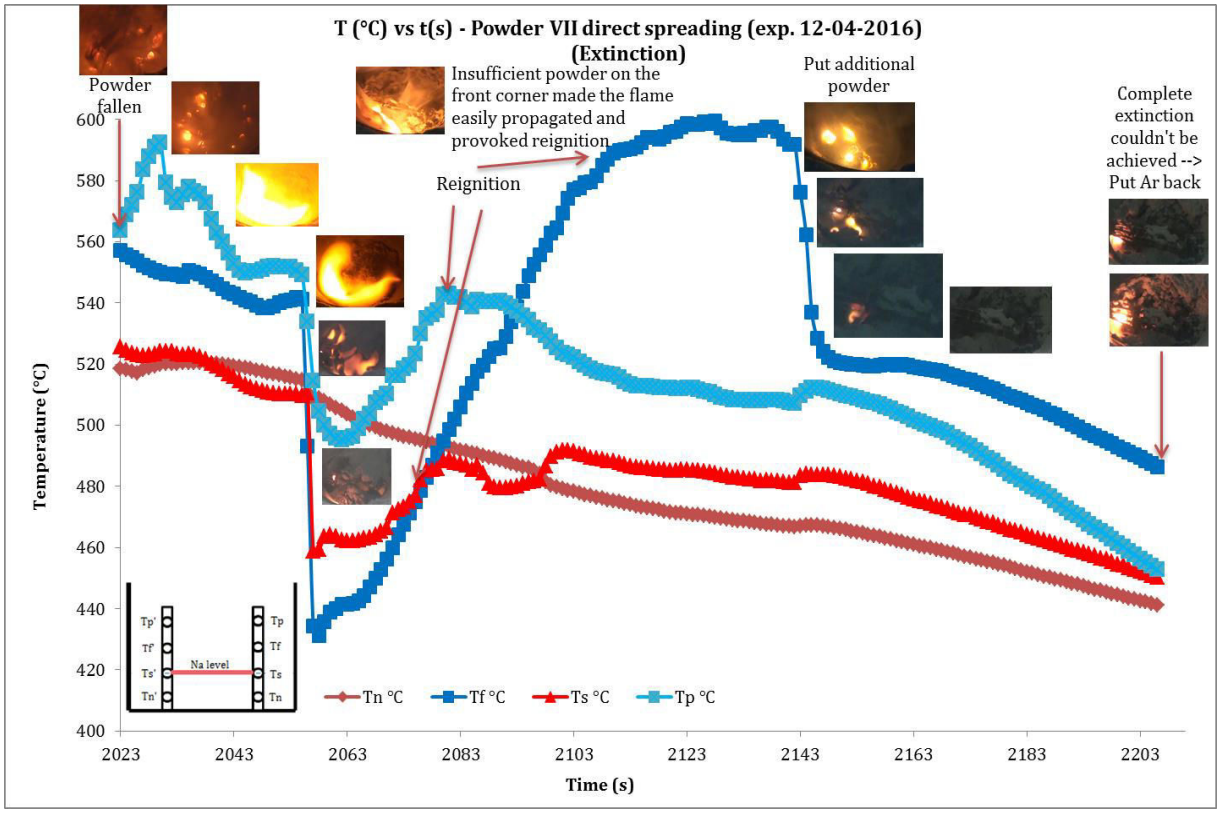

Figure 4-17. The temperature and video observations of the Chris(X)ti-Na experiment with direct spreading during extinction using powder VII

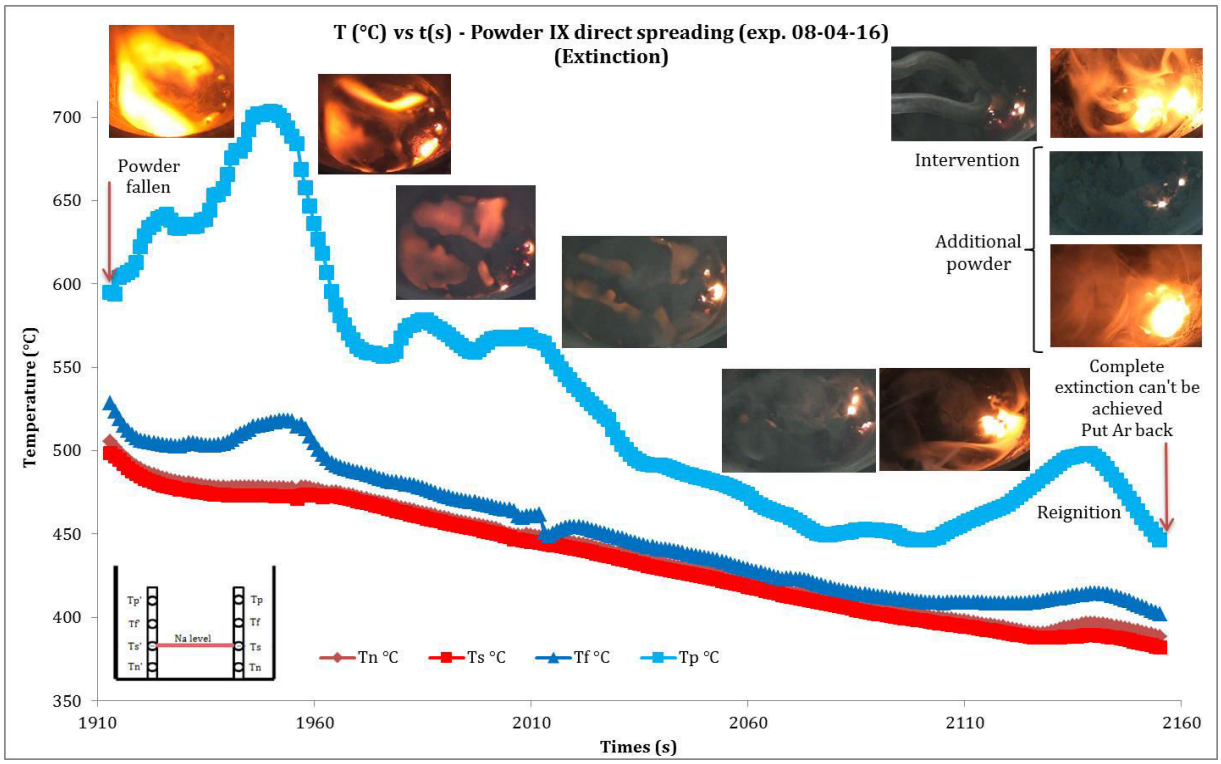

Figure 4-18. The temperature and video observations of the Chris(X)ti-Na experiment with direct spreading during extinction using powder IX

These tests allow us to evaluate the behavior of powders based on their composition. The test with powder II demonstrates the influence of water released, capable of increasing the temperature followed by a rapid temperature decrease. The presence of a flame (vigorous or not) appears also to be highly dependent on how much water release contributed to the extinction. $LiNaCO_3$ might be formed during extinction in the case of high sodium temperature (cf. test with powder IV), its melting may enhance the efficiency for extinguishing sodium fire especially at high temperatures. In the case of sodium fire starting at a lower temperature, it appears to be less supportive to the extinction as a longer time is needed to achieve its melting (cf. test with powder IX). Finally, no problem of extinction seems to appear when trona is present (cf. test with powder VII).

Table 4-8. Summary of Chris(X)ti-Na experimental results using synthetic powders II, IV, VII and IX with direct spreading

Test	Study	Powder composition (weight%)	Extinction time (s)	Powder quantity (g)	H_2O released (g)	XRD post test analysis	Temperature profile (°C/s)	Remarks
IId	**Direct spreading**	Powder II **(13.2% H_2O)** $Na_2CO_3.H_2O$ 91% Graphite 9%	78	5	0.7	NaOH ++++ Na ++	• T_n = cst @ 520.4°C • T_s↑ = 4.2°C/s then ↓ = 0.6°C/s and slightly ↑ = 0.5°C/s • T_f↑ = 8.7°C/s then ↓ = 6.4°C/s followed by ↑ = 0.6°C/s and finally ↓ = 1.3°C/s • T_p = cst @480°C then ↓ = 1.5°C/s	• Presence of high vigorous flame at the beginning of spreading • Flame appears for 47s • Slight reignition with rapid extinction observed • Complete extinction
IVd		Powder IV **(7% H_2O)** 1st test (A) $Na_2CO_3.H_2O$ 48% Li_2CO_3 43% Graphite 9%	102	5 (+1.8) = 6.8	0.5	NaOH + LiNaCO3 +	• T_n slightly ↓ = 0.5°C/s • T_s slightly ↓ = 0.6°C/s then rapid ↓ = 7.7°C/s, cst @470°C followed by rapid ↓ = 22.8°C/s and ↑ = 0.7°C/s • T_f ↓ = 4.1°C/s then ↑ = 0.9°C/s, cst 487.5°C, ↓ = 18.7°C/s, and ↑ = 0.2°C/s • T_p ↓ = 5.4°C/s then ↑ = 3.8°C/s, ↓ = 2.1°C/s, ↑ = 1.1°C/s and ↓ = 2.3°C/s	• No high vigorous flame • Flame appears for 20s • Reignition observed • O.I. (Operator Intervention) with additional powder. • Complete extinction
VIId		Powder VII **(5.6% H_2O)** 2nd test (B) $Na_2CO_3.H_2O$ 30% Li_2CO_3 30% Trona 6% $LiNaCO_3$ 25% Graphite 9%	104	5 (+2.4) = 7.4	0.4	NaOH +++ *LiNaCO3 +	• T_n↓ = 0.4°C/s • T_s slightly ↓ = 0.5°C/s then rapid ↓ = 25.6C/s, followed by slight ↑ = 0.8°C/s and ↓ = 0.4°C/s • T_f ↓ = 0.5°C/s then rapid ↓ = 36.6°C/s, followed by slight ↑ = 1.9°C/s and ↓ = 0.6°C/s • T_p fluctuations until 550°C then ↓ = 6.9°C/s, ↑ = 2.6°C/s and ↓ = 0.7°C/s	• No high vigorous flame • Flame appears for 18s • O.I. (Operator Intervention) with additional powder. • Temporary extinction • Cooling with argon
IXd		Powder IX **(2.9% H_2O)** $Na_2CO_3.H_2O$ 20% Li_2CO_3 21% $LiNaCO_3$ 50% Graphite 9%	242	5 (+5) = 10 insufficient	0.3	NaOH ++ *LiNaCO3 +	• T_n = T_s = ↓ 0.5°C/s • T_f cst @510°C then ↓ = 0.6°C/s • T_p ↑ = 3°C/s then cst @550°C, ↓ = 1.4°C/s, ↑ = 1.2°C/s and ↓ = 3.1°C/s,	• No high vigorous flame • Flame appears for 18s • Reignition observed • O.I. (Operator Intervention) with additional powder • No complete extinction • Cooling with argon

*) Uncertainty of the $LiNaCO_3$ formation during extinction due to its presence in the initial powder composition

4.3 Discussions

4.3.1 The role of chemical compounds on the extinction

Two methods of spreading were developed in these tests: continuous spreading with vibration and direct spreading using a powder trap. The first one is very sensitive to the external factors (i.e. convection flux, aspiration system), which might affect the trajectory of the powder. The homogeneity of spreading is difficult to maintain constant during each test. Besides, the vibration also causes several agglomeration problems that are encountered during various tests. However, this approach is more representative of the reality as the powder is normally spread continuously to cover the sodium surface until a complete extinction is achieved.

Meanwhile, the second approach, direct spreading, is employed to compare the role of chemical compounds in certain samples, for which the effect of spreading can be omitted. Additionally, the smothering effect is also studied as whether or not it is an essential element to obtain extinction.

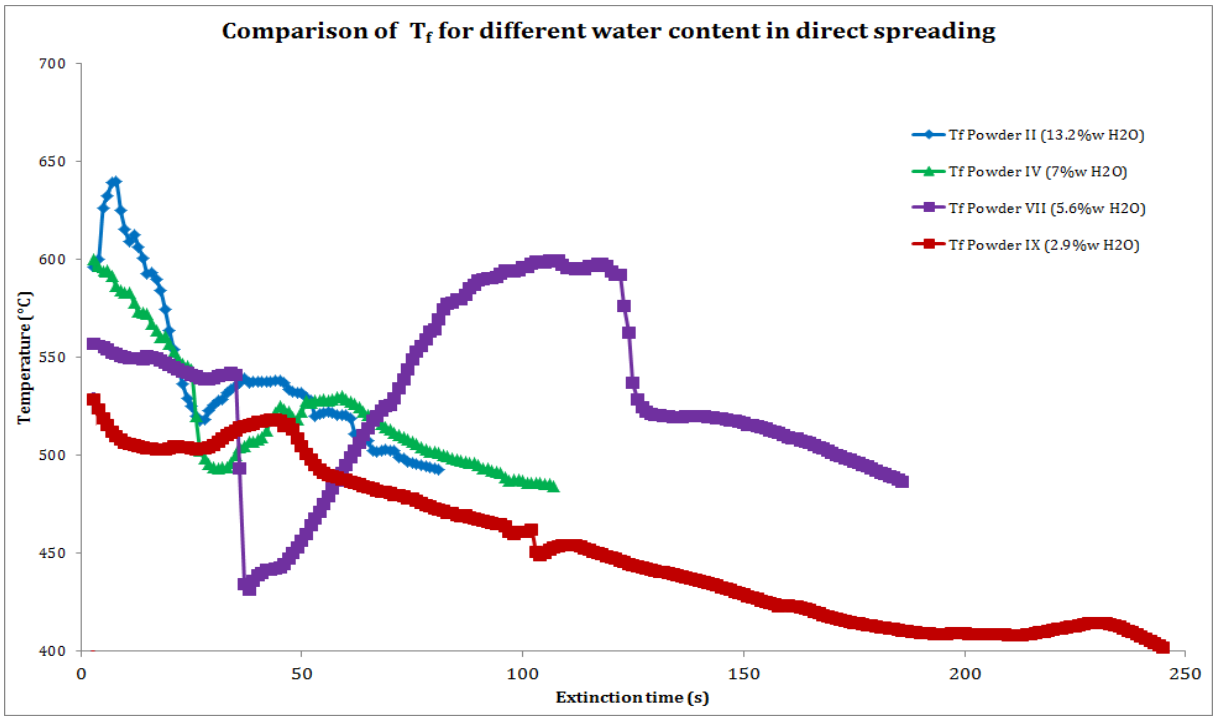

Figure 4-19. Comparison of temperature profile recorded by T_f for different water contents in direct spreading

Figure 4-19 shows the temperature profile comparison registered by thermocouples T_f for different water contents as a function of extinction time. The graph illustrates that more hydration water contributes to shorten the extinction time. The increase of temperature at the beginning of flame-powder contact recorded by T_f in powder II reflects the presence of a high vigorous flame observed in the video camera. However, the temperature drops significantly (ΔT = 120°C) shortly after 5s. This phenomenon is only observed with powder II. This temperature

increase might be interpreted as an exothermic reaction due to the reaction Na-H_2O as a consequence of the thermal decomposition of sodium carbonate monohydrate as a primary compound in powder II. Indeed, $Na_2CO_3.H_2O$ decomposes at low temperatures (63-127°C). As the temperature is much higher (600°C), the hydration water release might happen spontaneously. This statement is also supported by the thermal calculations conducted using HSC Chemistry that have been previously discussed in §2.1.2. The water reacts with sodium vapor to produce sodium hydroxide and hydrogen. Another possibility is that $Na_2CO_3.H_2O$ might react directly with the vapor of sodium (without undergoing decomposition). As reactions happen rapidly, it would be hard to distinguish which one took place. In any case, H_2 is produced by both reactions, which might explain the presence of the flash flame observed in the video. Nevertheless, a spectrometer measurement would be needed to support this statement. What must be emphasized is that it is only produced in a short time and is followed by what appears to be a liquid sodium hydroxide formation (XRD affirmation). The latter forms a sealed layer that secures sodium from a direct contact with oxygen, which succeed in achieving extinction.

Powder IV exhibits the same temperature profile as powder II, except for the temperature rise at the beginning. The temperature decrease was observed directly after powder spreading although it is much slower and the slope is not as steep as that in powder II. Both powders II and IV perform a complete extinction. The presence of $LiNaCO_3$ is also detected by XRD analysis. Figure 4-16 displayed that the temperature on the sodium surface attained 530°C, which is higher than the eutectic melting point (498°C). Therefore, it is possible that the liquid carbonate is formed during extinction. Moreover, the energy absorbed by its formation might reduce the effect of exothermic reaction produced during the formation of NaOH as the flame produced might be considered as less vigorous than that observed in powder II.

The temperature decreases slowly with powder VII, before a sharp temperature drop takes place from 540°C to 430°C. It seems that the latter is caused by the formation of liquid sodium hydroxide. However the temperature rises until reaching nearly 600°C, soon after the re-ignition is observed by video camera. It might be due to the fact that the water content is not enough significant to produce a sealed layer on the sodium surface. The temperature then drops back quite significantly to 520°C only after additional powder is added to the fire. Hence, the extinction is only temporary. The presence of $LiNaCO_3$ is also detected by XRD analysis. However, its formation during extinction is considered to be questionable since it is already a part of the initial powder composition.

Powder IX demonstrates a slow temperature decrease with several ignitions. Even if no significant temperature rise is recorded during extinction, the video recording shows that no complete extinction is obtained using this powder. The amount of water content is not enough to produce a sealed layer of sodium hydroxide, while the role of $LiNaCO_3$ is not significant at the temperatures under 498°C. Indeed, the powder temperature is too low to allow the $LiNaCO_3$ to melt and then to increase the sealing surface.

In general, the results display the significant impact of a minimum amount of hydration water in achieving extinction. As what has been previously demonstrated by Reuillon [4], a significant water content is necessary to achieve a complete extinction and this experimental result, using powder II particularly, were in accordance with Reuillon's finding. On the other hand, the high flame is present even at 13.5% of hydration water, which is rather different of what is stated in her work. According to Reuillon in [4], more re-ignitions are observed under the presence of

14.5-15% hydration water. However more elaborate explanation about the description of re-ignition (i.e. color, height, duration) was not clearly described in Reuillon's work. Nevertheless in our experiments, the high flame is followed by a complete extinction, which is in contradiction to what seems to be implied by Reuillon concerning the frequency of reignition in powders of high hydration water content.

The evolution of flame extinction using powder II is shown in figure 4-20. A high abrupt flame is produced, which is dominated by a yellow flame with a bright white center, for several seconds. The bright center slowly disappeared after the melting of powder at the surface that might be attributed to the formation of sodium hydroxide. During extinction with powder IV (cf. figure 4-21), the video camera demonstrated a relatively small flame as compared to the previous one. It has the same bright white light in the center, but the latter appears to be shorter than in the former test. The same flame pattern is also observed in powder VII (cf. figure 4-22) although in this case only temporary extinction was achieved. Lastly, more porous layer was performed with powder IX (cf. figure 4-23). Several re-ignition points were observed under the porous crust, and as a result, no complete extinction was achieved. It appears that the more hydration water is present in the powder, the longer the presence of flame is observed prior to the extinction (cf. table 4-8). The more hydration water, the more H_2 is produced which explained the longer flame appeared before NaOH formation (as a protective layer) that facilitates the extinction.

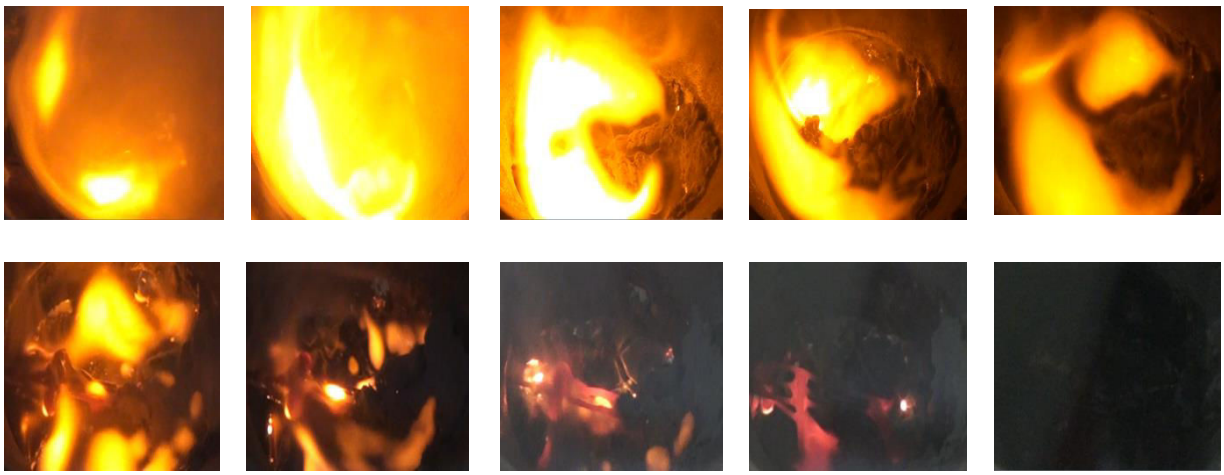

Figure 4-20. The evolution of flame prior to extinction using powder II

Figure 4-21. The evolution of flame prior to extinction using powder IV

Figure 4-22. The evolution of flame prior to extinction using powder VII

Figure 4-23. The evolution of flame prior to extinction using powder IX

The comparison of temperature evolution recorded by T_p is provided in figure 4-24. It shows the same trend as what was previously described. The more water content, the shorter is the time of extinction. T_p for powders II, IV, and VII shows a temperature decrease profile. This might indicate that the sodium flame detected might be of 1cm height from the surface, which corresponds to what is stated in literature [5]. Meanwhile powder IX shows a temperature rise which is due to the re-ignition observed. As the porous crust formed is not capable of ensuring the Na-O_2 separation, temperature profile shows several temperature fluctuations.

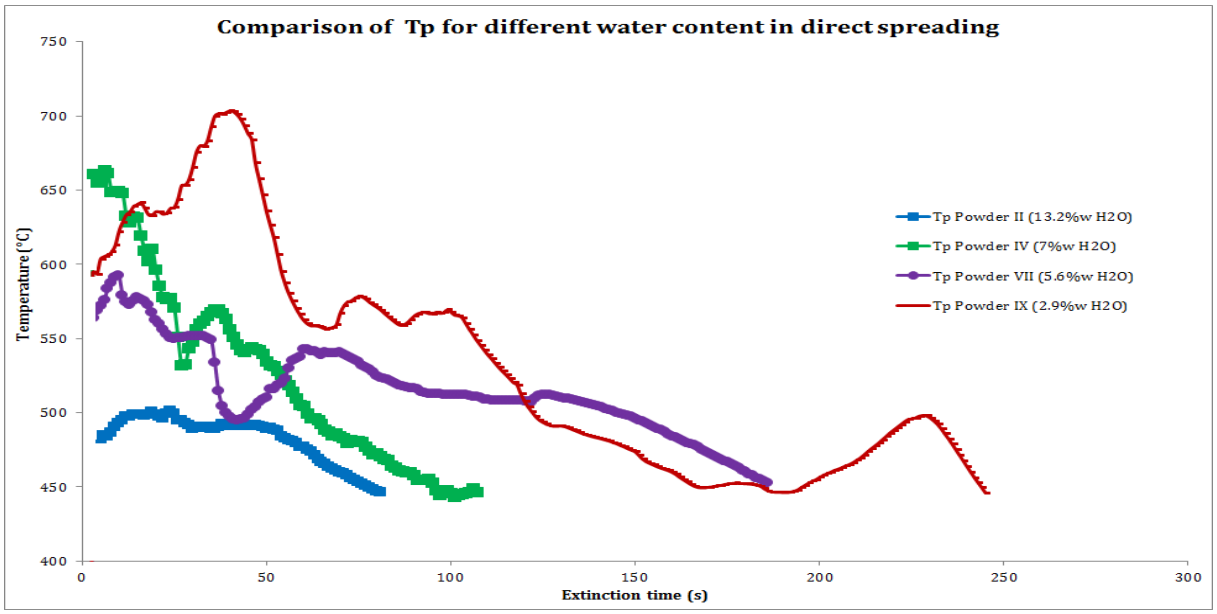

Figure 4-24. Comparison of temperature profile recorded by T_p for different water content in direct spreading

4.3.2 The effect of hydration water on the extinction capacity

Figure 4-25 displays the comparison of temperature profiles recorded by T_f for different water contents in continuous spreading. Tests at the beginning of spreading show that the temperature profile of powders with higher hydration water contents (i.e. powders II, III, VII, B, and C) tends to demonstrate a temperature rise prior to a relatively fast extinction. For instance, temperature of powder II can increase up to 800°C before decreasing down to 200°C in less than 60s. However, it should be emphasized that it is not suggested to compare the extinction times in the test using continuous spreading as the spreading performance is difficult to control. Taken powder C as an example, it has high hydration water content with 7.5w%, but its small particle size makes it longer to spread on the sodium surface. Nevertheless, it still has the same temperature profile as other powders of higher water content, with a rise before a rapid decrease. Powder A, which is of relatively small particle size, corresponds to a similar case than powder C. It also seems to experience difficulties in obtaining a complete extinction as the temperature decrease slowly. Powder A almost has a similar performance as powder I with no hydration water content. Having smaller water content, powder IX displays similar trend of temperature profile with a longer time for extinction.

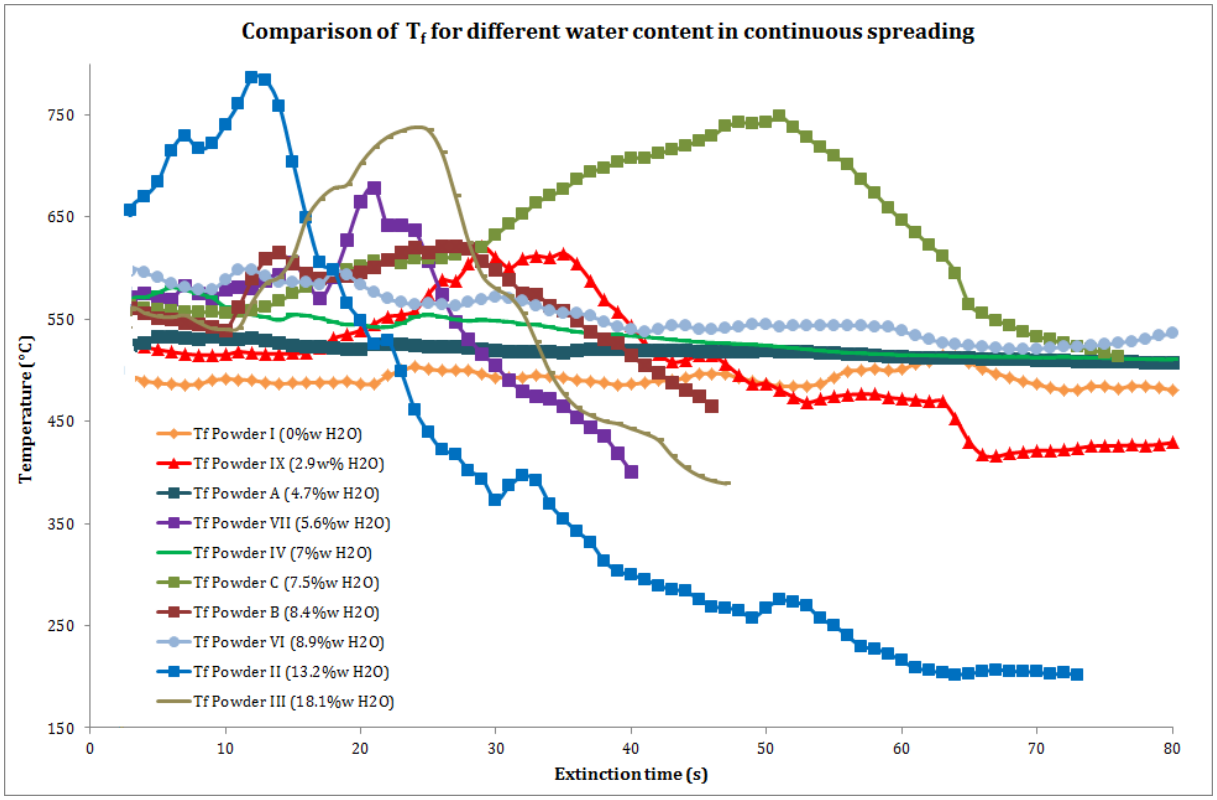

Figure 4-25. The comparison of temperature profile recorded by T_f for different water content in continuous spreading

T_p measurement results for powders II, III, VII, B, and C illustrate the same profile as previously discussed. The temperatures have more tendencies to decrease rapidly to 350°C as compared to the other powders. No temperature rise is observed in powder IV prior to the extinction. Powder VI shows a slight temperature rise before a slow decrease. The same profile is also observed in powder IX with more delay due to the spreading. Powder I displays a slow temperature decrease with still a relatively high temperature at around 600°C, while powder A seems to have the slowest decrease of temperature.

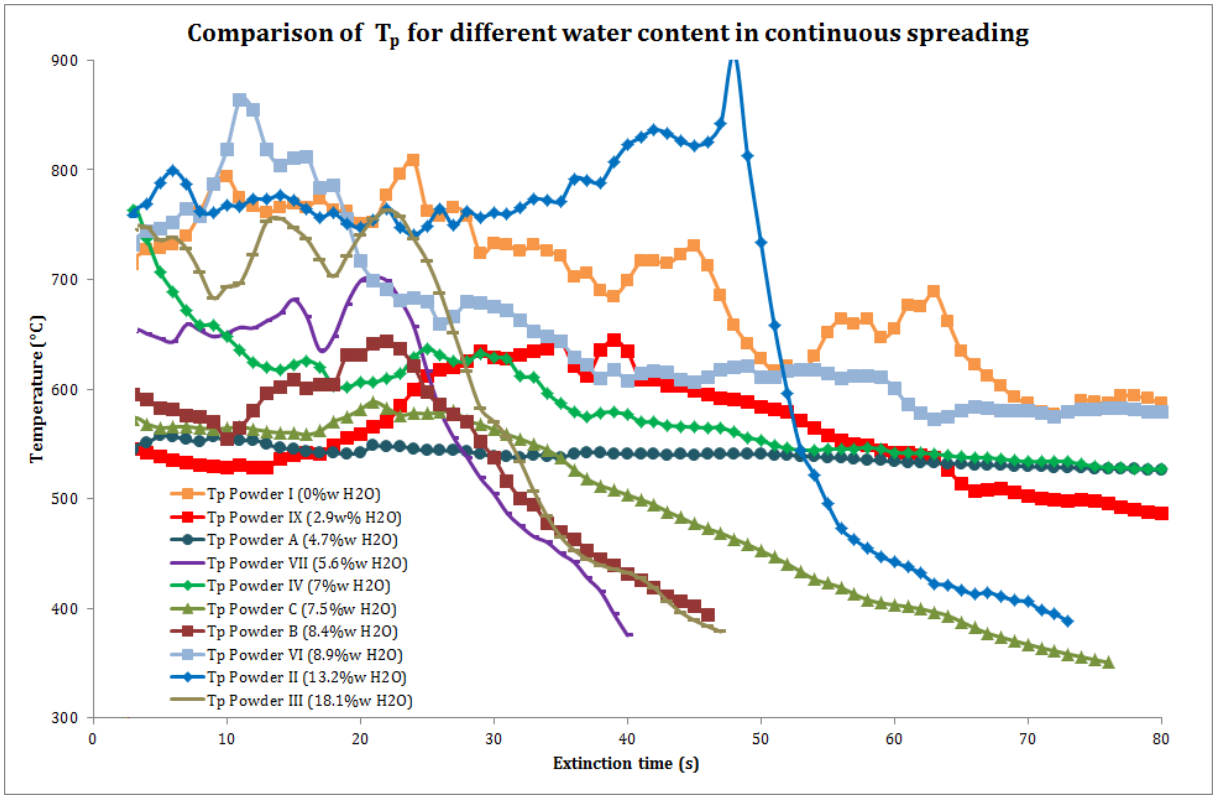

Figure 4-26. The comparison of temperature profile recorded by T_p for different water content in continuous spreading

Overall, figures 4-25 and 4-26 demonstrate the tendency of rapid temperature decrease down to less than 500°C (except for powders VI, IX, and A which experienced delay due to heterogeneity of spreading performance) after sudden rise on temperature at the beginning of spreading. It appears that this trend is observed in the range of 5.6 – 18.1w% of hydration water, with the exception of temperature rise only in powder IV (7%w of H_2O). This is might be related to its composition that will be more discussed later on. This rapid temperature decrease shows the valuable role of hydration water in terms of providing fast extinction as opposed to the one with a lower or even no hydration water content as illustrated in figure 4-27. In fact, 0.5-0.9 g of water is needed to extinguish a sodium pool fire of 19.6 cm^2, which means the average of 0.036 g of water/cm^2. It implies that 1-2 g of NaOH (equivalent to 0.3-0.6 mm height of NaOH for 19.6 cm^2) is actually required to completely cover the sodium surface. This value relatively

corresponds to 0.4 g of water used to extinguish 12 cm^2 of sodium pool fire presented in Reuillon thesis, which represents 0.033g of water/cm^2.

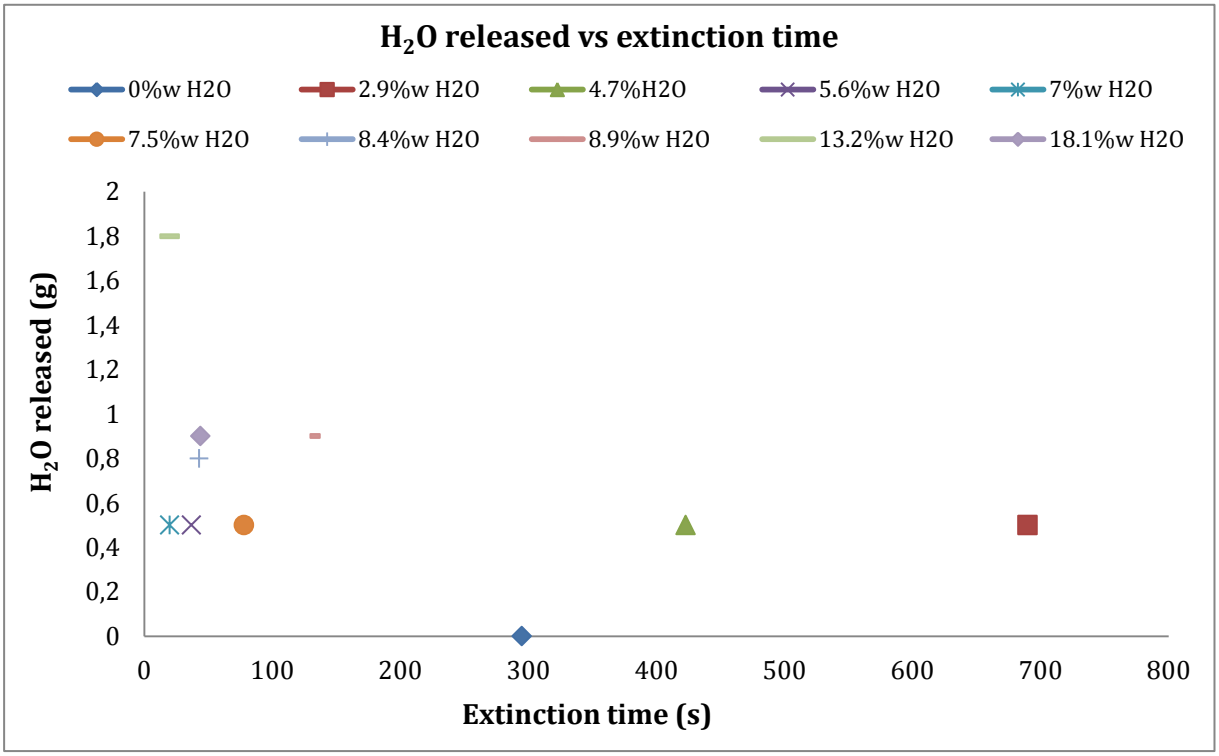

Figure 4-27. Contribution of hydration water in the function of extinction time for several powders with different hydration water contents

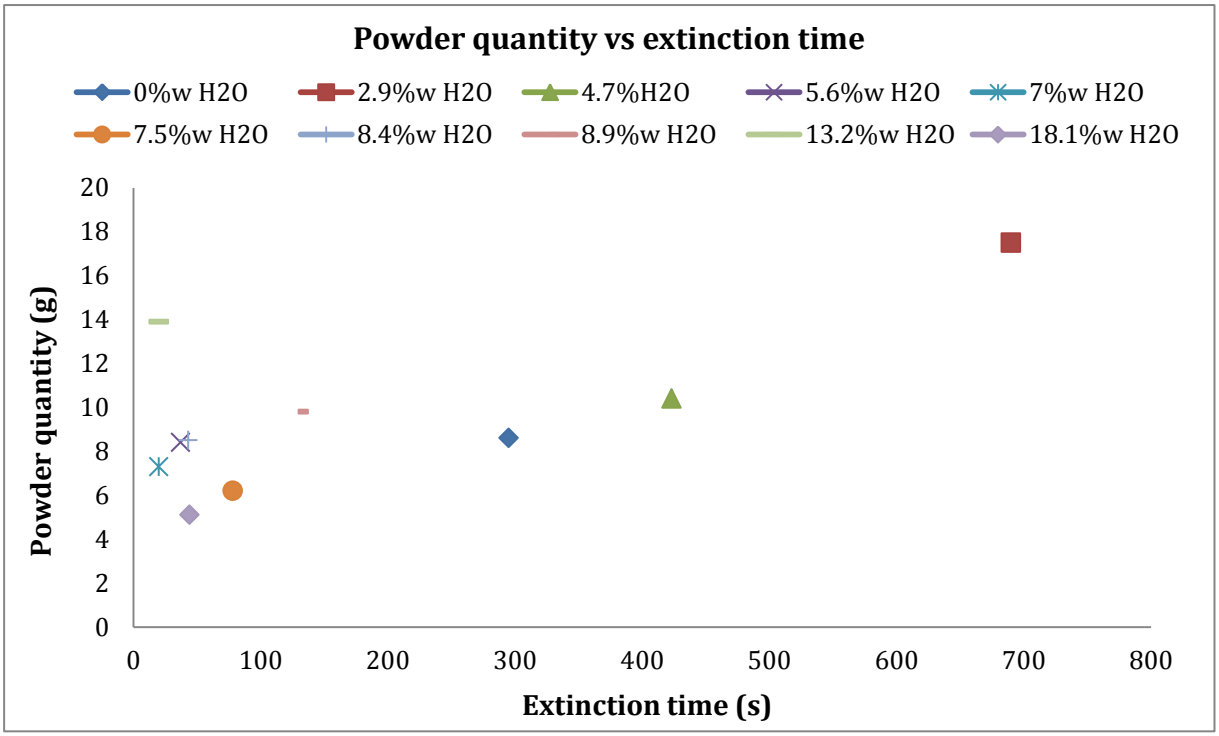

Figure 4-28. Comparison of powder quantity in the function of extinction time using several powders with different hydration water contents

Even though there is obviously a slight temperature rise due to the exothermic reaction of Na-H_2O in the surface, the decrease of temperature due to the formation of liquid NaOH is more important to ensure the separation of Na and O_2, which is the key role in the extinguishing performance. Insufficient hydration water content appears to be only capable to provide a slow smothering effect of the fire with the formation of a porous layer that favors re-ignition. These powders are still able to extinguish a fire, but it may take a much longer time and higher quantity (cf. figure 4-28) so it questions their efficiency.

The minimum water content, which corresponds to a powder that is still efficient in extinguishing a fire, is 5.6w% that is the upper limit range of water contents recommended by the producer several years ago. Meanwhile, powders that are close to 13w% of hydration water seem more likely to produce a high vigorous "H_2" flame prior to the extinction.

4.3.3 The effect of trona on the extinction capacity

As figure 4-29 illustrates, trona do not appear to have a negative effect in altering the extinction. Quite on the contrary, with 91w% of trona, powder III may extinguish a sodium fire in a relatively short time. However, there is a high temperature increase of about 200°C prior to a rapid extinction. This phenomenon is denoted for all powders presented in figures 4-29 and 4-30, although it is twice more significant for powder III in which trona is a main compound. Moreover, as illustrated in figure 4-30, a high rise of temperature is recorded by T_s that corresponds to the presence of the flame observed in the video. Indeed, the high water content may contribute to a higher production of H_2, but produces more liquid NaOH at the same time. The latter is the key factor in achieving rapid extinction as it allows the separation of Na and O_2. The reactions can be described as follows:

- Direct reaction of trona with $Na_{(g)}$ or $Na_2O_{(s)}$

$$Na_2CO_3.NaHCO_3.2H_2O_{(s)} + 3\,Na_{(g)} \rightarrow 2\,Na_2CO_3 + 2\,NaOH_{(l)} + \frac{3}{2}H_{2(g)} \qquad (4\text{-}1)$$

$$\Delta H_{r\,(500°C)} = -650\ kJ.mol^{-1}$$

or

$$Na_2CO_3.NaHCO_3.2H_2O_{(s)} + 3\,Na_2O_{(s)} \rightarrow 2\,Na_2CO_3 + 5\,NaOH_{(l)} \qquad (4\text{-}2)$$

$$\Delta H_{r\,(500°C)} = -286\ kJ.mol^{-1}$$

- Indirect reaction : decomposition reaction of trona followed by reaction with Na(g) or $Na_2O_{(s)}$

$$Na_2CO_3.NaHCO_3.2H_2O_{(s)} \rightarrow \frac{3}{2}Na_2CO_3 + \frac{5}{2}H_2O_{(l,g)} + \frac{1}{2}CO_{2(g)} \qquad (4\text{-}3a)$$

$$\Delta H_{r\,(500°C)} = 215\ kJ.mol^{-1}$$

$$\frac{5}{2}Na_{(g)} + \frac{5}{2}H_2O_{(g)} \rightarrow \frac{5}{2}NaOH_{(l)} + \frac{5}{4}H_{2(g)} \qquad (4\text{-}3b)$$

$$\Delta H_{r\,(500°C)} = -654\ kJ.mol^{-1}$$

or

$$\frac{5}{2}Na_2O_{(s)} + \frac{5}{2}H_2O_{(g)} \rightarrow 5NaOH_{(l)} \qquad (4\text{-}3c)$$

$$\Delta H_{r\,(500°C)} = -1348\ kJ.mol^{-1}$$

or combination of both $H_2O_{(g)}$ reactions with $Na_{(g)}$ and $Na_2O_{(s)}$, such as:

$$\frac{3}{2}Na_{(g)} + \frac{3}{2}H_2O_{(g)} \rightarrow \frac{3}{2}NaOH_{(l)} + \frac{3}{4}H_{2(g)} \quad \text{(4-3d)}$$

$$\Delta H_{r\,(500°C)} = -392\ kJ.mol^{-1}$$

$$Na_2O_{(s)} + H_2O_{(g)} \rightarrow 2NaOH_{(l)} \quad \text{(4-3e)}$$

$$\Delta H_{r\,(500°C)} = -148\ kJ.mol^{-1}$$

All these reactions are thermodynamically favored at 500°C ($\Delta G < 0$) and only the direct decomposition of trona is endothermic.

Depending on the reaction pathways (direct or indirect), 1 mole of trona might produce more or less NaOH and H_2. 2 moles and 5 moles of NaOH per mole of trona might be produced from direct reaction with sodium and sodium oxide respectively. The later reaction does not produce hydrogen, contrarily to the former that produce 1.5 moles of H_2. Indirect path produces at least 2.5 moles and 5 moles of NaOH via the reaction with sodium and sodium oxide respectively. In this case, 1.25 moles of H_2 can be produced as a by-product of the reaction with Na. Hence, the hydration water that reacts directly with Na_2O or with sodium in the gas phase changes considerably the number of gaseous hydrogen produced. As a hydrogen flame is likely observed in our experiment, obviously, at least one part of H_2O reacts with Na.
As a comparison, the reactions of Na and/or Na_2O via direct and indirect steps with $Na_2CO_3.H_2O$ are presented below:

- Direct reaction of $Na_2CO_3.H_2O$ with $Na_{(g)}$ or $Na_2O_{(s)}$

$$Na_2CO_3.H_2O_{(s)} + Na_{(g)} \rightarrow Na_2CO_3 + NaOH_{(l)} + \frac{1}{2}H_{2(g)} \quad \text{(4-4)}$$

$$\Delta H_{r\,(500°C)} = -184\ kJ/mol$$

or

$$Na_2CO_3.H_2O_{(s)} + Na_2O_{(s)} \rightarrow Na_2CO_3 + 2\,NaOH_{(l)} \quad \text{(4-5)}$$

$$\Delta H_{r\,(500°C)} = -71\ kJ/mol$$

- Indirect reaction: decomposition reaction of sodium carbonate monohydrate followed by reaction with Na(g) or $Na_2O_{(s)}$

$$Na_2CO_3.H_2O_{(s)} \rightarrow Na_2CO_3 + H_2O_{(g)} \quad \text{(4-6a)}$$

$$\Delta H_{r\,(500°C)} = 78\ kJ/mol$$

$$Na_{(g)} + H_2O_{(g)} \rightarrow NaOH_{(l)} + \frac{1}{2}H_{2(g)} \quad \text{(4-6b)}$$

$$\Delta H_{r\,(500°C)} = -262\ kJ/mol$$

or

$$Na_2O_{(s)} + H_2O_{(g)} \rightarrow 2NaOH_{(l)} \quad \text{(4-6c)}$$

$$\Delta H_{r\,(500°C)} = -148\ kJ/mol$$

In fact 0.008 mole of NaOH may be produced from 1g of trona. The same amount of NaOH is produced from 1g of $Na_2CO_3.H_2O$. However, the latter produce 1.5x less quantity of H_2 (0.004 moles) compared to the one resulting from the reaction with trona (0.006 moles). This comparison is based on the reaction 4-1 and 4-4 only. Besides, reactions with $Na_2CO_3.H_2O$ are less energetic than the ones with trona. This might indicate that $Na_2CO_3.H_2O$ is a more attractive compound as compared to trona for sodium fire extinction. Therefore, a high content of trona does not seem to actually improve the quality of extinction.

Figure 4-29 shows that a powder with 6w% of trona is of better performance than a powder of 23w% trona content. It even has almost the same efficiency as the one mainly composed of trona. Depending on the initial temperature of sodium, trona may or may not be favorable on extinction. As the sodium temperature T_n at which the combustion started is higher (cf. figure 4-30), a powder having less trona content but higher amount of $LiNaCO_3$ (powder VII) is able to fight fire better than one with an higher amount of trona but a lower $LiNaCO_3$ content. The role of $LiNaCO_3$ in this regard will be discussed in §4.3.4.

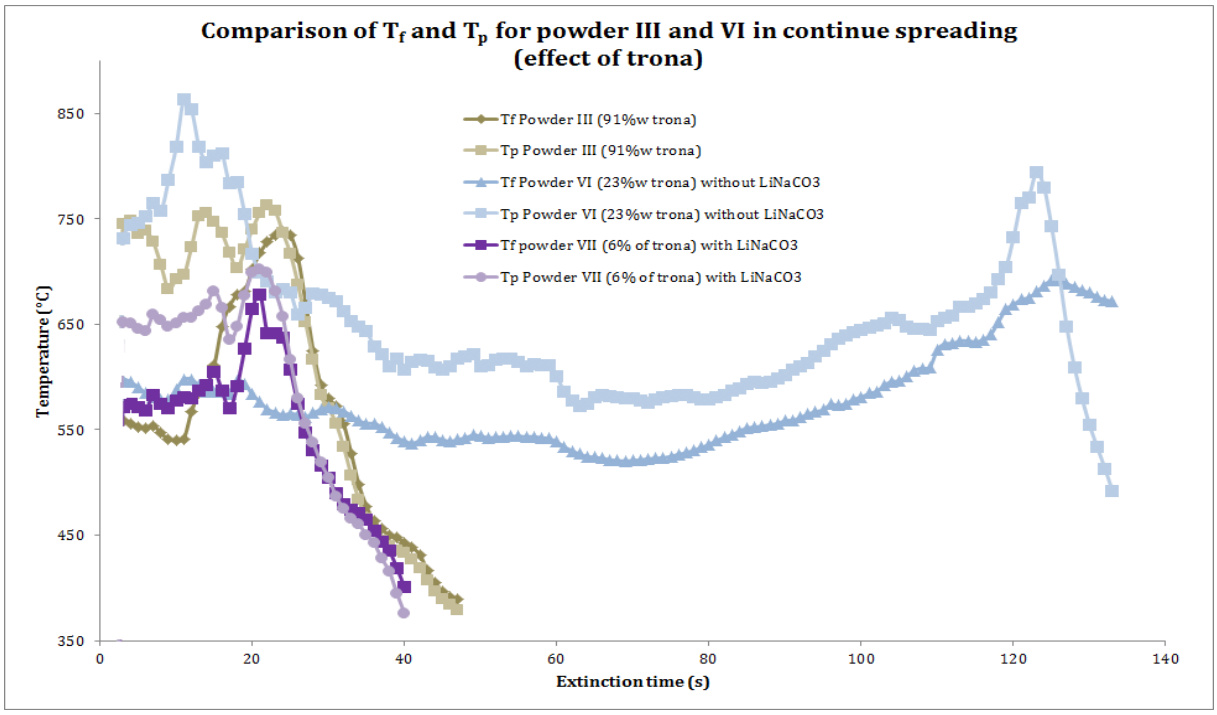

Figure 4-29. The comparison of temperature profile recorded by T_f and T_p for different trona contents in continuous spreading

However, high trona contents in the powder drives the tendency to produce a high flame (likely a H_2 flame) and exothermic reactions prior to the extinction, which eventually may harm the person who tries to extinguish the fire. This causes an increase of temperature on the sodium surface. Nevertheless, it is a relatively short flame that appears for 30s (cf. T_s of powder III in figure 4-30) and may not be dangerous if distance between the flame source and the person is long enough.

The maximum of trona produced during aging from Marcalina composition, as mentioned in the patent, is predicted to be as much as 58w%, which would yield 11.6w% of water (cf. §3.1.3). It is considered as being a slow transformation and to happen faster under a high relative humidity with no sealed condition (role of CO_2 is important in favoring the reaction). A regular control of relative humidity, as well as the choice of packaging during storage, might be essential to control the aging. As the chemical analysis previously discussed in §2.2 presents certain limitation in calculating the ratio of $Na_2CO_3.H_2O$ that may be transformed into trona, it can be suggested to still consider the total hydration water content rather than trona itself as the new threshold in powder quality insurance, but rather at an higher value than the present one.

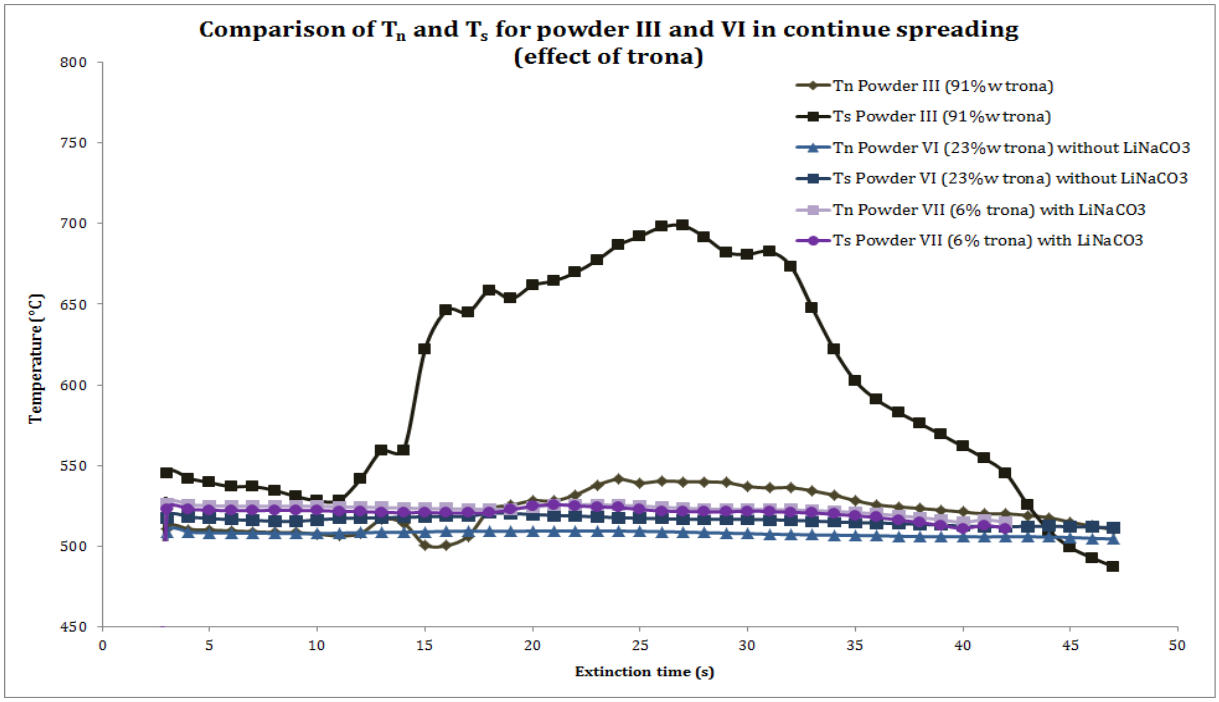

Figure 4-30. The comparison of temperature profile recorded by T_n and T_s for different water content in continuous spreading

4.3.4 The effect of $LiNaCO_3$ on the extinction capacity

$LiNaCO_3$ might eventually be produced as a result of a mechanochemical reaction during grinding. It is still questionable whether or not its presence is necessary in improving the extinction efficiency. Figure 4-31 shows the comparison of all powders in which the XRD residue of samples taken after extinction test contains $LiNaCO_3$. With $LiNaCO_3$ as the major component, powder VIII exhibits a relatively slow melting during extinction. The porous layer formed does not allow a complete separation of Na and O_2. As observed, the layers are continuously cracked, thus provoking re-ignitions. Meanwhile, powders VII and IX with 25w% and 50w% contents of $LiNaCO_3$ respectively, shows the same tendency of progressive temperature decrease, with slight temperature rise prior to extinction in the case of powder IX. However, it appears that even without $LiNaCO_3$ in the initial sample, its formation was evidenced in powder IV. The sodium surface temperature was recorded by T_s to be at 560°C, while T_n was at 530°C. These temperatures exceed the melting point of carbonates eutectic (498°C). As $LiNaCO_3$ may be formed after the cooling of melted carbonates at high temperature, it is possible that the thermal

exchange during extinction is high enough to allow the carbonates to melt. Thus, this component might not be essentially needed to improve extinction (by the formation of a liquid carbonate layer). Nevertheless, the presence of $LiNaCO_3$ in several cases (i.e. test with powder VII) might contribute to extinction as long as either the sodium or its surface has a relatively high temperature (superior to its melting temperature of 500°C). The temperatures in the sodium and at the surface have a tendency to slowly decrease as compared to a relatively constant temperature at around 500°C in powders of high hydration water content and no $LiNaCO_3$.

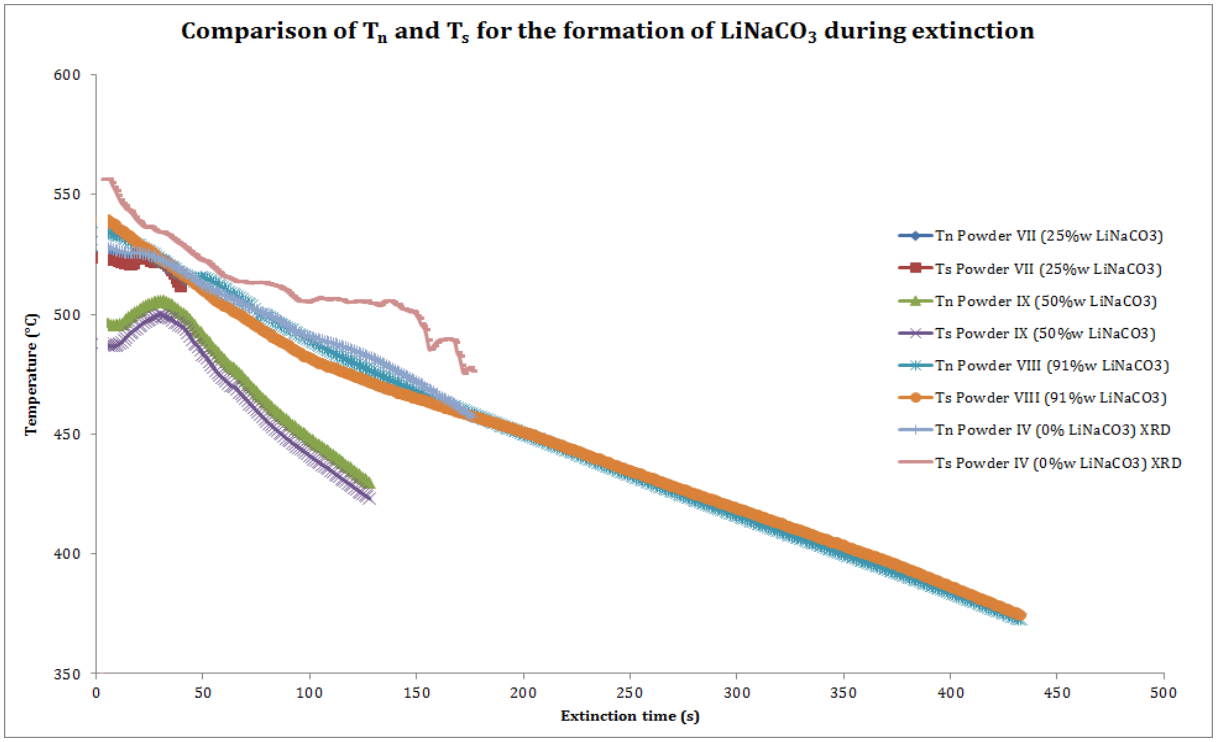

Figure 4-31. The comparison of temperature profile recorded by T_n and T_s for different content of $LiNaCO_3$ in continuous spreading

Considering that the melting point of carbonates is close to $LiNaCO_3$, it seems that this compound might not give an important contribution to improve the extinction quality as demonstrated in powder IV. Although, in certain cases, it may facilitate the melting of carbonates (i.e. powder VII with more $LiNaCO_3$ is more effective than that powder VI with less $LiNaCO_3$). $LiNaCO_3$ alone (powder VIII) is not capable to achieve complete extinction as the layer of $LiNaCO_3$ cracks easily, while the sodium temperature is still relatively high enough to provoke reignition.

4.3.5 The effect of particle size on the extinction capacity

The effect of particle size distribution on the extinction time is illustrated in figure 4-32. It appears that particles of small sizes (<20µm) do not contribute to improve the extinction performance unless the powder has a sufficient content of hydration water (i.e. powder C with 7.5w% of hydration water). Indeed, the ancient extinguishing powder, Totalit M2, of particle size

<35µm shows a better performance as compared to others of bigger particle sizes [4]. However it is not the case for powder II. With a particle size of 65µm but 13.2w% of hydration water, powder II performs a better extinction (in terms of extinction time) in comparison with the others. This demonstrates the important role of chemical composition in achieving sodium fire extinction.

In her work, Reuillon [4] recommended particle sizes to be less than or equal to 160µm, whilst several Marcalina batches produced by CACI have a dominant particle size <63µm. In both cases, the powders tested in this work have a size range between 5-65µm which is still within the range of particle size previously studied. Our results clearly demonstrate the small influence of particle size on improving extinction capacity. It only affects the spreading performance. The smaller particles struggle to achieve homogenization at the sodium surface, thus re-ignition was observed more often, contrarily to others of greater particle sizes. Besides, the test with direct spreading shows that the extinction time is actually decreased as the particle size increases (cf. figure 4-33).

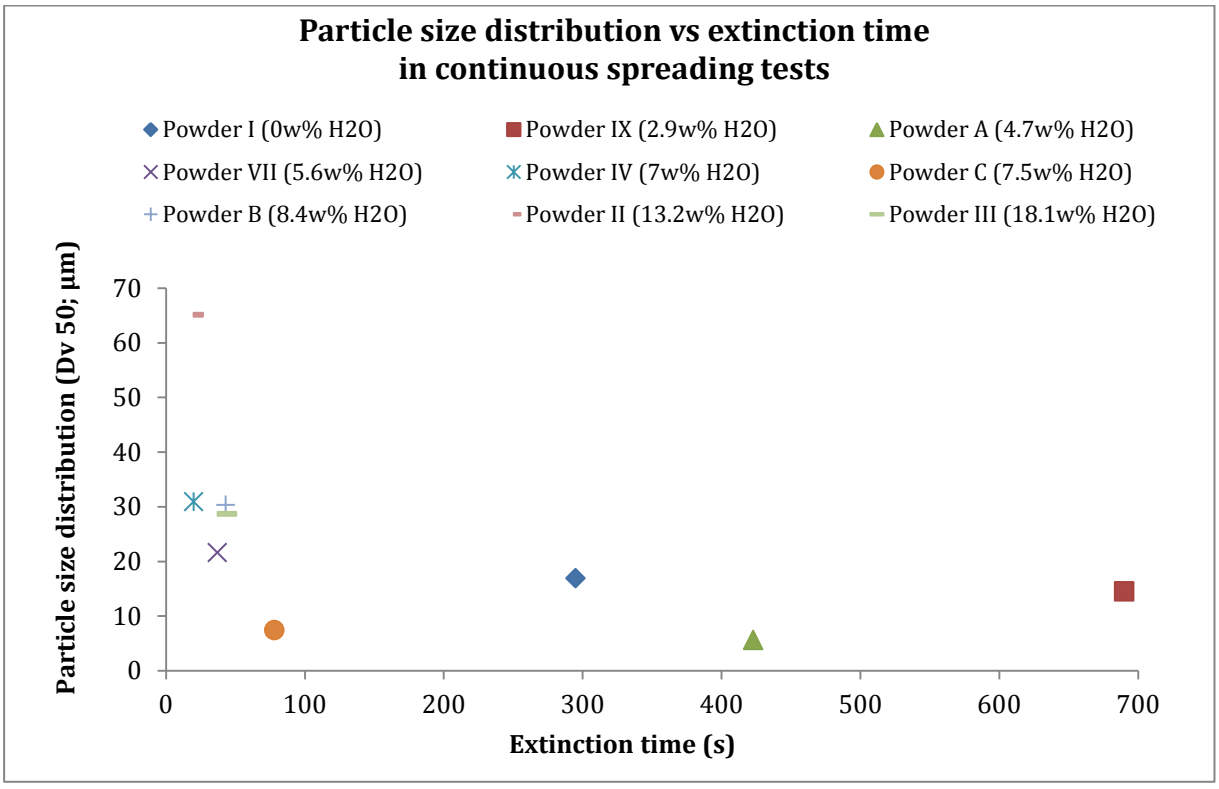

Figure 4-32. The influence of particle size distribution on the extinction time using continuous spreading tests

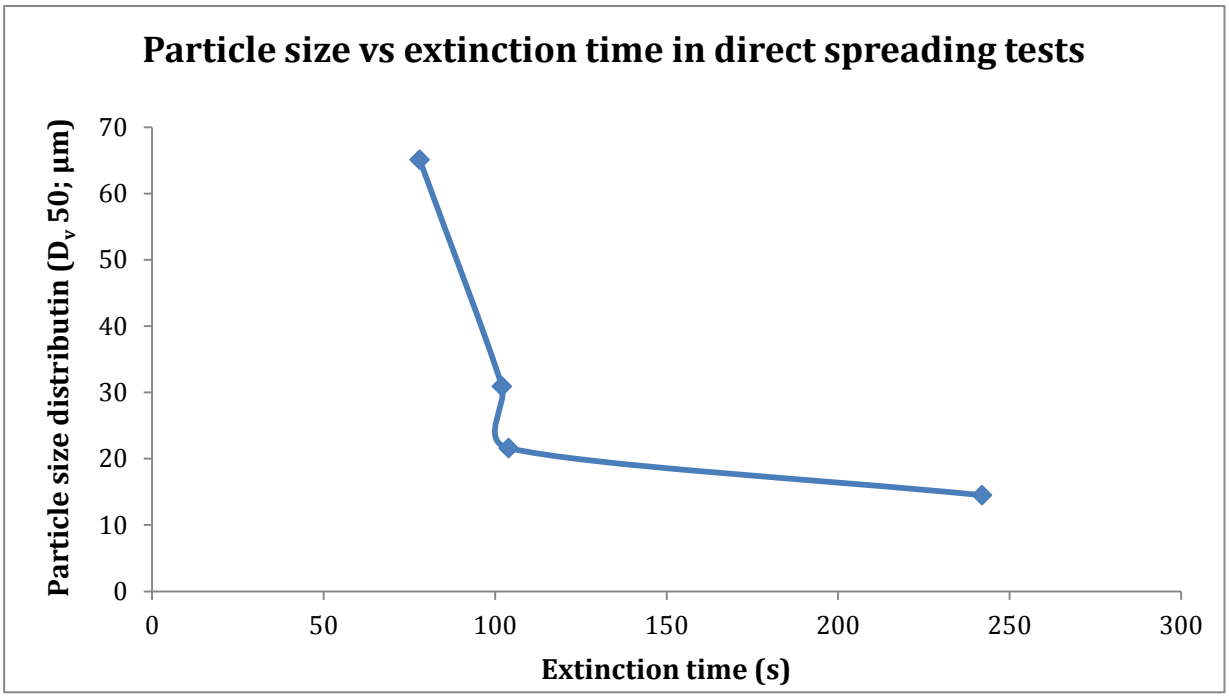

Figure 4-33. The influence of particle size distribution on the extinction time using direct spreading tests

4.3.6 The extinction mechanism

Based on the result of Chris(X)ti-Na experimental tests discussed above, two extinction mechanism steps might be proposed and illustrated in figure 4-34 (a) the formation of NaOH and (b) the melting of eutectic carbonates. The reactions proposed are detailed as follows:

1. The formation of NaOH (figure 4.34a)
   - Direct formation
     - From the reaction of trona with $Na_{(g)}$ and $Na_2O_{(s)}$: reactions 4-1 to 4-2
     - From the reaction of $Na_2CO_3.H_2O$ with $Na_{(g)}$ and $Na_2O_{(s)}$: reactions 4-4 to 4-5
   - Indirect formation
     - From the decomposition reaction of trona followed by reaction with $Na_{(g)}$ or $Na_2O_{(s)}$: reactions 4-3a to 4-3c
     - From the decomposition reaction of $Na_2CO_3.H_2O$ followed by reaction with $Na_{(g)}$ or $Na_2O_{(s)}$: reactions 4-6a to 4-6c

   These decomposition reactions are in contradictory with the extinction mechanism proposed by Birchall [8] in which a decomposition product might eventually contribute to improve the performance as the increase of specific surface (physical effect) might help favor the extinction. In our case, the decomposition reactions give more contribution to the formation of NaOH instead (chemical effect). The protective layer of sodium hydroxide allows a total separation of sodium and oxygen. In addition, the effect of small particle sizes is proved to be insignificant for sodium fire extinction.

   It is hard to distinguish which of these reactions (direct or indirect) actually happens as both might happen rapidly during extinction. Both mechanisms induce the formation of H_2 that might provoke the flash flame observed prior to extinction (need to be confirmed by

spectrometer measurement). These reactions are significantly contributing to the rapid decrease of temperature due to the formation of liquid sodium hydroxide as a protective layer to cover the sodium surface from prolonged contact with oxygen. Although most of the time the temperature in the sodium surface is still at relatively high temperature (around 500°C), the re-ignitions hardly happened.

2. The melting of eutectic carbonates

The melting of eutectic carbonates happened at 498°C with the enthalpy fusion of 11.1 kJ.mole^{-1}. After cooling until room temperature, $LiNaCO_3$ may be formed according to reaction 4-7. Hence, the presence of $LiNaCO_3$ is a proof that the melting of eutectic carbonates happened during extinction.

$$Na_2CO_3 + Li_2CO_3 \rightarrow LiNaCO_3 \qquad (4\text{-}7)$$

NaOH has smaller latent heat of fusion than that of $LiNaCO_3$with 6.8 kJ.mol^{-1}. However, the latter has higher viscosity (with 4.8 cP [7] for ternary mixtures of lithium, sodium, and potassium carbonates since there is no data for $LiNaCO_3$) than that of NaOH with 2.2 cP [6], This property might make the liquid eutectic carbonate less efficient to achieve the formation of a protective layer. Besides, the reaction happens more slowly than that of NaOH formation. Moreover as the sodium temperature is still high when it solidifies, the eutectic carbonates layer tends to crack easily so more susceptible to provoke re-ignitions. Since its formation takes a much longer time than that of liquid sodium hydroxide, its role is less significant especially if the sodium surface temperature is less or equal to 500°C (as it is close to its melting point). However, it is considered it could be more efficient for sodium fires with higher sodium surface temperature (more than 500°C).

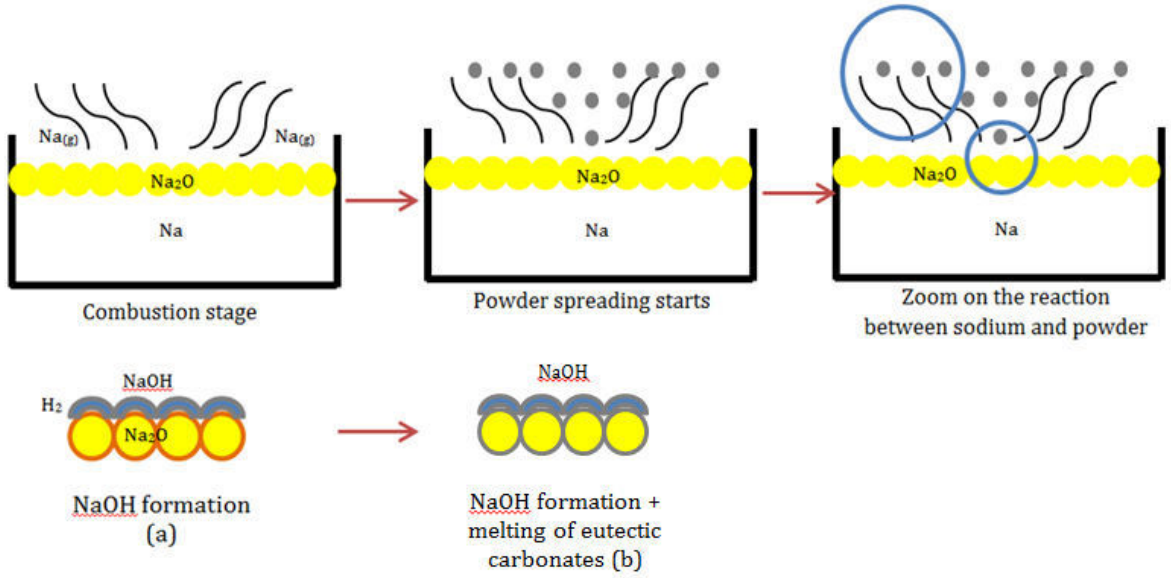

Figure 4-34. The mechanism of sodium fire extinction (a) with and (b) without formation of $LiNaCO_3$

4.4 Proposition of simulation approach to validate the mechanism of extinction

The experimental approach has been conducted to understand the extinction mechanism of sodium fire as well as the influence of aging on the extinction capacity,. A tentative of modelling approach involving energy and mass transfers during extinction is proposed here to complete observational results obtained in the experiments. This could be the basis of further simulation developments.

4.4.1 Phenomenological description of the extinction mechanism

As what was previously observed in the experimental tests, notably those using direct spreading, the phenomenology that would be interesting to simulate is related to the material and energy transfers within powder, sodium oxide layer, and sodium itself. Considering that these exchanges happen across porous materials (Marcalina powder but also sodium oxide layer), the oxygen comes downward (from the surrounding atmosphere towards the sodium pool surface) and the vapor of sodium comes upward through the porous media (Na_2O layer and Marcalina powder) as can be seen in figure 4-35.

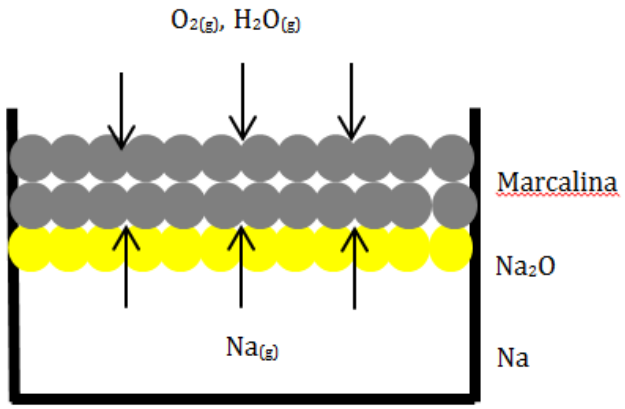

Figure 4-35. The phenomenological description of the mass exchange during extinction of a sodium fire

- *Chemical reactions*

The reaction of combustion between sodium and oxygen, as well as other reactions with water vapor or thermal decomposition of Marcalina compounds, should be taken into consideration. Powders containing hydration water may (or not) experience a decomposition and induce the formation of sodium hydroxide. The formation of $LiNaCO_3$ is also included as part of the reaction in favor of extinction. Thus, depending on the powder content, more or less reactions might take place. The substantial reactions are listed as follows:

- Sodium combustion (in gas phase and in liquid phase at the sodium pool surface)
  $2\,Na_{(g)} + \frac{1}{2}O_{2(g)} \rightarrow Na_2O_{(s)}$ (4-9)
- NaOH formation (in gas phase and in Na_2O solid phase at the sodium pool surface or in the powder media after deposition of Na_2O particles) according to reactions (4-1) to (4-7)

- $LiNaCO_3$ formation according to reaction (4-8) and the melting of carbonates.

- *Material transfer in porous media*

The migration of two gaseous reactants should be considered in the model:

- The downward diffusion of oxygen through the powder (Marcalina) layer and through the Na_2O layer.
- The upward diffusion of sodium vapor through the Na_2O layer and through the extinction powder layer.

For each gaseous reactant, the effective diffusion coefficient (D_e) in both porous media is evaluated from the classical value (D) in air or in nitrogen with a correction factor based on the porosity (ε): $De = \varepsilon.D$.

Moreover, if it can be considered that water vapor is effectively released during dehydration of sodium carbonate, then an isotropic diffusion transfer of this gaseous species should also be considered in the model as a transfer in the porous media.

- *Heat transfer in porous media*

The sodium combustion heat (in J/kg) coupled with the combustion kinetics of sodium vapor (in kg/s) must be taken into account as the major heat source during the extinction process of sodium fire.

Then different terms of heat transfer should be also implemented in the model in order to describe the extinction mechanism:

- Thermal conduction in the concerned porous media,
- Thermal radiation associated with the combustion flame temperature
- Endothermal or exothermal enthalpy associated with each chemical reaction or phase change

In the porous media, no convection will be considered for the gas phase which is supposed to be stagnant within the porosity. On the other hand, it would be interesting to take into account the convective heat removal at the upper surface of the powder bed.

4.4.2 Strategy of modelling development

Two stages of simulation are proposed: the simplified and complex model. Details of both models will be explained hereafter and are illustrated in figure 4-36.

- *"Simplified model" focused on the behavior in Marcalina porous media*

In this model, the phenomenon is more emphasized on what happens in the Marcalina layer. Two development steps are developed:

- First step: the single combustion phase

In order to simplify the model for this first step, we suppose that the thickness and porosity of Marcalina remains constant. As a preliminary step, this study should be conducted in a stationary regime, in which the sodium vaporization flux, as well as the air composition, remains constant. The insulator was used during the experiment; therefore the sodium container is suggested to be considered as thermally isolated. The sodium temperature is initiated at 500°C.

Only the reaction of combustion is taken into consideration in this configuration. It represents the initial condition when the powder is firstly spread on the sodium fire. Indeed, this configuration is close to the experiment of direct spreading, the fire still developed for certain time even after the powder has directly fallen on the sodium surface. In this case the sodium vapor diffuses through the pores of the powder bulk and can react with available oxygen supplied from the upper surface of the powder (cf. combustion reaction 4-9). The other reactions (especially for the NaOH formation) are not considered in this preliminary step.

In terms of expected results, this step will give a first idea of the temperature profiles as well as the concentration profiles of oxygen, sodium vapor, and sodium oxide within the powder layer. The influence of the quantity of Marcalina used, and consequently of its thickness above the sodium, should be studied.

- Second step: combustion coupled with NaOH formation

Two modeling options should be considered: either the NaOH formation takes place directly at the surface of the particles (without release of gaseous water molecules), or it takes place in gas phase when stoichiometric conditions are locally achieved (coupling with gas diffusion kinetics). In this former case, a convention will be adopted to calculate the initial concentration of H_2O vapor that is likely to be released from the powder composition and that will fill the pores of Marcalina. This data input can be estimated by the assumption that the whole water quantity is directly released in the pores.

Moreover, in order to evaluate the progress of the extinction mechanism, it seems interesting to calculate the filling of porosity (both in Na_2O layer and in the powder media) with liquid NaOH that may be formed progressively from sodium vapor reaction with water molecules coming from the powder decomposition. For this purpose, two calculations may be carried out:

a) Considering the NaOH formation at the surface of Na_2O layer (reaction 4-4), the thickness of NaOH liquid layer (h_{NaOH}) might be evaluated as follows:

$$m_{NaOH}(t) = F_{H_2O} * t \quad (4\text{-}10)$$

$$h_{NaOH} = \frac{V_{NaOH}}{area\ of\ container} = \frac{m_{NaOH}(t)}{d_{NaOH}} * \frac{1}{area\ of\ container} \quad (4\text{-}11)$$

Where $m_{NaOH}(t)$ is the mass of NaOH formed at time t due to the H_2O diffusion flux F_{H_2O} through the powder porous media and arriving at the Na_2O surface. This diffusion flux F_{H_2O} should be an output result calculated by the CFD software in the first step that could be used for the simulation. By multiplying the result with the time, the cumulate weight of NaOH formation could be estimated and compared to the time needed to obtain extinction taken

from the experiment. In addition, the thickness of NaOH to obtain a complete extinction might be evaluated to give complementary indication on extinction required conditions.

b) Considering the reaction (4-3) that may occur in gas phase within the powder porosity, another calculation is foreseen in order to determine the decrease of the powder porosity due to the filling with liquid NaOH. This modeling could also be applied to estimate an evolution of Na_2O porosity although it seems less realistic (since Na_2O is directly consumed by the reaction).

$$V_{powder} = area\ of\ container * h \quad (4\text{-}12)$$

$$V^0_{pores} = V_{powder} * \varepsilon^0_{powder} \quad (4\text{-}13)$$

$$V_{NaOH}(t) = F_{H_2O} / d_{NaOH} * t \quad (4\text{-}14)$$

$$\%\ porosity\ saturation(t) = \frac{V_{NaOH}}{V_{pores\ of\ Na_2O}} = \frac{F_{H_2O} * t}{d_{NaOH} * V_{powder} * \varepsilon^0_{powder}} \quad (4\text{-}15)$$

A saturation rate of the powder porosity by the accumulation of liquid NaOH can be estimated by this correlation (4-15) using also the H_2O diffusion flux F_{H_2O} expressed in ($kg.s^{-1}$) and the liquid NaOH density (in $kg.m^{-3}$). The time of extinction, then, might be evaluated whenever the NaOH fills the pores entirely (ε_{powder} = 0 or % porosity saturation = 1).

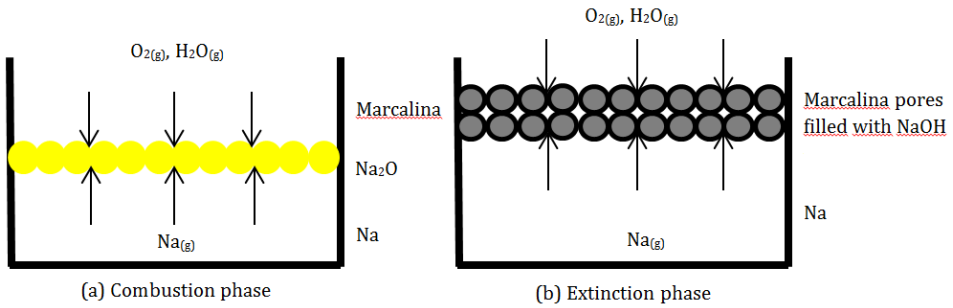

Figure 4-36. Simulation steps (a) combustion phase and (b) extinction phase in simplified model

- *"Complex model" implementing the coupled phenomena in the global system*

In this more complete model, the phenomenon is more representative of reality, as three layers are considered: the Marcalina powder layer, the porous Na_2O layer and the sodium layer. The calculation of the porosity decrease in Na_2O layer (which thickness will be considered as constant) will be used to apply a variable correction to the source term of sodium vapor diffusing from the sodium pool surface upward through the Na_2O layer. Obviously, the simulation with this "complex model" will take advantage to be performed in transient regime in order estimate the evolution of the different parameters and variables and to highlight the major influences of these coupled phenomena. Except from these major differences with the "simplified model", the modeling will also be carried out in two steps (cf. figure 4-37):

- First step: the single combustion phase

- Second step: combustion coupled with NaOH formation

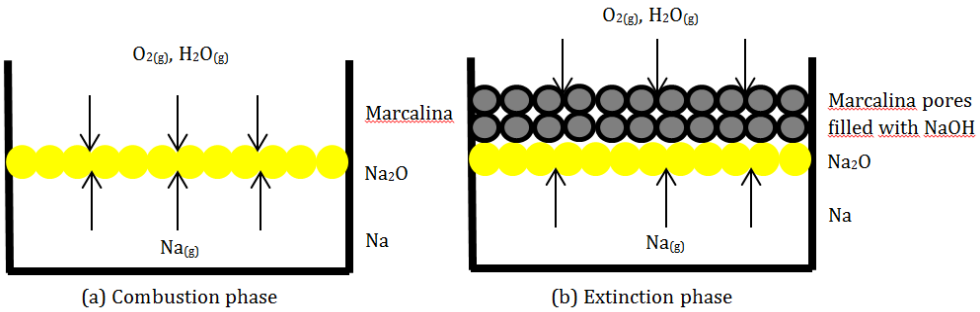

Figure 4-37. Simulation steps (a) combustion phase and (b) extinction phase in complex model

4.4.3 Description of physical parameters

Numerous parameters are needed to be taken into account in the models: Available literature was investigated in order to find numerical values or correlations (especially for temperature dependent parameters), which should be applicable to the conditions of sodium fire extinction.

- Properties of liquid sodium [9]

  - Density $Na_{(l)}$ $(\rho_{Na(l)})$
    $\rho_{Na\,(l)}[kg.m^{-3}] = 1037.1 - (0.268 * T)$

  - Viscosity $Na_{(l)}$ $(\mu_{Na(l)})$

    $\mu_{Na\,(l)}[Pa.s] = (0.089 * 10e^{-3}) * e^{\frac{770}{T}}$

  - Thermal conductivity $Na_{(l)}$ $(\lambda_{Na(l)})$

    $\lambda_{Na\,(l)}[W.(m.K)^{-1}] = 91.8 - [0.049 * (T - 273.15)]$

  - Specific heat $Na_{(l)}$ $(c_{p\,Na(l)})$

    $c_{pNa\,(l)}[J.(kg.K)^{-1}] = 1436 - \left[\frac{1}{5.8037} * (T - 273.15)\right] + \left[\frac{1}{4.6219 * 10^4} * (T - 273.15)^2\right]$

- Properties of sodium vapor [10]

  - Specific heat $Na_{(g)}$ $(c_{p\,Na(g)})$
    $c_{pNa\,(g)}[J.(kg.K)^{-1}] = 900$

  - Thermal conductivity $Na_{(g)}$ $(\lambda_{Na(g)})$

$$\lambda_{Na\,(g)}[W.(m.K)^{-1}] = (1.6343 * 10^{-2}) + (5.3243 * 10^{-5}\,T) - (6.2857 * 10^{-8}\,T^2) + (1.4425 * 10^{-10}\,T^3) - (2.2135 * 10^{-13}\,T^4) + (1.7096 * 10^{-16}\,T^5) - (5.0498 * 10^{-20}\,T^6)$$

- Viscosity $Na_{(g)}$ $(\mu_{Na(g)})$

$$\mu_{Na\,(g)}[Pa.s] = (2.1244 * 10^{-5}) + (6.4081 * 10^{-8}\,T) - (5.1874 * 10^{-11}\,T^2) + (6.5606 * 10^{-14}\,T^3) - (5.9325 * 10^{-17}\,T^4) + (2.9606 * 10^{-20}\,T^5) - (5.7636 * 10^{-24}\,T^6)$$

- Sodium diffusivity in nitrogen $(D_{Na(g)})$

$$D_{Na\,(g)} = \left(2.98\, e^{-\frac{778}{T}}\right)$$

- Rate of sodium vaporization $(F_{vap\,Na(g)})$

$$F_{vap\,Na\,(g)}[kg.(m^{-2}.h^{-1})] = \left(10^{8.062 - \frac{5426}{T} - 0.5 log_{10} T}\right)$$

- Sodium initial concentration $(c_{0\,Na})$

$$P_{sat} = 10000.\left[10^{(6.487538 - \frac{10020.6}{1.8 * T} - 0.5 log_{10}(1.8 * T))}\right]$$

- Properties of Marcalina and synthetic powders

The physical properties of powders were not measured specifically, but the thermal conductivity (λ), specific heat (Cp), and density (ρ) might be approached by using the properties of individual components contained in each powders and by the calculation of mixture properties based on mass fraction rating and the porosity (cf. table 4-9). However, this approach may present a downfall since the powder particle size distribution will influence these parameters. Each powder has experienced certain physical treatments such as grinding and mixing, thus influencing the particle size distribution. Considering the density as an example, a difference may appear between this approach and the actual density measured (cf. table 2-9 for powders A, B, and C). The particle size may affect the thermal conductivity due to the grain boundaries and their effect on the heat transfer. Besides, very few literature articles have mentioned relations to the specific heat. Therefore, a technical measurement of these parameters might be of interest for further development of the model.

Table 4-9. The estimation of thermal conductivity, specific heat, and density properties of each powder

Powder	λ (W/(m.K))	C_p (J/(kg.K))	ρ (kg/m³)
Powder I	22.3	1042	2497
Powder II	22.3	1042	2239
Powder III	26.4	1042	2130
Powder IV	22.3	1042	2188
Powder V	22.3	1042	2323
Powder VI	23.3	1042	2166
Powder VII	22.8	1042	2166
Powder VIII	23.1	1042	2130
Powder IX	22.7	1042	2154
Powder A	22.6	1042	2167
Powder B	20.8	1000	2080
Powder C	13.7	1042	2149

- Experimental evaluation of the sodium oxide (Na_2O) porosity

A first estimation of the porosity of the sodium oxide layer formed on top of the sodium pool surface was evaluated experimentally by monitoring the sodium oxide formed during the combustion (5 minutes were taken as the duration). The rate of Na_2O formation (r_{Na_2O}) was calculated using a majoring value of empirical combustion rate measured for sodium pool fires. The thickness (h_{Na_2O}) of Na_2O layer was then measured in order to estimate its porosity by using the correlation 4-24 between these two parameters.

- $r_{Na_2O}[kg.h^{-1}] = surface\ area\ of\ the\ container\ (s) * 40\ \frac{kg\ Na}{m^2.h} * \frac{M\ Na_2O}{2 * M\ Na}$ (4-16)

- $h_{Na_2O}[m] = \frac{V}{s} = \frac{m_{Na_2O}}{\rho_{bulk} * (1-\varepsilon) * s} = \frac{r_{Na_2O}\ x\ t}{\rho_{bulk} * (1-\varepsilon) * s}$ (4-17)

Figure 4-38 shows the influence of porosity towards the thickness of the sodium oxide calculated for 300 s combustion, equivalent to the duration of the combustion experiment (5 minutes). At the end of experiment, we measured the thickness of sodium oxide formed, which is 3.9 cm. According to the correlation 4-17, this corresponds to the thickness obtained for the porosity of 0.9. Considering this preliminary estimation of Na_2O porosity (assumed to remain constant), equation 4-17 is then used to determine the thickness of oxide obtained during the combustion time in each extinction experiment with the different powders (cf. figure 4-39). This estimation of Na_2O thickness will be used in the case of the "complex model" accounting for this porous layer.

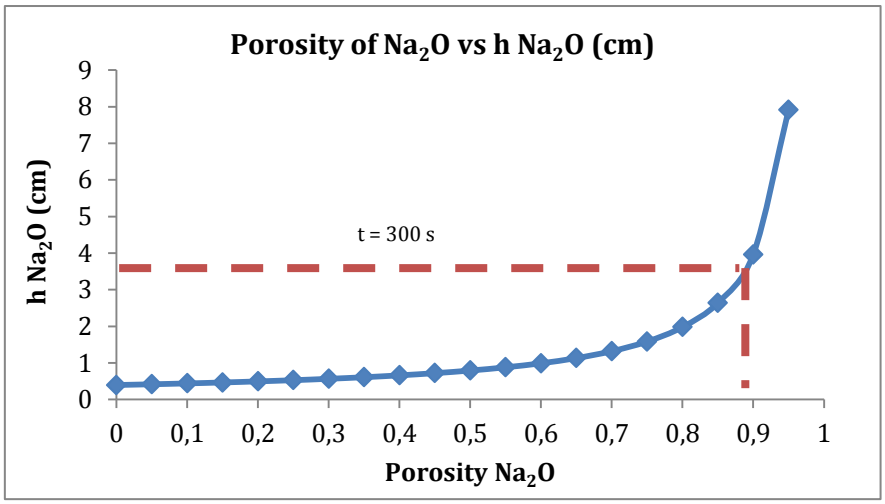

Figure 4-38. The thickness of Na_2O in a different porosity for 300 s

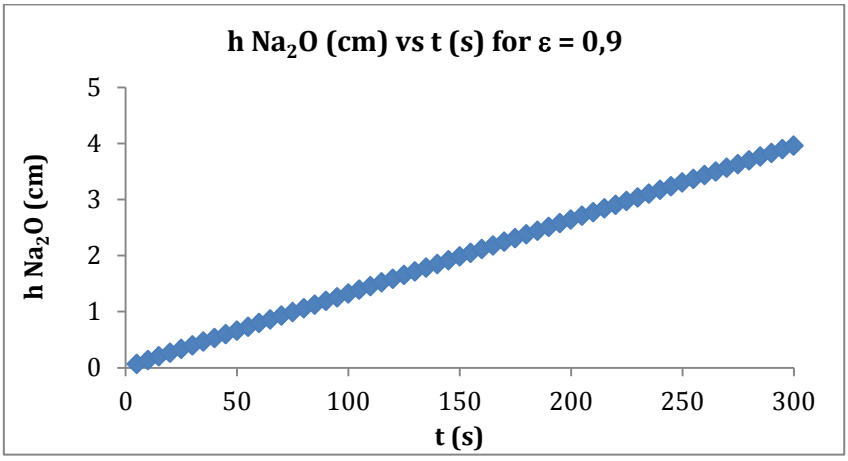

Figure 4-39. The thickness of Na_2O with ε = 0.9 throughout times

4.4.4 Modelling approach in COMSOL® software

Two physics modules should be chosen in the COMSOL® software in order to implement the proper equations sets necessary to represent the extinction mechanism:

- The module "Transport of diluted species in porous media"

This interface includes free and porous media flow with immobile and mobile phases, including diffusion, convection, dispersion, adsorption, and volatilization in porous media. It supports cases where the solid phase substrate is exclusively immobile, and when a gas-filling medium is also assumed to be immobile.

It applies to one or more diluted species or solutes that move primarily within a fluid that fills (saturated) or partially fills (unsaturated) the voids in a solid porous medium. The pore space not filled with liquid (like liquid sodium hydroxide) contains an immobile gas phase. We assume

that liquid sodium hydroxide filling the powder pores is able to seal the porosity and ensure the separation of sodium and oxygen.

- The module "Heat transfer in porous media"

It is used to model heat transfer by conduction, convection, and radiation in porous media. The following version of the heat transfer equation is used to model heat transfer in a porous matrix filled with a fluid:

$$(\rho C_p)_{eff}\frac{\partial T}{\partial t} + \rho C_p \boldsymbol{u}.\nabla T + \nabla.\boldsymbol{q} = Q$$

$$q = -k_{eff}\nabla T$$

with the following material properties, fields, and sources:

- ρ (SI unit: kg. m^{-3}) is the fluid density.
- Cp (SI unit: J.(kg^{-1}·K^{-1})) is the fluid heat capacity at constant pressure.
- $(\rho\ Cp)_{eff}$ (SI unit: J.m^{-3}·K^{-1})) is the effective volumetric heat capacity at constant pressure defined by an averaging model to account for both solid matrix and fluid properties.
- **q** is the conductive heat flux (SI unit: W.m^{-2}).
- **u** (SI unit: m.s^{-1}) is the fluid velocity field, either an analytic expression or the velocity field from a Fluid Flow interface. **u** should be interpreted as the Darcy velocity, that is, the volume flow rate per unit cross sectional area. The average linear velocity (the velocity within the pores) can be calculated as $\boldsymbol{u}_L = \frac{u}{\theta_L}$, where θ_L is the fluid's volume fraction, or equivalently the porosity.
- k_{eff} (SI unit: W.(m·K)$^{-1}$) is the effective thermal conductivity (a scalar or a tensor if the thermal conductivity is anisotropic), defined by an averaging model to account for both solid matrix and fluid properties.
- Q (SI unit: W.m^{-3}) is the heat source (or sink).

For a steady-state problem the temperature does not change with time and the first term disappears.

Figure 4-40 describes the geometry and boundary conditions chosen for the simplified model in COMSOL. The 2D-rectangle axisymmetric is used with the partial pressure of O_2 and rate of sodium evaporation assumed to be constant at the upper and lower boundaries, respectively.

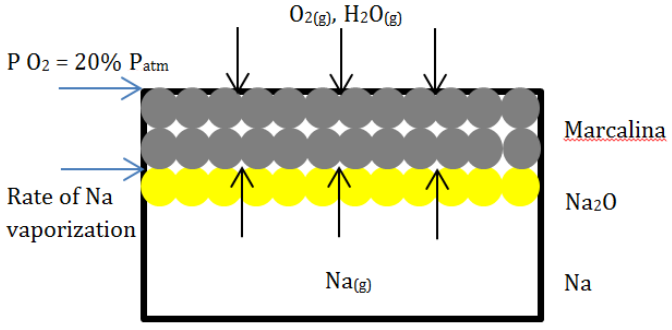

Figure 4-40. The geometry and boundary conditions for the simplified model applied in COMSOL

Heat of combustion depends on the rate of combustion itself, in which two approaches are considered:

- Rate of combustion (r_{comb}) based on the rate of sodium pool fire provided in literature and with a correction factor related to oxygen concentration

$$r_{comb}\left(\frac{mol}{m^3.s}\right) = \frac{40\frac{kg}{m^2.h}}{V_{powder}} x \frac{area\ of\ the\ container}{M\ Na} x \frac{c_{O_2}}{c_{0\ O_2}}$$

- Rate of combustion (r_{comb}) based on an extrapolation of the sodium drop combustion rate ("Spalding model" provided in literature [11]

$$r_{comb} = \frac{\pi\rho_l K}{4} d \text{ where } K = \frac{8.\lambda}{C_p\rho_l}\ln(1+B) \text{ and } B = \frac{1}{h_{fg}}\left\{C_p\left(T_g - T_s\right) + \frac{H_c Y}{i}\right\}$$

M = molecular weight
c $(kg.m^{-3})$ = concentration
λ $[W.(m.K)^{-1}]$ = gas thermal conductivity
C_p $[J.(kg.K)^{-1}]$ = gas specific heat
h_{fg} $[J.kg^{-1}]$ = latent heat of sodium vaporization
$T_g[K]$ = gas temperature
$T_s[K]$ = sodium drop temperature
$H_c[J.mol^{-1}]$ = heat of combustion
Y = weight fraction of O_2
i = stoichiometric ratio (O_2/Na)

Both of these approaches to calculate the sodium pool combustion rate could be investigated and compared in further modeling studies, as well as other sodium pool combustion models that might be identified in future literature review in this field.

The description of the modeling approach presented in this last section, and of the physical parameters to be used as input data, provides the major elements necessary for the implementation of the extinction model in the COMSOL® software. Preliminary work was carried out to build this calculation tool but needs complementary effort to finalize a first operational version able to provide meaningful results. Nevertheless, it seems a promising perspective, since the simulations should give very interesting information about the evolution of major parameters such as: the temperature profiles in the system (especially in the powder layer), the concentrations profiles of the different species ($O_{2(g)}$, $Na_{(g)}$, $Na_2O_{(s)}$, $NaOH_{(l)}$…) or the porosity profiles in porous media.

CONCLUSION

The Chris(X)ti-Na experimental tests allow us to understand not only the role of different chemical properties on the extinction, but also the influence of physical properties on the spreading. The results showed the significant role of hydration water that is demonstrated by a rapid temperature decrease. The NaOH formed due to the reaction of Na-H_2O, Na_2O-H_2O, $Na_2CO_3.H_2O$-Na, $Na_2CO_3.H_2O$-Na_2O and/or trona-Na, trona-Na_2O ensures the separation of sodium with oxygen that is essential during extinction. However, in most cases the latter is preceded by a sudden temperature rise that might correspond to the combustion of released H_2 as a by-product and exothermicity of reaction. Overall, 0.5-0.9 g of water is necessary to extinguish 19.6 cm^2 of sodium pool fire (equal to the average of 0.035 g per cm^2), which corresponds to 1-2g of NaOH. The more water contains in the powder, the easier will be to attain this amount so as to extinguish the sodium fire (consequently faster release of H_2). Nevertheless it should be emphasized that the flame produced is relatively short and is followed by rapid formation of NaOH. Moreover, study with continuous spreading displayed shorter flame as compared to direct ones. Trona is proven to not alter the extinction capacity of the powder. It contributes to increase the hydration water content that might eventually increase the production of both NaOH and H_2 during extinction. However, it should be noted that the same amount of NaOH might be produced by similar mass of trona and $Na_2CO_3.H_2O$. However, trona release almost twice higher amount of hydrogen, which makes its presence less interesting than that of sodium carbonate monohydrates

In the case of high sodium surface temperature, $LiNaCO_3$ might have more contribution by facilitating the melting of carbonates eutectic composition at 498°C. Nevertheless, its melting takes longer time than that of NaOH. It has a higher viscosity than NaOH, which makes it difficult for it to produce a liquid layer thick enough to ensure a total separation of sodium and oxygen. And most of all, the carbonates layer at freezing is susceptible to crack at a relatively high temperature, exposing fresh surface of hot sodium to the air, thus provoking re-ignitions.

The particle size apparently doesn't have a major influence on the extinguishing performance. The bigger particle sizes actually show faster extinction time. In fact it affects the spreading performance as the smaller particles struggle to cover the sodium surface homogeneously. Powders of small particle sizes perform well as long as they contain sufficient hydration water which is a key to achieve complete extinction rapidly. Powders of bigger particle size also have the same satisfying extinction performance as long as it has enough water content.

Furthermore, two steps of extinction mechanisms are proposed that includes (1) the formation of liquid sodium hydroxide and (2) the melting of eutectic carbonates. Step 1 can happen directly (via the direct reaction of trona and/or $Na_2CO_3.H_2O$ with $Na_{(g)}$ and/or $Na_2O_{(s)}$) or indirectly (via the decomposition reaction of trona and $Na_2CO_3.H_2O$ prior to reaction of $H_2O_{(g)}$ released with Na and Na_2O). However, as both reactions happen really fast during extinction, they are hardly distinguished in our experiments.

BIBLIOGRAPHY OF CHAPTER IV

[1] Reuillon M. , Mellottee H. , Devillers B. , Alfille L.,Duco J. , Fruchard Y. , Malet J.C. , et Chappellier A., "Procédé et poudre pour l'extinction des feux de métaux liquides," 75 36225, 03-Mar-1978.

[2] M. Reuillon *et al.*, "Powder for extinguishing fires of liquid substances or of a mixture of liquid substances," US Patent 4,149,976, Apr-1979.

[3] CACI, "Fiche technique de controle de la fabrication, condition de stockage, controle de reception de la poudre Marcalina." 22-Jan-1982.

[4] Reuillon M., "Etude de la combustion du sodium et de l'extinction de ses feux par les substances pulvérisees: Role des additifs," L'Université d'Orleans, France, 1976.

[5] JC. Malet., "Les feux de sodium (transparents)." Document CEA, DRN/DER/STPI Ecole du Sodium.

[6] G. . Janz and R. P. T. Tomkins, *Physical properties data compilations relevant to energy storage. Part IV Molten Salts: Data on additional single and multi component salt systems*. US Department of Commerce, 1981.

[7] G. J. Janz and F. Saegusa, "Molten carbonates as electrolytes: viscosity and transport properties," *J. Electrochem. Soc.*, pp. 452–456, May 1963.

[8] J. D. Birchall, "On the mechanism of flame inhibition by alkali metal salts," *Combust. Flame*, vol. 14, no. 1, pp. 85 – 95, 1970.

[9] G. Rodriguez and J. Desremaux, "Physico-chimie du sodium." Centre d'Etudes de Cadarache, 13-Nov-1997.

[10] Y. L. Sinai, I. J. Ford, J. C. Barrett, and C. F. Clement, "Prediction of coupled heat and mass transfer in the Fast Reactor cover gas: the C-GAS code," *Nucl. Eng. Des.*, vol. 140, no. 2, pp. 159–192, May 1993.

[11] A. Yamaguchi, T. Takata, and Y. Okano, "Numerical Methodology to Evaluate Fast Reactor Sodium Combustion," *Nucl. Technol.*, vol. 136, no. 3, pp. 315–330, Dec. 2001.

CONCLUSION

This study is proposed to respond to eventual issues regarding the safety of sodium related to sodium fire event, in the context of the development of ASTRID Sodium Fast Reactor project. Despite several advantages that sodium offers as a coolant, its reactivity with air and water might pose safety issues. Indeed, sodium ignites at a relatively low temperature. It is mostly preceded by an oxidation phase, before several nodulations leading to the combustion phase in the case of sodium pool fire. Sodium must be isolated from oxygen in order to ensure a complete extinction. Forty years ago, CEA developed an extinguishing powder, known as Marcalina, which is capable of extinguishing a sodium fire at low and high temperatures. It consists of a mixture of lithium carbonate and sodium carbonate monohydrate in eutectic proportion, together with graphite. After long term storage, the quality of this powder becomes questionable in terms of its performance in extinguishing sodium fire. In particular, their water content could exceed the original specifications of the producer. Furthermore, no information about how to manufacture this powder, as CACI, the producer, has ceased its activity, which makes this even more problematic.

For that reason, the physicochemical analyses of several powder batches have been performed. Three Marcalina samples (powders A, B, and C) were chosen as samples of interests. The chemical analysis with XRD highlights the presence of trona and $LiNaCO_3$, two compounds that are not mentioned in the patent. Coupled TGA-µGC and AAS allows the quantitative analysis of these powders. Several physical analyses (SEM, LASER particle size analysis, FT4 powder rheometry, and DVS) were also conducted. Two categories of powders can be distinguished based on the content of hydration water previously specified by the manufacturer (3.5 to 5.4 ± 1 w%):

- Powders in specifications (i.e. powder A), made of a high amount of $LiNaCO_3$ and a small amount of trona. It has small particle sizes and is considered to have cohesive properties.
- Powders out of specifications (i.e. powders B and C), made of a high amount of trona and a small amount of $LiNaCO_3$. Powder B has relatively large particles (easy flowing), while powder C has small particles but is considered to be less cohesive than powder A.

Trona ($Na_2CO_3.NaHCO_3.2H_2O$) is actually a product of aging whose formation depends on the storage conditions. Meanwhile $LiNaCO_3$ is supposed to be part of the initial composition of the powder due to its formation which would involve reaction of carbonates at high temperature.

The experimental results of aging have demonstrated two different mechanisms that might take place simultaneously during storage, whose reaction kinetics depends on the storage conditions:

- The high relative humidity conditions in the open atmosphere (presence of CO_2) promote the formation of trona.

$$3\ Na_2CO_3.H_2O + 2\ H_2O + CO_2 \rightarrow 2\ [Na_2CO_3.NaHCO_3.2H_2O]$$

- The high relative humidity condition in closed atmosphere (limited quantity of CO_2) is favorable to the decomposition of $LiNaCO_3$.

$$2\ LiNaCO_3 + H_2O \rightarrow Li_2CO_3 + Na_2CO_3.H_2O$$

Powder B happened to encounter both reactions, while the decomposition reaction of $LiNaCO_3$ in powder C is more rate-controlling. This might be due to the difference in storage conditions applied to these powders. If complete transformation of the powder might occur, it would yield a powder with 58w% of trona which corresponds to 11.6w% of hydration water. In order to prevent these reactions to occur, the regular control of storage conditions is necessary. Therefore, it is recommended to conserve the powders in sealed containers (impermeable of CO_2) with humidity conditions of not exceeding 50%RH.

Considering that Marcalina has relatively fine particles, hence a fine milling method is a definite prerequisite during the manufacturing process. Indeed, milling is not only capable of creating particles of a certain size, but may also be described as a mechanochemical treatment whose reactions induced by the mechanical energy known as mechanochemical reactions. Thanks to these mechanisms, reactions generally observed at high temperature can occur even at low temperature in a ball mill with no external heating needed. $LiNaCO_3$ appears to be produced through this type of reaction as what was demonstrated in the grinding experiments:

$$Li_2CO_3 + Na_2CO_3.H_2O \rightarrow 2\ LiNaCO_3 + H_2O$$

The decrease of water content down to the range of specification (3.9-5.4 wt%) might have been obtained by such a process, as if the composition was taken from the patent, the hydrated sodium carbonate would bring 7wt% of water. Furthermore, it is also possible that the manufacturer might not suspect that the release of water content may also cause the formation of $LiNaCO_3$, since only XRD analysis is capable of detecting the presence of this compound. Yet this analytical method was unlikely used back to the years of production for controlling the quality of products.

The Chris(X)ti-Na experimental facilities were developed in order to understand the extinction mechanism, notably related to the role of physicochemical properties of these powders as well as the effect of both trona and $LiNaCO_3$ on the extinction. The three Marcalina powders previously analyzed along with several synthetic powders with different compositions were tested in 10g of small sodium pool fire. Two methods of powder spreading (continuous and direct) were employed in these tests. The temperature profile, video recording of the experiment, mass of the powder used, time of extinction, and sampling of extinction residue are among certain parameters observed during each tests. The results highlight several points:

- The extinction time is considered to be much longer for powder with no and small amount of hydration water content (< 5.6%w).
- Hydration water appears to have an important role in facilitating extinction. This happens due to the presence of liquid sodium hydroxide (detected by XRD analysis of extinction residue) capable of forming an insulated layer that ensure the separation of sodium and oxygen. More hydration water contributes to shorten the extinction time. However, a rapid increase of temperature and flash flame are observed in certain tests prior to rapid

extinction. This temperature rise might be corresponds to the exothermic reaction and production of hydrogen.

- Trona is proven to not alter the extinction capacity of the powder. Powders with trona and $Na_2CO_3.H_2O$ even have similar performance during extinction, except for the fact that the flames are observed to be more frequent for the one with trona. Indeed, trona gives more hydration water content that might eventually increase the production of both NaOH and H_2 during extinction. However, with the same amount of sodium hydroxide produced by both compounds, trona releases more quantity of H_2 and more exothermic in terms of energy than that of sodium carbonate monohydrates.
- $LiNaCO_3$ as a main component seems to not give a significant contribution to the extinction as it may lead to several re-ignitions due to the long melting and cracking observed during cooling.

Two mechanisms of extinction are then proposed based on the results of these tests:

1. The formation of liquid sodium hydroxide via the direct reaction of trona and/or $Na_2CO_3.H_2O$ with $Na_{(g)}$ and/or $Na_2O_{(s)}$ or indirectly via the decomposition reaction of trona and $Na_2CO_3.H_2O$ prior to reaction of $H_2O_{(g)}$ released with Na and Na_2O.

Depending on direct or indirect pathways, more or less formation of NaOH might be produced. However, it is hard to distinguish which of these reactions that actually happens as both might happen rapidly during extinction. Besides, both reactions induces the formation of H_2 that might be the cause of the flash flame (need to be confirmed by spectrometer measurement)observed prior to extinction. The formation of liquid sodium hydroxide as a protective layer contributes to the rapid decrease of temperature and fire extinction. This layer is essential to cover the sodium surface from prolonged contact with oxygen. Overall, 0.5-0.9 g of water is necessary to extinguish 19.6 cm^2 of sodium pool fire (equal to the average of 0.035 g/cm^2), which corresponds to 1-2 g of NaOH. Based on these tests, the minimum water content required for extinction is 5.6w%. Meanwhile, powders whose hydration water content is close to 13w% seem more likely to produce a high vigorous "H_2" flame prior to the extinction.

2. The melting of eutectic carbonates.

The melting of eutectic carbonates happened at 498°C is followed by the formation of $LiNaCO_3$ during cooling. However, this process is considered to be slower than the previous step. The eutectic melting is observed to be slow to occur, eutectic carbonates layer tends to crack easily at cooling and has higher viscosity than sodium hydroxide. These facts prevent them to provide easily a sealed protector layer on the sodium surface. Therefore, its role might be less significant especially for the sodium fire started at low temperature.

The particle size apparently doesn't demonstrate a significant contribution in the extinguishing performance except for affecting the spreading performance. The bigger particle sizes actually show faster extinction time as they cover the sodium surface more homogeneously. Powders of small particle size may perform well as long as they contain sufficient hydration water, which is essential to achieve rapid complete extinction. This is also the case for powders of bigger particle size, which proves that the chemical properties are actually the limiting factors in sodium fire extinction.

PERSPECTIVES

The results of this study demonstrate the beneficial effect of hydration water which plays a major role on extinction, much more than the eutectic carbonate mixture. However, it is questionable if the exothermic reactions and the hydrogen formation induced by the reaction of water with sodium or sodium oxide might be an issue, in particular if the hydrogen flame might harm the person during intervention. Therefore it is first necessary to confirm the presence of such flame using appropriate technical measurement. Technologies to detect hydrogen fires include flame detectors that sense the non-visible spectrum of electromagnetic radiations, such as ultraviolet (UV) and infra-red (IR) radiations. Furthermore, the effect of this flame should be studied at a much bigger scale. This is important in order to know whether the phenomenon observed in the experiments at small scale conducted in Chris(X)ti-Na experimental facility is reproducible at other scales. A greater quantity of sodium should be used and thus, more important amounts of powder would be employed. The results of these tests will be valuable to evaluate the powder specification related to the hydration water content and what will be the tolerance limit of trona for effective employment. This information will be used to determine if powders currently in stock can be reused or if a new powder with different threshold needs to be developed. Besides, study regarding the employment of these powders on sodium pool fire at low temperatures (around 200°C) and much higher temperatures (above 500°C) might be interesting to explore as it will confirm the beneficial role of $LiNaCO_3$ for the extinction at higher temperatures.

The role of physical properties appears to be significant during powder spreading. Different amount of hydration water content might affect the particle sizes. Moreover, the phenomenon observed during the test related to caking, agglomeration, and homogenization might affect the spreading performance. Thus, the effects of chemical compositions on the spreading performance need to be studied. Powders with different chemical compositions can be tested in different spreading devices. The effects related to the composition evolution due to different powder handling such as transport, fluidization are needed in order to ensure the quality of powder used and whether or not new process or method of spreading need to be developed in the future.

The fabrication of new powders might be considered. The grinding process plays an important role in producing powders with good homogenization. Depends on the results of study obtained from extinction test in bigger scale and spreading test with different devices, new range of particle sizes can be proposed. The extinction test results on large scale fires may give the information of the necessity to have $LiNaCO_3$ in the powder. From the results of this thesis, this compound was found to be beneficial in some tests when hydration water content is low (5.6%w). If it is proved that it brings substantial effect on extinguishing efficiency on large scale, its formation needs to be studied by using different type of grinders and procedures (related to duration of grinding, atmosphere) to control its formation. The spreading test may give the indication about the range of particle sizes that might be used to improve the spreading performance. This value also contributes to determine an adequate grinding method during the manufacturing process. It should have to be kept in mind that producing $LiNaCO_3$ by a mechanochemical reaction might reduce the water content in the powder, so composition can be adjusted in order to provide the final target water content in the powder.

In terms of storage condition, it should be of great interest to keep the storage on sealed container and control regularly the humidity conditions of <50%RH. Regarding powder packaging, it is recommended to choose a package (ex: plastic) that impermeable of CO_2. These conditions might limit not only the chemical transformation into trona but also the decomposition of $LiNaCO_3$ (if it is proved to be an interesting compound for extinction on large scale experiment).

In order to anticipate the water uptake that might happen during powder handling and uncontrolled storage, it is suggested to have the initial powder compositions with hydration water content between 5.6-7w% from the mixture of sodium carbonate monohydrate, lithium carbonate, and graphite. 5.6w% is the minimum limit as the powder with less water contents are considered to have bad performance during extinction, while 7w% is the original composition of Marcalina as recommended in the patent. This maximum allows at least 5w% of gap to anticipate from the maximum content of 13w% that is not recommended in terms of hydrogen flame that might be produced. However, the determination of this range is based on the results obtained from this thesis that should be confront in terms of the effect in large scale fires and transport handling phenomena (such as caking, agglomeration,…) during powder handling.

Finally, a simulation approach might be developed based on the preliminary data collected and previously discussed. The thermal and material energy exchange during extinction is considered to be interesting to be analyzed in order to have more comprehension in regards to the mechanism of extinction proposed. Several possibilities of reactions that might happen during extinction can be analyzed so as to estimate how much sodium hydroxide and hydrogen that might be produced during extinction. As what have been previously discussed, depend on the different pathways (direct or indirect) the quantity of both compounds might be varied. It would also be interested to be able to predict the amount of sodium hydroxide needed to cover the sodium surface with different pool surface area. The results might be useful as a comparison of experiment result to help determine the best powder composition for different scenario of pool fires in case of accident.

Glossary

AAS	Atomic Absorption Spectroscopy
ASTRID	Advanced Sodium Technological Reactor for Industrial Demonstration
CEA	Commissariat à l'Energie Atomique et aux énergies alternatives
DSC	Differential Scanning Calorimetry
DVS	Dynamic Vapor Sorption
GIF	Generation IV International Forum
SEM	Scanning Electron Microscopy
SFR	Sodium cooled Fast Reactors
TGA	Thermo-Gravimetric Analysis
XRD	X-Ray Diffraction
µ-GC	Micro Gas Chromatography

Nomenclature

Latin alphabet	***Definition***	***Unity***
$\dot{q}_c$	Heat flux released	J/(s.m²)
S	Surface of the sample	m²
C	Overall heat capacity of the sample	J/K
h_c	Heat transfer coefficient by convection	J/(s.m².K)
T_s	Surface temperature	K
A	Pre-exponential factor of the reaction rate	$(g/cm^3)^{1-m-n}.sec^{-1}$
E_a	The activation energy	J/mole
R	Universal gas constant	J/(mole.K)
a	Mass of oxygen consumed per unit area and time (t)	kg/(m².s)
w	The rate of fuel consumption in the gas phase flame	g/cm³.s
c_F	The local fuel concentration	g/cm³
M	Molecular weight	mol/g

Greek alphabet	***Definition***	***Unity***
ρ	Density	kg/m³
ΔH_r	Enthalpie of the reactio	kJ/mol
λ	Thermal conductivity	$W.(m.K)^{-1}$
μ	Viscosity	Pa.s
c_p	Specific heat	$J.(kg.K)^{-1}$

Bibliography

A. Linan, 1973. The asymptotic structure of counterflow diffusion flames for large activation energies. Acta Astronaut. 1, 1007–1039.

A. N. Khlapova and V. M. Elenevekaja, 1968. The lithium carbonate - sodium carbonate systeme. Russ. J. Inorg. Chem. 610 – 613.

An, D., Sunderland, P.B., Lathrop, D.P., 2013. Suppression of sodium fires with liquid nitrogen. Fire Saf. J. 58, 204–207. doi:10.1016/j.firesaf.2013.02.001

Avvakumov, E., Senna, M., Kosova, N., n.d. Soft mechanochemical synthesis: A basics for new chemical technologies. Kluwer Academic Publishers.

Ball, M.C., Snelling, C.M., Strachan, A.N., Strachan, R.M., 1992. Thermal decomposition of solid sodium sesquicarbonate, Na2CO3· NaHCO3· 2H2O. J Chem Soc Faraday Trans 88, 631–636.

Baláž, P., 2008. High-Energy Milling, in: Mechanochemistry in Nanoscience and Minerals Engineering. Springer Berlin Heidelberg, pp. 103–132.

Bailly J., 1990a. Extinction des feux de sodium: Choix initial du type de poudre utilisée sur la base d'essais de laboratoire.

Bailly J., 1990b. Extinction des feux de sodium: Mise en œuvre de la poudre extinctrice Marcalina.

Baláž, P., 2008. High-Energy Milling, in: Mechanochemistry in Nanoscience and Minerals Engineering. Springer Berlin Heidelberg, pp. 103–132.

Birchall, J.D., 1970. On the mechanism of flame inhibition by alkali metal salts. Combust. Flame 14, 85 – 95. doi:http://dx.doi.org/10.1016/S0010-2180(70)80013-X

Bulmer, G.., Fire E, A.M.., 1972. Fire safety considerations related to the usage of sodium. Presented at the I.Chem.E Symposium Series, London.

Burgio, N., Iasonna, A., Magini, M., Martelli, S., Padella, F., 1991. Mechanical alloying of the Fe–Zr system. Correlation between input energy and end products. Il Nuovo Cimento D 13, 459–476. doi:10.1007/BF02452130

C. Casselman., 1979. Ignition of a liquid sodium pool., Report International Atomic Energy Agency, International Working Group on Fast Reactors, Vienna (Austria);

C. Casselman., 1978. Etude des processus conduisant à l'inflammation et à la combustion d'une nappe de sodium liquide. Université de Provence.

CACI, 1982. Fiche technique de controle de la fabrication, condition de stockage, controle de reception de la poudre Marcalina.

Cairns, E.J., MacDonald, D.I., 1962. Sensitive Thermal Analysis Establishing Formation of the Incongruently Melting Compound LiNaCO3. Nature 194, 441–442. doi:10.1038/194441a0

Carr, R., 1965. Evaluating flow properties of solids 72, 163–168.

Charles R. Schmitt, 1974. Extinguishant for metal fires. US Patent 3840075.

Coreño A., J., Coreño A., O., Cruz R., J.J., Rodríguez C., C., 2005. Mechanochemical synthesis of nanocrystalline carbonate-substituted hydroxyapatite. Opt. Mater., Proceedings of the First Topical Meeting on Nanostructured Materials and Nanotechnology CIO 2004 First Topical Meeting on Nanostructured Materials and Nanotechnology CIO 2004 27, 1281–1285. doi:10.1016/j.optmat.2004.11.025

Doyle, F.M., 1989. Crystallization and precipitation: Proceedings of the international symposium, Saskatoon, Saskatchewan, Canada, 5–7 October, 1987. Edited by G.L. Strathdee, M.O. Klein and L.A. Melis. Can. J. Chem. Eng. 67, 698–698. doi:10.1002/cjce.5450670428

D'yakov, V.A., Ebbers, C.A., Pchelkin, M.V., Pryalkin, V.I., 1996. Lithium sodium carbonate: A new nonlinear-optics crystal. J. Russ. Laser Res. 17, 489–494. doi:10.1007/BF02090628

Edgar CHahvekilian, Robert Peteri, et André Hennequart, 1972. Composition extinctrice pour feux de métaux. FR 2102424.

Ekmekyapar, A., Erşahan, H., Yapıcı, S., 1996. Nonisothermal Decomposition Kinetics of Trona. Ind. Eng. Chem. Res. 35, 258–262. doi:10.1021/ie950171q

Eitel, W., Skaliks, W., 1929. Über einige Doppelcarbonate der Alkalien und Erdalkalien. Z. Für Anorg. Allg. Chem. 183, 263–286. doi:10.1002/zaac.19291830119

F. A. Williams, 2000. Progress in knowledge of flamelet structures and extinction. Prog. Energy Combust. Sci. 26, 657–682.

F. A. Williams, 1974. A unified view of fire suppression. J. Fire Flammabl. 5, 54–63.

Formosa, J., Chimenos, J.M., Lacasta, A.M., Haurie, L., 2011. Thermal study of low-grade magnesium hydroxide used as fire retardant and in passive fire protection. Thermochim. Acta 515, 43–50. doi:10.1016/j.tca.2010.12.018

Fritsch, n.d. Operating instructions planetary mono mill PULVERISETTE 6 classic line.

Gärtner, R.S., Witkamp, G.-J., 2007. Mixed solvent reactive recrystallization of trona (sodium sesqui-carbonate) into soda (sodium carbonate anhydrate). Hydrometallurgy 88, 75–91. doi:10.1016/j.hydromet.2007.03.006

J. Desremeaux, M. Rodriguez, S. Trambaud., 2000. Compatibilité de la poudre extinctrice Marcalina avec le sodium, le potassium, et l'alliage NaK-56.

J.C. Malet, 1990. Les feux de sodium : Synthèse des résultats.

Janz, G.J., Lorenz, M.R., 1961. Solid-Liquid Phase Equilibria for Mixtures of Lithium, Sodium, and Potassium Carbonates. J. Chem. Amp Eng. Data 6, 321–323. doi:10.1021/je00103a001

JC Malet, 1980. Ignition and combustion of sodium – Fire consequences – Extinguishment and prevention.

JC. Malet., n.d. Les feux de sodium (transparents).

Jeong, Ji Young; Jeong, K. C.; Kim, B. H.; Kim, T. J.; Choi, J. H.;, n.d. Analysis of patents on extinguishing agent for sodium fires (No. KAERI/AR-624/2002).

Kuang, K., Huang, X., Liao, G., 2008. A comparison between superfine magnesium hydroxide powders and commercial dry powders on fire suppression effectiveness. Process Saf. Environ. Prot. 86, 182–188. doi:10.1016/j.psep.2007.11.002

L. Felician, N; Simon, n.d. Marcalina: Bilan bibliographique et caractérisation de produits disponibles (Document Technique DEN No. DEN/CAD/DTN/STPA/LIPC/2012-012).

La poudre Marcalina : Caracteristiques physiques, stockage et fluidisation, transport pneumatique, epandage (Rapport DSN/SRS/SESTR 80/44 No. 11), n.d.

Langlet, M., Benali, M., Pezron, I., Saleh, K., Guigon, P., Metlas-Komunjer, L., 2013. Caking of sodium chloride: Role of ambient relative humidity in dissolution and recrystallization process. Chem. Eng. Sci., 5th International Granulation Workshop 86, 78–86. doi:10.1016/j.ces.2012.05.014

LeRoy J. Leeper, St. Paul Park, and Gunther H., 1969. Fire extinguishing. US Patent 3475332.

Lobos, Z.J., 1965. Dry chemical fire extinguisher composition. US Patent 3,172,852.

M. Abdellaoui, E. Gaffet., 1994. Mechanical alloying in a planetary ball mill : kinematic description. Presented at the Journal de Physique IV Colloque, pp. pp.C3–291–C3–296.

Malet, J.C., 1972. Contribution à l'étude des processus d'inflammation et de combustion de métaux alcalins liquides en lit. Université d'Orléans.

Matthew C. Ball, Christine M. Snelling and Alec N. Stracha, 1985. Dehydration of sodium carbonate mnohydrate. J Chem Soc Faraday Trans 81, 1761–1766.

Matthew C. Ball, Rosemary A. Clarke and Alec N. Strachan, 1991. Investigation of the Formation of Wegscheiderite, Na2CO3.NaHCO3. J Chem Soc Faraday Trans 87, 3683–3686.

Markstein, G.., 1967. Heterogeneous reaction processes in metal combustion. Presented at the XIth Symposium (International) on Combustion, The Combustion Institute, Pittsburg, Pensylvenia, pp. 219–234.

Muller, M., 2013. Etude du processus d'initiation par laser de la combustion d'un alliage métallique sous atmosphère d'oxygène. École Nationale Supérieure De Mécanique et d'Aéronautique.

N. Kusumanindyah, L. Brissonneau, T. Gilardi, H. Berthiaux, and C. Gatumel, "Study of the physicochemical properties and the aging phenomena of an extinguishing powder for sodium fire," *Récents Prog. En Génie Procédés*, no. 107, 2015.

N. Kusumanindyah, L. Brissonneau, T. Gilardi, C. Gatumel, and H. Berthiaux, "Study of the aging impact on the extinction efficiency of an extinguishing powder for sodium fire," *Chem. Eng. Trans.*, vol. 48, 2016.

Porter, R.A., 1997. Fire extinguishing composition. US Patent 5,626,787.

Retsch, n.d. Retsch Mortar Grinder RM 200.

Reuillon, M., 1984. Etude thermodynamique et expérimentale des réactions intervenant dans la combustion du sodium. Université d'Orleans.

Reuillon M., 1976. Etude de la combustion du sodium et de l'extinction de ses feux par les substances pulvérisees: Role des additifs. L'Université d'Orleans, France.

Reuillon M. , Mellottee H. , Devillers B. , Alfille L.,Duco J. , Fruchard Y. , Malet J.C. , et Chappellier A., 1978. Procédé et poudre pour l'extinction des feux de métaux liquides. 75 36225.

Reuillon, M., Mellottee, H., Alfille, L., Duco, J., Fruchard, Y., Malet, J.C., Chappellier, A., Devillers, B., 1979. Powder for extinguishing fires of liquid substances or of a mixture of liquid substances. US Patent 4,149,976.

Richard, T., 1944. Extinguishing light metal fires. US Patent 2,346,627.

Riley, J.F., Stauffer, E.E., 1976. Extinguishing agent for combustible metal fires. US Patent No. 3985658.

Rodriguez, G., Desremaux, J., 1997. Physico-chimie du sodium.

Rojac, T., Šegedin, P., Kosec, M., 2012. Using Infrared Spectroscopy to Identify New Amorphous Phases - A Case Study of Carbonato Complex Formed by Mechanochemical Processing, Infrared Spectroscopy - Materials Science, Engineering and Technology, Prof. Theophanides Theophile (Ed.). ed.

Sarrut, J.P., 1979. Method of extinguishing metal fires. US Patent 4,177,152.

Société NEU, 1981. Etude du compprtement de la poudre extinctrice de feux de sodium (Marcalina) et de sa tenue dans le temps sous l'action de la fluidisation et de la pression dans un réservoir: Compte rendu d'essai 81 EC 35.M.

Spasic, A.M., Hsu, J.-P., 2005. Finely Dispersed Particles: Micro-, Nano-, and Atto-Engineering. CRC Press.

Takacs, L., McHenry, J.S., 2006. Temperature of the milling balls in shaker and planetary mills. J. Mater. Sci. 41, 5246–5249. doi:10.1007/s10853-006-0312-4

Teunou, E., Fitzpatrick, J.., Synnott, E.., 1999. Characterisation of food powder flowability. J. Food Eng. 39, 31–37.

Thierry Bonhomme, 2013. Maitrise risque sodium.

V. R. Lecoustre, P. G. Arias, S. Roy et al., 2013. Direct numerical simulations of diffusion flame extinction at different pressures. 8th US Natl. Combust. Meet.

William R. Warnock,, 1963. Fire extinguisher compositions for metal fires. US 790045.

William R. Warnock, Menominee, Mich, 1960. Extinguishing agent for combustible metals. US Patent 2937990.

Yamaguchi, H., 1989. Method for fire extinguishment of hardly extinguishable dangerous material. European Patent 0323350.

Appendixes

A.1 Kinetic energy during milling

The kinetic energy transferred at the collision event and the shock f requency in a planetary ball mill apparatus are calculated in [1]. Apparently, the end product depends not only on the kinetic energy but also the shock power. The kinetic energy, E_k, is given as:

$$E_k = 1/2.m.\left\|\overrightarrow{V_a}\right\|^2 \quad \text{(a-1)}$$

where m = the ball mass and $\overrightarrow{V_a}$ = the absolute velocity. The shock frequency, f, is the number of collision per second. It is expressed by:

$$f = \frac{1}{T} = \frac{1}{T_1+T_2} \quad \text{(a-2)}$$

where T = the cycle period, T_1 = the period of time needed by the ball to go from the detachment point up to the collision point and T_2= the period of time needed between the first collision event and the second detachment one.

Hence, the power released by the ball to the powders is the product of the frequency with the integral of the kinetic energy along one cycle period that is given by the following:

$$P = f.E_k \quad \text{(a-3)}$$

The shock power then needed to be multiplied by the ball milling duration (BMD) in order to obtain the total kinetic energy.

The calculations of E_k, f, and P for the G7 planetary ball mill have been conducted. The results showed that the kinetic energy and the shock power increase as a function of the disc and vial rotation speeds. The shock frequency drastically decreases and then increases almost linearly as the disc rotation speed increases.

Another attempt to quantitatively assess the mechanical energy transfer and its dissipation has been conducted by Magini et al [2] in the form of milling intensity (I). It is related to the frequency of collision and the average energy transferred to the powder at each impact. Generally in the case of multiple ball milling, f and E depend on their number and mass so that the relevant milling parameters should be adjusted to the respective mill considered. For the planetary ball mill, the intensity, I (Wh/g), may be interpreted as follows [2]:

$$I = \varphi_b.\Delta E_b.N_b.\frac{K(W_p-W_v)}{2\pi*PW} \quad \text{(a-4)}$$

where ΔE_b is the energy release; N_b is the number of ball used; K is the time necessary to dissipate the energy; W_p is the absolute angular velocity of the plate; W_v is the absolute angular velocity of the vial, and PW is the total powder weight.

Meanwhile φ_b is the assumption taken for which until one third of the inner surface wall is not covered, the reciprocal hindering of the ball is neglected. It is expressed by this equation:

$\varphi_b = (1 - n_v^{\varepsilon})$, where ε is a parameter depending on the ball diameter that can be evaluated by condition:

$$0.95 = [1 - \left(\frac{N_{b,s}}{N_{b,v}}\right)^{\varepsilon}] \quad \text{(a-5)}$$

$N_{b,s}$ is the number of balls needed to cover one third of the inner surface wall and is given by:

$$N_{b,s} = \pi(D_v - d_b)H_v/3d_b^2 \quad \text{(a-6)}$$

$N_{b,v}$ is the number of balls that can be contained in the vial and is given by:

$$N_{b,v} = \pi D_v^2 H_v/4d_b^3 \quad \text{(a-7)}$$

where D_v and H_v being the diameter and the height of the vial respectively and d_b is the ball diameter.

The milling intensity depends on the number of balls and angular velocity of supporting disc for two different vials charged and balls diameter. For given angular velocity, intensity increases with ball number up to some maximum values, after which intensity decreases due to hindering effect. Therefore it seems that the milling intensity is the characteristic milling parameter that defines final (steady-state) phase induced by milling [3].

A.2 XRD results of aging (8 months)

- 75%RH and open conditions (CO_2)
  - Powder A

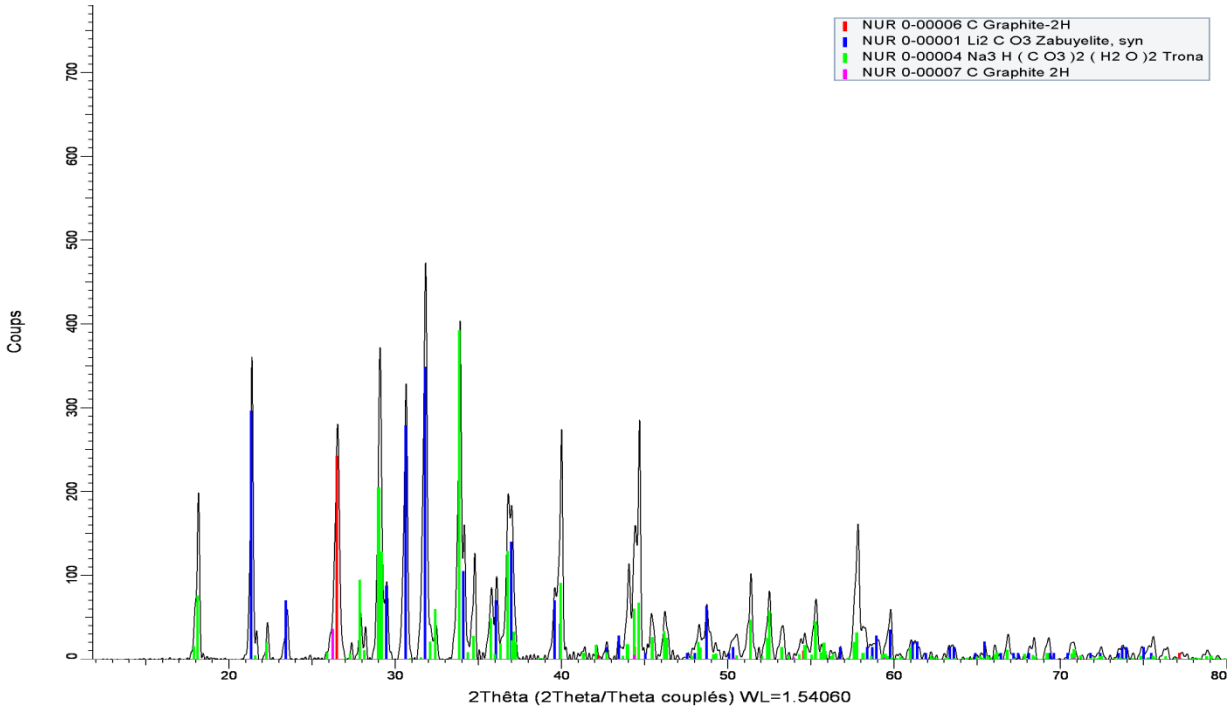

Figure A- 1. XRD diagram of powder A stored in 75%RH and open conditions after 8 months

- $Na_2CO_3.H_2O$

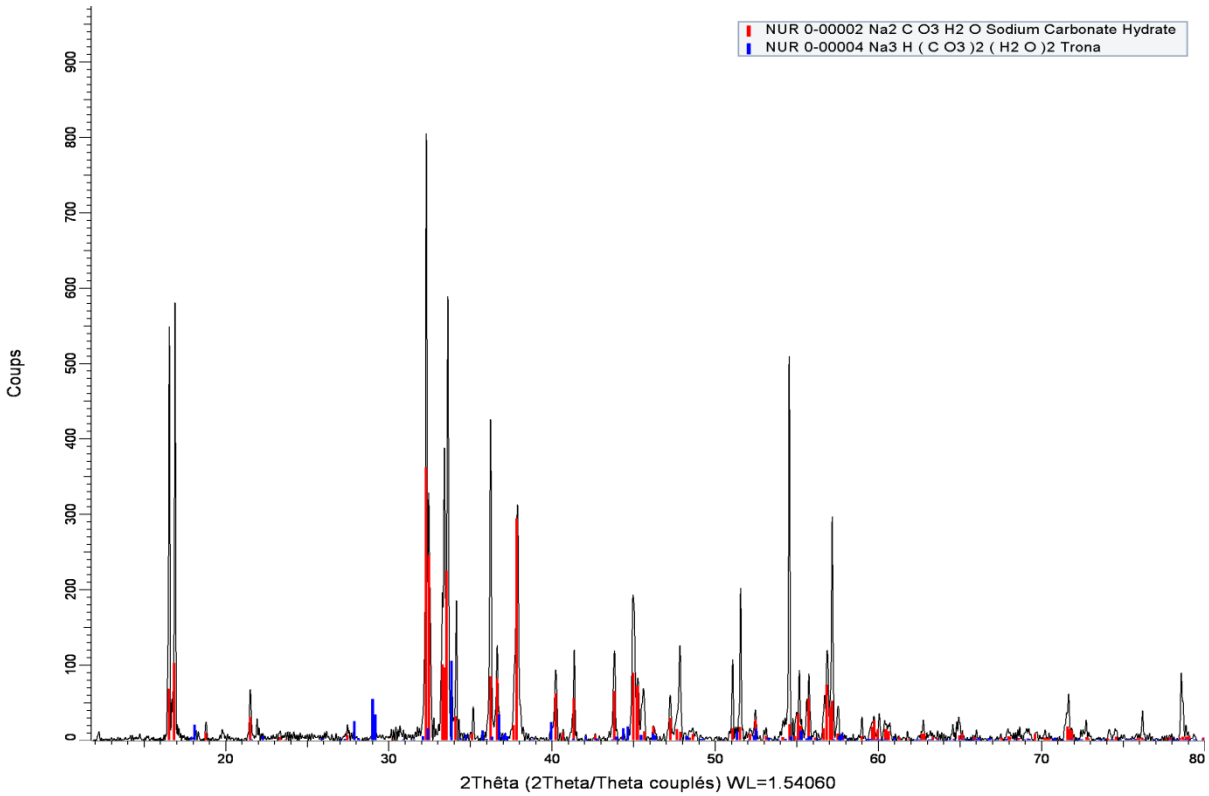

Figure A- 2. XRD diagram of powder $Na_2CO_3.H_2O$ stored in 75%RH and open conditions after 8 months

- $LiNaCO_3$

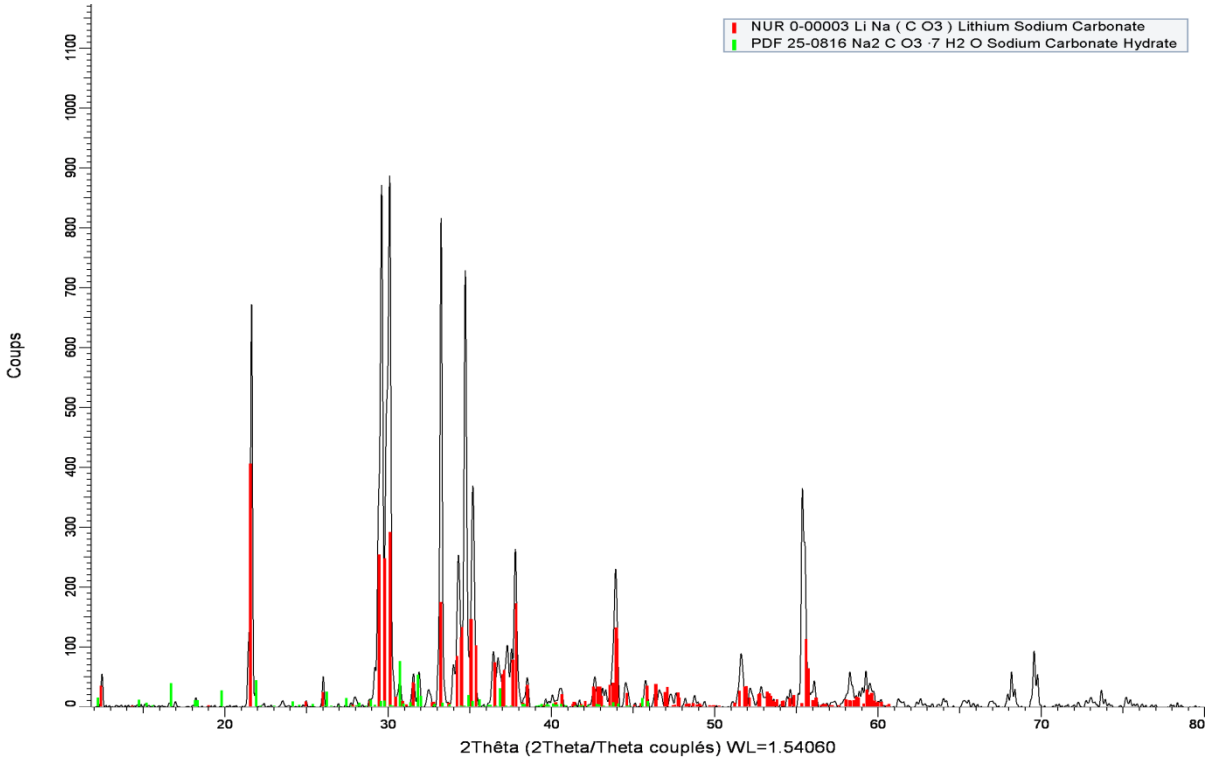

Figure A- 3. XRD diagram of powder $LiNaCO_3$ stored in 75%RH and open conditions after 8 months

- 75%RH and sealed conditions
  - Powder A

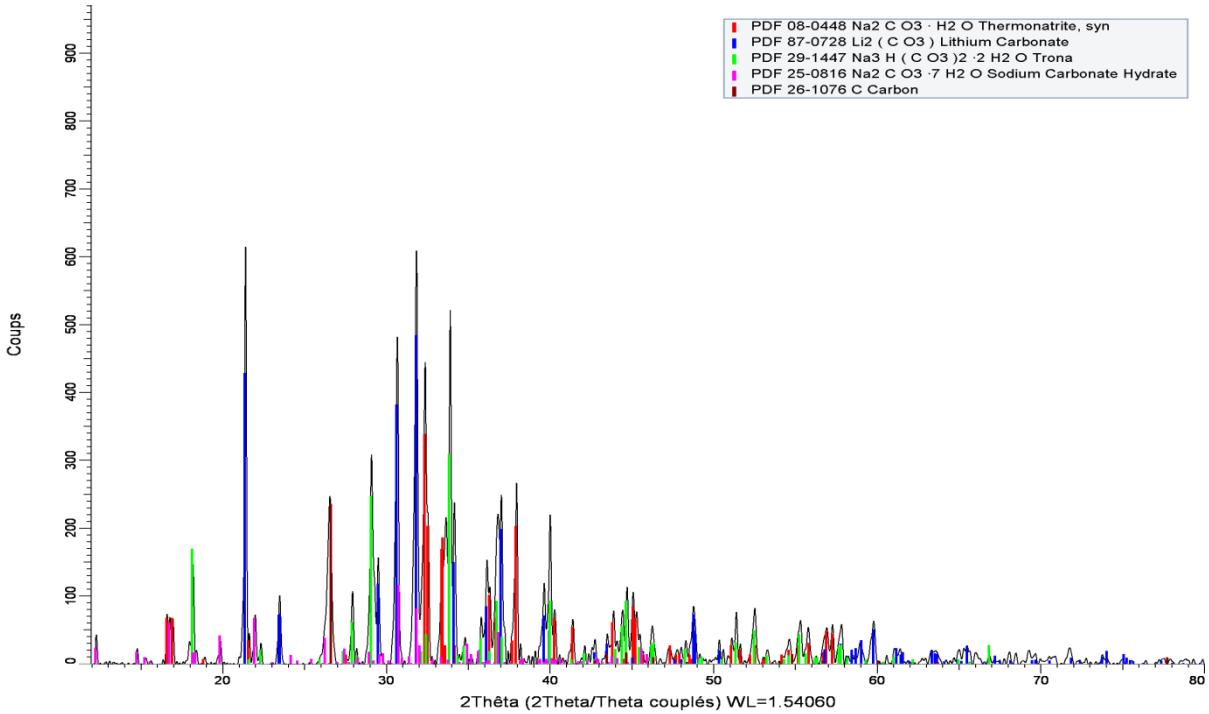

Figure A- 4. XRD diagram of powder A stored in 75%RH and sealed conditions after 8 months

- $Na_2CO_3.H_2O$

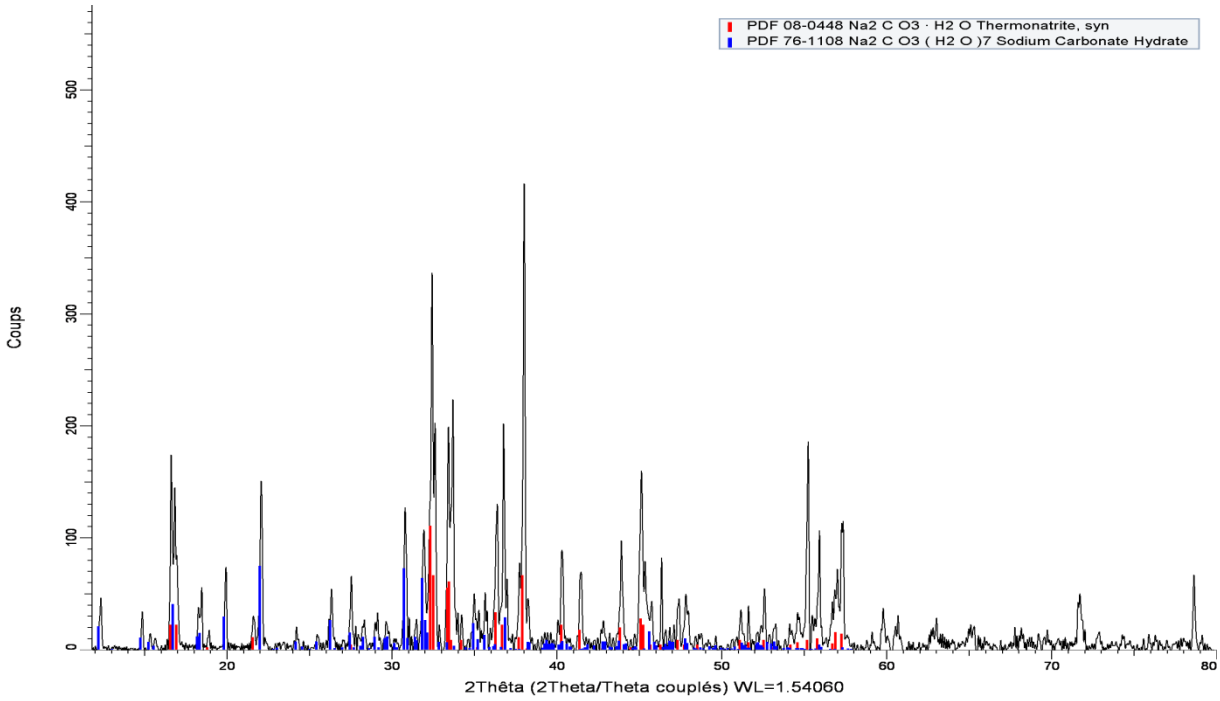

Figure A- 5. XRD diagram of powder $Na_2CO_3.H_2O$ stored in 75%RH and sealed conditions after 8 months

- $LiNaCO_3$

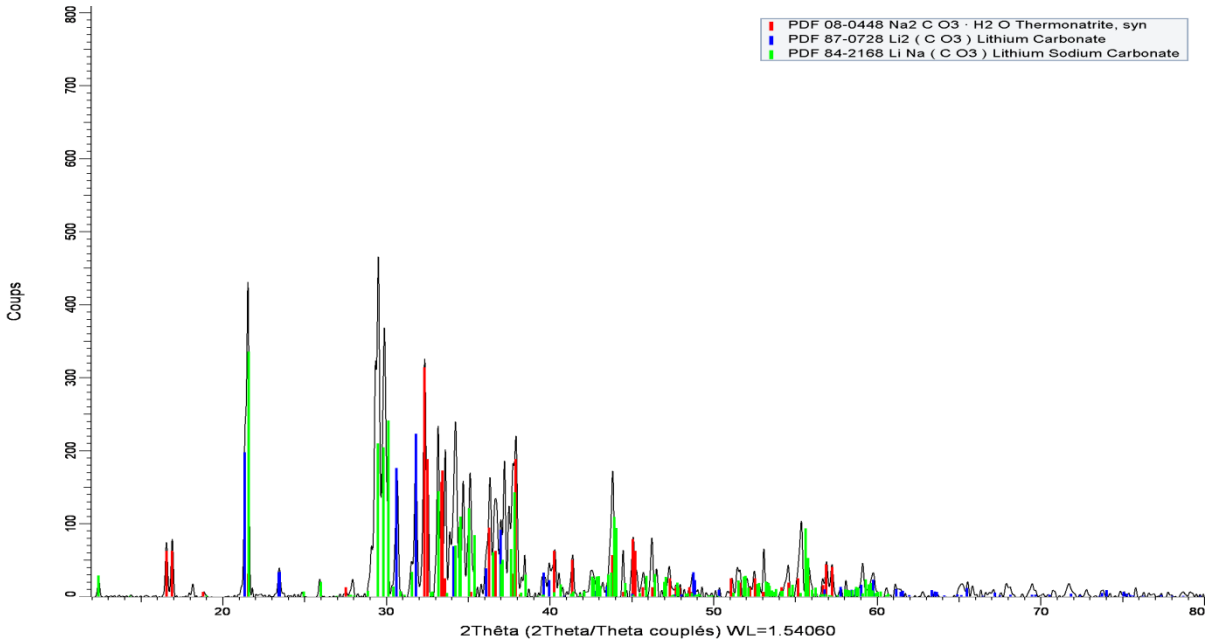

Figure A- 6. XRD diagram of powder $LiNaCO_3$ stored in 75%RH and sealed conditions after 8 months

A.3 Temperature profile and video observation during combustion

- Continuous spreading
  - Powder III

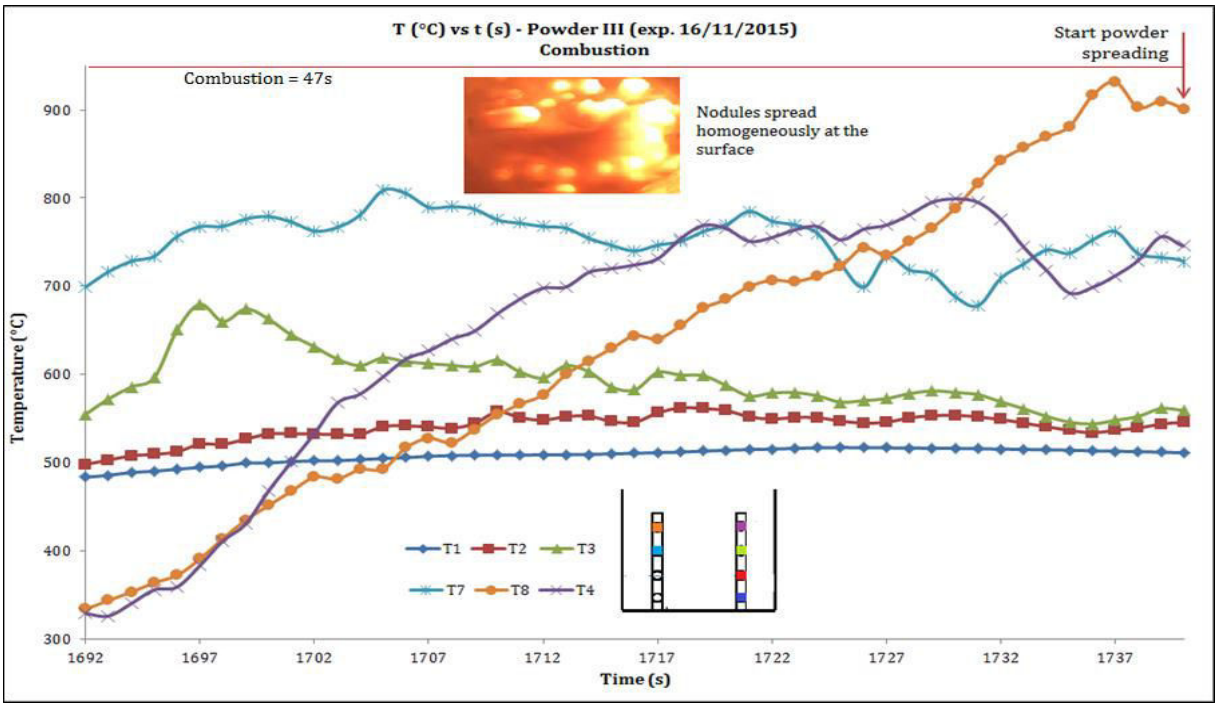

Figure A- 7. The temperature and video observations of the Chris(X)ti-Na experiment using powder III with continuous spreading during combustion

- Powder IV

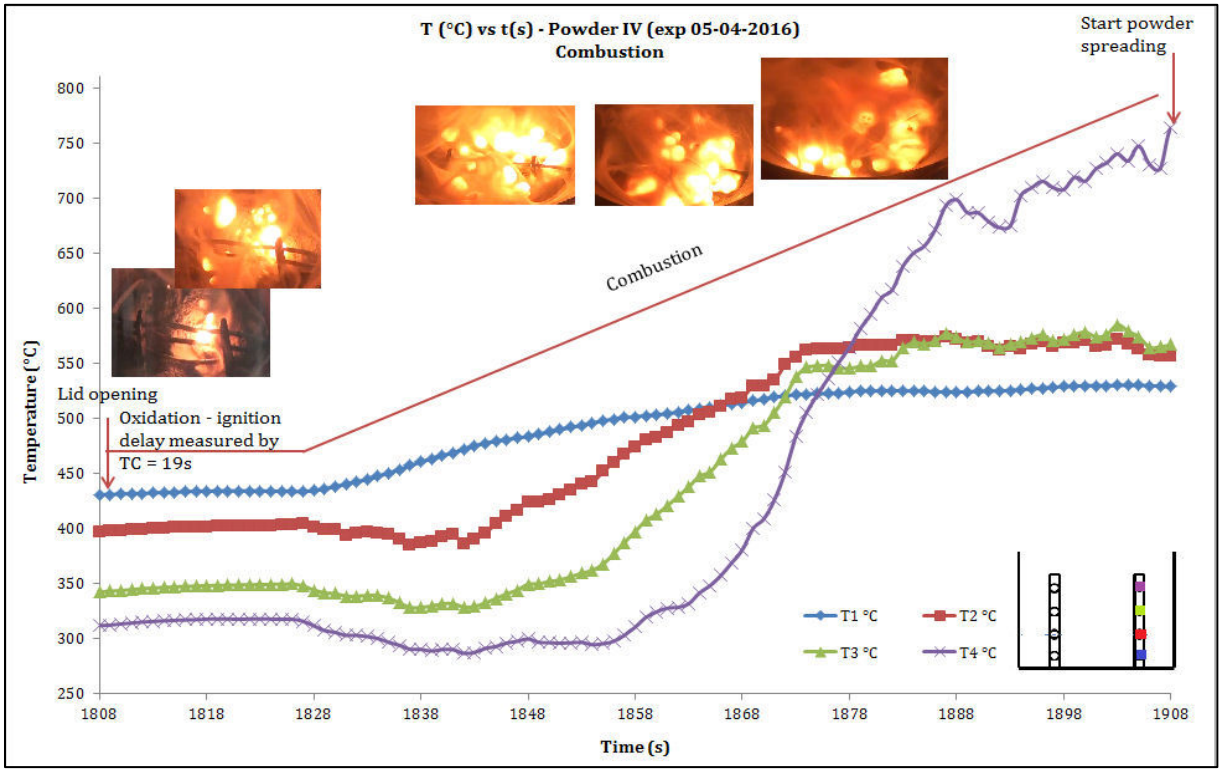

Figure A- 8. The temperature and video observations of the Chris(X)ti-Na experiment using powder IV with continuous spreading during combustion

- Powder V

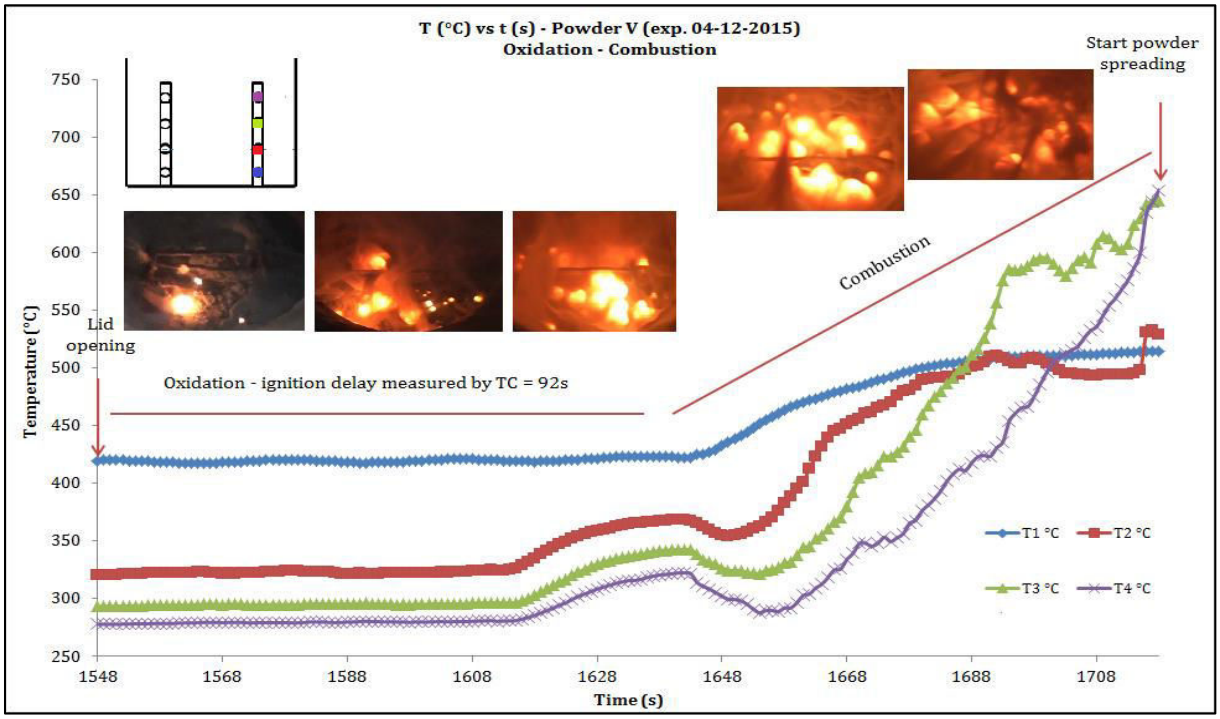

Figure A- 9. The temperature and video observations of the Chris(X)ti-Na experiment using powder V with continuous spreading during combustion

- Powder VI

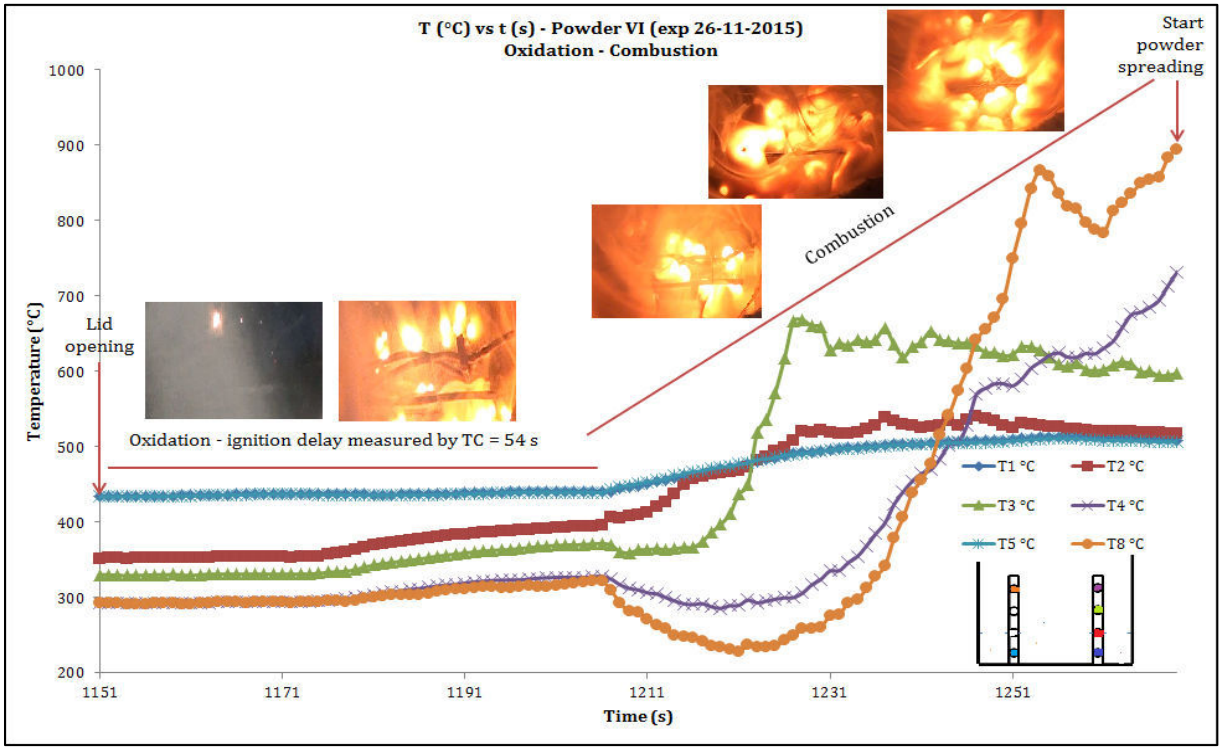

Figure A- 10. The temperature and video observations of the Chris(X)ti-Na experiment using powder VI with continuous spreading during combustion

- Powder VII

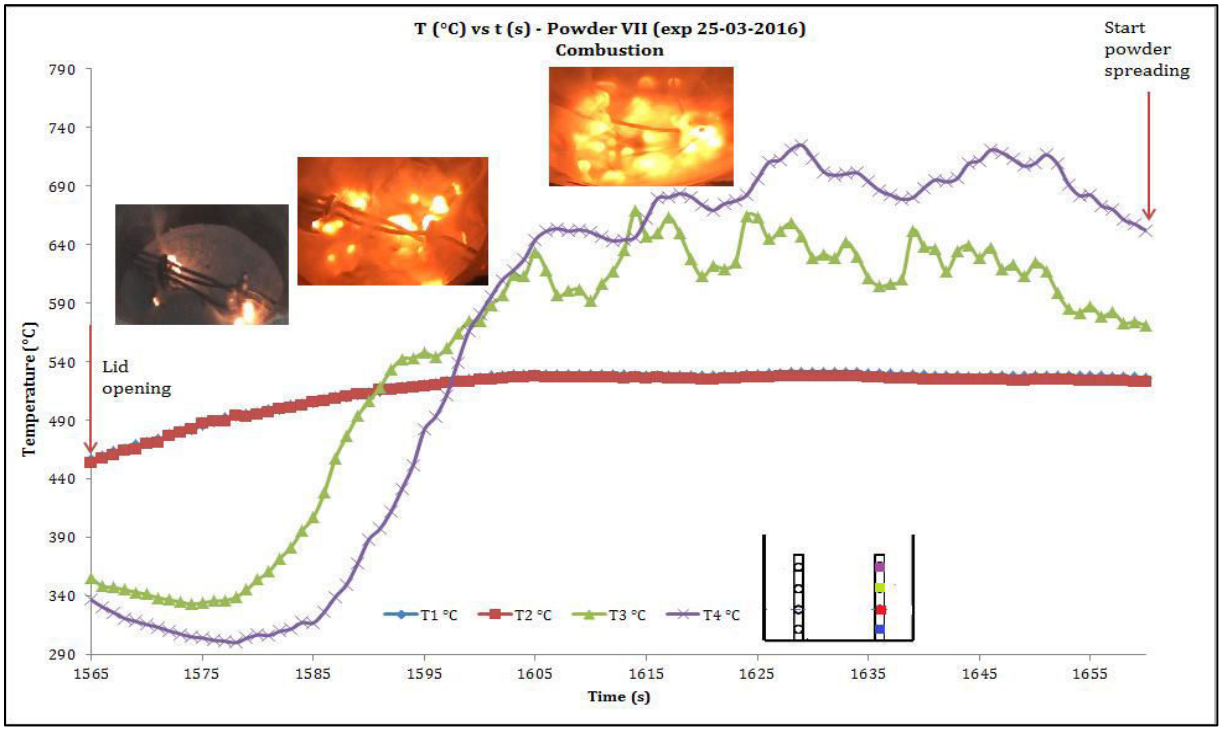

Figure A- 11. The temperature and video observations of the Chris(X)ti-Na experiment using powder VII with continuous spreading during combustion

- Powder VIII

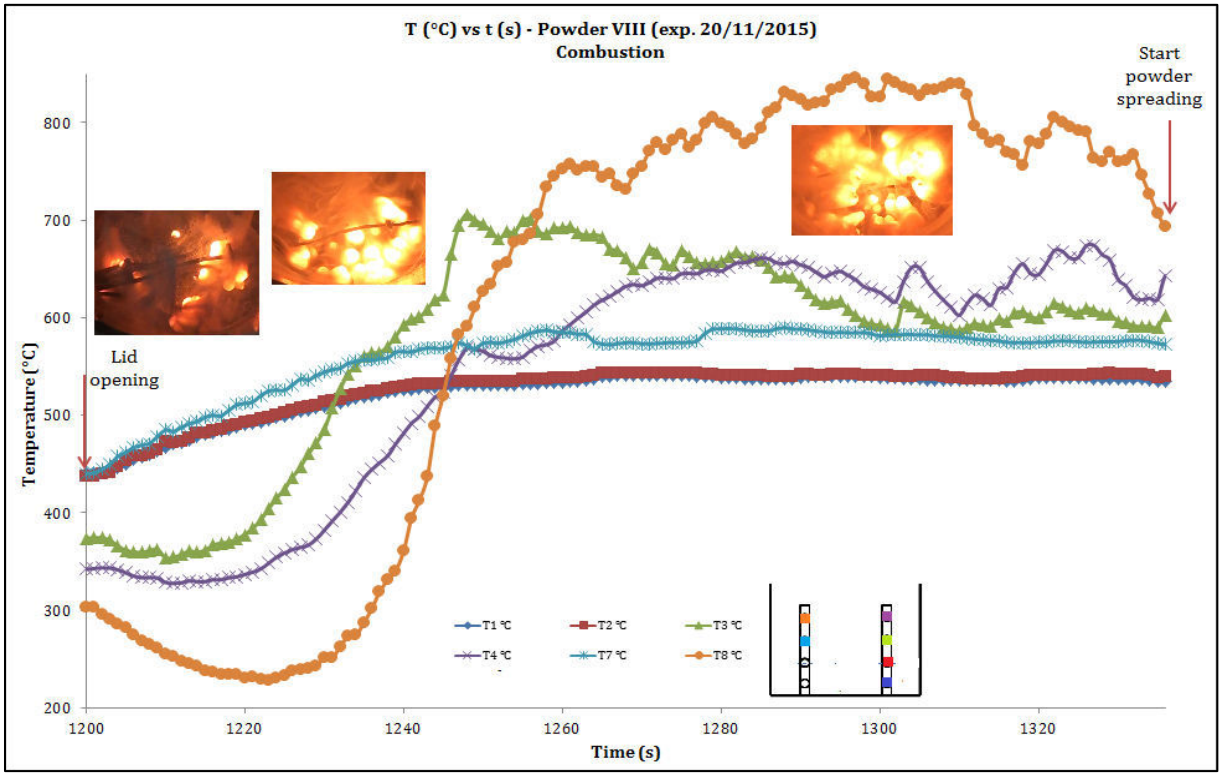

Figure A- 12. The temperature and video observations of the Chris(X)ti-Na experiment using powder VIII with continuous spreading during combustion

- Powder IX

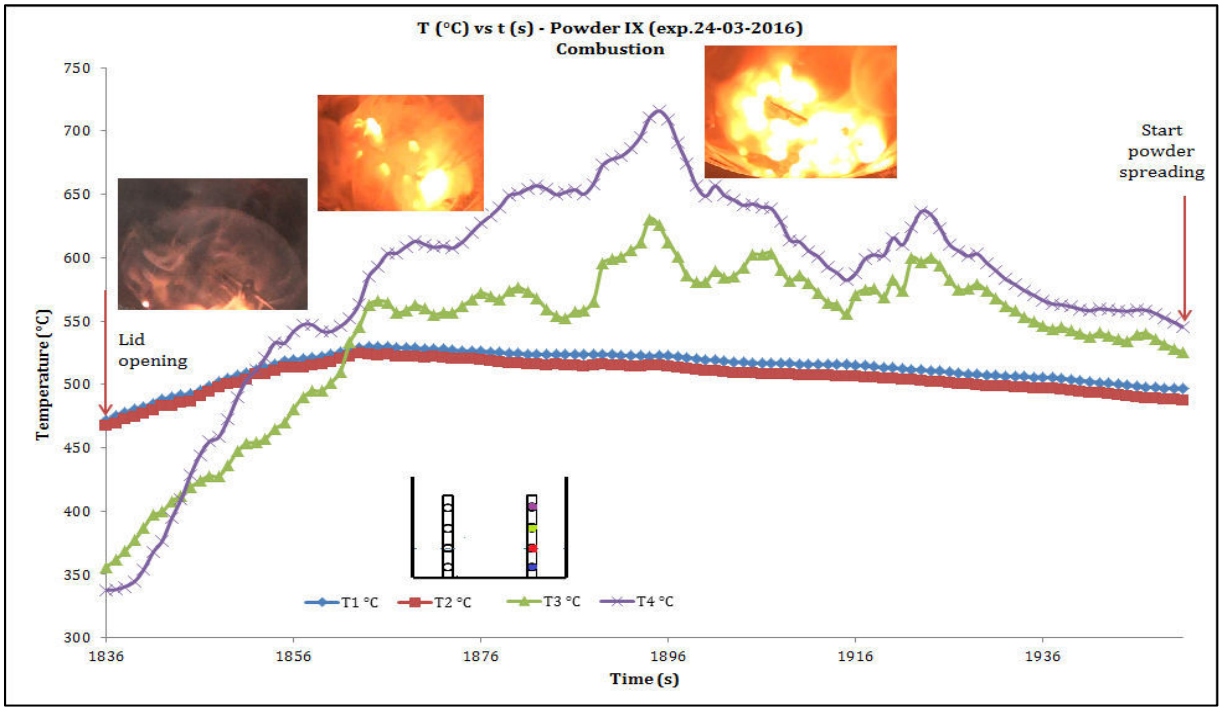

Figure A- 13. The temperature and video observations of the Chris(X)ti-Na experiment using powder IX with continuous spreading during combustion

- Direct spreading

  - Powder II

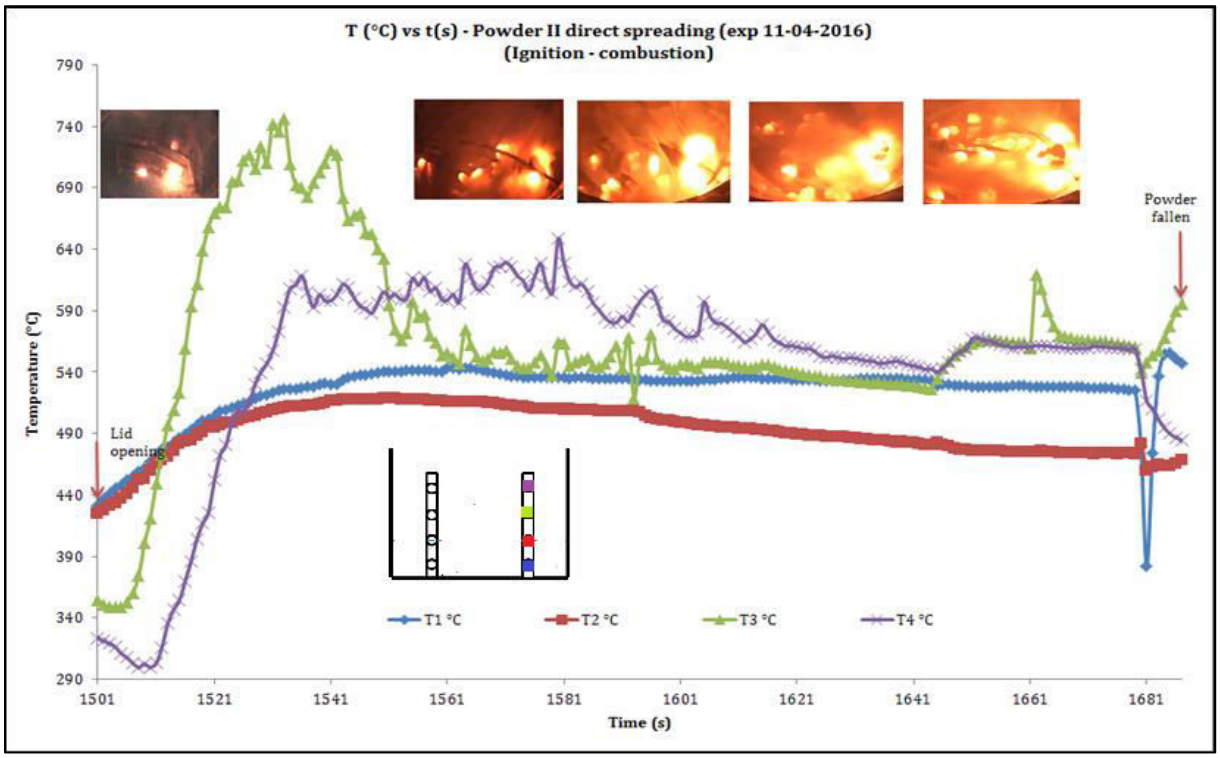

Figure A- 14. The temperature and video observations of the Chris(X)ti-Na experiment using powder II with direct spreading during combustion

  - Powder IV

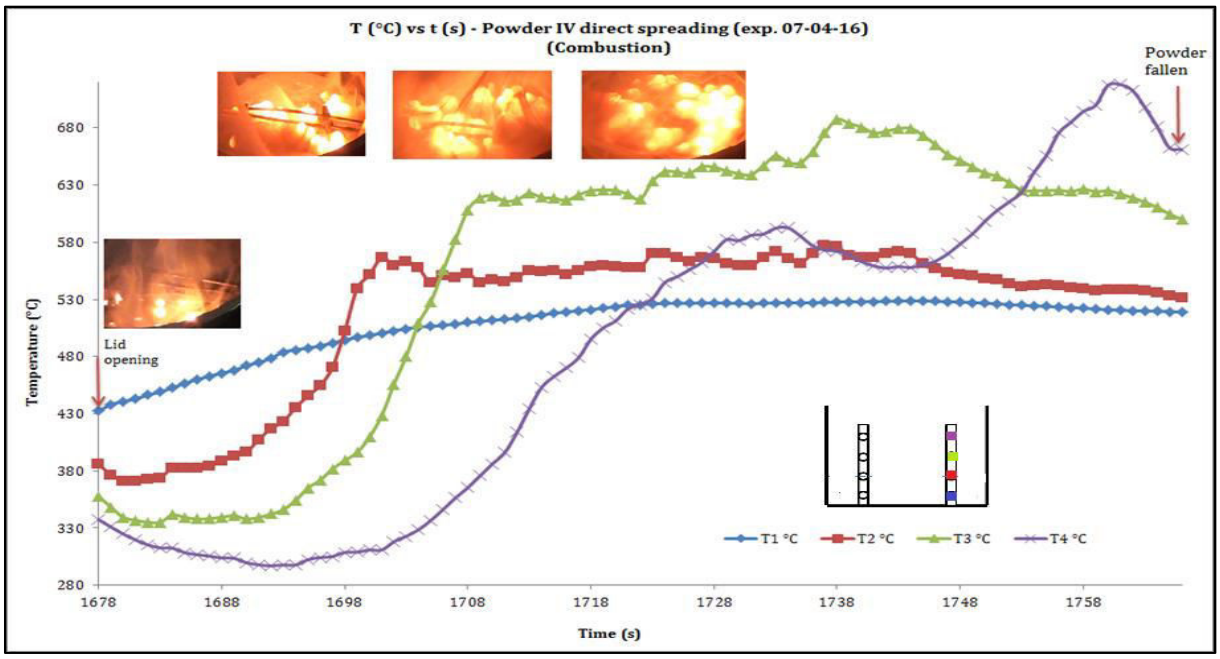

Figure A- 15. The temperature and video observations of the Chris(X)ti-Na experiment using powder IV with direct spreading during combustion.

- Powder VII

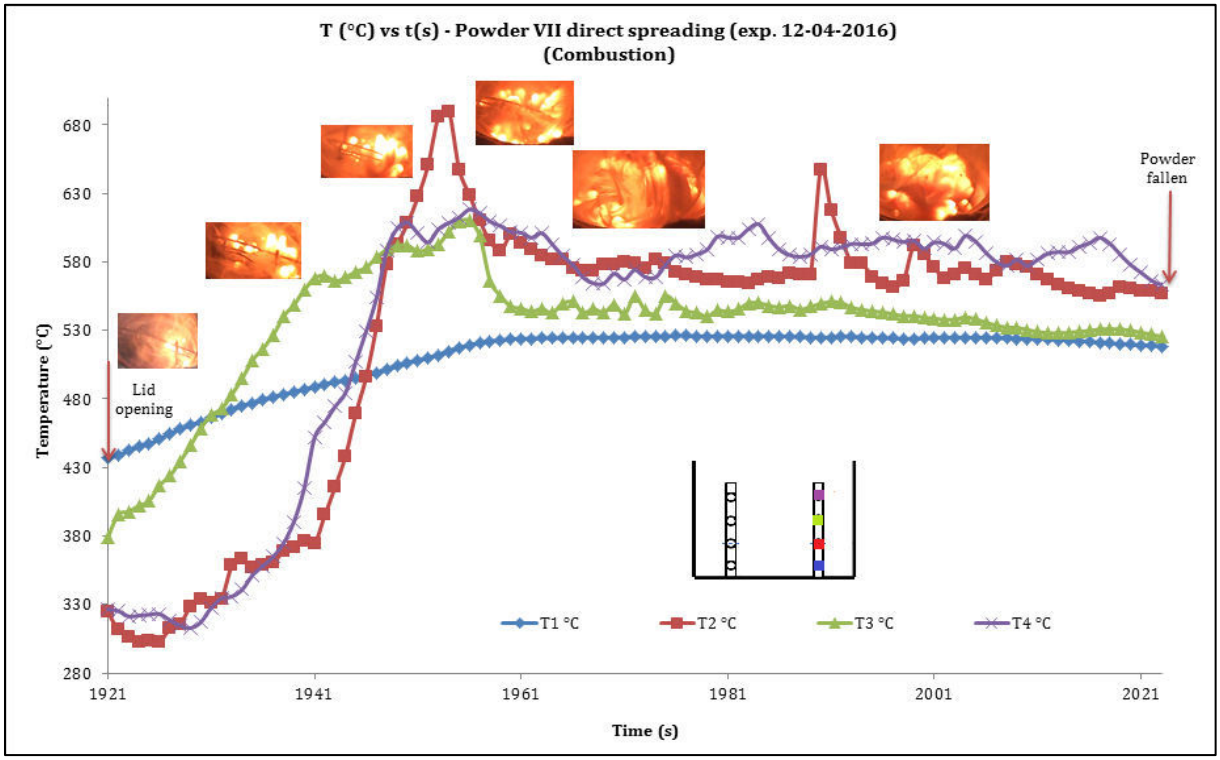

Figure A- 16. The temperature and video observations of the Chris(X)ti-Na experiment using powder VII with direct spreading during combustion

- Powder IX

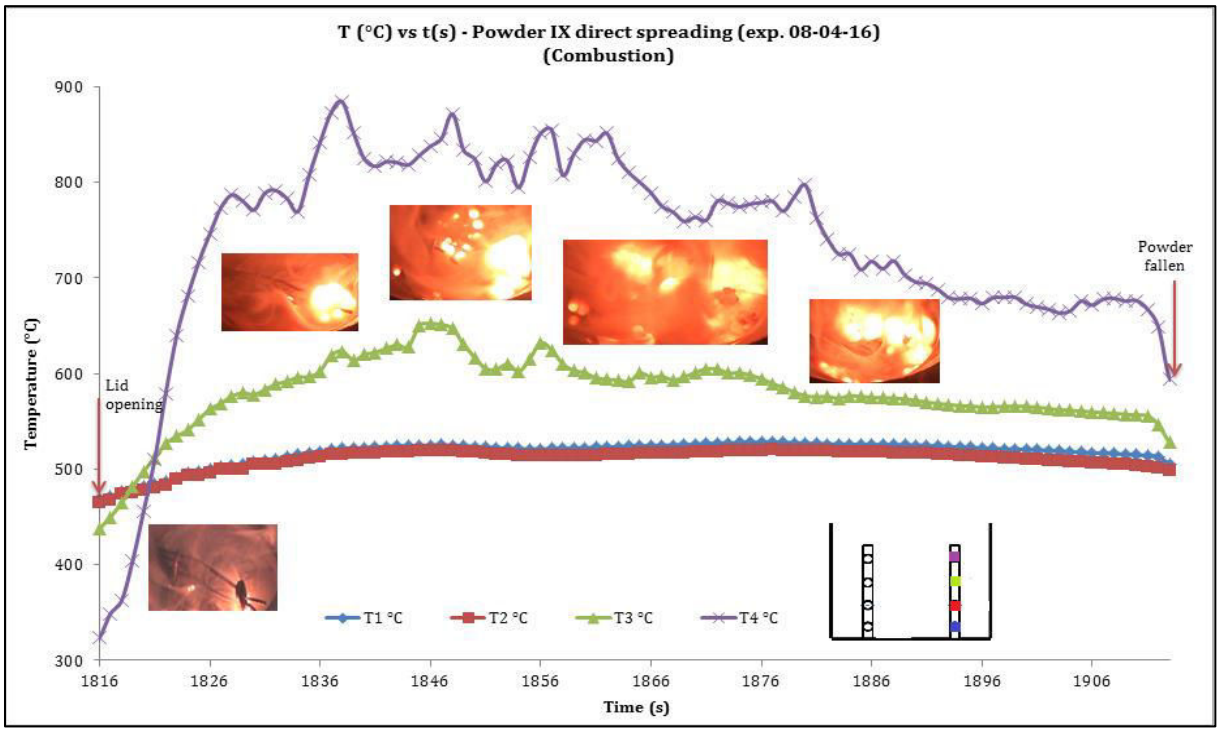

Figure A- 17. The temperature and video observations of the Chris(X)ti-Na experiment using powder IX with direct spreading during combustion

A.4 Optical microscope observation of extinction residue

The observation of extinction residue with powder II was taken under optical microscope. It showed that there is white and black part as can be seen in Fig. A-18a. Taken a closer look to the black part (cf. Fig. A-18b), it is actively reacts with air as a lot of liquid bubbles formed through the surface contrarily to the white part having no reaction whatsoever (cf. Fig. A-18c). We might suppose that the white part here represents the NaOH formed during extinction with powder II, while the black part is the sodium carbonate layer formed under which the unburnt sodium still present. As the observation were done in the ambient air, the residue of sodium and sodium oxide then reacts with humidity thus forming liquid bubble soaks through the powder layer according to reaction (a-8) and (a-9). It should be noted that the more water hydrate contained in the powder, the more white parts observed in the residue.

$$Na_{(s)} + H_2O_{(g)} \rightarrow NaOH_{(l)} + \frac{1}{2}H_2(g) \qquad \text{(a-8)}$$

$$Na_2O_{(s)} + H_2O_{(g)} \rightarrow 2NaOH_{(l)} \qquad \text{(a-9)}$$

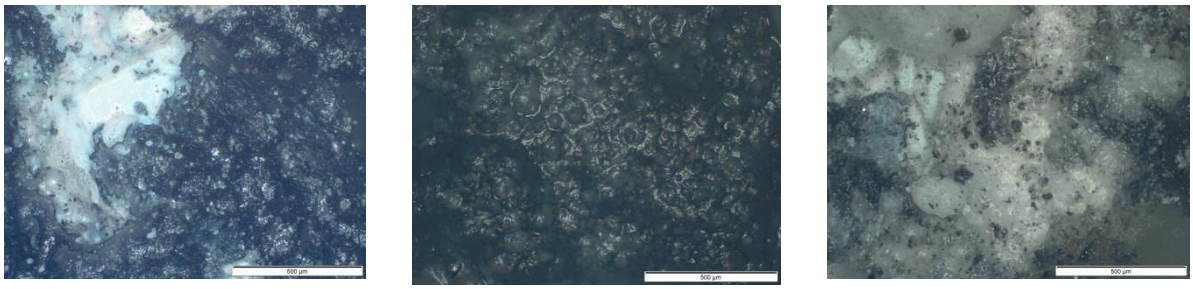

(a) (b) (c)

Figure A- 18. The optical microscopy observation of the extinction residue with powder II

A.5 XRD results of extinction residue

- Continue spreading
  - Powder A (14-03-2016)

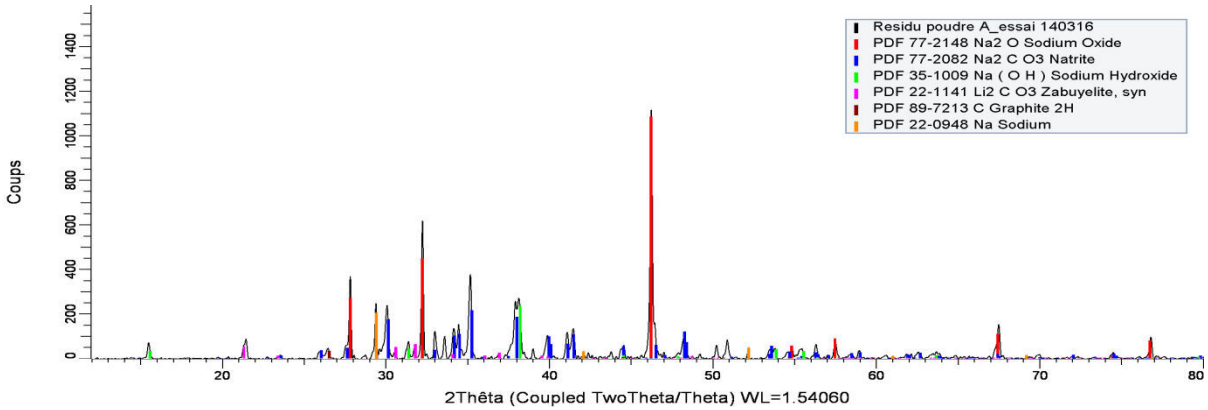

Figure A- 19. XRD diagram of extinction residue with powder A in continuous spreading

- Powder B (21-03-2016)

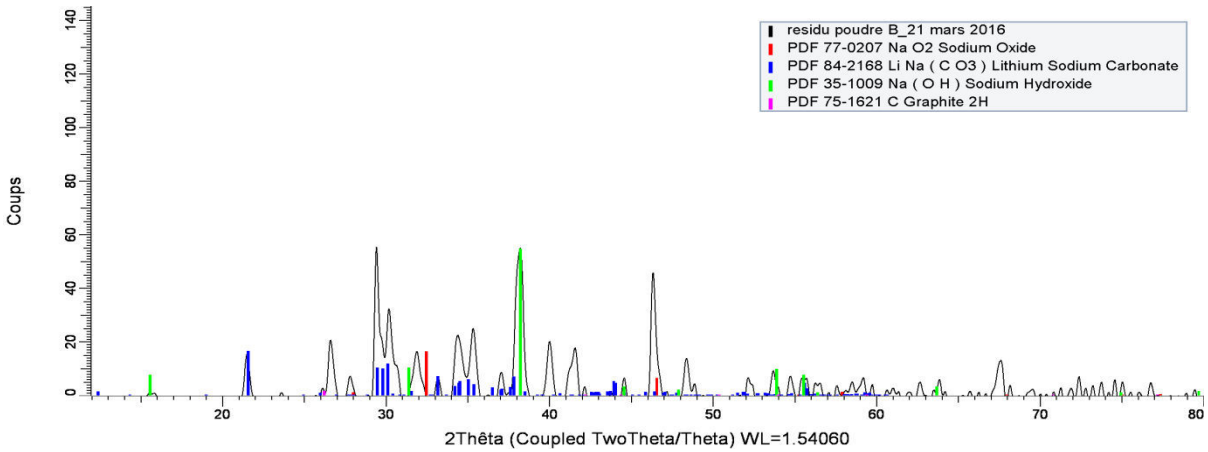

Figure A- 20. XRD diagram of extinction residue with powder B in continuous spreading

- Powder C (22-03-2016)

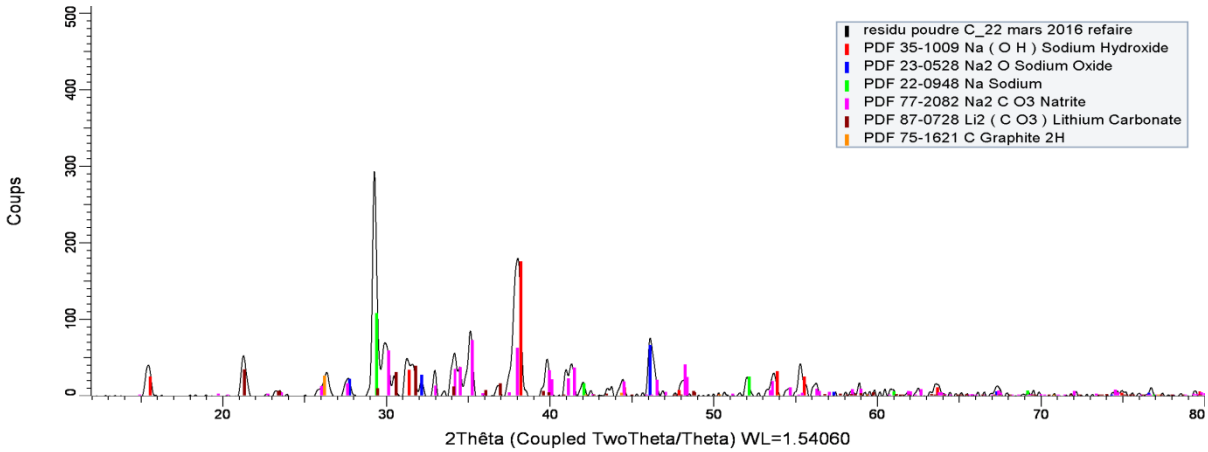

Figure A- 21. XRD diagram of extinction residue with powder C in continuous spreading

- Powder I (19-11-2015)

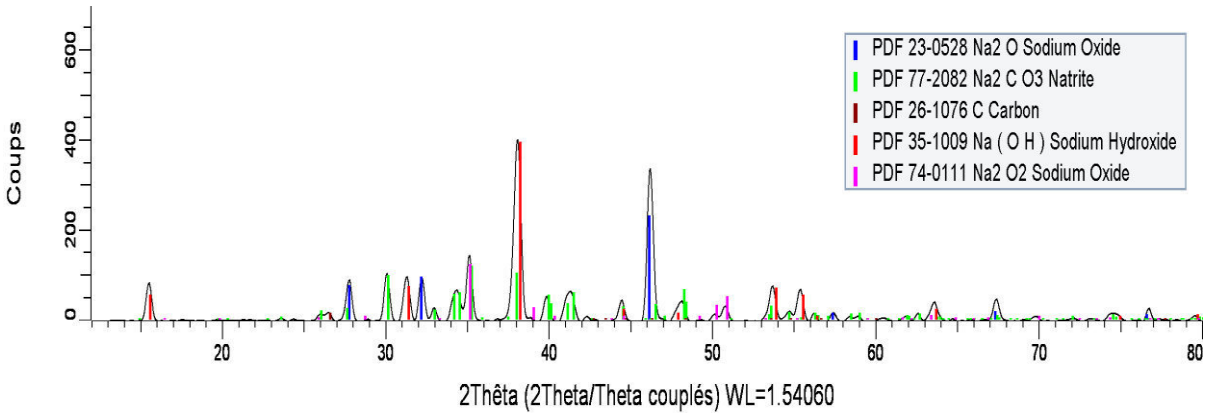

Figure A- 22. XRD diagram of extinction residue with powder I in continuous spreading

- Powder II (17-11-2015)

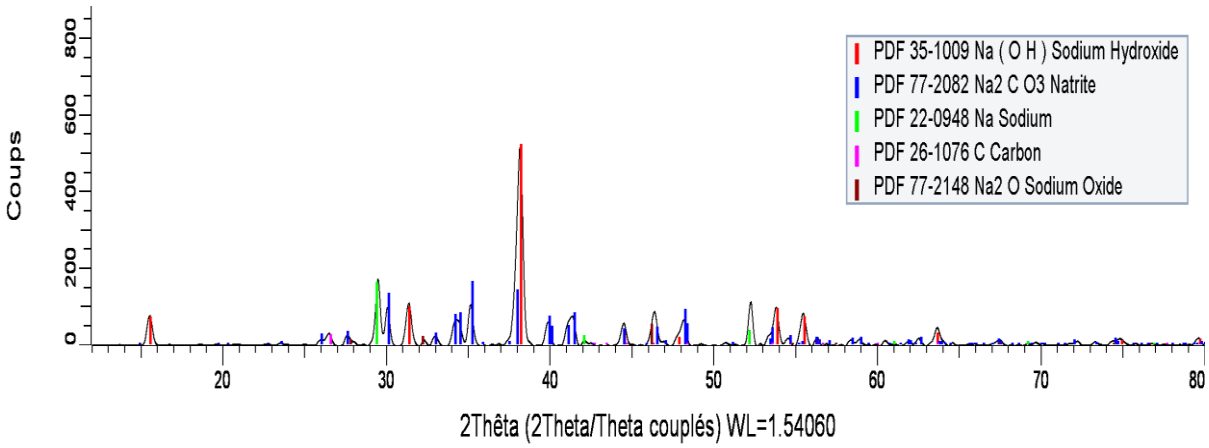

Figure A- 23. XRD diagram of extinction residue with powder II in continuous spreading

- Powder III (16-11-2015)

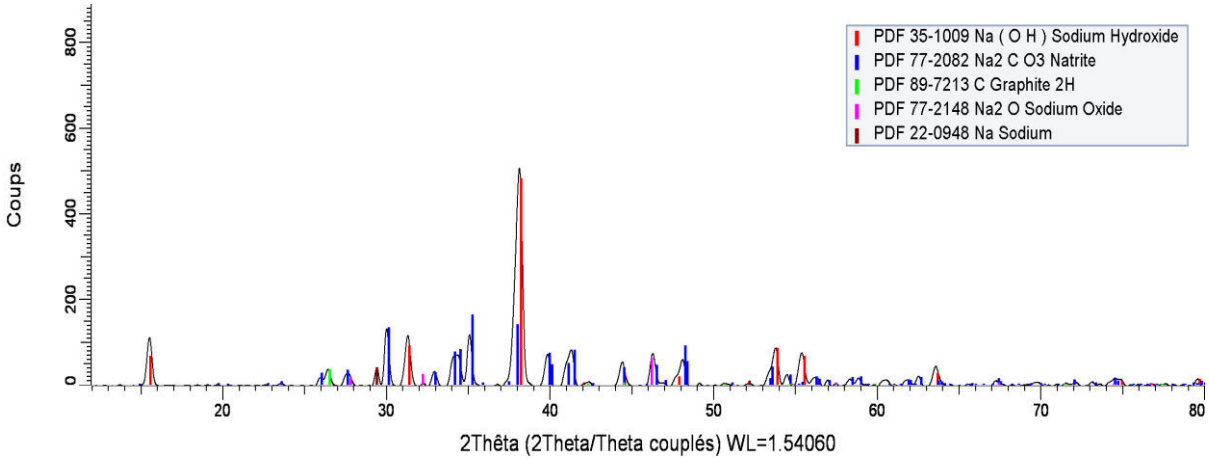

Figure A- 24. XRD diagram of extinction residue with powder III in continuous spreading

- Powder IV (05-04-2016)

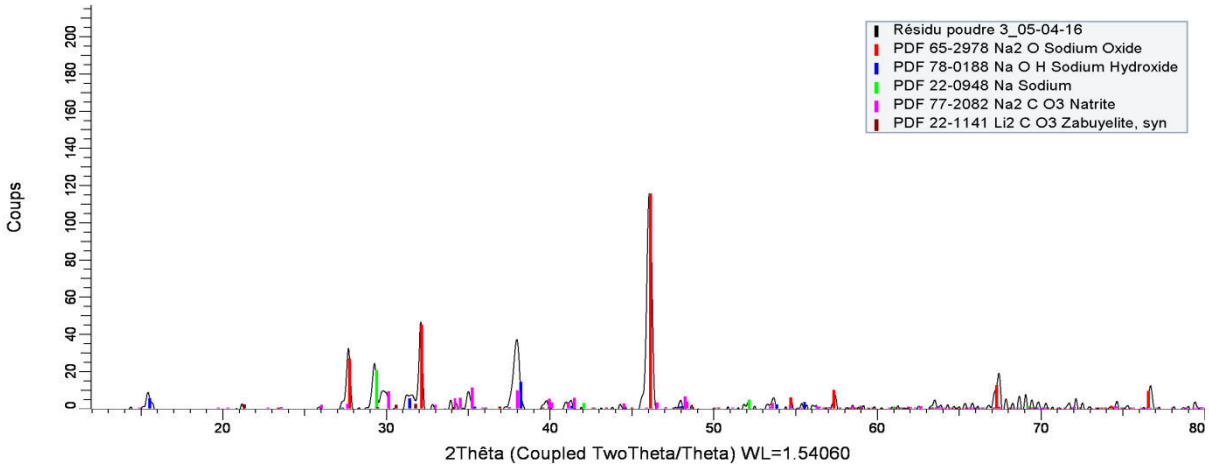

Figure A- 25. XRD diagram of extinction residue with powder IV in continuous spreading

- Powder V (04-12-2015)

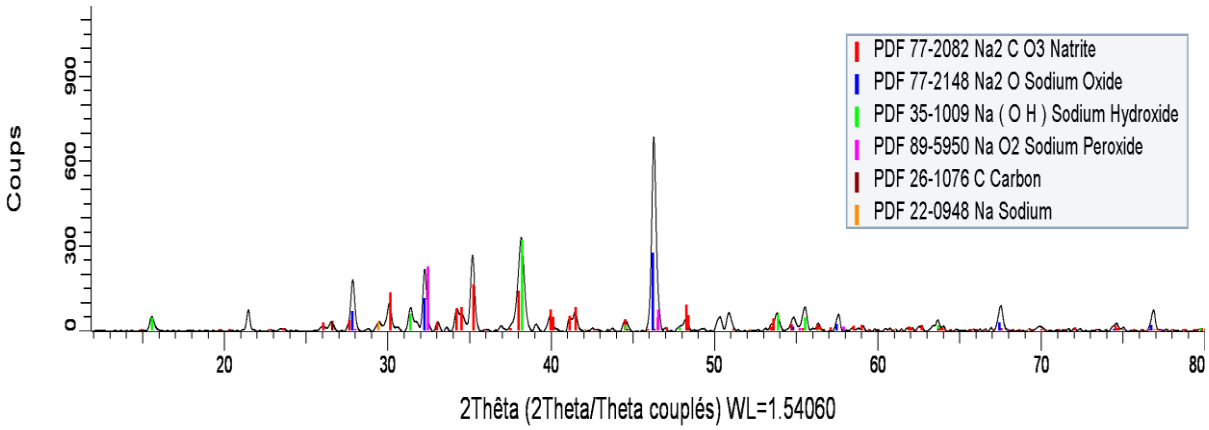

Figure A- 26. XRD diagram of extinction residue with powder V in continuous spreading

- Powder VI (26-11-2015)

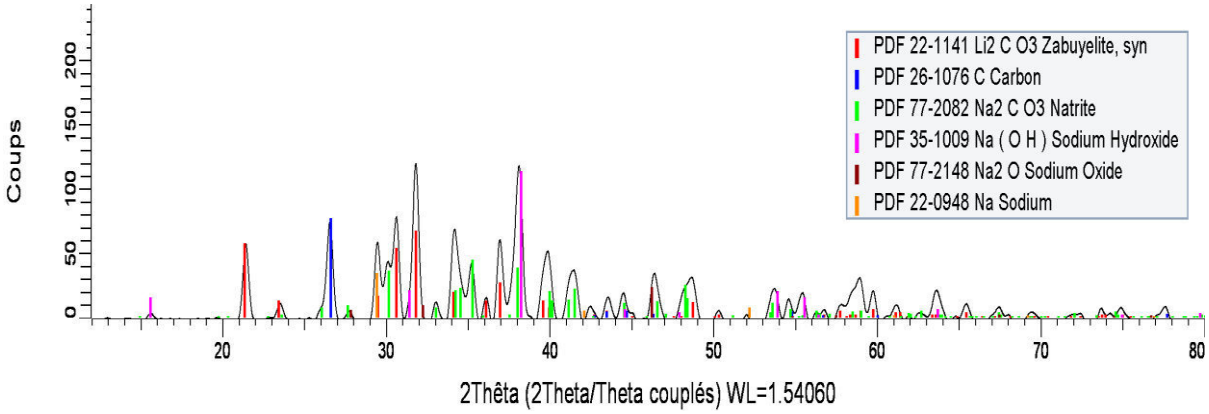

Figure A- 27. XRD diagram of extinction residue with powder VI in continuous spreading

- Powder VII (25-03-2016)

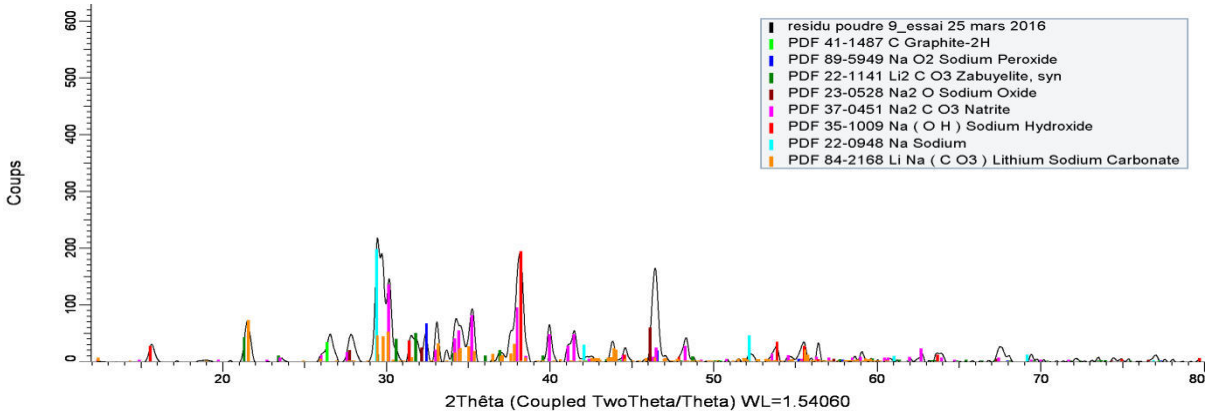

Figure A- 28. XRD diagram of extinction residue with powder VII in continuous spreading

- Powder VIII (20-11-2015)

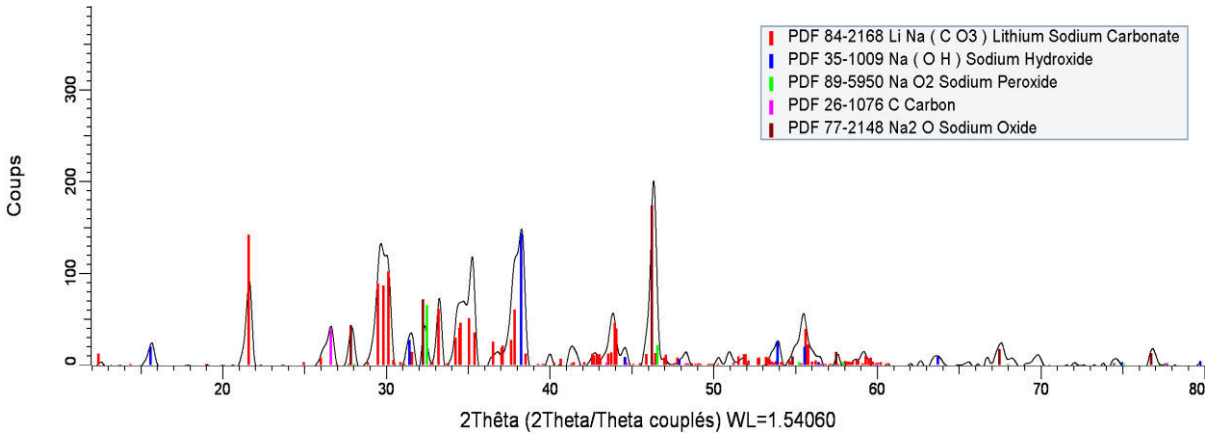

Figure A- 29. XRD diagram of extinction residue with powder VIII in continuous spreading

- Powder IX (24-03-2016)

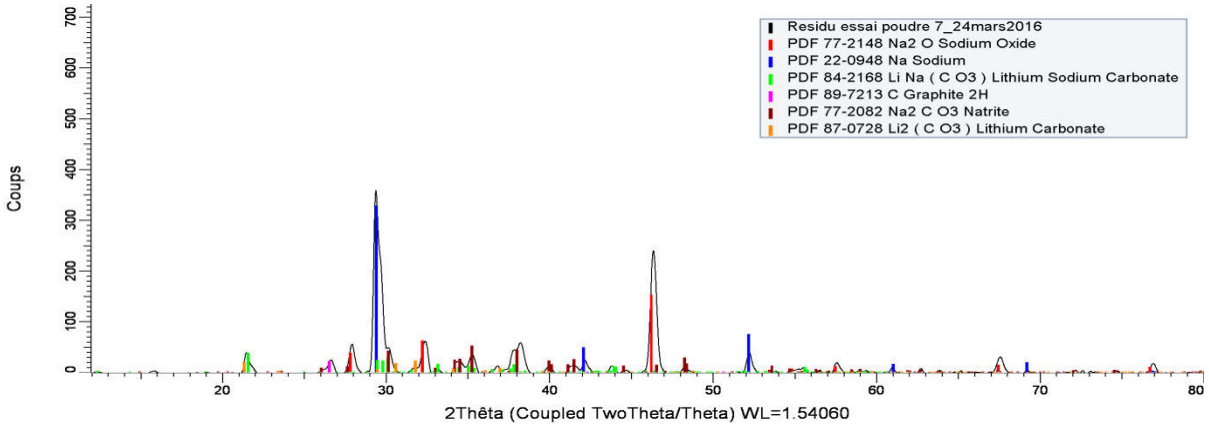

Figure A- 30. XRD diagram of extinction residue with powder IX in continuous spreading

- Direct spreading

- Powder II (11-04-2016)

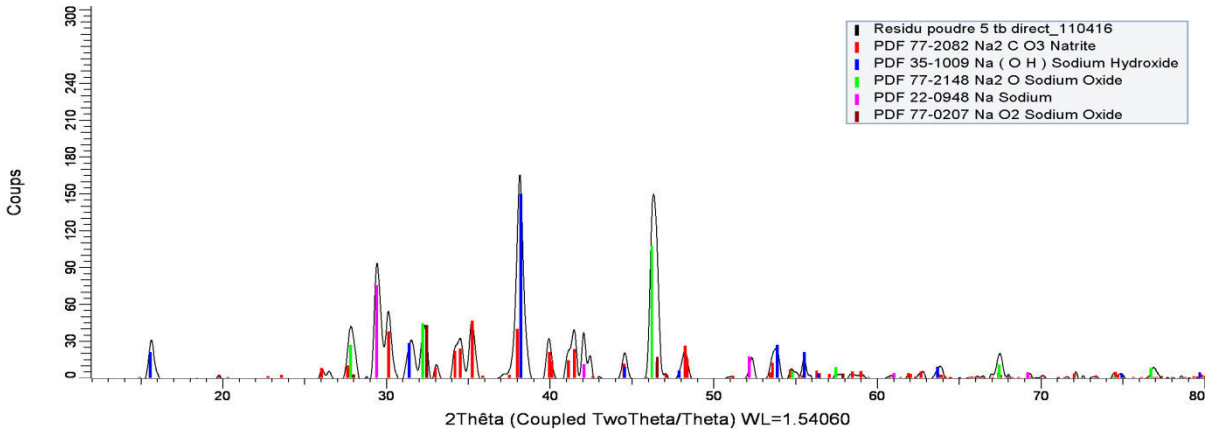

Figure A- 31. XRD diagram of extinction residue with powder II in direct spreading

- Powder IV (07-04-2016)

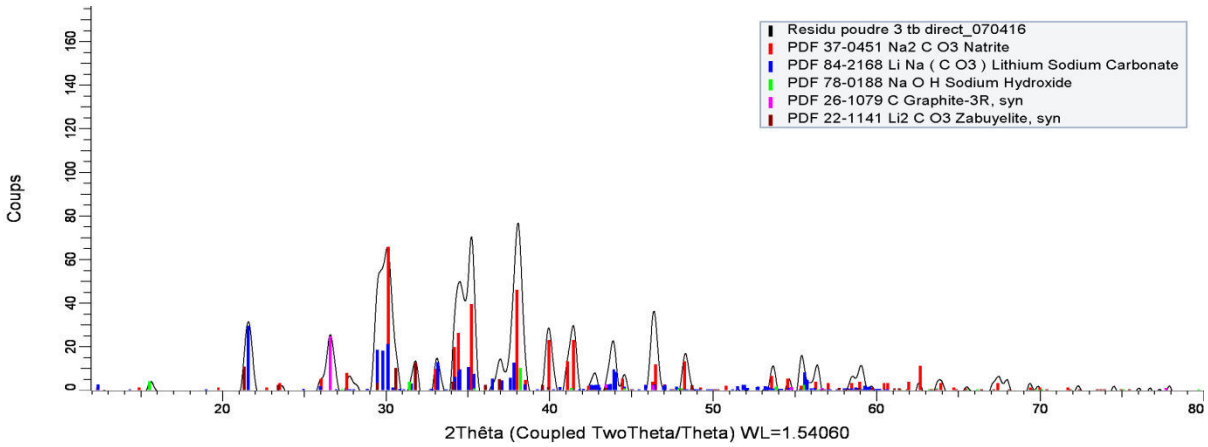

Figure A- 32. XRD diagram of extinction residue with powder IV in direct spreading

- Powder VII (12-04-2016)

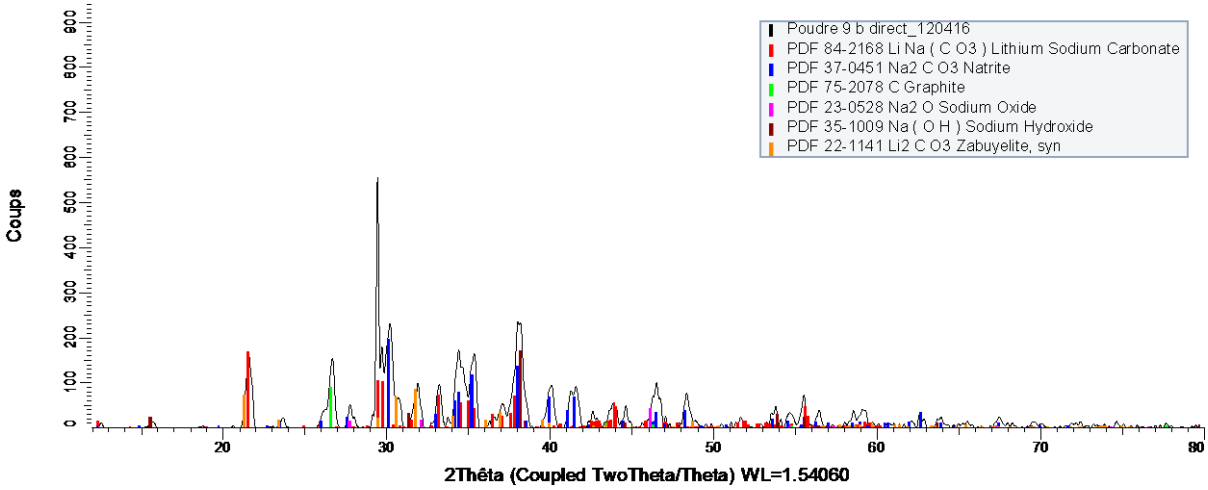

Figure A- 33. XRD diagram of extinction residue with powder VII in direct spreading

- Powder IX (08-04-2016)

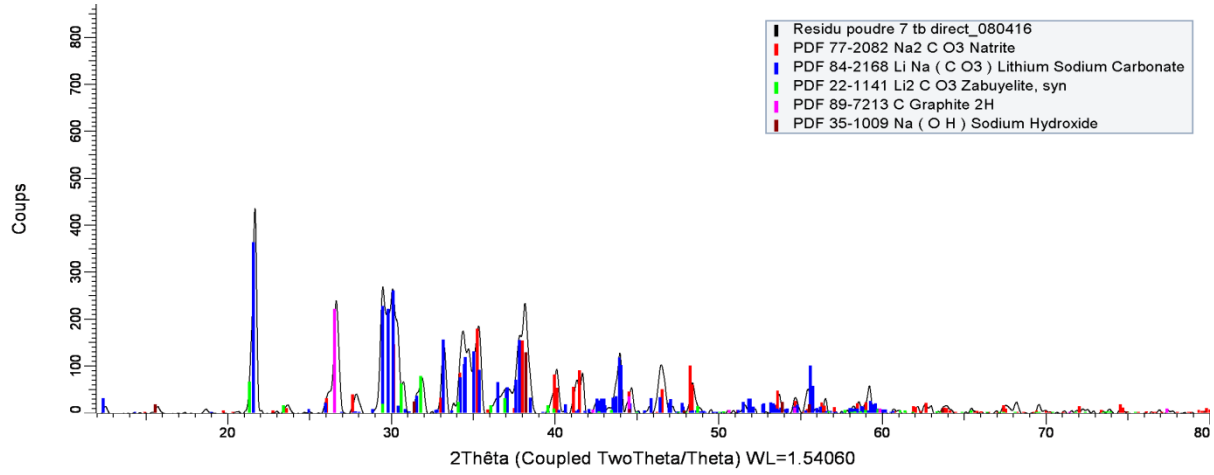

Figure A- 34. XRD diagram of extinction residue with powder IX in direct spreading

BIBLIOGRAPHY OF ANNEXE

[1] M. Abdellaoui and E. Gaffet, "The physics of mechanical alloying in a planetary ball mill: mathematical treatment," *Acta Metall. Mater.*, vol. 43, no. 3, pp. 1087–1098, 1995.

[2] N. Burgio, A. Iasonna, M. Magini, S. Martelli, and F. Padella, "Mechanical alloying of the Fe–Zr system. Correlation between input energy and end products," *Il Nuovo Cimento D*, vol. 13, no. 4, pp. 459–476, Apr. 1991.

[3] A. M. Spasic and J.-P. Hsu, *Finely Dispersed Particles: Micro-, Nano-, and Atto-Engineering*. CRC Press, 2005.

Etude des propriétés physicochimiques d'une poudre extinctrice pour les feux sodium: vieillissement, fabrication, et mécanisme d'extinction

Résumé

Le Commissariat à l'Energie atomique et aux énergies alternatives (CEA) a développé une poudre extinctrice efficace capable d'éteindre le feu de sodium. Elle est une poudre à base d'un mélange de carbonate de lithium (Li_2CO_3) et de carbonate de sodium à basse hydraté ($Na_2CO_3.H_2O$) dans une proportion proche de l'eutectique, avec une température de fusion d'environ 500°C, associée à du graphite. Cependant, depuis le démantèlement de plusieurs anciennes installations de sodium, le CEA dispose d'un stock important de lots de poudre inutilisés. L'idée de réutiliser ces poudres initie la question sur leur efficacité pour éteindre un feu de sodium après un stockage à long terme. Cette étude a proposé des analyses physico-chimiques de ces poudres afin d'identifier leurs compositions et les caractéristiques des différents lots. Les résultats mettent en évidence la présence de carbonate de lithium de sodium ($LiNaCO_3$) et trona ($Na_2CO_3.NaHCO_3.2H_2O$) qui ne sont pas mentionnés dans le brevet. Les expériences de vieillissement ont été développées pour étudier le rôle de l'humidité et du dioxyde de carbone à l'air ambiant au cours du stockage. Les résultats montrent que $LiNaCO_3$ est sensible à la présence d'humidité, capable de transformer en carbonate de lithium et le carbonate de sodium monohydrate, quant à celui-ci réagit avec de l'eau et du dioxyde de carbone pour former du trona. Une étude de la formation de $LiNaCO_3$ a permis d'avoir la compréhension du procédé de fabrication de la poudre. Ce composé se trouve à se produire grâce aux réactions mécanochimique entre Li_2CO_3 et $Na_2CO_3.H_2O$ au cours du processus de broyage. Le Chris(X)ti-Na installation expérimentale est construit pour comprendre les mécanismes d'extinction en particulier concernant le rôle des propriétés physicochimiques sur l'extinction. Deux étapes de mécanismes d'extinction sont proposés, qui comprend (1) la formation d'hydroxyde de sodium liquide (NaOH) et (2) la fusion des carbonates eutectique. La première étape peut se produire directement (par la réaction directe du trôna et / ou $Na_2CO_3.H_2O$ avec $Na_{(g)}$ et / ou $Na_2O_{(s)}$), soit indirectement (par l'intermédiaire de la réaction de décomposition du trôna et $Na_2CO_3.H_2O$ avant la réaction de $H_2O_{(g)}$ libéré avec $Na_{(g)}$ et / ou $Na_2O_{(s)}$). Les deux réactions mènent la possibilité de la formation d'hydrogène (H_2) qui pourrait être représenté par la flamme flash observée avant l'extinction. Ils contribuent également à la diminution rapide de la température due à la formation d'hydroxyde de sodium liquide (NaOH) en tant que couche protectrice. Cette couche est nécessaire pour couvrir la surface de sodium d'un contact prolongé avec de l'oxygène. La présence de trona semble ne pas altérer la capacité d'extinction de la poudre. Avec la même quantité de NaOH produit par les deux composés, trona libère plus de quantité de H_2 et plus exothermique que celle de $Na_2CO_3.H_2O$. Dans l'ensemble, 0,5-0,9g d'eau est nécessaire pour éteindre 19,6 cm^2 de sodium feu en nappe, ce qui équivalent à 1-2g de NaOH. Sur la base de ces tests, la teneur minimale en eau nécessaire à l'extinction est 5.6w%. Les poudres dont la teneur en eau d'hydratation est proche de 13w% semblent plus susceptibles de produire une flamme vigoureuse élevée avant l'extinction. La deuxième étape est considérée comme étant plus lent que l'étape précédente. La couche de carbonates eutectique a une viscosité supérieure à celle de NaOH qui le rend moins avantageux pour former la couche étanche à la surface de sodium. Par conséquent, son rôle pourrait être moins important en particulier pour le feu de sodium ayant commencé à basse température. Néanmoins, son effet est considéré comme plus important lorsqu'il est appliqué au feu de sodium à température élevée (supérieure à 500°C). Enfin, la taille des particules apparemment ne démontre pas une contribution significative à la performance d'extinction outre qu'affecter les performances d'épandage.

Mots clés: Sodium, Feu, Poudre, Physico-chimique, Vieillissement, Fabrication, Extinction.

Study of physicochemical properties of an extinguishing powder for sodium fires : aging, fabrication, and mechanism of extinction

Abstract

The French Atomic and alternatives Energy Commission (CEA) developed an effective powder capable of extinguishing sodium fire. It is a powder based on a mixture of lithium carbonate (Li_2CO_3) and low-hydrated sodium carbonate ($Na_2CO_3.H_2O$) in a near eutectic proportion, with a melting temperature of around 500°C, associated with graphite. However, ever since the dismantling of several old sodium installations, CEA has at its disposal an important stock of unused powder batches. The idea of reutilizing these powders initiates the question about their efficiency to extinguish a sodium fire after long term storage. This study proposed the physicochemical analyses of these powders in order to identify their compositions and characteristics for different batches. The results highlight the presence of lithium sodium carbonate ($LiNaCO_3$) and trona ($Na_2CO_3.NaHCO_3.2H_2O$), which are not mentioned in the patent. The aging experiments were developed to study the role of moisture and ambient carbon dioxide during the storage. The results showed that $LiNaCO_3$ is sensitive to the presence of moisture, able to transform it into lithium carbonate and sodium carbonate monohydrate, meanwhile the latter reacts with water and carbon dioxide to form trôna. A study of the formation of $LiNaCO_3$ allowed the understanding of the fabrication method of the powder. This compound is found to be produced as the results of mechanochemical reactions between Li_2CO_3 and $Na_2CO_3.H_2O$ during the grinding process. The Chris(X)ti-Na experimental facility is built to understand the mechanisms of extinction especially related to the role of physicochemical properties on extinction. Two steps of extinction mechanisms are proposed that includes (1) the formation of liquid sodium hydroxide (NaOH) and (2) the melting of eutectic carbonates. The first step can happen directly (via the direct reaction of trona and/or $Na_2CO_3.H_2O$ with $Na_{(g)}$ and/or $Na_2O_{(s)}$) or indirectly (via the decomposition reaction of trona and $Na_2CO_3.H_2O$ prior to reaction of $H_2O_{(g)}$ released with $Na_{(g)}$ and $Na_2O_{(s)}$). Both reactions explore the possibility of hydrogen (H_2) formation that might be represented by the flash flame observed prior to extinction. They also contribute to the rapid decrease of temperature due to the formation of liquid sodium hydroxide (NaOH) as a protective layer. This layer is essential to cover the sodium surface from prolonged contact with oxygen. The presence of trona appears to be not altering the extinction capacity of the powder. With the same amount of NaOH produced by both compounds, trona releases more quantity of H_2 and more exothermic in terms of energy release than that of $Na_2CO_3.H_2O$. Overall, 0.5-0.9 g of water is necessary to extinguish 19.6 cm^2 of sodium pool fire, which equivalent to 1-2g of NaOH. Based on these tests, the minimum water content required for extinction is 5.6w%. Meanwhile, powders whose hydration water content is close to 13w% seem more likely to produce a high vigorous H_2 flame prior to the extinction. The second step is considered to be slower than the previous step. The eutectic carbonates layer has higher viscosity than NaOH that makes it less beneficial to form sealed layer on the sodium surface. Therefore, its role might be less significant especially for the sodium fire starts at low temperature. Nevertheless, the effect is considered to be more important when applied to sodium fire at higher temperature (more than 500°C). Finally, the particle size apparently doesn't demonstrate a significant contribution in the extinguishing performance other than affecting the spreading performance.

Keywords: Sodium, Fire, Powder, Physicochemical, Aging, Fabrication, Extinction.